CITY UNIVERSITY LONDON

School of Engineering and Mathematical Sciences

Fundamental Behaviour of Valves Used in Diesel Fuel Injection Equipment

Michael James McLorn

Thesis submitted for the degree of Doctor of Philosophy

April 2013

I hereby declare that the work presented in this thesis is my own work, was developed in a joint effort, or has been built upon existing knowledge as stated and acknowledged in the text accordingly.

Date Michael James McLorn

Disclaimer

The views and findings are those of the author and are not necessarily endorsed by Delphi Diesel Systems, the company providing the facilities and finance for this research.

ABSTRACT

Engine manufacturers have acknowledged that in order to meet future strict emission regulations, greater optimisation of the combustion process is necessary. They are also aware that in a direct injection diesel engine, the Fuel Injection Equipment (FIE) plays the most critical role in the combustion efficiency and the formation of exhaust pollutants. In fact, the engine torque curve, fuel consumption, smoke, noise and exhaust emissions are all determined by the quantity and manner in which the fuel is injected into the engine cylinder. In modern high speed diesel engine applications, it is the inwardly-opening needle valve which fulfils this purpose. Its location, being situated within the tip of a fuel injector nozzle, ensures that the needle valve is the ultimate link between the FIE and the combustion process. This arguably makes this valve the single most important component within the whole fuel injection system, or in other words, the most important piece of the puzzle.

This thesis details a series of experimental projects which were carried out to study the internal flow inside some common types of valves found within diesel FIE. Although primarily focusing on the needle valve design, both ball and cone check valves were also considered. The typical approach of visualising the internal flow structure involved the use of enlarged transparent models and a refractive index matched working fluid. Laser Light sheet illumination and Particle Image Velocimetry techniques were adopted to provide qualitative and quantitative analysis of the internal flow structure within the aforementioned types of valves. In the case of the needle valve, two reported flow phenomena, the 'flow transition' and the 'flow overshoot' were confirmed to occur within the nozzle sac, whilst a third previously unknown flow structure, the 'reverse overshoot' was exposed. PIV analysis has quantified flow structures within the injection holes and these have been associated with vortical structures known to exist within the emerging spray plumes. Additional observations were made of the growth of the separated region and the influence of hole entry cavitation on the bulk flow within the injection hole. In the case of an un-sprung ball check valve, a novel design of lift stop was put forward and found during steady-state flow to improve the operational performance and neutralise some undesirable behaviour. This effect was especially apparent at the full lift condition.

It is anticipated that knowledge gained and described within this thesis will have commercial value to assist with design optimisation of future FIE components and for the validation of simulation data, in particular with regard analysis of the flow within the injection hole.

ACKNOWLEDGEMENTS

Firstly I would like to give thanks to my academic supervisor at City University. Throughout the 5 year duration of this PhD, Professor Manolis Gavaises provided me with direction yet freedom whilst offering meaningful advice and guidance when sought.

Secondly I would like to thank the significant input from the Advanced Engineering Group at Delphi Diesel Systems technical centre in Gillingham, Kent. In no particular order, Dr Celia Soteriou, Mark Winterbourn, Satish Sankhalpara, Abdul Aziz, Daniel Bush, Dr Larry Yu and Marion Balin. This is not a conclusive list so I would like to extend thanks to the dozens of other colleagues who let me 'pick their brains' on regular occasions.

I wish also to thank the City University faculty staff who contributed to the projects discussed within this thesis, in particular Dr Nicholas Mitroglou.

Finally I would like to give thanks to Delphi Diesel Systems for the financial support in funding this PhD, the use of their excellent research facilities and for providing access to unpublished internal reports and papers.

TABLE OF CONTENTS

ABSTRACT **5**

ACKNOWLEDGEMENTS **7**

LIST OF FIGURES **14**

LIST OF TABLES **16**

LIST OF EQUATIONS **16**

NOMENCLATURE **17**

Abbreviations 17

Non-Dimensional Numbers 19

Symbols 19

1. CHAPTER 1 INTRODUCTION **21**

1.1. Development of the Diesel Engine 21

1.2. Fuel Injection 23

1.2.1. Indirect Injection 23

1.2.2. Direct Injection 24

1.2.3. Evolution of the Fuel Injection Equipment 26

1.2.4. Multiple Injection Strategy 27

1.2.5. Injection Rate Shaping 28

1.2.6. Recent & Future FIE Trends 29

1.3. Combustion 30

1.3.1. Main Combustion Products 32

1.3.2. Lesser combustion products 33

1.3.3. Fuel Distribution 35

1.4. Fuel Quality 36

1.4.1. Calibration Oil 36

1.5. Emission Standards 37

1.5.1. European Exhaust Emission Standards 37

1.5.2. Worldwide Exhaust Emission Standards 39

1.5.3. Exhaust After-Treatment 40

1.5.4. FIE After-Treatment Approaches 42

1.6. Modern Fuel Injection Strategies 43

1.6.1. High Pressure Rotary Pumps 43

1.6.2. Electronic Unit Injectors 45

1.6.3. Common Rail Systems 47

1.6.4. Hybrid FIE systems 51
1.6.5. Summary of FIE systems 53
1.6.6. Future Trends for FIE 54
1.7. Multi-hole LD Nozzles 56
1.7.1. Nozzle Design 56
1.7.2. Nozzle Manufacture 58
2. CHAPTER 2 – EXPERIMENTAL TEST FACILITIES 63
2.1. High Pressure Rig 63
2.2. Low Pressure Rig 64
2.3. Spray Visualisation Rig 66
2.4. Laser Based Flow Rig 67
2.4.1. Laser Light Sheet Illumination 69
2.4.2. Particle Image Velocimetry 70
2.4.3. Laser Doppler Anemometry 73
2.5. Other Experimental Facilities/Techniques 75
3. CHAPTER 3 – FLUID THEORY 77
3.1. Fluid Cavitation Theory 77
3.1.1. Cavitation Number 78
3.1.2. Reynolds Number 79
3.1.3. Weber Number 79
3.1.4. Coefficient of Discharge 80
3.1.5. Choked Coefficient of Discharge 81
3.1.6. Geometry Induced Cavitation 81
3.1.7. Dynamically Induced Cavitation 81
3.1.8. Cavitation Bubble Growth 82
3.1.9. Cavitation Erosion 83
3.1.10. High C_d Nozzles 84
3.2. Injector Nozzle Flow 85
3.2.1. Low needle Lift 86
3.2.2. Intermediate Needle Lift 86
3.2.3. Large Needle Lift 86
3.3. Mechanism of Fuel / Air Mixing & Atomisation 87
3.4. Valve Overview and Description 87
3.4.1. Ball Check Valve Design 88
3.4.2. Cone Check Valve Design 93

3.4.3. Needle Valve Design 95
3.5. Injector Nozzle Design 95
3.5.1. Needle Valve Wander 97
3.5.2. Needle Lift Sensor 97
3.5.3. Relationship between Valve Lift & Seat Area 97
3.6. Check Valve Behaviour 98
3.6.1. Check Valve Closure 98
3.6.2. Check Valve Slam 99
3.6.3. Pressure Surge 99
3.6.4. Check Valve Clatter 100
3.6.5. Check Valve Performance 100
3.6.6. Check Valve Selection 101
4. CHAPTER 4 – LITERATURE REVIEW 103
4.1. Check Valve Review 103
4.1.1. Ball Check Valves 103
4.1.2. Cone Check Valves 105
4.2. Needle Valve Review 107
4.2.1. Real Size Study 107
4.2.2. Large Scale Models 111
4.2.3. Limitations of Large Scale Modelling 114
4.3. Scaling Between Real Size & Large Scale Models 115
4.3.1. Deriving Scaling Equations 116
4.4. Summary of Literature Review 117
5. CHAPTER 5 – EXPERIMENTAL PROJECTS 119
5.1. Ball Delivery Valve LSM 119
5.1.1. Eccentric Flow Insert – LLS Analysis 120
5.1.2. Eccentric Flow Insert – PIV Analysis 123
5.1.3. Project Conclusions 125
5.2. 120° Seat Nozzle Project 126
5.2.1. LSM Design & Manufacture 126
5.2.2. AFM Method for Nozzle LSMs 128
5.2.3. Flow Transition 131
5.2.4. Flow Overshoot 132
5.2.5. LBFR Reference Needle - Opening CN 3 132
5.2.6. Spray Visualisation – Real Size Nozzle 134

5.2.7. FEATS Needle Design Variant 136
5.2.7. LBFR Reference needle – Opening 20 l/min 138
5.2.8. LBFR Reference needle - Closing 20 l/min 143
5.2.9. LBFR FEATS needle - Opening CN 3 147
5.2.10. LBFR FEATS needle - Opening 20l/min 149
5.2.11. LBFR FEATS needle - Closing 20l/min 152
5.2.12. Flow Transition Plots - 20l/min 155
5.2.13. Summary of Flow Transition & Hysteresis 158
5.2.14. Reference Needle PIV - Eccentric Light Sheet Positions 159
5.2.15. Project Conclusions 166
5.2.16. Summary of FEATS Needle Concept 169
5.3. 60° Seat Nozzle Project 171
5.3.1. Research Visualisation Nozzle (RVN) 171
5.3.2. RVN Real Size Nozzle testing 173
5.3.3. LBFR RVN - LSM Design & Manufacture 177
5.3.4. LPR RVN - LSM Design & Manufacture 179
5.3.5. Scaling Between LSM & Real Size 181
5.3.6. LBFR Hole 1 Internal Flow at CN 3 184
5.3.7. LBFR Hole 1 Internal Flow at ΔP = 0.87 bar 191
5.3.8. LPR Hole 1 Plume Structure 197
5.3.9. LBFR Hole 2 Internal Flow at CN 3 201
5.3.10. LBFR Hole 2 Internal Flow at ΔP = 0.87 bar 204
5.3.11. LBFR Hole 2 Vortex Activity 207
5.3.12. Project Conclusions 216
5.4. Real Size Transparent Nozzle Tip 219
5.4.1. Transparent Tip Design 219
5.4.2. Real Nozzle Modification 221
5.4.3. Acrylic Tip Manufacture 222
5.4.4. Experimental Testing 223
5.4.5. Project Conclusions 224
6. CHAPTER 6 – CONCLUSIONS & RECOMMENDATIONS 227
6.1. Thesis Overview 227
6.2. Statement of Findings 228
6.3. Project Synopsis 229
6.4. Recommendations for Future Work 230

REFERENCES **233**

APPENDIX **240**

LIST OF FIGURES

Figure 1 - HSDE LD, MD & HD divisions 22
Figure 2 - IDI Engine Design 23
Figure 3 - DI Engine Design 25
Figure 4 - Multiple Injection Strategies 28
Figure 5 - Boot-shaped Main Injection Profile 29
Figure 6 - Two-actuator EUI single-cylinder engine data 31
Figure 7 - NO_x / PM Trade Off 35
Figure 8 - Tightening LD emission legislations 39
Figure 9 - Rotary Injection Pump 44
Figure 10 - EUI cross-section 46
Figure 11 - Delphi's Common Rail system 49
Figure 12 - Delphi's DFI 1.5 Fuel Injector 51
Figure 13 - F2 distributed pump CR system 52
Figure 14 - MD past and projected trends 55
Figure 15 - SEM images of an impression of injection hole entry 61
Figure 16 - High Pressure Rig image 64
Figure 17 - Low Pressure Rig Schematic 65
Figure 18 - Low Pressure Rig image 65
Figure 19 - Spray Visualisation Chamber image 67
Figure 20 - Laser Based Flow Rig Schematic 68
Figure 21 - Schematic & LLS image of an entry-throttled orifice 70
Figure 22 - Schematic of PIV setup 71
Figure 23 - PIV system in operation on LBFR 71
Figure 24 - Laser Doppler Anemometry system 74
Figure 25 - Evidence of nozzle cavitation 84
Figure 26 - Typical C_d versus CN relationship 85
Figure 27 - Conical seat ball valve (type 1) 89
Figure 28 - Conical seat ball valve (type 2) 90
Figure 29 - Spherical seat ball valve 91
Figure 30 - Flat seat ball valve 92
Figure 31 - Pressure limiting valve CAD model 92
Figure 32 - CR high pressure pump – Head assembly 93
Figure 33 - Cone check valve 94
Figure 34 - Guided cone inlet valve 94
Figure 35 - Section view of a fuel injector nozzle tip 96
Figure 36 - Relationship between lift and seat angle 98
Figure 37 - Ball check valve lift with increasing RPM 106
Figure 38 - Side and end views of the CAD model assembly 120
Figure 39 - Eccentric flow insert 120
Figure 40 - LLS images with insert at 5mm lift – Stable behaviour 121
Figure 41 - LLS images with insert at 2.5mm lift – Unstable behaviour 122
Figure 42 - Ball valve PIV measurement locations 123
Figure 43 - Mean PIV velocity contours regions 1 – 4 124
Figure 44 - Hole entry rounding 127

Figure 45 - 120° seat nozzle LSM nozzle and needle valve 128
Figure 46 - CAD section view of 120° seat nozzle LSM with Reference needle..... 129
Figure 47 - 120° Reference needle flow areas 130
Figure 48 - Reference Needle Flow versus Lift 131
Figure 49 - PIV velocity contours - Reference needle opening – CN 3 133
Figure 50 – 400 bar Spray Visualisation Images 135
Figure 51 - 120° FEATS needle flow areas 137
Figure 52 - FEATS needle Flow versus Lift 138
Figure 53 - LLS images with Reference needle opening – 20 l/min..... 140
Figure 54 - PIV velocity contours - Reference needle opening – 20 l/min 142
Figure 55 - LLS images with Reference needle closing – 20 l/min 144
Figure 56 - PIV velocity contours - Reference needle closing – 20 l/min..... 145
Figure 57 - RMS velocity contours - Reference needle closing – 20 l/min 146
Figure 58 - Mean PIV and raw images - FEATS needle opening - CN 3..... 147
Figure 59 - LLS images - FEATS needle opening - 20l/min..... 150
Figure 60 - PIV velocity contours - FEATS needle opening - 20l/min..... 151
Figure 61 - LLS images - FEATS needle closing - 20l/min..... 152
Figure 62 - PIV velocity contours - FEATS needle closing - 20l/min 153
Figure 63 - RMS velocity contours - FEATS needle closing - 20l/min 154
Figure 64 - Transition plots measurement location..... 155
Figure 65 - Mean V_X & V_Y component plots 156
Figure 66 - Eccentric laser light sheet positions..... 160
Figure 67 - PIV velocity contours, 0.2mm lift - CN 3..... 160
Figure 68 - PIV velocity contours, 0.4mm lift - CN 3..... 162
Figure 69 - V_X and V_Y component plots - CN 3..... 165
Figure 70 - Design A nozzle with plumes attached..... 171
Figure 71 - RVN design with plumes attached 172
Figure 72 – 2000 bar Spray visualisation - Design A and RVN at full lift 173
Figure 73 - 60° Seat Nozzle - Average plume penetration 175
Figure 74 - Liquid Phase Volume Fraction (LPVF) for RVN design 176
Figure 75 - RVN LBFR nozzle LSM and needle valve 178
Figure 76 - RVN LPR nozzle model and needle valve 179
Figure 77 - RVN LSM flow areas 181
Figure 78 - LSM and Real Size - Flow versus Lift plots 183
Figure 79 - Hole 1 PIV velocity contours - CN 3..... 185
Figure 80 - Hole 1 RMS PIV velocity contours - CN3..... 187
Figure 81 - Boundary layer measurement location..... 188
Figure 82 - V_X and V_Y components - CN 3 189
Figure 83 - Separated region reduction with lift - CN 3 190
Figure 84 - Hole 1 PIV velocity contours and LLS images - 0.87 bar ΔP..... 192
Figure 85 - Hole 1 RMS PIV velocity contours - 0.87 bar 194
Figure 86 - V_X and V_Y component plots - 0.87 bar ΔP 195
Figure 87 - Emerging spray plume un-submerged - 2.27 bar ΔP 198
Figure 88 - Emerging spray plumes submerged - 2.27 bar ΔP..... 199
Figure 89 - Enlarged image at 3.0mm lift submerged - 2.27bar ΔP 201
Figure 90 - Hole 2 PIV velocity contours - CN 3..... 202

Figure 91 - PIV raw images of cavitation within hole 2 204
Figure 92 - Hole 2 PIV velocity contour and LLS images - 0.87 bar ΔP 206
Figure 93 - Hole 2 eccentric laser light sheet positions 207
Figure 94 - Hole 2 position A & B section views 208
Figure 95 - Position A - mean PIV vector images at CN 3 209
Figure 96 - Position B – mean PIV vector images at CN 3 209
Figure 97 - Position A - mean PIV vector images at 0.87 bar 210
Figure 98 - Position B – mean PIV vector images at 0.87 bar 211
Figure 99 - Hole 2 possible vortex activity - CN 3 213
Figure 100 - Hole 2 possible vortex activity - 0.87 bar ΔP 215
Figure 101 - Transparent tip geometry flow areas 220
Figure 102 - CAD side and plan views of transparent nozzle tip 221
Figure 103 - Modified nozzle body 221
Figure 104 - Transient nozzle cavitation and flow – 300 bar 223

LIST OF TABLES

Table 1 - Summary of different FIE strategies 53
Table 2 - Observed flow transition lift location 158
Table 3 - Observations from FEATS needle testing 169
Table 4 - Injection hole inlet edge conditions 180
Table 5 - Fluid properties for model scaling 182
Table 6 - Scaling of pressure and flow 182

LIST OF EQUATIONS

Equation 1 – Overall Engine Efficiency 30
Equation 2 – K-factor 60
Equation 3 – LDA velocity at a point 74
Equation 4 – Cavitation Number 78
Equation 5 – Reynolds Number 79
Equation 6 – Flow Velocity 79
Equation 7 – Weber Number 80
Equation 8 – Coefficient of Discharge 80
Equation 9 – Area of a Frustum 97
Equation 10 – Joukowsky formula 99
Equation 11 – Re with C_d equation substituted 116
Equation 12 – Model Pressure Drop 116
Equation 13 – Model Flow 116
Equation 14 - Effective C_d relationship 126
Equation 15 – Plume penetration length 174

NOMENCLATURE

Abbreviations

1D	One Dimensional
2D	Two Dimensional
3D	Three Dimensional
ABS	Anti-lock Braking System
AFM	Abrasive Flow Machining
CAD	Computer Aided Design
CCD	Charge Coupled Device
CFD	Computational Fluid Dynamics
CO_2	Carbon Dioxide
CR	Common Rail
DDS	Delphi Diesel Systems
DFI	Diesel Fuel Injector
DFP	Diesel Fuel Pump
DPF	Diesel Particular Filter
DI	Direct Injection
DTI	Dial Test Indicator
ECU	Engine Control Unit
EDM	Electrical Discharge Machining
EGR	Exhaust Gas Recirculation
EPIC	Electronically Programmed Injection Control
EU	European Union
EUI	Electronic Unit Injector
EUP	Electronic Unit Pump
FIE	Fuel Injection Equipment
GVW	Gross Vehicle Weight
H_2O	Water
HD	Heavy Duty
HPR	High Pressure Rig
HPRP	High Pressure Rotary Pump
HSDE	High Speed Diesel Engine
IDI	Indirect Injection
IID	Internal Injector Deposits
INO	Inlet Nozzle Orifice
KE	Kinetic Energy
LBFR	Laser Based Flow Rig
LD	Light Duty
LGV	Large Goods Vehicle
LHS	Left Hand Side
LIF	Laser Induced Fluorescence
LLS	Laser Light Sheet
LNT	Lean NO_X Trap
LPR	Low Pressure Rig
LSM	Large Scale Model
MD	Medium Duty
MRI	Magnetic Resonance Imaging
MUI	Mechanical Unit Injector
MUP	Mechanical Unit Pump
Nd:YAG	Neodymium doped Yttrium Aluminium Garnet
NO	Nitrogen Oxide

NO_2	Nitrogen Dioxide
NOP	Nozzle Opening Pressure
NO_X	Nitrogen Oxides
NPO	Nozzle Path orifice
NVH	Noise Vibration Harshness
OEM	Original Equipment Manufacturer
PCD	Pitch Circle Diameter
P_{dn}	Pressure downstream
PE	Potential Energy
PIV	Particle Image Velocimetry
PLN	Pump-Line-Nozzle
PM	Particulate Matter
P_{up}	Pressure upstream
P_{vapour}	Vapour pressure
RHS	Right Hand Side
RIM	Refractive Index Matching
RMS	Root Mean Square
RVN	Research Visualisation Nozzle
RW	Reference Weight
SCR	Selective Catalytic Reduction
SNCR	Selective Non-Catalytic Reduction
SEM	Scanning Electron Microscope
SOI	Start of Injection
SPO	Spill Path Orifice
SVR	Spray Visualisation Rig
TDC	Top Dead Centre
TON	Time On
UBHC	Un-burnt Hydrocarbon
ULSD	Ultra Low Sulphur Diesel

Non-Dimensional Numbers

C_d	Coefficient of Discharge
C_dC	Choked Coefficient of Discharge
CN	Cavitation Number
RE	Reynolds Number
WE	Weber number

Symbols

Δ	Delta
A	Area [m²]
c	Speed of sound [m/s]
d	Distance [m]
d_f	Fringe distance [m]
f_D	Doppler frequency [Hz]
l	Length [m]
Ø	Diameter [m]
P	Pressure [Bar]
Q	Volumetric flow [m³/s]
v	Kinematic Viscosity [m²/s]
r_c	Compression ratio
V	Velocity [m/s]
γ	Heat capacity ratio
η	Efficiency
θ or α	Angle [°]
λ	Wavelength [m]
μ	Dynamic Viscosity [Pa.s]
ρ	Density [kg/m³]
σ	Surface tension [kg]

City, University of London
Northampton Square
London
EC1V 0HB
United Kingdom

T +44 (0)20 7040 5060

THE FOLLOWING PARTS OF THIS THESIS HAVE BEEN REDACTED FOR COPYRIGHT REASONS:

Figure 2 - IDI Engine Design 23

Figure 3 - DI Engine Design.....25

Figure 9 - Rotary Injection Pump.....44

Figure 10 - EUI cross-section.....46

1. CHAPTER 1 INTRODUCTION

1.1. Development of the Diesel Engine

It was in 1893 that Rudolf Diesel first demonstrated his single-cylinder, four-stroke, compression ignition engine. Today, regarded as being the most efficient of all internal combustion engine designs, the diesel engine has found applications in sectors as diverse as automotive, marine, power generation and even the aerospace industries. The development of Rudolf Diesel's original design into something recognizable as a modern High-Speed Diesel Engine (HSDE) may be considered to have occurred through small incremental improvements, with perhaps the most significant of these being the introduction of the common rail system in 1997. Whereas the first 100 years of diesel engine development could be generally characterized by power output and fuel efficiency driven improvements (Clemens, et al., 2007), the emphasis has shifted so that in recent years it has been the changing and tightening exhaust emission regulations that have been the driving force in the development and refinement of this engine. In fact it is anticipated that more than ever, diesel engine development will be driven by reducing emissions, lowering fuel consumption and improving the acoustic characteristics of the engine through optimisation of the combustion process (Schoppe, et al., 2012). Ignoring the low-speed marine and stationary power generation applications, this thesis shall focus on the HSDE commonly found within the automotive sector. To further clarify this, the automotive sector in Europe may be considered to be divided up into three divisions, Light Duty (LD), Medium Duty (MD) and Heavy Duty (HD). These divisions along with representative images of vehicle class are shown in Figure 1; however, this is intended for reference purposes only.

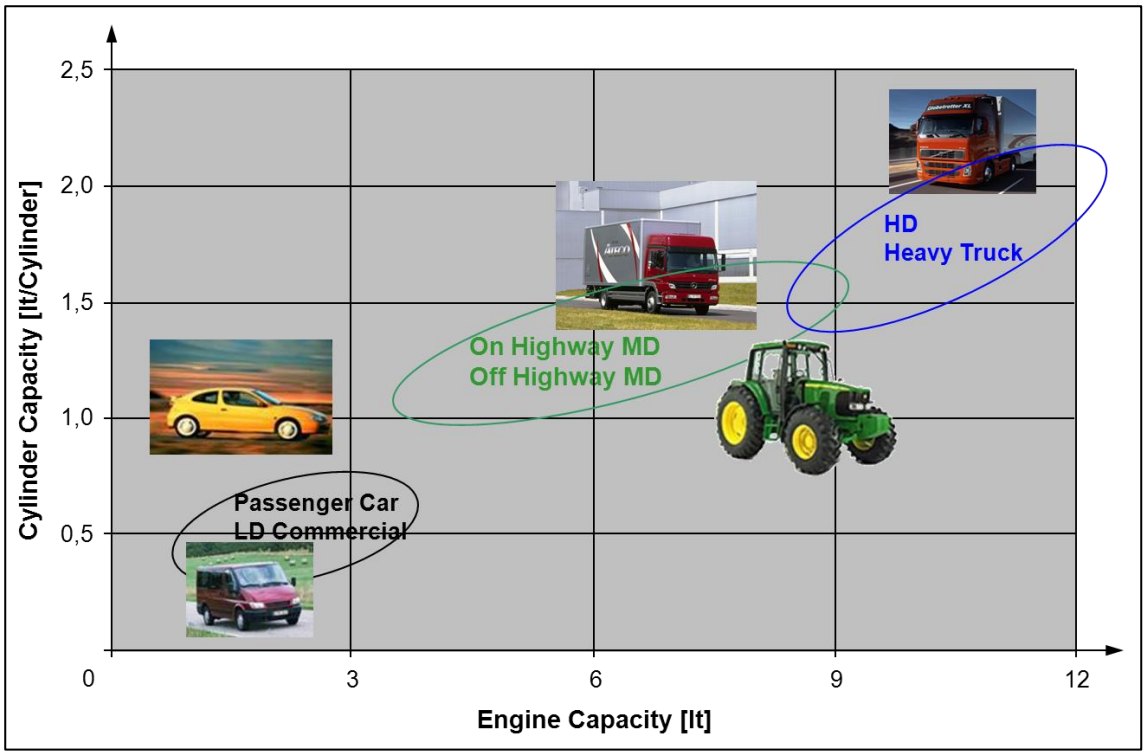

Figure 1 - HSDE LD, MD & HD divisions (Zülch, et al., 2006)

LD and MD often share similarities in terms of engine design and Fuel Injection Equipment (FIE) strategy, owing to the fact that they share principal driving factors of cost and performance. However, within the same division, duty or load cycles can differ wildly. For instance in the MD division a fork-lift truck will spend a lot of its time at low load idle, whereas an excavator can spend much of it operation at loads above 75%. Additionally, agricultural tractors and back-hoes stem from the same origins and have engines of similar displacement and power, yet both experience very different duty cycles in regard to engine speed and torque. An agricultural tractor can be expected to spend the majority of its operation in excess of 90% full load, whereas a back-hoe will typically experience long periods of idling interspersed with small periods of high load as the hydraulics are actuated. Duty cycles which demonstrate this for both tractors and back-hoes are included in the appendix of this thesis.

Within the HD division the principal driving factors are fuel economy and robustness, owing to the greater distances HD vehicles are expected to travel in their projected lifespan[1]. Secondary driving factors which may also apply include maintenance and service intervals, driveability and engine refinement.

[1] Vehicle life can be up to 1 million miles for HD vehicle (Lacey, et al., 2012)

1.2. Fuel Injection

With HSDEs, there are two basic fuel injection approaches, indirect and direct injection.

1.2.1. Indirect Injection

Pre-chamber Indirect Injection (IDI) was patented by Prosper L'Orange as early as 1909 (Bosch, 2004). With IDI, the fuel is injected into an auxiliary combustion **pre-chamber**, which is separated from the main combustion chamber by a flow restriction or throat, as is shown in Figure 2. Air displaced by the moving piston is forced through this restriction into the pre-chamber as a highly turbulent flow. Injected fuel in the pre-chamber partially ignites and this forces the hot burning mixture back through the restriction into the main combustion chamber where intensive mixing and further ignition can occur. The benefits of this design are a short ignition delay and a controlled release of energy at a low overall pressure level. This produces a softer combustion with low noise and less mechanical stress on the engine.

Figure 2 - IDI Engine Design (How cars work, n.d.)

A variation of the IDI engine design features a **whirl-chamber** with a throat area opening tangentially into the main combustion chamber. During the piston's compression stroke a strong air vortex is generated in the whirl chamber. Fuel

injected into this swirling air is thoroughly mixed and at the start of combustion the hot air/fuel mixture is forced into the main combustion chamber by way of the throat. Compared with the pre-chamber the whirl-chamber design features a greater throat area which results in lower flow losses and hence greater efficiency.

IDI engines typically operate with very high compression ratios to ensure adequate cold start ability. This is required on account of the energy losses that occur between the pre- and main combustion chambers. On the other hand, as mixing is heavily assisted by turbulence, IDI engines generally operate with a relatively low fuel injection pressure.

1.2.2. Direct Injection

The more modern approach to diesel engine design is Direct Injection (DI), as illustrated in Figure 3. In a DI engine the fuel injector is mounted directly into the main combustion chamber and injects the fuel into the cavity formed between the cylinder head and the piston at Top Dead Centre (TDC). Unlike IDI, DI engines do not feature the aforementioned energy losses that occur between the pre- (or whirl) chamber and main combustion chamber. This generally results in a 5-10% increase in overall engine efficiency over IDI engines.

Unlike IDI, DI requires that the injection pressure provide the kinetic energy for fuel atomisation, evaporation, mixing and combustion to occur in rapid succession. For this reason substantially higher injection pressures are required than for IDI.

Figure 3 - DI Engine Design (How cars work, n.d.)

With DI there are two mixing methods adopted;

1. **Air-distribution method**. In order to ensure rapid mixing the fuel is distributed uniformly in the combustion chamber. Atomisation is achieved by means of small spray-hole diameters which necessitate very high injection pressures to deliver the required quantity of fuel within a very short injection duration. This is the method usually adopted by HSDEs.
2. **Wall distribution method** or M-system (Heywood, 1988). This method has only been included in this thesis for completeness as it is mostly used in large stationary or marine diesel engines. With a substantially lower injection pressure than the air-distribution method, the injected fuel is deposited upon the combustion chamber walls where it evaporates and is picked up by the air motion inside the cylinder. With correctly manipulated cylinder air motion, extremely homogeneous air/fuel mixtures can be obtained with long combustion durations to provide a relatively quiet combustion.

1.2.3. Evolution of the Fuel Injection Equipment

The biggest difficulty facing early diesel engine designers was obtaining the high pressures necessary for high levels of engine efficiency. This is in regard to:

1. The peak cylinder compression pressure created by the piston to create enough heat to allow the injected fuel to auto-ignite.
2. The pressure at which the fuel is injected into the cylinder to ensure good atomization and hence efficient combustion.

Both peak cylinder and fuel injection pressures were initially limited by a lack of metallurgical knowledge and poor manufacturing tolerances which have obviously improved over time. Similar to Rudolf Diesel's original design, early engines featured an air-blast fuel injection system that used compressed air to force the fuel through a nozzle into the engine cylinder. This was a necessity due to the lack of a high-pressure pump to enable atomisation of liquid fuel to promote good fuel-air mixing.

The general development of the diesel engine saw air-blast injection soon replaced with a mechanical high-pressure pump called the **Jerk pump,** named due to the sudden loss of line pressure once injection has begun. This saw the arrival of the Pump-Line-Nozzle (PLN - sometimes referred to as Pump-Pipe-Nozzle) FIE system with injection being initiated by a pressure wave sent from the pump and injection timing dictated by the pump's camshaft. Control over the quantity of injected fuel (or delivery) was controlled by a number of methods ranging from mechanically varying the pumping stroke, throttling the fuel arriving into or spilling the fuel leaving the pumping chamber. With a single pumping element per engine cylinder and owing to these pumping elements being arranged in series, the jerk pump is also referred to as an **Inline pump.**

Jerk or inline pumps are still found mostly on large, medium-speed engines; however, since the 1950's and particularly on smaller diesel engines, they have been largely replaced with the **Rotary** or **Distributor pump.** This is due to rotary pumps being more compact, quieter and lower-cost, with an ability to easily advance their injection timing. Although of greater manufacturing complexity than inline pumps, the reduction in the number of components has meant that Rotary pumps have proved cheaper to manufacture, at least in the developed world where labour costs are high. Being entirely mechanical, the

rotary pump proved to be extremely robust approach with excellent serviceability due to its relatively simple, interchangeable components. In the early 1990s however, it became clear that rotary pumps would need to produce injection pressures greater than currently obtainable for better fuel atomization and more efficient combustion. A limitation with this pump design was that the maximum pressure was limited by the Hertzian contact stress[2] on the nose of the pumping cam (Mardell, 2003). By spilling high-pressure fuel prior to cam TDC this limitation was overcome, thus allowing the latest evolution of this design, the High Pressure Rotary Pump (HPRP) to generate injection pressures in excess of 1000bar. More shall be mentioned of HPRPs later in this thesis.

A different approach to FIE architecture arose in part due to occasional failures with the high pressure pipes connecting the injection pump to the nozzles on PLN systems. With this solution the pump and nozzle were combined in a single component which became simply referred to as a **unit injector**. Although this concept was patented in the early 1900's, it only found commercial acceptance in the 1930's.

1.2.4. Multiple Injection Strategy

In recent years a multiple injection strategy consisting of pilot, post and split-main injections has arisen to not only reduce exhaust emissions but provide Noise Vibration Harshness (NVH) refinement and increased performance whilst maintaining the fuel economy advantage of a diesel engine. The multiple injections are each precisely timed in order to improve fuel-air mixing and achieve combustion under conditions that do not favour pollutant formation. With enhanced fuel atomisation and vaporisation, a more homogeneous fuel-air mixture can be created within the engine cylinder whilst maintaining combustion at temperatures lower than ~2300K to limit the formation of Nitrogen Oxides (NO_x) (Kontoulis, et al., 2008). A multiple injection strategy consists of the following:

A **pilot injection** injects a small part of the required fuel delivery[3] into the combustion chamber to ignite before the main injection. This has the effect of

[2] Hertzian contact stress is the localised stresses that develop between two curved surfaces that come into contact and deform slightly under the imposed loads.
[3] A pilot injection on a LD engine may contain as little as 0.5mm³ of fuel (Schoppe, et al., 2008)

shortening the period before the main injection undergoes combustion, whilst providing a controlled combustion heat release and associated pressure rise to minimise noise and NO_x formation.

A **post injection** is a small injection after the main and much later in the expansion process where the combustion charge is at a lower temperature in order to reduce particulate matter (PM) or smoke emissions.

A **split-main injection** is used to separate the fuel rich regions within the engine cylinder where PM is formed thus allowing increased oxidation to occur to reduce PM emissions. With modern fast-acting injectors, a secondary injection can occur directly after a main injection whilst combustion is still taking place, allowing PM to be reduced by as much as 70%. An example of a split main with 3 pilot and 2 post injections is shown in the bottom image of Figure 4.

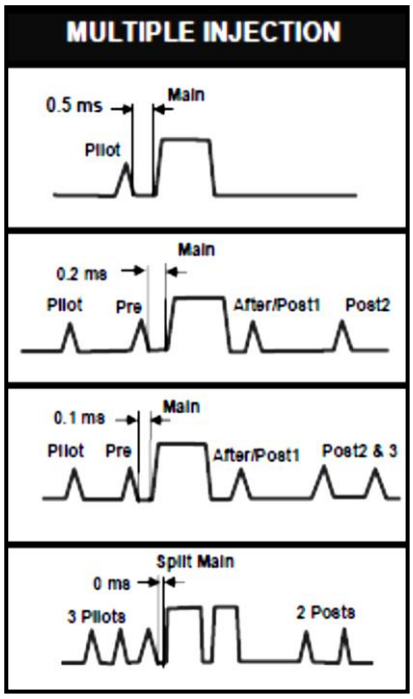

Figure 4 - Multiple Injection Strategies (Delphi, 2012)

1.2.5. Injection Rate Shaping

Additional to having a multiple injection strategy, the injection rate profile has been recognised as a key factor in minimising pollutant formation. By tailoring different injection strategies throughout the entire engine map, it is possible to adapt the mixture preparation and rate of heat release rise for optimal trade-off

between PM formation and combustion noise. Figure 5 is an example of a boot-shaped main injection (alongside twin pilots and a post injection), with a low initial rising rate of pressure to reduce NO_x emissions and combustion noise yet a sudden high pressure end-of-injection to minimise PM formation.

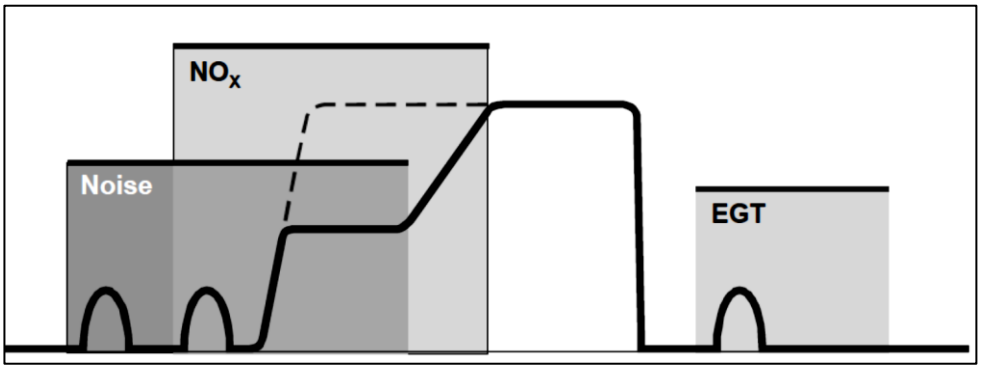

Figure 5 - Boot-shaped Main Injection Profile (Mahn B., 2002)

1.2.6. Recent & Future FIE Trends

To keep pace with the ever-increasing demands placed upon the diesel engine, it has been necessary to continually develop and optimise the FIE. Recent increases in engine power density have resulted in higher peak cylinder pressures and temperatures, to which the injector nozzle tip is directly exposed. This higher power rating has also required that the FIE operate more frequently and at a higher injection pressure to ensure that fuel atomisation and combustion occur in even shorter durations. To prevent leakage at these higher injection pressures, closer manufacturing tolerances between mating surfaces have been required since the pressures used are beyond the capability of conventional seals which would likely add undesirable compliance and dead volume to the system (Dingle & Lia, 2005). Additionally it is required that the FIE be designed with the same service life as that of the base engine or vehicle to which it is fitted whilst being able to operate with the range of diesel fuel blends and fluid properties that exist around the world.

Notwithstanding the above, perhaps the most significant driving force in the development and refinement of the HSDE has been the frequent changing and tightening of the emission regulations. This is potentially a huge topic and will be mentioned later on in this thesis.

1.3. Combustion

Due to the fact that within diesel engines the fuel is injected at the end of the compression process (or just prior to TDC); high compression ratios are possible. Compression ratio is directly related to the fuel conversion efficiency ($\eta_{f,i}$) via the expression:

$$\boldsymbol{\eta_{f,i} = 1 - \frac{1}{r_c^{\gamma-1}}}$$

Equation 1

where r_c is the engine's compression ratio and γ is the heat capacity factor. Since diesel fuel contains approximately 15% more energy by volume that petrol, diesel engines typically have 40% better fuel economy and therefore emit 40% less Carbon Dioxide (CO_2) emissions compared to a petrol engine of the same power (Heywood, 1988).

The whole combustion process is actually an extremely complex process that depends on the fuel quality characteristics, the engine's internal geometry, the FIE and the engine's operating condition (rpm and load). In light of this only a general overview shall be given as the intricacies of combustion are considered beyond the scope of this thesis.

Mechanism of Compression Ignition

Within a diesel engine, as the piston approaches the end of its stroke towards top dead centre (TDC), the injector's needle valve lifts off its seat allowing fuel to pass through the injection holes and enter the engine cylinder. The process then occurs in the following four stages:

1. **Fuel atomization.** Ideally entering as a high velocity liquid jet, the fuel is atomized into small droplets through the mechanisms of cavitation and aerodynamic shear as it encounters the dense hot air within the engine cylinder.
2. **Fuel vaporisation**. The small droplets of fuel mix with the hot cylinder gases and vaporise.
3. **Fuel-air mixing**. Vaporised fuel and air interact to create regions of mixed fuel and air.

4. **Combustion**. Small pockets of mixed fuel and air undergo spontaneous combustion which has the effect of further increasing the cylinder pressure. This further compresses the unburned portion of the injected fuel and shortens the delay before the remainder of the fuel underdoes ignition.

The delay between stage 1 or start of injection (SOI) and start of combustion (SOC) at stage 4 is referred to the 'ignition delay' and this is known to be strongly dependent on the instantaneous cylinder compression temperature at the point of injection (Gilkin, 1985). The ignition delay is known to affect the pattern of burning and the resulting heat release, which in turn has a significant effect on the combustion noise and production of exhaust emissions. Generally speaking the SOI is taken as being the time when the needle valve lifts off its seat. The SOC is best identified from the change in the slope of the heat release rate graph; however, this is typically detectable on the cylinder pressure trace. Figure 6 is an experimental trace from a Ricardo Proteus single-cylinder engine, consisting of cylinder pressure, injection rate, injection pressure, and needle lift data for a HD injector at 1550rpm and 50% load. The SOI, SOC and ignition delay have all been identified.

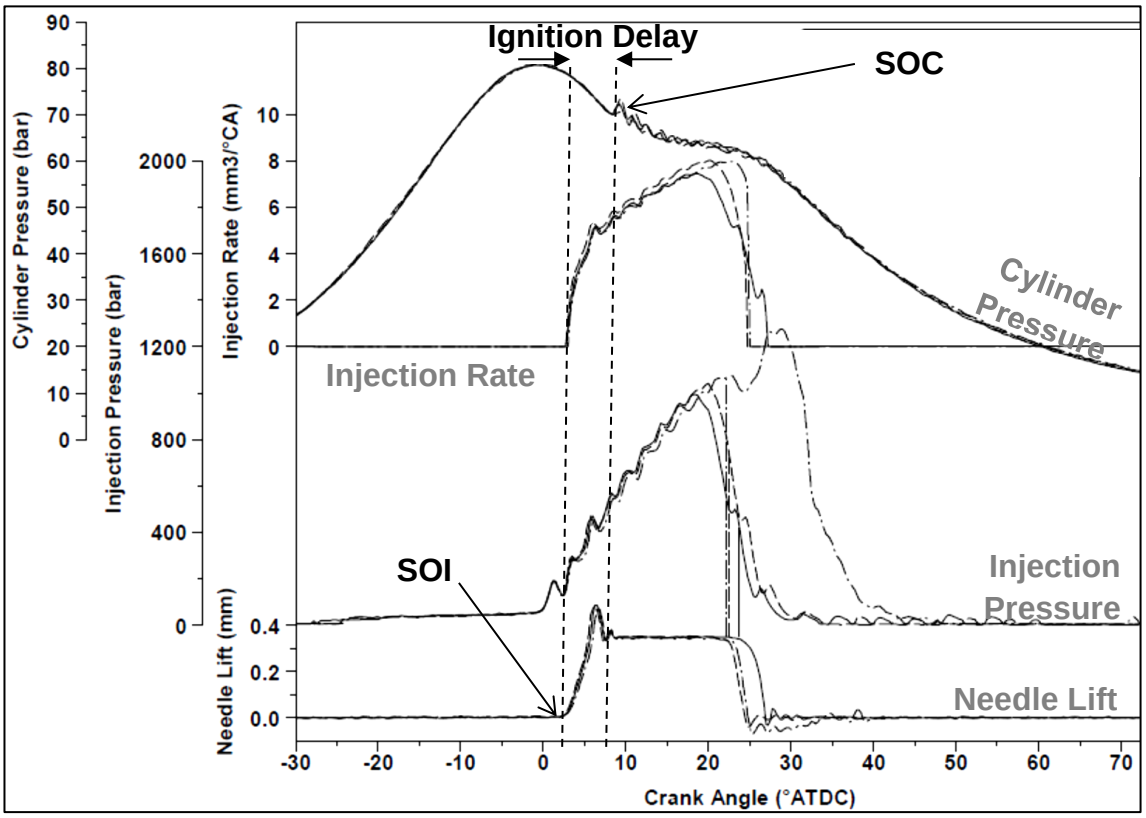

Figure 6 - Two-actuator EUI single-cylinder engine data (Greeves, et al., 2003)

1.3.1. Main Combustion Products

When diesel fuel undergoes combustion, a variety of combustion products are formed depending upon the engine design, power output and working load. These include in no particular order, Nitrogen Oxides (NO_x), Particulate Matter (PM), Carbon Dioxide (CO_2), Carbon Monoxide (CO), Un-burnt Hydrocarbon (UBHC) and Sulphur. Although CO and UBHC are considered toxic, these can be limited by maximising fuel combustion and the adoption of a diesel oxidation catalyst (as complete combustion of all the fuel is very difficult due to crevice losses[4] etc.).

Nitrogen Oxide (NO_X)

NO_X formation occurs through an endothermic reaction between excess Oxygen and Nitrogen (present in the inducted air and to a lesser extent within the fuel) creating either Nitrogen Oxide (NO) or Nitrogen Dioxide (NO_2). NO may oxidise to NO_2 or form nitric acid, which has been attributed as being a leading cause of acid rain. NO_2 is toxic by inhalation and has been linked to an increased risk of respiratory ailments.

Particulate Matter (PM)

PM is the product of incomplete combustion at fuel rich regions within the engine cylinder. It has been reported that about 0.2 and 0.5% of the injected fuel mass is emitted as small particles which consist primarily of soot with some additional absorbed hydrocarbon material (Heywood, 1988); however, this is from an old source and likely to be very specific to (older) FIE architecture. Typically PM consists of clusters of small spheres with a diameter ranging between 15 and 30nm (Heywood, 1988) which are readily inhaled into the lungs being too small to be removed by the body's natural defences. Not only has there been evidence linking the inhalation of PM to respiratory diseases such as asthma, but PM is now reasonably anticipated as being a human carcinogen, based on limited evidence of carcinogenicity from studies in humans and supporting evidence from trials on experimental animals and mechanistic studies (National Toxicology Program, Department of Health and Human Sciences, 2011).

[4] Small volumes with narrow entrances - into which the flame is unable to penetrate, have been shown to be a major source of UBHC, the largest being the volumes between the piston, piston rings and cylinder wall (Heywood, 1988).

Carbon Dioxide (CO_2)

Presently within the European Union, road transportation is responsible for about 20% of all CO_2 emissions with 12% being attributed to passenger cars alone (European Union, 2012). Due to this, in Europe and around the world, a shift is occurring to force engine manufacturers to strive to minimise these CO_2 emissions. In fact the end consumer is now increasingly aware of the direct link between CO_2 emissions and fuel economy with this data regularly being used for marketing purposes as an indication of how efficient or 'green' a vehicle is.

Sulphur (S)

Sulphur contained within Diesel fuel is oxidised or burned within the engine cylinder to form Sulphur dioxide of which a fraction my further oxidise to form Sulphur trioxide which then combines with water to form a Sulphuric acid aerosol. As sulphur is known to deteriorate exhaust after-treatment performance, the fuel is usually processed to remove almost all of the Sulphur at the refining stage. In 2000 the European standard for diesel fuel was a Sulphur content of ≤300ppm, yet by 2009 this had fallen drastically to ≤10ppm. This is referred to as Ultra-low-sulphur-diesel (ULSD) and this trend is being reflected to varying degrees around the world.

1.3.2. Lesser combustion products

Coking is the term given to combustion products which are deposited within the holes and on the outside of the fuel injector nozzle tip. Coking deposits commonly consist of carbon and oxygen and are formed from components within the fuel and engine lubricant in the presence of zinc which is thought to act as a catalyst. Within the injection holes this is problematic as any reduction in the hole cross-sectional area could potentially change the injection characteristics and deteriorate the combustion efficiency leading to increases in fuel consumption and exhaust emissions. This effect has perhaps become more pronounced in recent years with smaller injection holes which are more sensitive to deposit formation as they will result in a proportionately greater reduction in hole flow area. Cavitation within the hole is thought to be effective at dislodging and even preventing injection hole coking; however, the recent increase in tapered holes with smooth honed entries, has resulted in the reduction or even elimination of in-hole cavitation. Additionally, the higher

nozzle tip temperatures which have accompanied engine downsizing are further known to promote coking deposit build-up (Tang, et al., 2009).

Internal Injector Deposits (IIDs) can form either inside the nozzle or within the injector body. These deposits can inhibit the performance of the fuel injector or even cause sticking of moving internal parts, which may result in loss of control over injection timing and injection quantity (Quigley, et al., 2011). Higher injection pressures significantly increase the fuel operating temperature and with modern injection pressures within the 2000 to 3000 bar range, peak fuel temperatures are likely to exceed 150 °C, with nozzle tip temperatures being appreciably higher still. At locations of rapid pressure drop, such as at the needle seat or across the control valve, localised temperature rises occur in the fuel before the heat can be dissipated into the surrounding metal. These locations all tend to contain close fitting and moving components which are potentially affected by IID accumulation.

Two broad categories of IID exist:

1. Relatively soft metal soaps which tend to be water soluble
2. Hard Poly-metric lacquers that are impervious to most solvents

The mechanism of IID formation is likely to be different to those observed in nozzle coking, since there is no possibility of exposure to combustion gases or evaporation of fuel from the wetted surface. Within the nozzle tip, after an injection, any remaining fuel is heated during combustion and is expanded during the power stroke. It is a combination of degradation and evaporation of lighter fractions within the fuel which is thought to lead to sticky deposits or lacquers forming at this location.

IID's are being reported by most major FIE and Original Equipment Manufacturers (OEMs) yet occur sporadically in specific geographical areas, indicating a close relationship to fuel and additive composition. In developing markets, IID's have occasionally been observed in higher sulphur fuels, typically in combination with traces of copper which is thought to act as a catalyst. In Europe however, soap deposits have been observed with ULSD fuel but this is generally thought to be due to sodium present in additives such as lubrication enhancers or corrosion inhibitors. In fact sodium has been found as being present in approximately 75% of analysed IIDs (Lacey, et al., 2012).

1.3.3. Fuel Distribution

The fuel distribution within the cylinder of a diesel engine is of utmost importance to the combustion process. Unlike a traditional spark ignition engine, the fuel is injected into the cylinder just before the start of combustion. Therefore the fuel distribution which is critical to pollutant formation, is provided by the FIE and the interaction of the injected fuel with the in-cylinder air motion, be it swirl or squish. If high temperatures exist in fuel-lean regions of the cylinder, the amount of NO_x formed increases, whereas if high temperatures exist in fuel-rich regions, PM formation occurs. Unfortunately this produces a balancing act where factors that reduce PM have the opposite effect on NO_x. Figure 7 illustrates this and is well known within the automotive industry as the NO_x/PM trade-off.

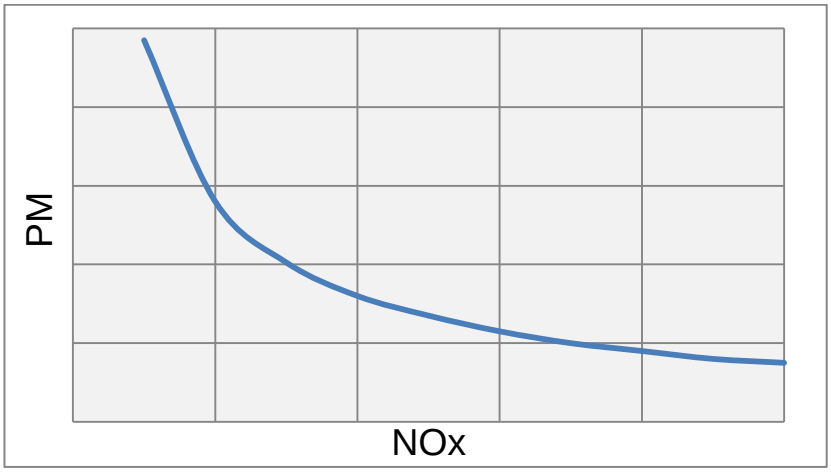

Figure 7 - NO_x / PM Trade Off

Injector Orientation

In order to improve air utilisation and volumetric efficiency, engine designers have adopted the four-valve per cylinder configuration which has had the drawback of limiting the space available for the fuel injector. To overcome this and provide the best arrangement for uniform spray distribution and penetration, a centrally mounted multi-hole injector at the centre of the combustion bowl has become the standard arrangement (Mardell, 2003). In light of this, unless otherwise stated any referencing of injector positioning in this thesis shall refer to an axially centred injector.

1.4. Fuel Quality

Significant variations in fuel quality exist around the world yet it is a requirement that the FIE operates within its specifications whilst running on a range of different diesel fuel blends. There are 5 key parameters used to measure and compare fuel quality, Cetane number, density, lubricity, cold flow properties and sulphur content. Sulphur content has already been covered but Cetane number and lubricity shall be expounded upon here.

Cetane number is a dimensionless parameter used to measure a fuel's ignition characteristics. For road vehicles in the EU, the Cetane number is legally required to be between 52 and 54, between 40 and 50 in the US and in Japan it has to be above 45. Therefore a vehicle designed to operate on EU diesel fuel may experience poor starting particularly in cold conditions when running on diesel fuel in the US or to a lesser extent Japan. Therefore worldwide fuel variability has to be taken into account when designing and validating diesel FIE.

Lubricity is very important to the robustness of the FIE as with most LD and MD systems the diesel fuel provides sole lubrication for the moving components within the pump and the fuel injector. If the lubricity of the fuel is too low increased wear will occur potentially leading to failure. Even if this wear does not lead to component failure any removed material will remain within the fuel system and may potentially lead to a blockage of the injection holes leading to increased emissions and fuel consumption. To protect against poor fuel lubricity it is sometimes common in HD applications for the FIE to be separately lubricated by the engine oil circuit.

1.4.1. Calibration Oil

In order to ensure repeatability during FIE testing and validation, it is essential to use high quality fuel. For this reason a standardised fluid for the testing and calibration of diesel FIE is used. This is referred to as calibration oil or ISO4113. Unlike regular diesel fuel which may see significant variation in fluid properties between different regions and manufacturers, calibration oil has close tolerance ranges for kinematic viscosity and density. Additionally for health and safety reasons, calibration oil has a much

reduced flammability[5] and odour. The spec sheet for ISO4113 has been included in the appendix of this thesis.

1.5. Emission Standards

Automotive emission standards which vary depending on vehicle class and/or size have been introduced to set specific limits on the amount of pollutants that can be released into the environment. The following sections with focus on the European exhaust emission standards but will also encompass the other major regional emission standards from Japan and the United States of America.

1.5.1. European Exhaust Emission Standards

European emission standards define acceptable limits for the exhaust emissions of new vehicles sold within the European Union (EU). These standards are a progressive series of increasingly stringent limits prefixed with the term Euro. For HD vehicles these standards use Roman numerals, whereas the standards for LD and MD vehicles use Arabic numerals.

The regulations are quite complicated and differ depending not only on the vehicle class but also Gross Vehicle Weight (GVW) and load carrying ability or Reference Weight (RW). Additionally for passenger vehicles, the emission standards are defined in terms of mg/km, however, for HD vehicles they are defined in terms of mg/kWh which complicates any direct comparison between different vehicle classes. Furthermore, vehicles and engines have to conform to these emission standards for what is regarded as a normal life of the engine or vehicle. For passenger cars and light commercial vehicles this is a period of 5 years or 100,000 km. For buses, coaches and Large Goods Vehicles (LGV) this can be 200,000 km or 6 years and 500,000 km or 7 years for the very biggest LGVs (Delphi, 2011). A complete review of the European emission standards is considered beyond the scope of this thesis; however, a table summarizing the Euro 5 & Euro V standards for a range of different vehicle classes has been included in the appendix.

Over the past two decades the Euro emission regulations have been successively tightened and in the future will continue to be so with the introduction of Euro 6 and 7. The successive tightening of the LD and MD

[5] For combustion testing of FIE, standard diesel fuel is used

emission standards up to Euro 6 is summarized in the text below with any reference to actual values referring to those for passenger cars and light commercial vehicles less than 1305 kg, GVW.

Euro 1

The first emission standards to define acceptable limits for exhaust emissions for new passenger cars sold in EU member states were introduced in 1993. These were denoted as Euro 1 and identified acceptable limits for exhaust emissions of CO, PM and also UBHC, defined in terms of milligrams emitted per Kilometre (g/km). The PM limit only applied to diesel engines. In 1994 additional categories were introduced with differing limits for light commercial vehicles depending on GVW. These vehicle categories are class 1 (<1305 kg), class 2 (>1305 kg to 1760 kg) and class 3 (>1761 kg to 3500 kg).

Euro 2

The introduction of Euro 2 in 1996 saw the introduction of different emission limits for diesel and petrol engines with diesel engines having more stringent CO standards but a higher allowance for NO_X emissions.

Euro 3 & 4

Euro 3 and Euro 4 were introduced in 2000 and 2005 respectively and are generally regarded as the being the start of a successive trend towards greater reductions of NO_X and PM in diesel engines.

Euro 5

Euro 5 was introduced in October 2009 for new car models but existing models were allowed until January 2011 to comply. Euro 5 saw a further tightening of the emission restrictions, for example the regulations for diesel engines require an 80% reduction in PM (5 mg/km, down from the Euro 4 limit of 25 mg/km) and a 28% reduction in NO_X (180 mg/km, down from 250 mg/km). In light of this it is expected that diesel vehicles need to be equipped with a particulate filter to meet this PM reduction. Unlike previous standards, Euro 5 also sees the introduction of a PM limit for DI spark ignition engines too.

Euro 6

Expected in 2014, the Euro 6 regulations will impose a further 10% reduction in PM (to 0.0045 g/km) and a 56% reduction in NO_X (to 0.08 g/km) over the Euro 5 limits. For both diesel and petrol engines the limits for CO have remained unchanged since the Euro 4 limits. It is expected that diesel vehicles will require exhaust gas after-treatment to achieve these NO_X reduction targets.

Tightening Euro European Emissions

Figure 8 is a graphical illustration of the reduction that has occurred to both PM and NO_X emission limits between the introduction of Euro 1 and Euro 6 for passenger cars and class 1 light commercial vehicles.

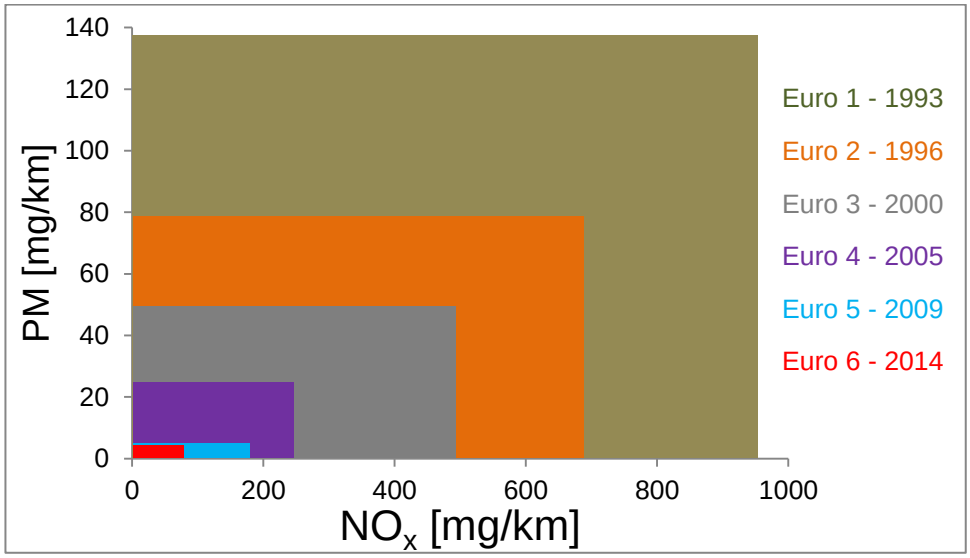

Figure 8 - Tightening LD emission legislations

1.5.2. Worldwide Exhaust Emission Standards

Whilst other regional standards exist, Japan and the US are the other two main counties which dictate automotive emission regulations.

1. Japan introduced emission standards for on-road vehicles in the late 1980's; however, these remained relaxed throughout the 1990's. More recently the Ministry of the Environment has adopted very stringent emission standards similar to the European and US requirements. In addition, 'The Motor Vehicle NO_x Law' was introduced to reduce Nitrogen oxide pollution in highly populated metropolitan areas. This has forced the replacement of older more polluting vehicles with newer cleaner ones and in some cases the retrofit of approved NO_x and PM control devices to used vehicles.
2. In the United States the emission standards are managed by the Environmental Protection Agency. These standards are known as 'Tiers' and unlike Tier I which classified vehicles on GVW, for passenger cars and light commercial vehicles, Tier II classified vehicles into initially

eleven certification bins, with bin 1 being the cleanest and bin 11 the most polluting. Naturally a different series of tiers applies to HD vehicles which for non-road diesel engines are currently at Tier III. A different system is adopted in the state of California which has special dispensation to put forward even more stringent vehicle emission regulations by way of the California Air Resources Board (CARB). US states are able to adopt either regulation.

1.5.3. Exhaust After-Treatment

The usual methodology is to exploit the FIE's capabilities to the fullest. This is because the cost-to-benefit ratio has almost always favoured minimising engine-out emissions with advanced FIE, rather than requiring expensive exhaust after-treatment from a less than capable FIE. Additionally, FIE sophistication has tended to bring further benefits such as reduced noise or NVH that the consumer is prepared to pay for, whereas exhaust after-treatment provides few consumer-perceived benefits and a likely fuel consumption penalty (Dingle & Lia, 2005). More recently it has become increasingly difficult for diesel engines to satisfy stringent exhaust emission standards, and unlike petrol engines the excess oxygen in the exhaust gas prevents the use of well-established stoichiometric 'three-way catalyst' technology (Lüders, et al., 1995). In light of this, a number of after-treatments technologies have had to be incorporated alongside advanced FIE for a diesel engine to achieve the emissions levels of a petrol engine.

The following are some examples of after-treatment technologies:

1. **Exhaust Gas Recirculation** (EGR) is not technically after-treatment but has been included here for completeness. EGR reintroduces a proportion of cooled exhaust gas into the combustion charge to reduce the excess quantity of oxygen present during part-load operation. The higher specific heat capacity of cooled exhaust gases when compared to air also helps to reduce the combustion charge temperature. A reduction in combustion charge temperature combined with a reduced oxygen concentration has the effect of minimising NO_x formation. It is important to accurately control EGR when engine load varies, as excessive

quantities in the combustion charge may result in increased UBHC and PM.

2. **Selective Catalytic Reduction** (SCR) usually involves the injection of a liquid urea or Ammonia solution into the hot exhaust flow. In the presence of a catalyst the NO_x is reduced forming N_2, H_2O and CO_2. This technology along with Selective Non-Catalytic Reduction (SNCR) was pioneered for stationary and heavy-duty applications but is only recently being customised for LD vehicle applications. Due to its relative size and weight, a vehicle fitted with an SCR system may expect to occur a <1.5% fuel economy penalty (Brogan, 2011). Solid state SCR systems are also being developed and benefit by having longer service intervals between reductant replacement compared to liquid systems and without the need for costly heated tanks and supply lines.
3. **Lean NO_x Trap** (LNT) is an alternative to SCR. A LNT contains three active components, an oxidation catalyst such as Platinum, an absorbent such as Barium and a reduction catalyst such as Rhodium. The absorbers chemically bind NO_x until they become saturated, at which point the system is regenerated by a period of rich engine operation allowing the NO_x to be reduced to nitrogen. This need for periodic regeneration and an increase in the exhaust back pressure is unfortunately thought to incur a 1.5 - 3% fuel economy penalty (Brogan, 2011). As the engine size and hence quantity of NO_x to be converted is increased, the cost of an LNT escalates as its volume needs increasing along with the quantity of precious metals contained within. Concerns with 'sulphur poisoning' of the LNT has contributed to the introduction of ULSD fuel.
4. **Diesel Oxidation catalyst.** Excess oxygen in the exhaust gas is used to oxidise CO and UBHC to CO_2 and H_2O in the presence of a catalyst. The catalyst provides a large surface area for the reaction to occur and is typically a noble metal, such as Platinum, Palladium or Rhodium (Bosch, 2004).
5. A **Diesel Particulate Filter** (DPF) is used to trap significant quantities of PM from the exhaust gases. By forcing exhaust gases to flow through a porous ceramic honeycomb structure, PM in the exhaust gases is deposited on the structures walls. Periodic regeneration is required

typically every 500km (Bosch, 2004) to remove these collected particulates which if unchecked would increase engine backpressure and in extreme cases lead to engine damage. Regeneration may be carried out by injecting fuel late in the expansion or power stroke so that the fuel will not undergo combustion but will evaporate and be forced out of the cylinder during the exhaust stroke. Oxidation of this evaporated fuel within the oxidation catalyst can sufficiently increase the exhaust gas temperature to allow trapped particulate matter to reach combustible temperatures to regenerate the DPF.

Engine and FIE manufactures may decide to adopt a certain specific after-treatment strategy. For Instance Ford Europe for Euro 6 LD applications believe that LNT's are better suited to small vehicles whereas SCR is better suited for larger vehicles. This is primarily due to the larger initial cost and size of an SCR system compared to a small volume LNT for a small vehicle (Brogan, 2011). It is generally considered that in order to satisfy Euro 5 regulations, DPFs were necessary but not NO_X after-treatment systems. However, to meet Euro 6 regulations NO_X after-treatment will also be needed at least on heavier vehicles, although this can deliver fuel consumption benefits by running at a higher NO_X forming level (Johnson, 2008). Cost of course is an issue as this remains one of the principal driving factors within the LD division.

1.5.4. FIE After-Treatment Approaches

Higher injection pressures may be used as a means to reduce the quantity of PM formation by improving the fuel/air mixing process. To suppress NO_X, high levels of cooled EGR may be used to reduce the quantity and temperature of excess oxygen present within the engine cylinder. A high level of EGR leads to increased PM formation which results in a requirement for even higher injection pressures. SCR after-treatment to reduce NO_X emissions can allow engines to operate with lower levels of EGR and hence produce lower quantities of PM. Unfortunately on a LD vehicle there is a reasonable limit to the quantity of SCR reductant, either liquid or solid state that can be carried and hence the consumption rate dictates that a minimum amount of EGR will always be required.

With future emission standards likely to even further reduce NO_X and PM emission limits, it is expected that a combination of high injection pressures, SCR (or LNT), EGR and a DPF will be required for Euro 7, if not for Euro 6. Although lean-burning gasoline direct injection is beginning to require after-treatment additional to the traditional 3-way catalyst, the extra cost of these after-treatment devices may likely offset the fuel-economy and hence financial gain that may be expected with choosing a diesel over a petrol engine vehicle.

1.6. Modern Fuel Injection Strategies

Four distinct fuel injection strategies have emerged to meet the requirements of the HSDE. In chronological order of their development, they are:

1. High Pressure Rotary Pumps
2. Electronic Unit Injectors
3. Common Rail systems
4. Hybrid FIE systems

1.6.1. High Pressure Rotary Pumps

Rotary Pump Design

With the rotary pump design, a single pumping element is capable of delivering the fuel to all the engine cylinders. This pumping element incorporates a plunger which is made to describe a combined rotary and stroke movement by a rotating eccentric disc or cam plate. For distributing the fuel, a single inlet and outlet port, each connected to an engine cylinder, are exposed to the pressurised fuel in the firing order of the engine (Heywood, 1988).

In the past fifty years the High Pressure Rotary Pump (HPRP) has undergone continual development and optimisation being not only responsible for generation of the fuel injection pressure but also for control over injection timing and fuel delivery. HPRPs are also able to operate at the speeds necessary for greater power density which is a necessity within the automotive sector. This higher speed rating, a proven robustness of the design and the fact that they are readily packaged on an engine, has meant that HPRP became the standard

choice for PLN systems on LD vehicles. Whereas historically, fuel metering and injection timing was solely mechanically controlled, the introduction of electronic control allowed greater precision over the injected fuel quantity and injection timing in order to meet increasingly stringent emission legislations. An example of this is the Lucas EPIC (Electronically Programmed Injection Control) HPRP introduced in 1991, Figure 9.

Figure 9 - Rotary Injection Pump (Lucas EPIC)

In the past decade PLN systems have in automotive applications been largely replaced by Common Rail (CR) and now only really remain an option for simple, low-cost installations or where emission standards are much more lenient. Prior to the emergence of CR systems, HPRPs seemed to have a promising future within the automotive sector due to their sophisticated control mechanisms and being able to operate at high speeds and loads. In fact their designers and developers even believed it would be possible to improve HPRPs to satisfy increasingly stringent emissions standards. This however, would have necessitated additional electronic control hardware to be integrated into a largely mechanical pump, which was likely to prove costly and therefore made the HPRP less attractive against its CR rival. This was further compounded by customer demands for the more ‘fashionable’ CR system and a large reduction in both PM and NO_X required with the introduction of Euro 4 in 2005, which would have necessitated a significant financial investment to develop HPRPs to meet these new standards.

Features of High Pressure Rotary Pumps

1. With a relative lack of complexity and being a mature technology that has been continually developed by a number of manufacturers over more than a 50-year period, HPRPs as part of a PLN system can provide a low-cost, reliable fuel injection system. Coupled with excellent serviceability and versatility of application, HPRPs have been employed on such equipment ranging from small electrical generators to large agricultural and construction vehicles. More recently, stringent exhaust emission legislation may have limited their application but they are still being used in automotive applications were these standards are lower, particularly in the developing world.
2. Being camshaft driven, the injection rate and pressure is dependent on engine speed and the HPRP's cam profile
3. PLN systems have limited pilot and post injection capabilities. This is due to the compressibility of the fuel, such that the high pressure pipes between the pump and injector modify the initial pressure wave causing pressure appreciation and wave front bunching (Mardell, 2003). This creates two detrimental effects.
    a. Firstly, the shape of the rate of injection diagram is changed so that the rate of injection at the injector nozzle is less than the rate of pump plunger displacement.
    b. Secondly, the start of injection is delayed relative to the events at the pump. Both of these are a function of pump speed and become more pronounced as the speed is increased. This makes it difficult for a PLN system to ensure consistent behaviour over a wide engine operational speed range.

1.6.2. Electronic Unit Injectors

The design of an Electronic Unit Injector (EUI) is very similar to that of a Mechanical Unit Injector (MUI) having the injector and pumping unit combined in a single component. Unlike a MUI, a EUI incorporates an electronically controlled spill valve allowing fine control over injection quantity and duration.

Figure 10 is a cross-section of a EUI showing the pressurised fuel circuit in Red. When the rocker arm (operated by an auxiliary cam on the overhead cam-shaft)

drives the pumping plunger, fuel is displaced into the feed hole. With the spill valve normally open, the displaced fuel is allowed to drain. To initiate injection the solenoid is energised, thus closing the spill valve and pressurising the fuel contained below the plunger. When the pressure in this pressurised circuit is sufficient to overcome the nozzle opening pressure (NOP) fuel injection occurs. Injection is terminated by de-energising the solenoid, thus opening the spill valve and reducing the pressure in the pressurised circuit below that of the NOP.

Figure 10 - EUI cross-section

Similar in design to a EUI is the Electronic Unit Pump (EUP), derived from the Mechanical Unit Pump (MUP). In many ways the EUP is similar to a PLN system where the pump is separated from the injector by a high-pressure pipe. This arrangement provides a modular high-pressure injection system which is suitable for a wide range of different system installations, particularly suitable for small displacement engines that do not feature an overhead camshaft.

Features of Electronic Unit Injectors

1. Being engine camshaft driven, the injection rate and pressure is dependent on cam profile and engine speed. However, with EUI's under normal operation this constraint is normally not a problem as injection and combustion always fall within a few crankshaft degrees of TDC.

2. The location at the EUI at the top of the engine makes it difficult to shield the vehicle interior from the mechanical noise or 'clatter' between the rocker arm and the pumping plunger.
3. Packaging is often an issue when trying to accommodate the EUI with the usual four valves per cylinder found in a modern HSDEs.
4. Having a small high-pressure volume ensures a high hydraulic efficiency in contrast to a large volume where every time fuel is injected this volume would be pressurised and depressurised resulting in large compressive losses (Bosch, 2004). This high efficiency allows EUIs to easily generate peak injection pressures in excess of 2500Bar. This is necessary within the HD division as the almost quiescent cylinder nature required for high levels of efficiency requires that the injection pressure provide the energy for fuel-air mixing.
5. The aforementioned small hydraulic volume also provides a responsive performance that is generally free from reflected pressure waves which are known to interfere with delivery and injection timing on PLN systems (Knight, 1960).

Towards the end of the 1990's, light duty EUIs were successfully introduced by Bosch for Volkswagen and Lucas for the Land Rover TD-5 engine. However, these have both been superseded by CR systems and currently no known manufacturers offer LD vehicles with EUIs, although they remain the most common FIE approach for HD vehicles which typically feature engines of capacity between 1.5 and 2.6 litres per cylinder.

1.6.3. Common Rail Systems

A principal factor in CR development has been the desire to create a fuel injection system where the injection pressure remains constant throughout an injection to provide a more accurate fuel delivery quantity. A simple method of providing this constant pressure was through pressurizing a large volume of fluid.

Common Rail Development

In 1913 Vickers Ltd. first produced a primitive CR system. Their design comprised a large capacity accumulator and header tank with the fuel pressure maintained at approx. 350Bar and the injectors mechanically actuated by pushrods. Rather unbelievably as early as 1933, the Atlas-Imperial Diesel Engine Company produced a similar system but replaced the mechanical actuation of the injectors with solenoid control (DeLuca, n.d.). Another example is the Helios system developed by Lucas Diesel Systems in the early 1980's for research purposes which utilised piezoelectric actuators to operate relatively heavy hydraulic control valves. Considerable energy was consumed with the operation of these control valves and for this reason there was little chance of reaching affordable production costs. Whilst vehicle manufacturers such as Renault and Iveco actively pursued the development of a CR system, it was Fiat who developed the first production system. Following their success from introducing the first passenger car with a turbocharged DI diesel engine in 1986, Fiat began to assess the feasibility of a CR system. Following development and testing in the late 1980's and early 1990's, the system, named UNIJET, was licensed in 1994 to Bosch for industrialisation and further development (Knecht, 2004). This led in 1997 to the first production CR passenger car, the Alfa Romeo 156 JTD, being introduced with two DI diesel engine variants equipped with the Unijet system.

Since CR's introduction, higher injection pressures, reductions in parasitic losses and more elaborate multiple injection strategies have all resulted in even greater fuel economy and reduced exhaust emissions from a diesel engine. However, it is fully expected that further improvements are attainable with a greater understanding of not just the combustion process but also the behaviour of diesel fuel at these high injection pressures.

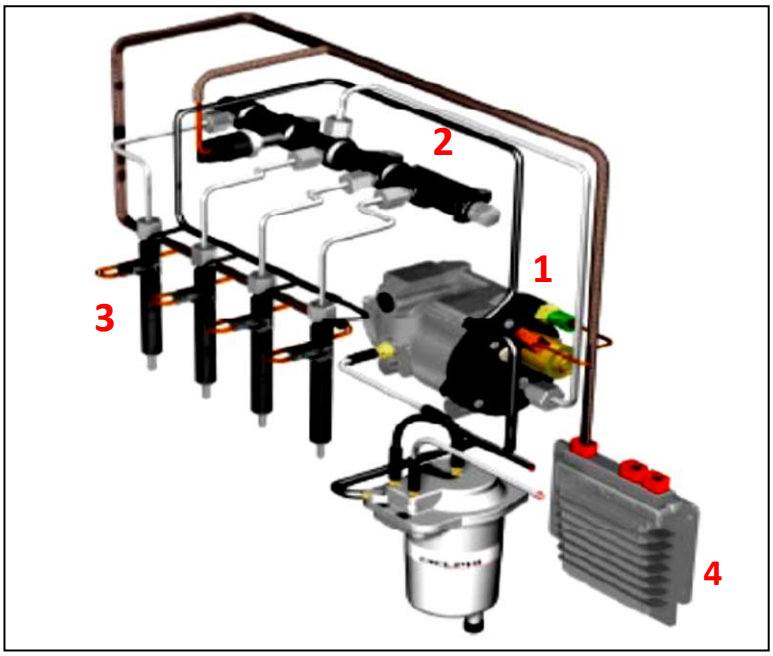

Figure 11 - Delphi's Common Rail system

Common Rail System Components

Figure 11 is a schematic of a Delphi Diesel System's (DDS) Multec CR system. The Key components have been numbered and their purposes are described as follows:

1. High-pressure pump - The purpose of the pump is to ensure that there is always sufficient pressurised fuel for all engine loads.
2. Common rail - The common rail must contain a volume large enough to ensure that during an injection the pressure remains constant, yet be small enough to allow a rapid pressure rise at engine start-up. It has a further purpose of damping out compression waves produced by the pump and decompression waves induced from the start of an injection event. It is common for the rail to contain orifices within each outlet port to damp out the waves.
3. Injectors - The injectors must consistently and accurately meter and inject the correct amount of fuel at the correct injection timing. The operation of a solenoid injector shall be detailed later.
4. Electronic Control Unit (ECU) - The ECU must read and interpret real-time data from sensors located on the engine in order to calculate fuel demand and injection timing. The ECU must then communicate with actuators on the engine to satisfy performance requirements whilst minimising exhaust emissions over a wide range of operation conditions.

Features of Common Rail

1. Having a (relatively) constant injection pressure, the fuel delivery quantity is proportional to the length of time that the injector is electronically activated. Therefore accurate regulation over the quantity of injected fuel is possible for optimum control over the combustion process.
2. Independence of engine speed and load allows for an almost square rate of injection curve providing almost constant high velocity fuel spray plumes at full load, thus permitting higher specific power outputs (Bosch, 2004).
3. An advantage of the high-pressure pump being driven by the engine continuously is that the drive torque is much lower than with either rotary pumps or EUIs. In fact the drive torque is typically only 1/9th of the torque required for a comparable rotary pump (Bosch, 2004).
4. As the high-pressure pump is typically driven from the engine crankshaft, it does not impart a large stress on the camshaft as with EUI's. This requires less modification to retro-fit CR systems to existing engine designs.

Solenoid Injector Opening Behaviour

Taking a typical solenoid CR fuel injector as an example, the injector assembly (comprising the injector body, the nozzle, the control valve and the cap-nut) contains three control orifices which are designed to provide the injector behavioural characteristics as required for a particular engine calibration. By altering the sizing of these orifices at the design stage, the needle opening and closing rates can be manipulated. These orifices are described as follows:

1. **Spill Path Orifice** (SPO). This orifice controls the flow of fuel leaving the nozzle's control chamber which is the region above the needle valve where the valve spring is located.
2. **Inlet Nozzle Orifice** (INO). This orifice controls the flow of fuel entering into the control chamber.
3. **Nozzle Path Orifice** (NPO). This orifice controls the flow of pressurised fuel to the nozzle gallery and thereafter the nozzle tip.

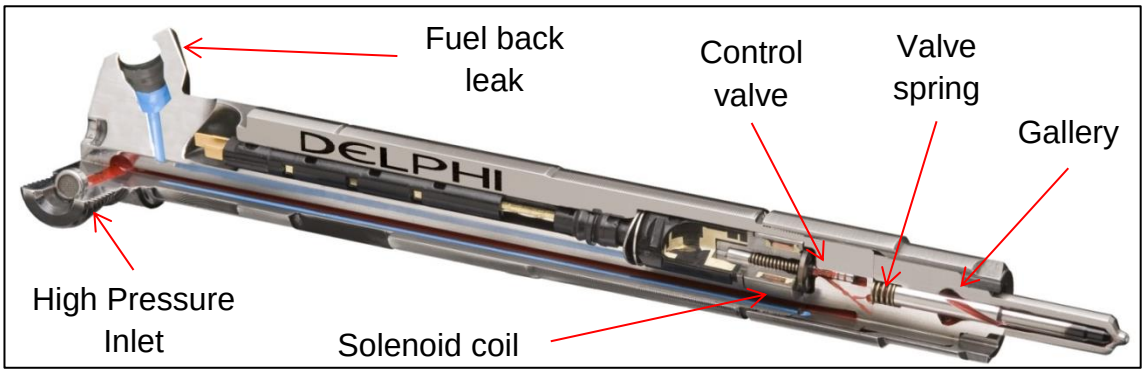

Figure 12 - Delphi's DFI 1.5 Fuel Injector

Figure 12 is a section-view a solenoid fuel injector. When the control valve is triggered electronically, fuel in the control chamber is allowed to drain via the SPO to the back-leak where it returns to the fuel tank. By having the INO smaller than the SPO, the fuel departs the control chamber before it can be re-filled via the INO, causing the pressure to fall. The resultant pressure in-balance across the ends of the needle causes the needle to lift and injection to commence. To end an injection, the control valve closes so that the SPO leakage path is closed and fuel through the INO refills the control chamber causing the pressure to rise. A third orifice, the Nozzle Path Orifice (NPO) in the flow path to the nozzle gallery induces a slight pressure drop so that the pressure in the gallery is slightly lower than that of the control chamber. This slight pressure in-balance acting on either end of the needle, acts in combination with the spring force to close the needle and terminate the injection. From this basic description it should be quite obvious how the simple sizing of these control orifices can dictate the rate of filling and draining of the control chamber, which in turn controls needle opening and closing rates. Due to this, extensive research is carried out to ensure the correct orifice sizing for optimum injector performance to suit a particular engine calibration.

1.6.4. Hybrid FIE systems

Hybrid FIE systems are a recent development designed to combine the individual advantages of differing FIE approaches. An example of this is DDS F2 distributed pump CR system which is designed for Euro VI HD engines between 9 and 16 litres. This system is rated to 3000 bar peak injection pressures to improve fuel atomisation and minimize the need for after-treatment

devices (Delphi.com, 2012). Effectively this F2 system combines the advantages of both EUI and CR systems by removing the need for the high pressure pump and allowing the entire FIE to be packaged within the suitably designed cylinder head. A typical six cylinder arrangement is shown in Figure 13 with three pumping and three non-pumping injectors which provide obvious cost-reduction benefits over a traditional EUI system with six pumping units.

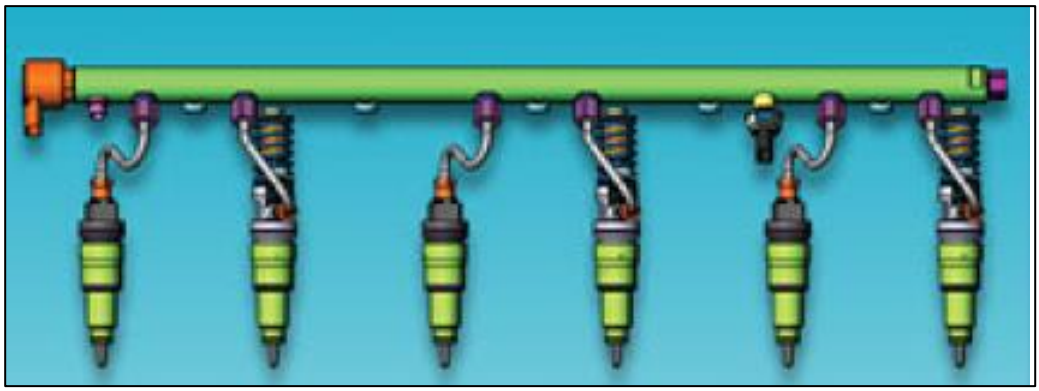

Figure 13 - F2 distributed pump CR system

1.6.5. Summary of FIE systems

Table 1 compares the pros and cons for each FIE system discussed previously.

FIE System	Pro's	Con's
High Pressure Rotary Pump (HPRP)	Low-cost system Easy to repair with interchangeable components[6] Easily packaged on an engine	Very limited multiple injection strategy Difficulty in meeting >Euro 3 emission regulations Peak injection pressures limited due to Hertz stresses Injection rate shape dependant on engine speed & load Long HP piping required Significant HP volume Large pump drive torque
Electronic Unit Injector (EUI)	High hydraulic efficiency High peak injection pressure Reduction in the number of components Nearly square or ramped rate shaping capability No HP external connections - robustness	Limited multiple injection strategy High levels of noise Difficult to package on all engine designs without robust cam train Engine oil lubricated with risk of fuel in lub oil or vice versa Pressure control of pilot / post difficult
Common Rail (CR)	Independent from engine speed & load Nearly square injection rate shape capability Fully flexible injection strategy potential Low pump drive torque	Higher system cost Components exposed to continuous pressure loading May require a fuel cooler to remove heat from spilled fuel Significant HP volume
Hybrid F2 Distributed Pump CR system	Independence from engine speed & load Nearly square injection rate shape Fully flexible injection strategy potential Small footprint - space saving Scalable, modular design Ultra high pressure potential Selective replacement of pumping injectors if performance declines Double lobed cam - lower pump drive torque	Higher system cost Components exposed to continuous pressure loading Difficult to package on engine designs without robust cam train Engine oil lubricated with risk of fuel in lubrication oil or vice versa

Table 1 - Summary of different FIE strategies

[6] Important for 3rd world and off-highway applications

Comparison between Fuel Injection Strategies

It is a difficult task to quantify the fuel economy and emission improvements that have occurred over the past decade with HSDEs moving from a PLN system with a HPRP to either a CR or an EUI system. This is due to the fact that it is not just the FIE architecture that has changed during this transition, but also the basic engine design. For instance, as power and torque are proportional to the mass of air inducted per cycle, the performance of an engine may be increased by compressing the air prior to it entering the cylinder. In modern HSDEs this is routinely accomplished by super or more commonly turbo-charging. To prevent peak pressures and thermal loading from moving outside of acceptable limits, intake-charging is usually associated with a reduction in the compression ratio when compared to a naturally aspirated engine. Much more recently, new cylinder head designs have emerged with more complicated intake and exhaust valve arrangements to accommodate the higher airflow rates found with higher-revving engines.

In summary, whereas increased FIE sophistication has led to significant reduction in fuel consumption and exhaust emissions, it cannot be ignored that improvements in the basic engine design necessary to fully utilise the improved FIE, may have somewhat contributed towards this. In light of this, the four main FIE manufactures (Bosch, Delphi, Continental and Denso) all work in partnership with engine manufacturers to exploit their FIE to the fullest to suit a particular engine installation and calibration.

1.6.6. Future Trends for FIE

PLN systems with rotary or inline injection pumps have largely fallen out of favour with the introduction of the more flexible EUI and CR systems for the reasons that have been given previously. Figure 14 is an analysis of the past and future trends within the MD sector since the introduction of CR. It can easily been seen that besides an expansion in MD engine production, a massive growth has occurred within CR at the expense of mostly Inline and Rotary systems.

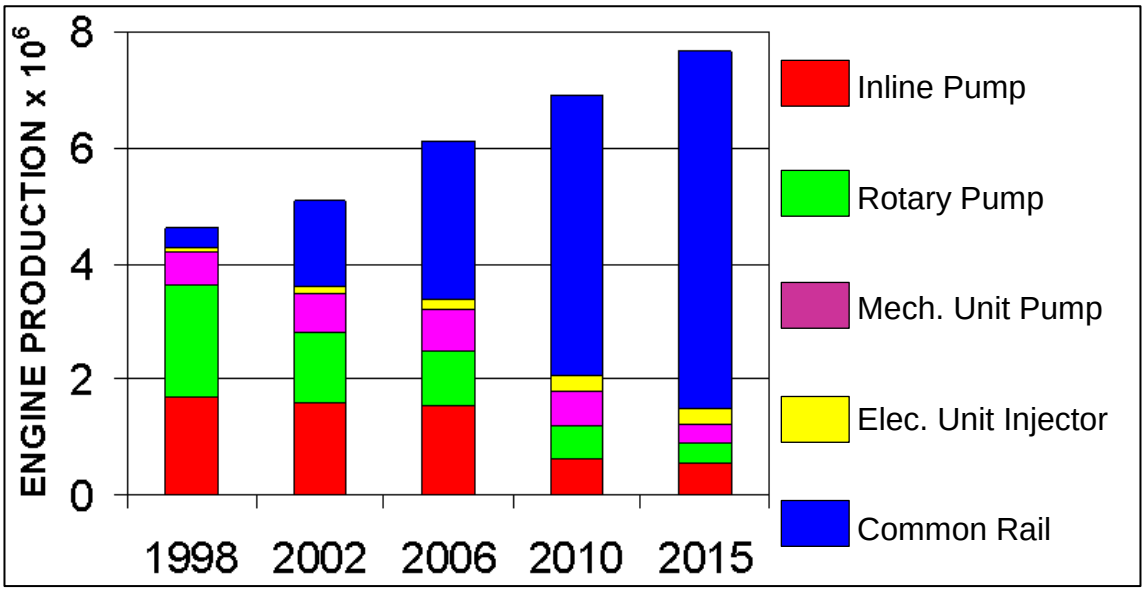

Figure 14 - MD past and projected trends (Zülch, et al., 2006)

PLN systems still remain attractive for low-cost applications; however, with likely future increases in fuel prices, stricter emission standards and a possible reduction in the cost of CR systems as the technology matures, it is likely that CR will gain even further market dominance. EUIs did have a brief flirtation with the LD market at the end of the 1990's but they cannot deliver the multiple injection flexibility and true independence from engine speed and load that a CR system can offer. Having high hydraulic efficiency, EUIs are able to generate very high peak injection pressures which are perfectly suited to the low swirl and low squish combustion that heavy duty engines utilise. However, with further expected increases in CR injection pressures and greater use of more elaborate multiple injection strategies, it is expected that CR will gain market share at the expense of EUI systems. Newly-introduced hybrid FIE designs such as the F2 system will also likely see increasing adoption to satisfy likely even more stringent future emission legislation.

Having now past ten years since the introduction of CR systems, small yet significant incremental gains are being sought within the system components and in the software which controls them. ECU's are getting more powerful, components are being treated with wear resistant coatings and efforts are being made to reduce parasitic losses to further reduce specific fuel consumption. A highly significant recent development has been the utilization of the

piezoelectric effect[7] for actuation of CR injectors. An example of this is Delphi's DFI3, direct acting injector where the needle valve is set in motion directly by a piezoelectric-ceramic actuator, rather than an electro-hydraulic circuit as is the case with a solenoid controlled injector. The DFI3 injector has the advantages of having more precise control over needle valve lift, no wasteful fuel back-leak, a needle lift rate approaching 3 m/s and the potential for up to seven injections per engine power stroke. With this design the effects of the improved spray quality and fuel-air mixing alone have been attributed as having the potential for up to a 7% reduction in specific fuel consumption over a comparable solenoid controlled injector (Schoppe, et al., 2008).

1.7. Multi-hole LD Nozzles

In compression ignition engines, for combustion to occur the injected fuel must encounter temperatures above the fuel's auto-ignition temperature in the presence of oxygen. For the entirely of this fuel to undergo combustion it needs to be injected in a finely atomised plume or jet, allowing the fuel to rapidly vaporise within a very short duration. Whereas PLN systems often featured a Pintle type nozzle producing a single, large hollow-cone spray, CR systems utilise a number of very small injection holes and very high injection pressures to ensure the necessary short injection duration. For instance, current LD CR systems feature 7 or 8 injection holes as little as 100 µm in diameter with peak injection pressures exceeding 2000 bar.

Nozzle design is a complicated process with recent developments likely attributed to the significant increase in injection pressures over the past 15 or so years. As the intricacies and development of nozzle design are considered to be beyond the scope of this thesis, only some note-worthy basics shall be mentioned here.

1.7.1. Nozzle Design

The rated engine power of the intended installation is used to determine the injection hole sizing as the hole cross-sectional area dictates the maximum fuel

[7] This is the production of stress or strain when an electric field is applied.

flow into the engine cylinder. A combination of past experiences, simulation and experimental testing is used to determine the inlet rounding and taper to ensure the most efficient atomization and hence combustion efficiency. A cone angle[8] is selected to ensure compatibility with the intended engine so that the fuel is injected into the piston bowl without impinging upon the cylinder walls (air-distribution method). Modern HSDEs tend to have the injector axially centred within the cylinder-head with equispaced injection holes which all lie on the same Pitch Circle Diameter (PCD) to ensure they all experience similar fuelling and have equal spray plumes.

For modern multi-hole nozzle designs, a range of different nozzle and sac designs have developed and are explained below. The terminology used has the sole purpose of describing the different designs and is therefore likely to be manufacturer specific, hence may be different to terminology found elsewhere.

Hemi-Sac

This is a type of HD nozzle design. It contains a large sac volume allowing for a number of large injection holes ensuring a good fuel flow capacity. This large sac volume is also its main disadvantage in that it experiences a large UBHC penalty. More modern designs are moving to a reduction in sac volume.

Mini-Sac

This is a slightly smaller version of a Hemi-Sac for LD and MD applications. It still has a relatively large sac volume so has similar advantages and disadvantages as the Hemi-Sac.

Micro-Sac

This is a LD design containing a small sac volume and may be found denoted µSac. Due to the small sac volume it has low UBHC emissions but is limited in terms of the maximum fuel flow and hence engine power which it can accommodate.

NSac

This name derives from the fact that unlike a Micro-Sac, the NSac initially featured a 90° seat whereas 60° was common on most other types of nozzles. It was designed to allow for more fuel to enter the sac and therefore be suitable for higher power applications.

Valve Covered Orifice (VCO)

[8] The included angle between the spray plumes

The design of a VCO has almost no sac volume and has the injection hole openings located immediately after the valve seat. The main benefit of a VCO is the very small sac volume leading to very low UBHC emissions. However, with sac-type nozzles, the benefit of having a sac volume is that it acts as a buffer providing a more even flow distribution to the holes whilst allowing for a smoother flow turn into them. In contrast, with VCO nozzles the flow feeding the injection holes is constrained between the needle valve and nozzle body resulting in the flow being forced to undergo a sharp flow turn within a small clearance region. For this reason VCO nozzles generate more turbulence, are more susceptible to cavitation and generally speaking will have a lower coefficient of discharge than a sac-type nozzle with the same injection hole diameters (Dingle & Lia, 2005). Additionally, the proximity of the needle valve to the entry of the injection holes makes VCO nozzle designs sensitive to any needle eccentricity often resulting in an irregular plume distribution especially at low lift.

1.7.2. Nozzle Manufacture

The nozzle of a diesel fuel injector could be regarded as being relatively simple owing to the fact that it consists of only two components, the nozzle body and the needle valve. This simplicity of design is essential owing to the fact that the nozzle tip is situated within the engine cylinder and exposed not only externally to cyclic combustion heat and pressures, but also to the pressurised fuel internally. Peak engine cylinder temperatures can be in excess of 700 °C, yet at temperatures above 350 °C a reduction occurs in the material hardness of the nozzle. For this reason it is necessary to always have fuel moving through the nozzle to provide internal cooling, which is not always possible in certain driving conditions[9]. Furthermore the robustness of the nozzle is paramount as during the lifespan of the engine the needle is expected to open and close millions of times with minimal drift to its performance. In light of this, the manufacturing process is necessarily complex and requires the utilisation of high quality chromium steel alloys.

[9] During engine exhaust braking in HD vehicles no fuel is passing through the nozzle tip such that it may over-heat leading to an increased risk of failure.

As not much published literature exists regarding the modern nozzle manufacturing process, some major processes are mentioned here.

Grinding

Firstly the sac and then the nozzle body's conical seat are ground to the required depth from a blank nozzle piece. The needle valve then has it seat ground with a differential angle of about 0.5° to that of the nozzle body. This allows for contact between the nozzle body and needle valve at a precise point to provide a good seal. It is common practice for robustness reasons to have the needle harder than the nozzle body so that the body wears faster.

Case Hardening

After grinding the nozzles are case-hardened, which as the name suggests infuses elements into the surfaces of the nozzle to form a thin layer of a harder alloy. Carbon migration into the surface of the nozzle forms a thin layer of higher carbon steel, with the carbon content gradually decreasing deeper from the surface. This ensures that the nozzle retains the internal toughness of the original steel with the hardness and wear resistance of the outer high-carbon steel. It may be necessary to re-grind important geometry such as the valve seat after the case hardening process.

Addition of injection holes

Very small injection holes with diameters as little as 100µm are created by Electrical Discharge Machining (EDM). EDM is a process where material is removed from the work piece by a series of rapidly recurring electrical discharges between two shaped graphite or copper electrodes. Without direct contact with the work piece, the electrical discharges are transmitted through a dielectric fluid, (typically light oil) resulting in a characteristic cratered appearance in the work piece. The advantages of EDM over traditional machining techniques is that it is capable of achieving difficult geometries, free from burrs and is insensitive to work piece hardness, the latter being especially important owing to the hardness of the nozzles (Fuller John E., 1989). As the EDM process has improved it has been possible to accurately and repeatedly produce even smaller injection holes. However, reduced injection hole sizes require a greater number of holes to maintain the same nozzle flow and this

number is limited by the size of the sac and the material strength of the nozzle. Therefore a manufacturing requirement to ensure robustness is to have at least a wall thickness of 0.2mm between adjacent holes. This has resulted in most LD nozzles having approximately 7 or 8 injection holes.

Since the introduction of Euro 4 emission standards, it has been common practice to manufacture injection holes with a negative taper, or with a larger hole inlet than exit. This can be obtained by accurately tilting and rotating the EDM head during the machining process.

K-Factor

The degree of injection hole taper can be expressed in terms or µ/mm or more commonly by the use of K-factor. This is given by the following equation:

$$\boldsymbol{K_{factor}} = \frac{\left[\emptyset_{\boldsymbol{entry}} - \emptyset_{\boldsymbol{exit}}\right]}{\mathbf{10}}$$

Equation 2

where the units of hole diameter are microns (µm).

Honing

Once the injection holes have been created by the EDM process, the nozzles undergo an Abrasive Flow Machining (AFM) procedure. This procedure involves hydraulically pumping an abrasive laden polymer media through the nozzles for the purpose of internal deburring, surface smoothing and producing controlled radii at the inlet to the injection holes. The unique properties of the media permit it to flow through small passages and conform to the shape that requires finishing (Kennametal Inc., 2012). To control the process, the flow rate is monitored for a constant applied pressure with the process being halted when the required increase in flow is observed. Figure 15 consists of Scanning Electron Microscope (SEM) images of a silicone impression of the inlet to an injection hole before (left) and after the honing process. Note the differing radii's at top and bottom of the injection hole post honing.

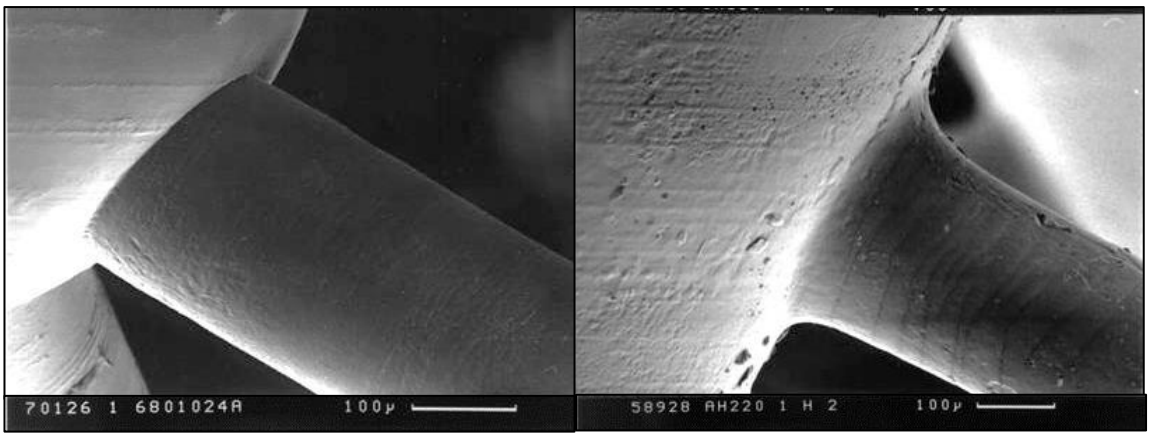

Figure 15 - SEM images of an impression of injection hole entry (Images obtained by colleague in DDS)

2. CHAPTER 2 – EXPERIMENTAL TEST FACILITIES

It is perhaps prudent to mention the experimental test facilities and techniques that are available within Delphi Diesel Systems (DDS) Technical Centre in Gillingham, where the vast majority of the experimental testing for this thesis was carried out.

2.1. High Pressure Rig

The High Pressure Rig (HPR) consists of a swash-plate pump which driven by a variable speed electric motor is able to provide a steady flow of calibration oil at up to 1000 bar pressure. Oil temperature is regulated by means of a heat exchanger and manual control over forced convection. A LD rail is installed between the pump and the test piece to introduce a pressurised volume for the purpose of damping out the pressure pulses induced by the pump. Figure 16 is an image of the HPR with the pump's control unit on the right and a protective enclosure containing the rail and test piece on the left. The upstream pressure is controlled by varying the pump speed while the downstream pressure is controlled by throttling the flow with a regulator valve. A needle valve was chosen for his purpose as it was found to be in-sensitive to pressure oscillations produced from the test piece. Instrumentation on this rig includes upstream and downstream pressure gauges, fluid temperature measurement and a piston-displacement flow meter situated on the return line back to the tank.

By varying the upstream and downstream pressures across a test piece, a range of Cavitation Numbers (CNs) can be applied which is a parameter used to indicate the likelihood of cavitation occurrence. This allows for characterisation of simple orifices or fuel injector nozzles. More shall be mentioned of CN and some other non-dimensional parameters later on in this thesis.

Figure 16 - High Pressure Rig image

2.2. Low Pressure Rig

The Low Pressure Rig (LPR) is part of the backbone of the steady-state large scale modelling technique used within DDS. Further information about large scale modelling will be disclosed later in this thesis.

With enlarged models the increased dimensions require large flow rates to match the Reynolds numbers found within real-size components. In light of this the LPR contains two large-capacity pumps that can deliver a steady flow of calibration oil at rates exceeding 450 l/min. The rig's working fluid is calibration oil which is tightly maintained at 35 °C to ensure its fluid properties remain constant. Coupled with a large, optically accessible vacuum chamber, the rig is able to apply a range of pressure drops and cavitation numbers across a test piece. Instrumentation on the LPR includes a Dial Test Indicator (DTI) for accurate linear measurement (such as of needle valve lift), a temperature regulation system, an upstream turbine flow meter and numerous pressure gauges. Figure 17 is a system schematic and Figure 18 is an actual image of the LPR testing a scalar model of an injector nozzle at un-submerged conditions. Injecting into air with a downstream vacuum is the most common arrangement to obtain similar CNs as real size components; however, it is also possible to inject into liquid which in the case of spray plume visualisation, aids optical access as the atomised spray around the periphery of the plumes can be supressed.

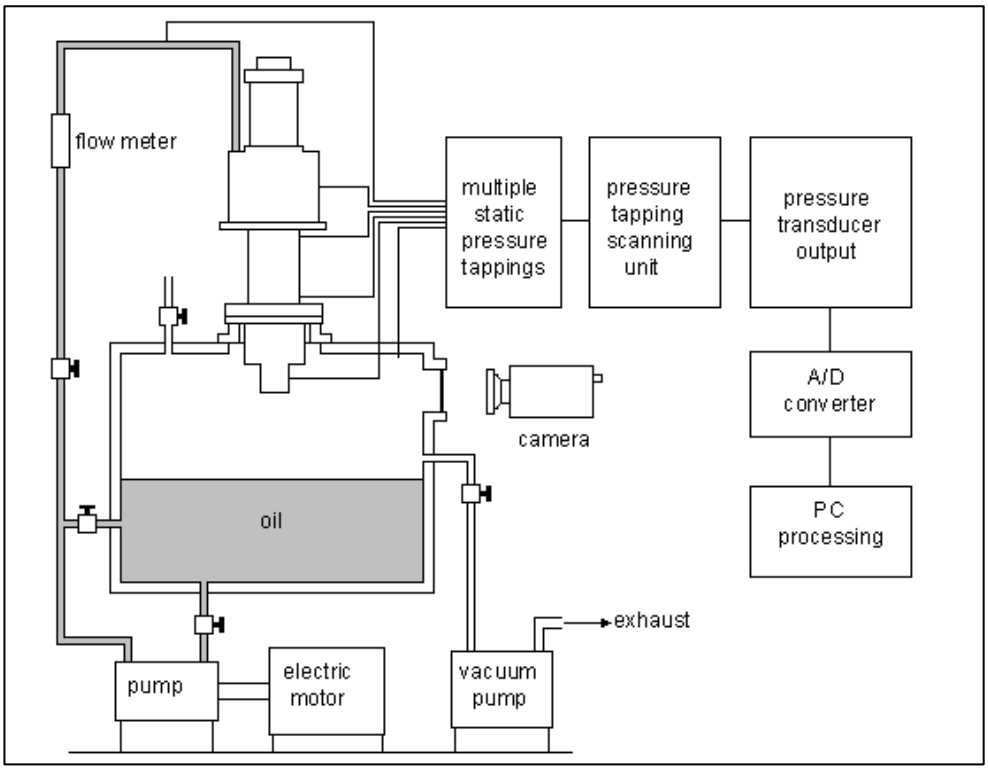

Figure 17 - Low Pressure Rig Schematic (Andrews R.J., 2004)

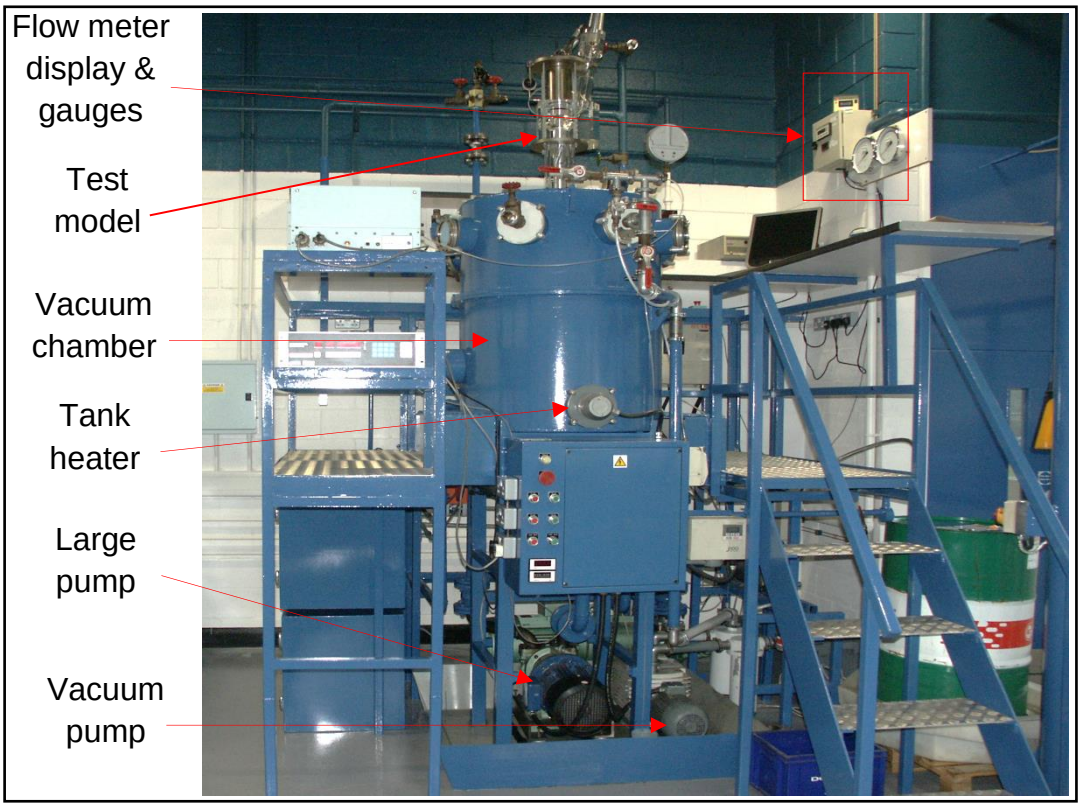

Figure 18 - Low Pressure Rig image

2.3. Spray Visualisation Rig

Unlike the previous two rigs, the Spray Visualisation Rig (SVR) is operated transiently and allows a real injection event to be viewed inside a pressurised non-combusting chamber, as shown in Figure 19. This chamber is made from chemically blackened mild steel and is rated to an internal pressure in excess of 100 bar. Pressurisation of the chamber is through inert Nitrogen gas, which although at room temperature allows replication of real 'hot' engine cylinder air densities without risk of combustion. The chamber contains three quartz windows which provide simultaneous front and two side views of the injected spray plumes. High intensity flash lighting is used to illuminate the spray plumes to provide effective shutter speeds of between 1 & 2 µs.

The FIE used with this rig is a standard LD CR system with the only modification being to the ECU software to allow it to operate on a single-injection mode. A high-pressure pump and in-house software is used to manipulate the ECU to produce the desired rail pressure and dictate the injection duration, which is referred to as Time ON or TON. Imaging software is used to synchronise the camera with the injection event as well as providing data analysis such as measurement of the spray plumes jet angle and penetration.

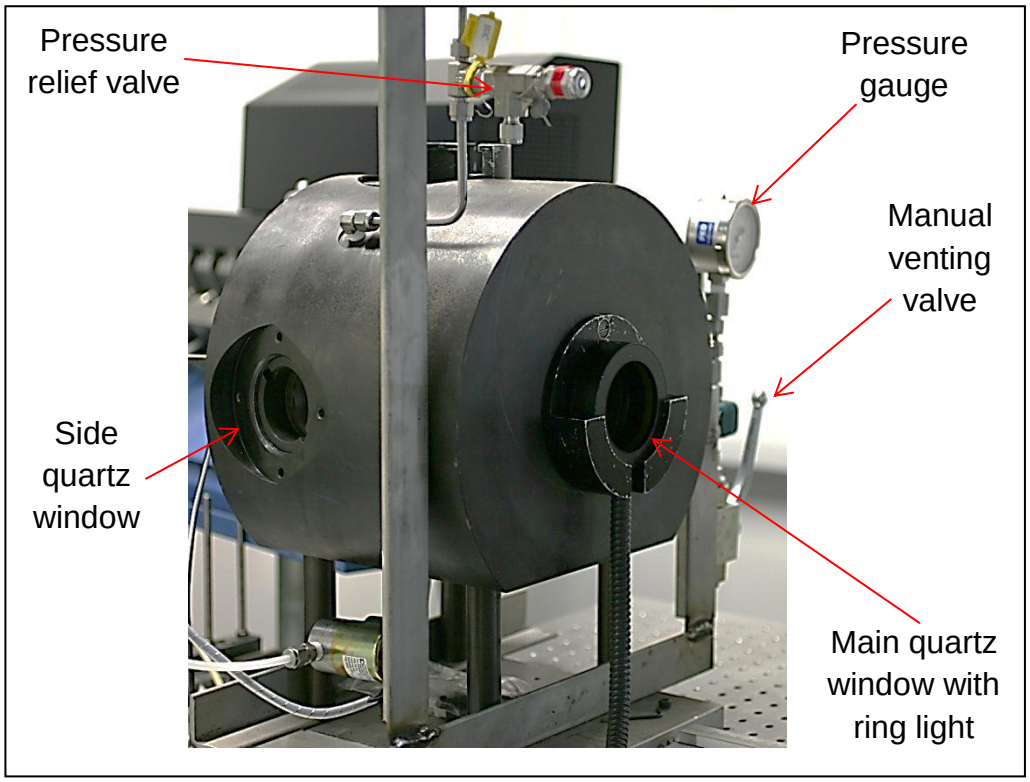

Figure 19 - Spray Visualisation Chamber image

2.4. Laser Based Flow Rig

Similar in nature to the LPR, the Laser Based Flow Rig (LBFR) is operated steady-state and adopts the large scale modelling technique to allow a vastly reduced pressure with a scaled-up flow rate (this is explained in the Scaling Between Real Size & Large Scale Models section later in this thesis). The LBFR rig also incorporates a vacuum chamber and can be operated over a similar range of cavitation and Reynolds numbers as the LPR. Unlike the LPR however, the LBFR adopts the Refractive Index Matching (RIM) technique. The principals of the RIM technique is that if the refractive index of the working fluid is matched to that of the transparent boundary, the physical flow boundaries irrespective of their complex geometry become optically invisible (Arcoumanis, et al., 1992). For this reason RIM necessitates an unusual working fluid consisting of a mixture of Turpentine and 1,2,3,4-tetrahydronaphthalene (commonly known as Tetralin) which at 25ºC has density and kinematic viscosity values of 896kg/m³ and 1.63×10^{-6} m²/s[10]. This mixture results in a fluid

[10] Turpentine and Tetralin mixing ration is 1:0.466418

with the same refractive index of 1.49 as acrylic[11] from which the test models are commonly fabricated (Gavaises, et al., 2002). The working fluid is seeded at a ratio of 1cc per 140 litres with hollow glass spheres of 10µm diameter which have neutral buoyancy and are assumed to faithfully follow the fluid flow path (this is elaborated on in the error section within the appendix). The rig is enclosed in a secure shielded room allowing the use of two Laser based, non-intrusive flow velocity measurement techniques, these are Laser Doppler Anemometry (LDA) and Particle Image Velocimetry (PIV). A third technique adopted for qualitative studies of the flow field is referred to as Laser Light Sheet (LLS) illumination.

Figure 20 is a schematic of the rig as it would be operated to test a nozzle scalar model. Two pressure pumps and a vacuum pump are able to apply a range of pressure drops and flows across the model to represent the (scaled) conditions a real size component is exposed to. Instrumentation on the rig includes a turbine flow meter, upstream and downstream pressure gauges and a DTI for accurate control over valve lift.

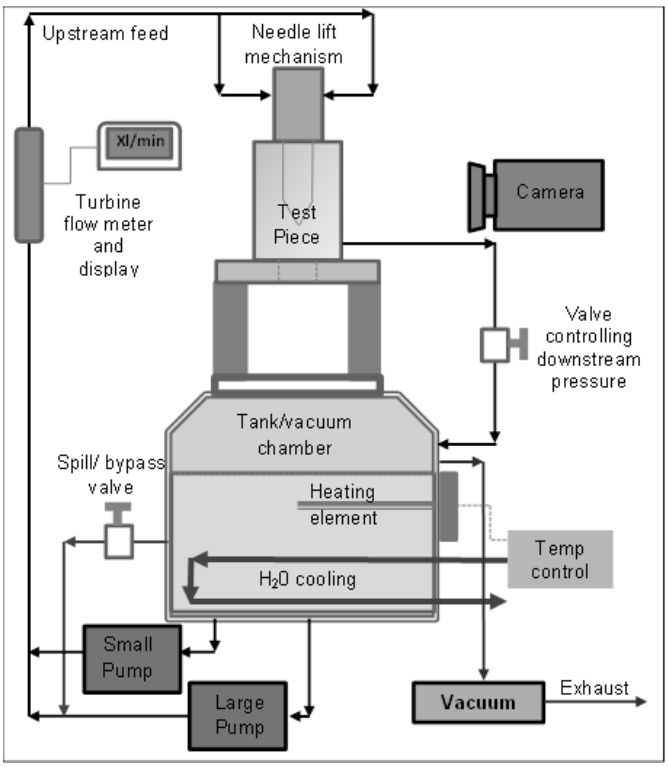

Figure 20 - Laser Based Flow Rig Schematic

[11] Poly(methyl methacrylate or PMMA is the chemical name

The rig tank's capacity is approximately 140 litres and to ensure tight control over the refractive index, the working fluid is maintained at exactly 25 °C by an electrical heating element and a chilled cooling water circuit. In order to obtain the required illumination intensity for very fast camera shutter speeds, illumination is typically from a laser light sheet situated directly below the test piece/model.

2.4.1. Laser Light Sheet Illumination

The experimental flow visualisation and measurement techniques mentioned in this thesis utilise an illuminating light sheet with is orientated parallel to the general flow direction. This light sheet is generated by passing coherent laser light through a fitting incorporating a cylindrical lens. This has the purpose of creating a thin sheet of light which although not technically 2D, only compromises a small 3D volume. Adjustment optics on the light sheet fitting enable focusing of the light sheet to minimise its thickness in the target region, however for the testing detailed in this thesis it was found that the light sheet was typically 0.8mm thick in the target region. A thinner light sheet will be of greater intensity and reduces the effect of any z-component within the flow (across the light sheet), however illuminating a smaller 3D volume will require a greater fluid seeding density for accurate flow information. Therefore there is a compromise between having the light sheet too thick and too thin. This is how the 0.8mm light sheet thickness was derived.

Using a high–resolution camera with manual control over exposure and aperture, the time history of tracer or seeding particles can be captured as they pass though this light sheet and scatter the laser light. Typically five or so laser light sheet (LLS) images are captured at each test condition and a single image considered to be an average is then selected to be representative of the flow structure. The RHS image in Figure 21 is an example of a LLS image of an entry throttled orifice with the light sheet located at the central axis and the flow entering from the left. In this arrangement approximately 50% of the orifice is being throttled at entry. The LLS image shows a primary flow clearing the flow throttling obstacle and moving downwards to enter the orifice. A secondary flow can be seen in the top right hand corner in the form of a single large vortex and two much smaller interconnected vortices. It is likely that the flow associated

with this main vortex moves out of the light sheet plane to enter the orifice in a manner which is not immediately obvious from this image. To avoid situations such as this, it is possible by moving the light sheet in successive slices through the model, to construct a 3D image of the flow structure to assist with understanding of complex flows.

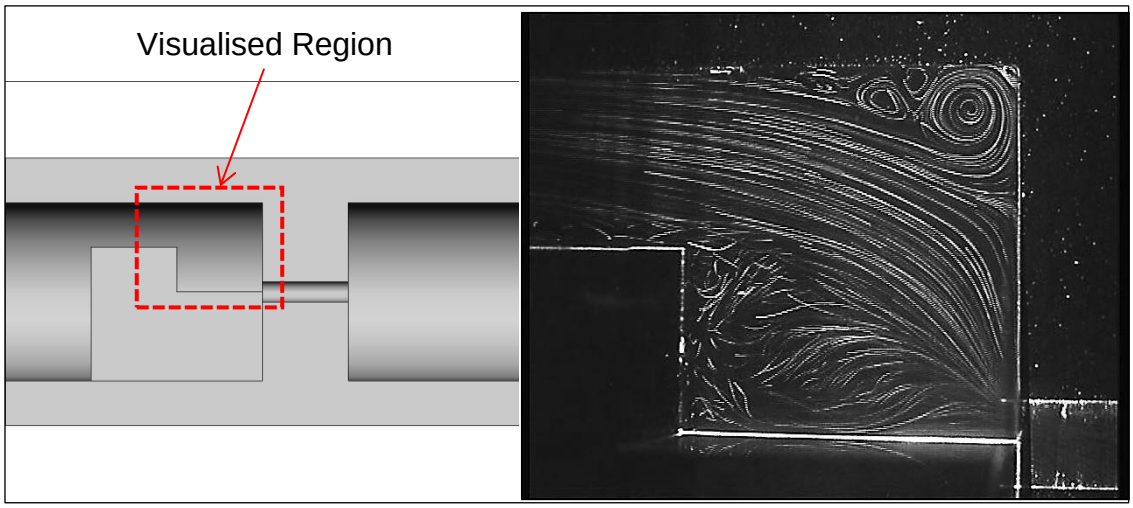

Figure 21 - Schematic & LLS image of an entry-throttled orifice (Soteriou, et al., 2000)

2.4.2. Particle Image Velocimetry

Particle Image Velocimetry (PIV) is a whole flow-field technique providing instantaneous velocity vector measurements in a cross-section of a flow. Compared with LLS imaging, a comparably much higher power Nd:YAG pulsed laser is used to produce the thin light sheet to illuminate the flow within a target 2D area. Seeding particles within the flow scatter laser light as they encounter the light sheet and this reflected light is captured in two successive image frames by a CCD camera. PIV software divides each frame into small sub-sections called ‘interrogation areas’ which are then cross-correlated to determine the particle displacement in each area. Knowing the time duration between the successive images, the particle displacement in each area can be equated to a velocity to produce a vector map over the whole target area. Figure 22 is a representation of the experimental setup.

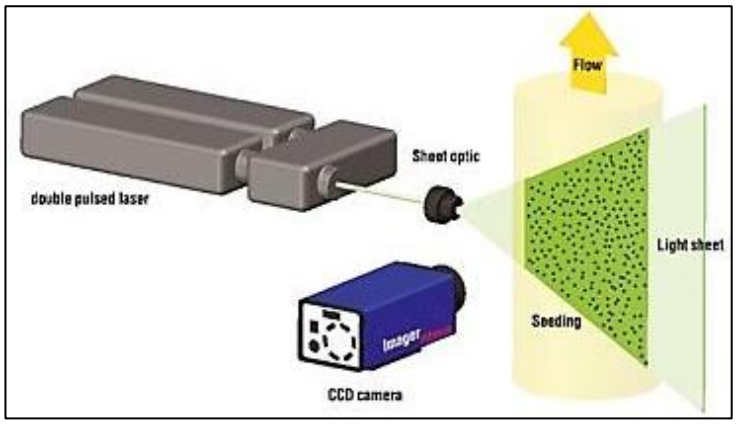

Figure 22 - Schematic of PIV setup (LaVision, 2012)

Figure 23 shows the PIV system as installed on the LBFR with the pulsed laser mounted on a traverse table to illuminate the test piece/model from below. The blue PIV camera on the right of the image is mounted perpendicular to the light sheet plane for optimum V_X & V_Y vector calculation.

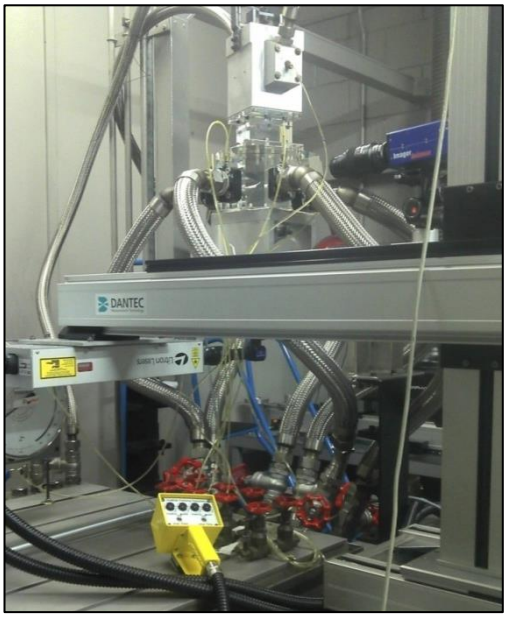

Figure 23 - PIV system in operation on LBFR

A further three-dimensional (3D) version of this technique called Stereo PIV uses two cameras ideally orientated 90° to each other to capture four separate image frames for determination of not only V_X and V_Y but also the V_Z component of the flow.

PIV System Specifications

The PIV system uses a two-frame cross-correlation method to determine the velocity vector field. The specifications of the three main pieces of hardware are as follows:

1. A PIV system controller able to control the camera and laser synchronisation and running LaVision's Davis PIV v7.2 software
2. A 532nm Nd:YAG laser with twin heads and a maximum power of 60mJ per pulse.
3. 1280x1024 pixel CCD camera(s) able to capture twin frames in quick succession

PIV Data Processing

1. For the experimental testing described in the coming sections of this thesis, a first pass interrogation window size of 64 x 64 cells was adopted before a second pass of 32 x 32 cells with a 50% cell overlap. These values were chosen to suit the seeding density and the typical target visualisation area with in the case of a nozzle model, the camera positioned to allow imaging of the entire sac and part of the injection holes. It is possible to use smaller or larger cell sizes and different amounts of overlap, but these values were obtained by a trial-and-error process and produced the most reliable results which required less interpolation from surrounding areas to fill-in missing vectors whilst providing a good signal to noise ratio. A further explanation of this shall be included in the error section in the appendix of this thesis.
2. To reduce vector calculation time, the application of a mask allowed the removal of areas containing irrelevant vector information, such as at solid wall boundaries.
3. During vector post-processing, global and local filtering was used to remove erroneous vectors which were then replaced with interpolated data from the surrounding areas.
4. To ensure statistically independent sampling, at each test condition a number of double image pairs were captured and the calculated velocity vectors were then averaged. Therefore unless otherwise stated, the vector images included in this thesis shall be the mean with the units of velocity being m/s.

Laser Induced Fluorescence PIV

To improve upon the quality of the PIV data collected within strongly cavitating flows, Laser Induced Fluorescence (LIF) PIV was adopted. This technique differs from normal PIV in that the seeding consists of nominally 10µm acrylic spheres containing a Rhodamine B fluorescent dye which is excitable at the 532nm wavelength (λ) of the illuminating laser. An edge-filter fitted to the PIV camera's lens, only allows light at wavelengths greater than 540 nm to pass, hence only fluorescent light (at 584 nm) reaches the camera. This method prevents laser light scattered off cavitation bubbles from overloading the camera, which is a concern with normal PIV. LIF PIV therefore allows for significantly higher laser intensities and the testing of flows at cavitation numbers more akin to actual engine conditions. One downside with LIF PIV is that due to the opacity of intense cavitation it is possible that fluorescent light from the seeding is obstructed from reaching the camera which can result in areas of poor quality or missing vectors. Normal PIV on the other hand is able to track and follow the cavitation bubbles in lieu of seeding, although it should be noted that cavitation bubbles when compared with normal seeding particles are less likely to follow the flow faithfully due to buoyancy forces and their low density/relatively large size.

2.4.3. Laser Doppler Anemometry

Laser Doppler Anemometry (LDA) allows the velocity to be calculated at a specific point by crossing two beams of collimated, monochromatic and coherent laser light within the flow to be measured. The principal relies on the fact that when light is reflected from a moving object, the frequency of the scattered light is shifted (the Doppler shirt) by an amount proportional to the speed of the object.

As LDA is point based it differs from both PIV and LLS techniques which utilise a light sheet plane. The basic components of the system are a continuous laser, a beam splitter, transmitting/receiving optics, a photo-detector, a signal processor and a data analysis system. A Bragg Cell is usually used to obtain the two beams by splitting a single laser beam, thus ensuring coherency between the two. By intersecting the two beams at their focal points, they interfere and generate parallel planes of high intensity light known as 'fringes'.

With the photo-detector aligned to the flow such that the fringes are perpendicular to the flow direction, when the seeding particles pass through these fringes they reflect light from the regions of constructive interference and produce a signal at the Doppler frequency f_D. The velocity at the specific point can then be calculated from the Doppler frequency and the fringe distance as given by the equation:

$$\boldsymbol{V = d_f \cdot f_D = \frac{\lambda}{2sin\left[\frac{\theta}{2}\right]} \cdot f_D}$$

Equation 3

where the fringe distance d_f is defined by the wavelength λ of the laser light and the angle between the two laser beams θ.

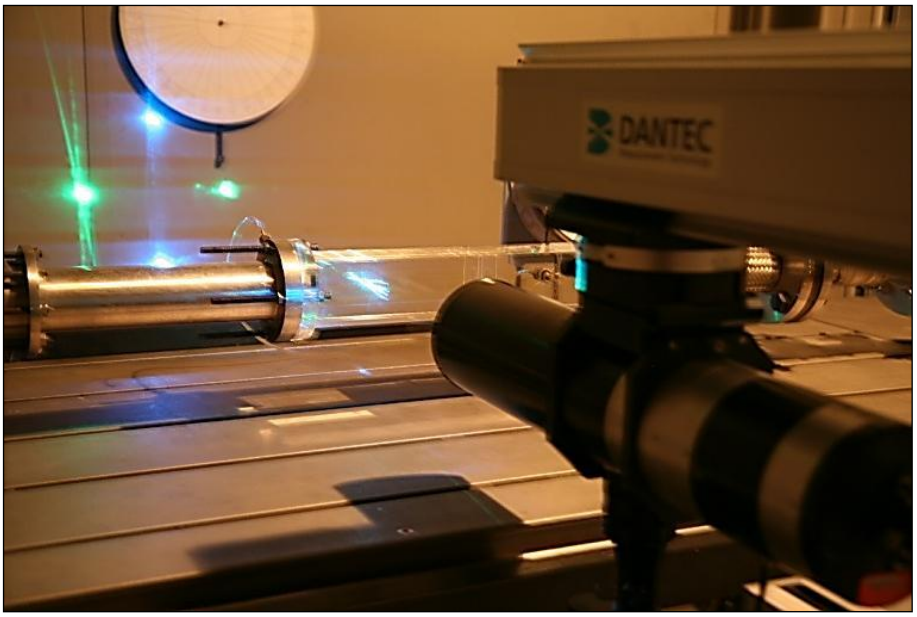

Figure 24 - Laser Doppler Anemometry system

Figure 24 shows the LDA beam splitter mounted on a traverse table and measuring the velocity at a point within an orifice plate model being ran on the LBFR.

2.5. Other Experimental Facilities/Techniques

A number of other experimental test facilities were available within DDS.

1. The **Curtis rig** is a steady-state test rig for the purpose of characterising real size nozzles. Similar in function to the HPR, the Curtis rig has the advantage of being able to mechanically control needle valve lift and accurately measure the hydraulic lifting force. The Curtis rig is therefore able to produce plots of flow and force against valve lift.
2. The **iAV injection analyser** is a device capable of computing the injection rate as a function of the dynamic increase in pressure in a fuel-filled measurement tube (iAV, n.d.). The injection analyser is an industry standard piece of measurement equipment able to simultaneously measure injection rate as well as injected fuel quantity to a very high precision.

Silicone Impression Measurement

Whereas it is easy to measure the external geometry of small items with conventional measurement tools such as microscopes and micrometres, it is somewhat more difficult to measure their internal geometries. For this reason silicone impressions are taken of the internal geometries which can then have their external geometries measured through conventional optical techniques. Although time consuming, the use of silicone impressions is essential during nozzle manufacture, for instance to ensure that the injection holes are not only the correct size and taper but also that they are free from defects which could produce a flow discontinuity. Although it is possible to optically measure sizing and positioning of the hole exit and to a lesser degree the hole inlet (being located deep inside the nozzle sac), silicone impressions are the only known method of determining the injection hole profile along its length. There are various types of impression media available for this task but the product used most frequently during this research was designed for dental purposes and goes under the Xantopren brand.

3. CHAPTER 3 – FLUID THEORY

3.1. Fluid Cavitation Theory

Numerous papers exist regarding cavitation and its discovery at the turn of the 20th century at the trailing edge of marine propellers on high-speed naval vessels (Wilczynski, 2003). Following its discovery, extensive research was initiated to try and understand the mechanism of cavitation bubble growth and collapse, through both experimental study and theoretical analysis. For this reason a wealth of literature exists on the subject not only with regard to naval applications, but also in medical and power generation fields amongst others. In light of this, it was decided in this thesis to not place too much emphasis on the well-studied phenomenon of cavitation, whilst not completely ignoring it either. Therefore, a certain past knowledge regarding the subject of cavitation has been assumed on behalf of the reader with the philosophy adopted that **cavitation is a potentially damaging mechanism and its occurrence should be understood and controlled whenever possible**.

Owing to the successive increases in fuel injection pressure, seen especially in the past 20 years, cavitation has featured ever more prominently within diesel FIE. In fact cavitation within the injection holes has been accredited as being the principal mechanism for fuel break-up and atomisation of the injected fuel sprays (Soteriou, et al., 1995) (Mardell, 2003). In contrast to this obvious beneficial effect of cavitation on fuel spray break-up, its occurrence inside the various components of the FIE is largely destructive. Cavitation generates substantial disturbances thus reducing the flow efficiency resulting in greater component losses and reduced flow rates which may contribute to diminishing spray penetration and deteriorating engine performance. Collapsing cavitation bubbles have also been known to cause surface erosion which is not only detrimental to the behaviour of the FIE but can also introduce contaminants into the system (Gao, et al., 2006).

Mechanism of Cavitation bubble formation

With a high-pressure flow, if the fluid velocity increases the pressure will decrease as the Potential Energy (PE) of the fluid is converted into Kinetic Energy (KE). If this pressure decrease is significantly large, the pressure of the fluid may drop to that of its vapour pressure. In such situations nucleation occurs with vapour bubbles forming and being carried away with the bulk flow to a region of higher pressure (lower velocity), where they collapse. The increase in fluid velocity necessary to cause the formation of these vapour bubbles is typically caused by a flow disturbance such as a sharp directional change in the flow or by a sudden fall in pressure perhaps due to the opening of a control valve.

3.1.1. Cavitation Number

A common method of representing the likelihood of cavitation occurrence across an orifice or flow discontinuity is the Cavitation Number (CN), with a higher value indicating an increased probability. Although different definitions of this dimensionless parameter may be found in other literature, the definition used throughout this thesis shall be the ratio of the pressure drop to the downstream pressure as given by the following:

$$\boldsymbol{CN = \frac{P_{up} - P_{dn}}{P_{dn} - P_{vapour}}}$$

Equation 4

The intensity of cavitation increases with increasing CN and it can be seen from Equation 4 that even with large pressure drops, cavitation can be suppressed if the downstream pressure is sufficiently high.

3.1.2. Reynolds Number

Another commonly used dimensionless parameter found in fluid mechanics is the Reynolds number (Re), which is a measure of the ratio of the inertia forces to the viscous forces acting on an element of fluid. When the Reynolds number is very small, this is an indication that the viscous forces are dominant and thus the density of the fluid may not be an important variable. Re is given by the following:

$$\boldsymbol{Re = \frac{\rho \cdot V \cdot d}{\mu}}$$

Equation 5

where ρ is the density, V is the fluid velocity, μ is the viscosity and d is a dimension although typically the hydraulic diameter is used for flow in a pipe. The fluid velocity is given by:

$$\boldsymbol{V = \frac{Q}{A}}$$

Equation 6

where Q is the flow rate and A is the flow area.

For Re < 2100, a steady flow in a round straight pipe is considered to be laminar (although this may not always be the case), but at RE > 4000 the flow in a round pipe is assumed to be turbulent (Munson, et al., 2006).

3.1.3. Weber Number

The Weber number (We) is another dimensionless parameter often used in fluid mechanics as a measure of a fluids inertia compared to its surface tension. For this reason it is particularly useful in analysing thin film flows and the formation of droplets and bubbles. With most fluid flows only the inertia and gravitation forces are dominant, however, in thin-film flows where surface tension forces

are dominant, the Weber number is an important parameter. We is given by the following equation:

$$\boldsymbol{We = \frac{\rho \cdot V^2 \cdot l}{\sigma}}$$

Equation 7

where ρ is the density, V is the fluid velocity, l is a characteristic length and σ is the surface tension. The critical Weber number is a useful parameter and is defined as being the number where values larger than this result in breakup of a droplet.

3.1.4. Coefficient of Discharge

The Coefficient of Discharge (C_d) is the fourth dimensionless parameter that warrants mentioning. The C_d is the ratio of the actual mass flow through a nozzle to that of an ideal nozzle expanding an identical working fluid from the same initial conditions to the same exit pressure. This is given by the following:

$$\boldsymbol{C_d = \frac{Q}{A \cdot \sqrt{\frac{2\Delta P}{\rho}}}}$$

Equation 8

where Q is the flow rate, A is the flow area, ΔP is the pressure drop and ρ is the density. It should be noted that an increase in the level of cavitation intensity (or CN) causes a decrease in the C_d. Generally speaking in the case of an orifice, as CN increases the onset of cavitation reduces the effective flow area causing the C_d to decrease.

3.1.5. Choked Coefficient of Discharge

A less-commonly used parameter is the Choked Coefficient of Discharge (C_dC). This is derived by neglecting the P_{dn} term from Equation 8 so that ΔP is replaced with P_{up}. This is representative of a choked[12] situation where the downstream flow cannot communicate with the upstream flow due to a reduction in the fluid density and hence the sonic velocity. This reduction in density is explained by the presence of low density cavitation bubbles within the flow.

3.1.6. Geometry Induced Cavitation

Geometry induced cavitation occurs in both steady-state and transient flows within the orifices and injection holes of FIE. A good example of this type of cavitation is within multi-hole nozzles, where sudden directional changes occur to the flow at the upstream entry "12 o'clock'' of the injection holes. At this location the boundary layer is likely to separate generating a highly turbulent region with high local velocities were cavitation is likely to occur. Steady-state transparent scalar models are an excellent way to observe geometrically induced cavitation at the entry to the injection holes and across the needle valve seat. Through research of this kind, it has been noted that nozzles with tapered injection holes[13] suppress the formation of geometric cavitation. However, it needs added that tapered holes with a sufficiently large sac volume have also been associated with a type of unsteady cavitation referred to as string cavitation (Arcoumanis, et al., 2008) which has been observed to initiate well inside the sac volume and progress along the length of the injection hole (Arcoumanis, et al., 2000).

3.1.7. Dynamically Induced Cavitation

Dynamically induced cavitation has often been associated with PLN FIE systems due to the long pipe lengths between the pump and the fuel injectors allowing pressure waves to proliferate. When a decompression wave travels

[12] Choked flow is a limiting condition which occurs when the mass flow rate will not increase with a further decrease in the downstream pressure while upstream pressure is fixed

[13] Since the introduction of Euro 4 in 2005 it has been standard practice to manufacture converging tapered injection holes on production nozzles.

down through the pipeline to terminate an injection, the pressure wave may overshoot and the local pressure may drop below the vapour pressure allowing cavitation bubbles to form at this location (Soteriou, et al., 1993). Due to its appearance, dynamically induced cavitation has also been referred to as **string** or **vortex-type cavitation**. Often occurring infrequently, this type of cavitation develops at the core of vortices where it acts as a cavitation bubble transport mechanism and upon reaching the injection hole exit, induces instability in the emerging spray (Mitroglou, et al., 2011). Although multiple studies have proven the existence of string or vortex cavitation in differing multi-hole nozzle designs, the formation process has been found to be relatively irregular whilst the interaction between string cavitation and the main flow is still poorly understood (Andriotis & Gavaises, 2009).

3.1.8. Cavitation Bubble Growth

The main factors that influence cavitation inception are the cavitation susceptibility of the liquid and the turbulence level of the flow (Zhiming & Yujian, 2003). Cavitation susceptibility can be altered if the fluid contains small contaminants or dissolved gases where cavitation nuclei are able to collate and grow (Breenan, 1995). In fact, studies have shown that the onset of cavitation inception can be significantly delayed by the removal of these contaminants.

Taking the fuel injector nozzle as an example**, cavitation inception** begins at a high velocity region such as at the inlet to an injection hole. Initially a series of small bubbles of uniform size begin to form which may resemble a slightly opaque cloud. With increasing CN the bubbles become more opaque and the individual bubbles begin to merge into large cavitation voids although there is some doubts about how this differs between real size and enlarged models (Soteriou, et al., 1998). With even further increasing CN, cavitation intensity increases and a vortex structure may develop within the nozzle hole allowing string-type cavitation structures to form at the centre of this vortex.

Once cavitation occurs, a **two-phase fluid** exists where the analysis of the flow is much more challenging due to the large density variations between the cavitating and non-cavitating regions. For instance, both one-dimensional (1D) and Computational Fluid Dynamic (CFD) simulation have to be tailored to accommodate a two-phase flow and tend to require a much greater

computational time to solve. Additionally, as cavitation bubbles are opaque and reflect illumination light, it is difficult to observe the non-cavitating regions during the experimentation techniques mentioned in the previous section.

3.1.9. Cavitation Erosion

Cavitation bubbles tend to be carried with the flow and migrate towards the surface of a rigid boundary upon which they collapse (Shervani-Tabar, et al., 2003). This collapse tends to be a violent destructive process which is known as cavitation erosion. It is believed that this bubble collapse produces a high velocity liquid micro-jet which impinges on the rigid surface. Pressure waves created partly by this micro-jet and its resultant local shockwave are believed to induce a frequent strain on the material and over time cause surface erosion. Consensus is divided between whether it is the implosion of this micro-jet or the local shockwave that is the actual cause of the material erosion.

Cavitation Erosion is thought to occur in three periods.

1. The first period is known as the *incubation period* and during this period there is a non-measurable material loss.
2. In the second period the erosion is almost constant resulting in a strongly fractured surface of which the area and depth of damage increases with time.
3. In the third period, as the surface is already strongly fractured, there is a reduced probability for an implosion close to the surface. For this reason the erosion rate is reduced.

Figure 25 is an example of cavitation erosion occurring to both the needle valve and the nozzle body of a HD CR injector. The left hand image of the needle shows cavitation erosion across its seat and in the vicinity of where the needle would penetrate into the nozzle sac. The right hand SEM image is of a nozzle silicone impression. The cavitation erosion here is confined to the region at sac entry which correlates well with the erosion seen on the needle's surface.

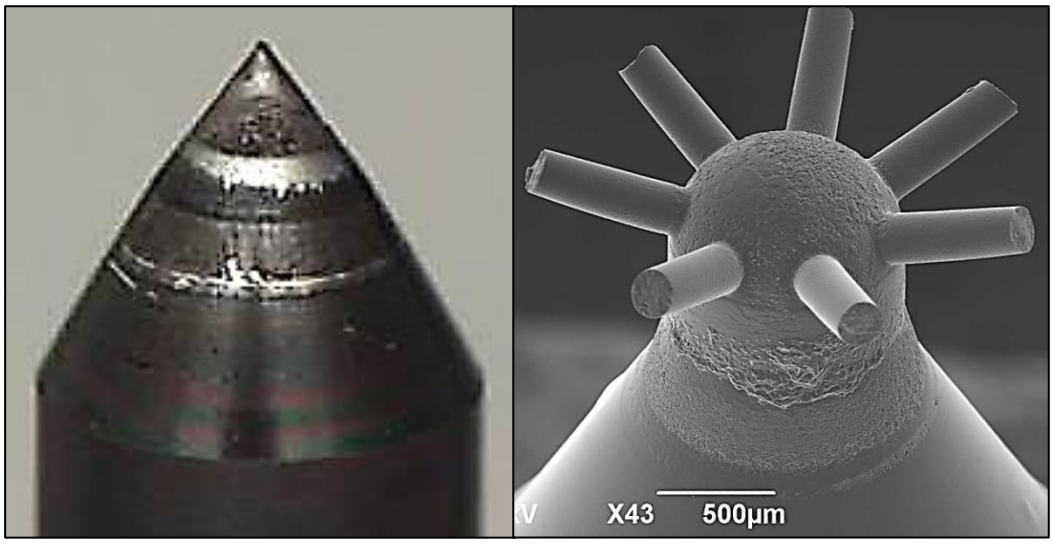

Figure 25 - Evidence of nozzle cavitation (Image obtained by colleague in DDS)

3.1.10. High C_d Nozzles

Alongside advances in injection system design and increasing injection pressures, the requirements for the spray plumes have been modified such that the injection holes have needed to become smaller. This has resulted in traditional geometry holes producing a non-optimum balance between atomisation and spray plume penetration. Modifications to the traditional, cylindrical hole shape to feature a smooth rounded entrance and a converging taper along the hole length, have resulted in significant reductions in engine exhaust emissions (Soteriou, et al., 2006). These designs are referred to as high C_d or K-factor nozzles and are designed to retain more of the energy from the injection pressure for fuel-air mixing whilst suppressing cavitation so that only a minimal drop in C_d occurs across the whole operational range.

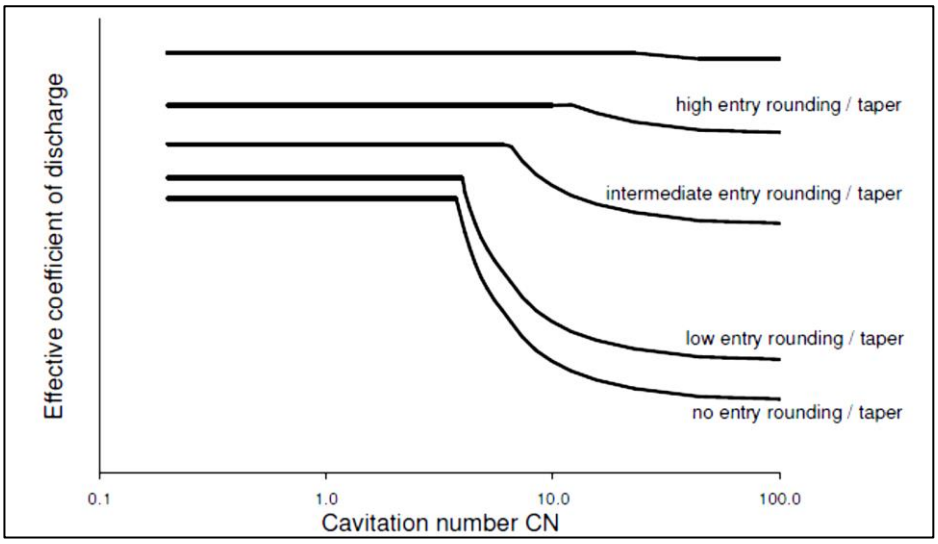

Figure 26 - Typical C_d versus CN relationship (Soteriou, et al., 2006)

In Figure 26 it can be seen that with no taper or rounding, the coefficient of discharge decreases with increasing CN once a certain value has been reached. The addition of entry rounding and taper increases the C_d overall, but this is significantly more apparent at higher CNs. Additionally, the CN at which the curves begin to decay is progressively delayed to higher CN values, indicating that the onset of cavitation is delayed with the addition of entry rounding and taper.

3.2. Injector Nozzle Flow

This section deals solely with the flow within the fuel injector nozzle and neglects the not inconsiderable path that the fuel takes to arrive there. For instance, in the case of a CR system, to get to the nozzle the flow must exit the pump, pass through the rail and travel down through the injector body. It is quite likely that the numerous orifices and restrictions within the rail and injector body, never mind the pressure pulsations induced from the pump, will all impart a considerable influence on the flow arriving within the nozzle sac. Under such transient conditions and with the many restrictions and discontinuities in the flow path, it is possible that laminar flow is never actually present within a fuel injection nozzle (Burman & DeLuca, 1962). For this reason, the flow within the nozzle is expected to be turbulent across the whole operational range even at

low RE conditions such as at the beginning and the very end of an injection event.

3.2.1. Low needle Lift

As the needle valve lifts to initiate fuel injection, a minimum flow area exists between the needle's seat and the nozzle body. Fuel passing this area is highly influenced by this restriction and cavitation is possible if the static pressure falls below the vapour pressure of the fuel. This could result in a complicated two-phase flow which may then result in further cavitation within a multi-hole nozzle as the fuel is forced to turn and enter the injection holes on a multi-hole nozzle. The formation of string cavitation has also been found to be sensitive to small variations in needle eccentricity due to this resulting in a non-uniform flow entering the injection holes (Gavaises, et al., 2009) which is likely to result in increased in-hole vortex activity. Even where cavitation does not occur, this may still be significant as in-hole vortex activity has been observed to continue within the dense core of the spray plume even after it has left the injection holes (Soteriou, et al., 2001).

3.2.2. Intermediate Needle Lift

As the needle valve lifts further, the pressure within the sac increases which has the effect of suppressing cavitation formed in the vicinity of the seat. At a predetermined lift which is dependent on the geometry of the nozzle, the minimum flow area (or area of greatest restriction) moves to the injection holes. However, even at lifts above this predetermined point, research within DDS has indicated that the needle valve may continue to significantly influence the flow by influencing the direction in which it arrives at and ultimately enters the injection holes.

3.2.3. Large Needle Lift

At large lifts the influence of the needle valve on the flow can be assumed to be largely insignificant which simplifies the analysis of the flow through the nozzle as will be made clear later in this thesis. Owing to the fact that at large lifts the

needle valve tip is typically situated further from hole entry, the flow is less constrained when turning to enter the injection holes. This results in the flow entering the injection hole more smoothly, resulting in lower levels of in-hole turbulence and possibly cavitation.

3.3. Mechanism of Fuel / Air Mixing & Atomisation

An important observation touched on earlier has been that the composition of the injected plume of fuel is extremely important to the combustion process. In light of this is it surprising that very little evidence exists concerning the structure of this plume at realistic running conditions. The general consensus is that this plume consists of a dense core (some literature refers to this as liquid core) with a cloud of atomized fuel droplets around its periphery. There is however, much ambiguity concerning the structure of this core as the peripheral fuel droplets scatter visible light, thus limiting traditional measurement techniques (Powell, et al., 2004).

As the combustion process occurs after the fuel plume has left the nozzle, it can easily be argued that the nozzle and more specifically the needle valve, affects, but is not effected by the combustion process itself. Purists may argue that exhaust blow back and to a lesser extent the effects of coking, may all indicate the contrary, but it is necessary at some point to draw a line. Therefore beyond what has already been mentioned, the combustion process is considered to be outside the remit of this thesis.

3.4. Valve Overview and Description

Valves are of utmost importance to the operation of the FIE, they are used not only for system control purposes but also to isolate, meter and spill the fuel. The three most common types of valves used within the FIE are **ball**, **cone** and **needle valves**. Between them these three types of valves are used for a wide variety of tasks including pump intake and delivery, rail pressure regulation, injector control and fuel injection metering. The opening and closing behaviour of these valves is often assumed to be simple 1D motion, however, there is past evidence within DDS that this is not the case, with free-floating (or un-sprung)

ball valves in particular being observed to be highly unstable (Knight, 1952). Additionally, successive increases in the FIE's system pressure and increasingly elaborate injection strategies have placed greater demands on the operation of these valves. Moreover, cost reduction has moved designers to select lower cost valves which tend to show the least robust and more complicated performance.

Check valve terminology

For clarification purposes it is necessary to refer to the ball and cone valves used within FIE as being check valves. Check valves (also referred to as non-return or reflux valves) are used where it is necessary to prevent the reversal of flow. They do so by means of a moveable valve element, which through activation by fluid forces (although movement may be assisted) prevents any reversal of flow. Check valves are a common component in most fluid transfer systems and for this reason a variety of differing designs exist across a wide range of applications. However, only ball and cone check valves have the ability to withstand the high pressures found within diesel FIE, therefore only they shall be considered in this thesis.

3.4.1. Ball Check Valve Design

Ball check valves use a spherical ball to block the flow in one direction. They are simple, compact, low-cost, and provide self-centring of the ball as it approaches the seat. In many applications the ball is spring-loaded (sprung) to ensure the valve remains shut with the ball on its seat until the pressure forces are sufficient to move the ball and allow the passage of fluid. Contrary to logic, ball check valves are actually more difficult to seal at lower pressures as at high pressures the fluid forces are substantial enough for the ball and seat to undergo elastic deformation, which takes account of any manufacturing imperfections on either surface. The size of the ball required is dependent on the seating arrangement and the required flow rate; hence a large flow will require a large ball which will have a high inertia. For an un-sprung valve design, a large ball with a large inertia will have a poor closing performance. For high-pressure applications, the ball is usually manufactured from steel and heat treated for hardness, however, there are cases where ceramic balls have

been adopted. Compared to a steel ball, a ceramic ball has a reduced mass which due to its lower inertia provides a more rapid response and generates a smaller impact force on the valve seat upon closing.

With ball check valve design, there are three approaches to the seating of the ball, a **conical seat**, a **spherical seat** and a **flat seat**.

Conical Seat

The conical seat is a very common arrangement with the advantage that the ball will self-centre as it moves towards its seat. There are two functional variants of this design.

1. In the first variant, the contact point of the ball is tangential to the seating cone, as shown in Figure 27. This allows the manufacturing tolerances to be liberal as the ball contact only needs to fall somewhere along the conical surface. The arrow shows the direction of flow which is referred to as being in the positive direction when the valve is opening.

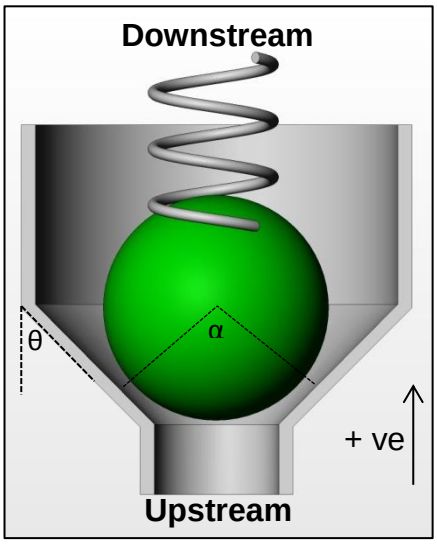

Figure 27 - Conical seat ball valve (type 1)

2. In the second variant, the ball makes contact at the intersection of the seating cone and the valve inlet, as shown in Figure 28. For the same seat angle θ as in variant 1, this design yields a much higher sealing force. It is for this reason that a leak-free valve is much easier to produce whilst still maintaining good self-centring properties of the ball.

As the ball must seat exactly at the intersection of the cone and inlet, the manufacturing tolerances for this design are tighter than with type 1.

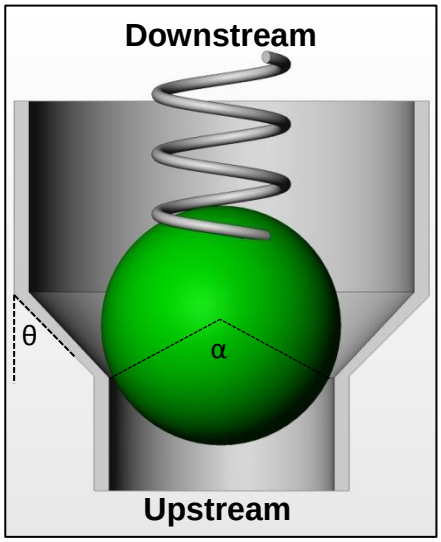

Figure 28 - Conical seat ball valve (type 2)

A common conical seat design features a 90° seat (θ x 2). This angle plays a critical role in the opening and closing behaviour of the valve. For instance a steep cone angle (small θ) will be better at self-aligning the ball during closing, whereas a flatter cone angle (large θ) will have a greater opening throat area for a given ball lift.

The Spherical Seat

A check valve with a spherical seat (Figure 29) offers greater sealing ability than a design with a conical seat. This is because the valve seat has a similar radius of curvature as the ball in two directions so that the point of contact between the seat and the ball (although theoretically the same as a conically seated valve), has a greater contact surface area when elastic deformation is taken into account. Upon flow reversal and valve closing, a layer of fluid trapped between the seat and the ball must be displaced, thus the ball is cushioned and prevented from slamming into its seat. The radius of curvature of the ball is always smaller than that of the seat and it is the ratio of these two curvatures that determines the opening and closing behaviour of the valve. The

disadvantage of this design is that its complexity requires a greater manufacturing cost and the valve seat may need to be lapped[14].

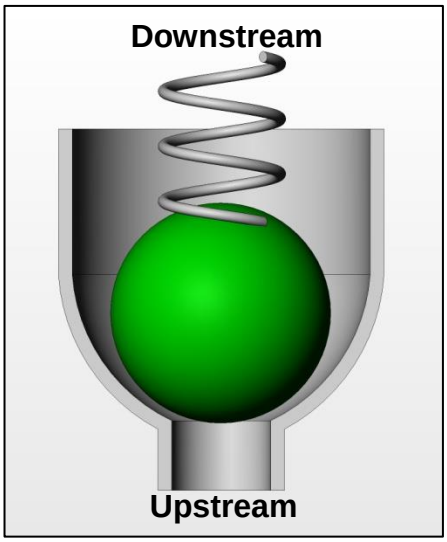

Figure 29 - Spherical seat ball valve

The Flat Seat

Due to having a smaller contact area, a flat seat offers a much higher elastic load on the seat for a given fluid pressure than both conical and spherical seat designs. For this reason a flat seat provides a better seal at lower pressures. A flat seat can easily be produced to a high quality; however, the design lacks the self-centring nature of the conical or spherical seat. In Figure 30 the ball contact angle α is determined by the ratio of the inlet diameter to the ball diameter. The smaller the contact angle α, the better the seal but the poorer the opening behaviour. An α-angle of 90° tends to be common.

[14] Lapping is an operation where two surfaces are rubbed together with an abrasive compound between them in order to produce smooth matched surfaces

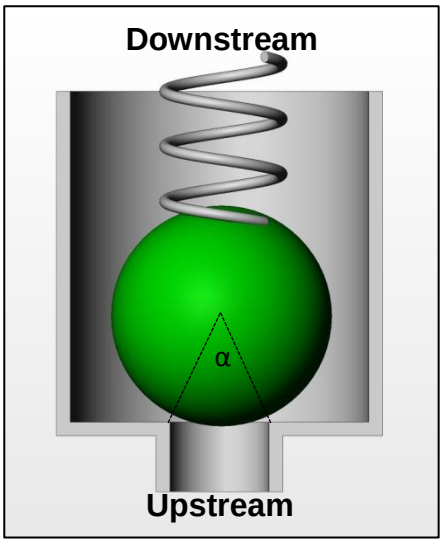

Figure 30 - Flat seat ball valve

Ball Check Valve Applications

Although the previous illustrations all featured a sprung ball element, each variant could amply function without a spring, with valve closure being actuated solely through fluid forces when neglecting the effects of gravity. Unlike un-sprung designs, with a light spring the ball is moved towards its seat once the flow has started to deteriorate but before any flow reversal has begun. This has obvious benefits for system efficiency. In the case of a pressure relief valve, a heavy spring is necessary with a spring force equivalent to the maximum force with which the fluid acts on the valve element. Figure 31 is a CAD model of a pressure relief valve (or pressure limiting valve) with a conical seat as found within a high-pressure CR fuel pump (Balin, 2004). When the fluid pressure exceeds the spring force the ball lifts off its seat and the pressurised fuel is allowed to drain by way or the spill pathway.

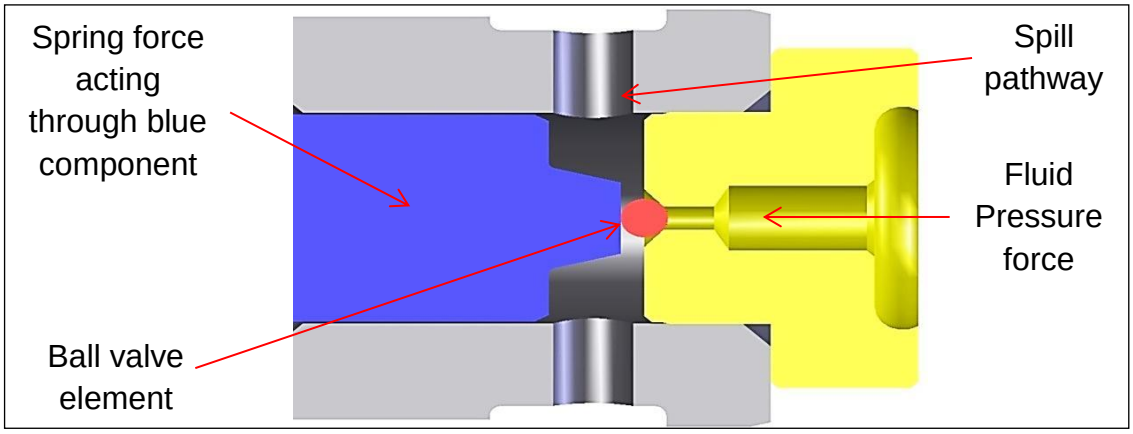

Figure 31 - Pressure limiting valve CAD model

Figure 32 contains a schematic of the cam and radial plunger arrangement within a CR fuel pump alongside an enlarged view of the delivery (outlet) valve which features a sprung ball with a spherical seat. During the filling phase, transfer pressure is sufficient to open the inlet valve and move the plungers apart allowing the dead volume between the plungers to fill with fuel. As the cam ring rotates, the diametrically opposite plungers are pushed inwards causing the pressure in the space between them to rise. The inlet valve then closes once the pressure becomes higher than the transfer pressure. The pressure continues to rise until the pressure exceeds that within the rail[15], at which point the delivery valve opens and the rail is filled with pressurised fuel.

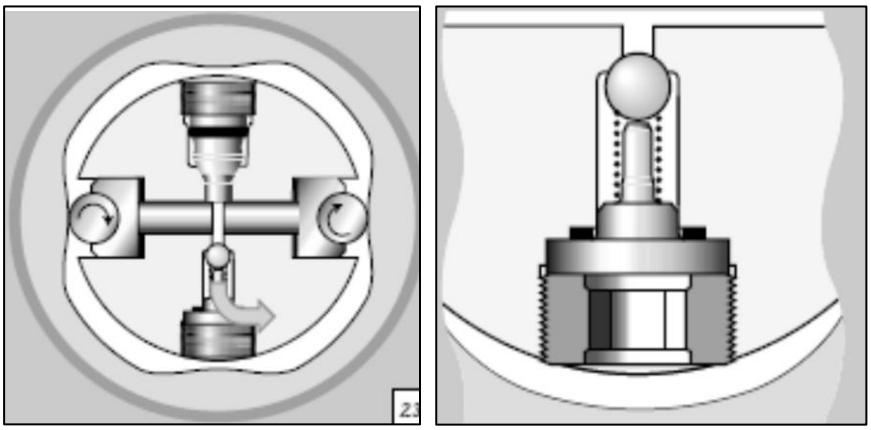

Figure 32 - CR high pressure pump – Head assembly

3.4.2. Cone Check Valve Design

Cone check valves are also known as poppet or plug check valves and are similar to ball check valves except they use a free-floating or spring-loaded tapered cone as the closure element, (Figure 33). Similar to ball check valves, the seat angle (and hence angle of the cone) is crucial to the opening and closing performance of the valve. However, unlike ball valves, cone valves need to be guided which results in increased complexity and hence greater cost of manufacture.

[15] Spring force is negligible compared to pressure forces at this point

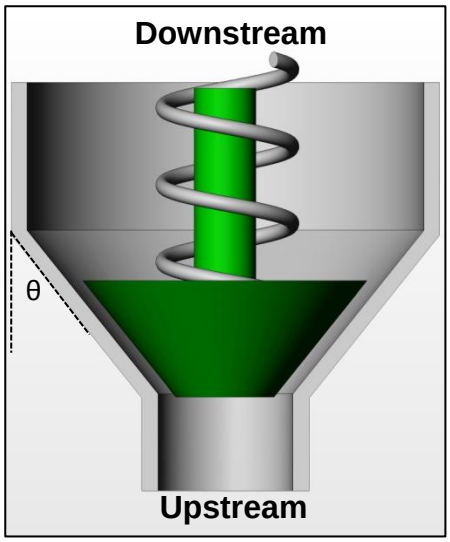

Figure 33 - Cone check valve

It is worth mentioning that like with ball check valves, it is possible to have a cone check valve with a flat seat, although this has not be illustrated in this thesis.

Cone Check Valve Applications

The aforementioned description of the operation of a CR fuel pump referred to but did not identify the inlet valve. A more recent design of fuel injection pump, (DDS DFP6) is a roller shoe configuration which incorporates a cone check valve as its inlet valve. This is shown in Figure 34.

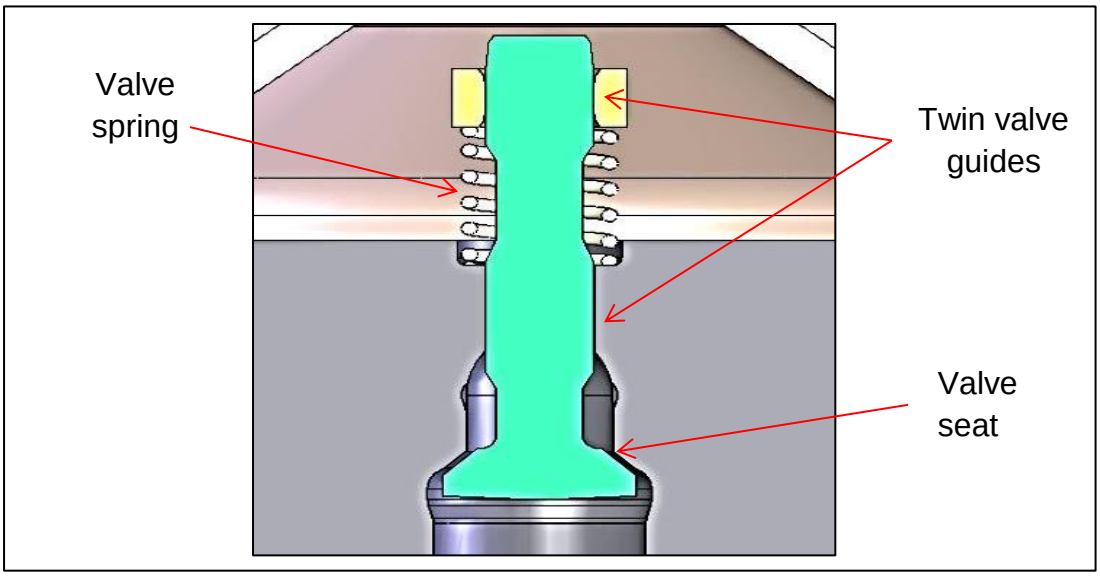

Figure 34 - Guided cone inlet valve

3.4.3. Needle Valve Design

Due to its location within the nozzle of a fuel injector, the needle valve is considered to be a critically important part of the fluid link between the FIE and the combustion process.

Needle valves are so named as they contain an elongated, conically-tapered needle and matched seat. Unlike ball and cone check valves, needle valves are capable of fine flow control and it is for this reason that they are integrated within the nozzle of a fuel injector to accurately and consistently meter fuel delivery to the engine cylinders. Although not considered as being a non-return valve in the same sense as ball or cone check valves, the needle valve (often referred to as just the needle) is required to inject fuel whilst preventing any reverse flow of the hot pressurised combustion gases[16].

Needle eccentricity particularly at low lift, may not only lead to a significant spray imbalance with subsequent combustion efficiency penalties, but as has already been mentioned, may set up an asymmetrical flow pattern within the sac of a multi-hole nozzle. Asymmetry in the flow entering the injection holes has not only been associated with vortex motion and vortex induced cavitation within the injection holes (Gavaises, et al., 2009) but this has also been associated with an increase in spray plume angle[17] (Andriotis & Gavaises, 2009). Furthermore, poor behaviour of the needle valve does not only have the potential to cause the engine to run poorly with emission and fuel economy penalties, but in the case of a dribbling injector, where the needle valve does not seal, it has the potential to damage the engine.

3.5. Injector Nozzle Design

Nozzle design is a complicated process beset with rules and understanding which has been amassed over decades of diesel engine research and development. For this reason FIE manufacturers remain guarded where nozzle design is concerned and this has probably been exuberated in recent years with increasing competitiveness for CR market share. Due in part to this, only a brief

[16] Known as ‘Exhaust Blowback’
[17] Spray plume included angle is commonly referred to a jet angle

overview will be given concerning nozzle design as a full explanation would quite possibly be beyond the scope of this thesis.

Figure 35 is a section view of a CAD model of the tip of µSac nozzle with the needle set to full lift (300µm) and some of the important features identified.

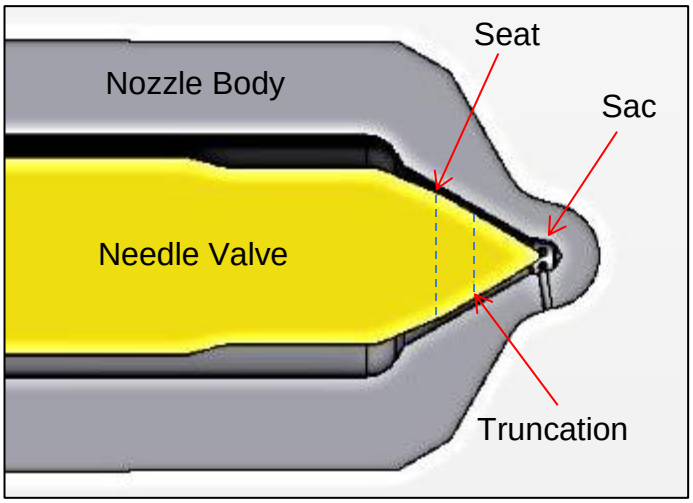

Figure 35 - Section view of a fuel injector nozzle tip

A differential angle between the needle valve and the nozzle body ensures that upon closing, the two parts contact along the valve's seat. The diameter of this seat and its angle are all crucial to the transient performance of the nozzle such that extensive research has been carried out to study variations in these parameters. The most common seat angle remains 60° although 90° and even 120° designs have been investigated as a means to provide a higher flow at low needle lift. The truncation point refers to a geometry change on the profile of the needle tip which due to the small cross-sectional area can actually be highly influential to the flow entering the sac. Higher flow nozzles tend to have a large truncation angle to permit a greater flow into the sac; however, a smaller truncation angle is advantageous for reduction in exhaust emissions as it serves to reduce sac volume when the needle valve is seated. This is due to the fact that during combustion, liquid fuel remaining in the sac volume and the injection holes may be released at the end of the power stroke, contributing detrimentally to UBHC and PM emissions (Dingle & Lia, 2005).

3.5.1. Needle Valve Wander

Needle valve eccentricity has a significant affect upon spray symmetry especially at the start of injection (SOI) where the needle valve is at low lift. Despite precision manufacture, lateral articulation or 'wander' as the needle lifts is possible due to the distance from where the needle is guided and possible pressure in-balances within the nozzle sac. To minimise needle wander and the resulting preferential flow that causes asymmetric spray plumes, dual-guided or extended guide nozzles have been introduced.

3.5.2. Needle Lift Sensor

For research and development purposes it is common to install a needle lift sensor within a modified fuel injector body to indicate the axial position of the needle valve. A typical approach to this involves the installation of a small probe onto the top of the needle which passes through a small coil installed within the injector body. The movement of the probe generates an eddy current which can be calibrated to correspond to an axial distance or valve lift. Using this technique the needle's axial motion can easily be observed with regards to its effect on spray plume development. However, due to the high temperatures and pressures to which a nozzle is subjected, needle lift sensors are not considered robust enough for actual CR production nozzles.

3.5.3. Relationship between Valve Lift & Seat Area

As has already been mentioned, at low needle lift the minimum flow area (or the area of maximum restriction) occurs between the needle valve's seat and the nozzle body. This restriction is very important to the developing flow and is given by the equation for a frustum of a cone:

$$\boldsymbol{A = \frac{\pi(d_1 + d_2)}{2} \cdot L}$$

Equation 9

where d_1 is the diameter of the body seat, d_2 is the diameter of the valve seat and L is the distance the valve moves away from the seat. The relationship between L and d_2 with the seat/cone angle θ can be seen in Figure 36.

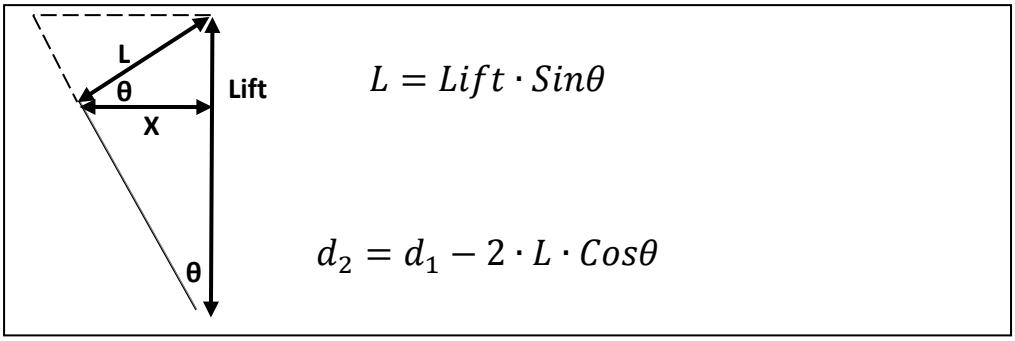

Figure 36 - Relationship between lift and seat angle

3.6. Check Valve Behaviour

The behaviour and performance of check valves has been investigated for over forty years, however, this has mostly with respect to power generation installations where the flows are large and the fluid pressures are relatively low. One key fact that is known and utilised with check valve selection is that the closing behaviour is strongly dependant on the rate of deceleration of the flow. The following section shall elaborate upon this.

3.6.1. Check Valve Closure

In the case of a slowly diminishing flow, when the flow velocity has reached a value smaller than the fully open velocity of the valve, the valve element starts to move towards its seat. This fully open velocity is dependent on the density of the working fluid, the valve design or even the valve's orientation within the system. Due to inertia of the valve element and the distance it has to travel to reach its seat, it is likely that a degree of backflow will have occurred before the valve has closed (Perko, 1986). Generally speaking, check valve behaviour in a slowly diminishing flow is predictable; however, it is the behaviour in a quickly diminishing flow that is most taxing.

3.6.2. Check Valve Slam

For a quickly decreasing flow as is typical within FIE systems, the flow is likely to have obtained a significant reverse velocity before the valve can close. As the valve element approaches its seat, the restriction of this backward flow causes an increase in the pressure. This rise in pressure further accelerates the closure of the valve element on to its seat, resulting in check valve Slam. This slamming is often accompanied by an audible noise regarded as being caused by the physical impact between the valve element and the valve seat. It has been claimed that the noise associated with check valve slam is not the impact of the movable valve element into the seat but rather the rapid stretching of the pipe due to the pressure wave travelling through the fluid. However, the report in question does not offer any experimental evidence to substantiate this claim (Val-Matic Valve and Manufacturing Corp., 2003).

3.6.3. Pressure Surge

At the instant of valve closure, the abrupt arresting of the reversed flow is likely to result in the compression of the fluid adjacent to the valve element and a resultant pressure rise which is reflected throughout the pipeline. This is referred to as either fluid hammer[18] or pressure surge and its magnitude is dependent on the deceleration of the flow and the line pressure. The Joukowsky formula can be used to estimate the maximum pressure variations at upstream and downstream sides of the valve (Perko, 1986) and this is given by the expression:

$$\Delta \boldsymbol{P} = \boldsymbol{\rho} \cdot \boldsymbol{c} \cdot \boldsymbol{V_{rev}}$$

Equation 10

where c is the speed of sound and V_{rev} is the maximum velocity of the reverse flow during valve closure.

An additional concern with value closure is that the kinetic energy of the column of fluid that is brought to an abrupt halt, is imparted through the check valve into the pipeline structure leading to large forces to prevent the pipeline travelling in

[18] Often referred to as Water Hammer

the same direction in which the fluid was going (Goodwin & Jenkins, 2000). This is especially problematic in large pipeline installations where the column of fluid is sufficient in size so that large forces may be transmitted to the pipeline and its foundations. In order to overcome such potentially damaging pressure surges in large pipeline systems, it is not uncommon for air traps or stand pipes to be installed to act as dampers to provide a cushion to absorb the force of the arrested fluid.

3.6.4. Check Valve Clatter

High transient pressures are not only restricted to the downstream side of the check valve. On the upstream side, as the reverse velocity is reduced to zero, the falling pressure may easily drop to the vapour pressure of the liquid allowing a vaporous cavity to form (Thorley, 1989). This cavity will normally rapidly collapse in response to pressure waves reflected from further upstream giving rise to large pressure increases which may be the same order of magnitude as the maximum pressure variation occurring downstream. In some circumstances this pressure rise may cause the check valve to re-open momentarily and then crash back onto its seat leading to resonance in a process often referred to as valve clatter (Provoost, 1982) (Provoost, 1983). This mechanism is also referred to as valve flutter and may result in a check valve experiencing a larger number of opening-closing cycles than the designer and/or manufacturer had anticipated. For this reason valve clatter has been suggested as the leading cause of wear in situations where check valves have consistently failed to meet the long-life specifications postulated by their manufactures (Potter, et al., 2008).

3.6.5. Check Valve Performance

An ideal check valve would have no resistance to flow in the positive direction yet infinite resistance to flow in the reverse direction (Kruisbrink, 1996). It would contain moving parts of a low inertia that would only travel a short distance to close with their movement being assisted so that they would close before any appreciable reverse flow had developed. In order to approach this ideal, the following techniques are adopted:

1. The addition of a spring to assist the valve element is a simple and low-cost method to lessen the degree of reverse flow that occurs before valve closure.
2. Hydraulic damping mechanisms are often adopted within the power generation industry to dramatically slow down the closure speed of the valve element over its final distance of travel. Extensive modelling and testing is required to determine the adjustment of the damping mechanism which is decisive in judging the valves performance within the system in which it is installed. Additionally, damping characteristics are highly system dependant since the valve closure may be influenced by reflections of pressure waves and would not suit a range of operating flow rates and pressures. Due to cost and sizing limitations the addition of a damping mechanism would not be practical for FIE applications, therefore damping mechanisms shall not be considered further.
3. An improvement in check valve performance can be made by using a valve of a smaller nominal diameter than that of the surrounding piping. The reduction in throat area results in an increase in the fluid velocity and also therefore an increase in the flow deceleration upon valve closure. However, this has the beneficial effect of reducing the pressure rise that occurs on closure which may minimise any fatigue problems. Using a valve of smaller nominal diameter is also beneficial for spring-loaded valves on account of the higher flow velocity, they can be fitted with stronger springs (Perko, 1986). A downside to this method is that the use of smaller valves will increase the frictional head loss that occurs across the fully open valve with the flow in the positive direction.
4. Generally speaking, the bigger the valve, the further the distance that the valve element has to move, the greater its inertia and therefore the larger the backward flow. Therefore the degree of pressure surge and ferocity of check valve slam will increase with increasing valve size (Koetzier, et al., 1986).

3.6.6. Check Valve Selection

Incorrect selection of check valves has for many years been a source of troublesome pressure transients in pipeline systems. In fact it has been

attributed to have been the cause of numerous catastrophic failures across a wide range of industries. For this reason numerous papers have been written to assist pipeline engineers with the selection of the correct valve for a given application (Provoost, 1982). These papers aim to provide criteria for check valve selection which may include; suitability for the working fluid, working pressure range, head loss, limitations on weight, size, cost, ease of transportation and maintenance, dynamic behaviour, flexural strength, fatigue and corrosion potential (Ellis & Mualla, 1986). Moreover these papers attempt to determine system independent characteristics for the hydrodynamic effects of valve closure in a decreasing flow, such that these characteristics may be used as a tool in pipeline design, valve selection and pressure surge analysis.

For applications within FIE, a check valve or any valve for that matter is expected to be robust and operate maintenance-free for the lifetime of the vehicle to which it is fitted, which for HD vehicle can be up to 1 million miles (Lacey, et al., 2012). Additional requirements are that the valve should operate with a minimal pressure or energy loss, withstand very high static and dynamic pressures, be extremely small in size and very low-cost. With ever increasing injection pressures, higher-revving diesel engines and further demands for increased hydraulic efficiency, the correct design and selection of valves for FIE applications is expected to become even more tiresome.

4. CHAPTER 4 – LITERATURE REVIEW

This section is devoted to the discussion of both published and unpublished research that is considered of relevance to this thesis.

4.1. Check Valve Review

During the Literature review it was found that most of the prior research into check valve behaviour has been focused at hydroelectric and nuclear power installations. Applications such as these typically involve large, low pressure flows which are in direct contrast to FIE, where the flow rates are low but at very high pressures. For this reason the large majority of existing research into check valve behaviour was reviewed but thought not directly relevant.

4.1.1. Ball Check Valves

The discontinuity over the usage of the terminology 'Ball valve' led to optimism in finding published research of direct relevance to this thesis. An example of this was several papers mentioning transparent modelling of ball valves. Upon reviewing these papers it was unfortunately found that the experimental testing had been carried out on a transparent model of what could be described as a quarter-turn ball, shut-off valve; however, the experimental methodology was relevant and interesting. Particle tracking flow visualisation with laser light sheet illumination had been adopted to study the flow and onset of cavitation at a range of Reynolds numbers and valve opening angles (Chern, et al., 2007). The experimental data was compared with CFD simulation of the internal flow to determine the flow and loss coefficients for various valve opening angles (Moujaes & Jagan, 2008). Further experimental testing was also performed in order to investigate the effect of control devices mounted downstream of the valve in order to provide a linear relationship between valve opening angle and volumetric flow rate. Finally measurements were taken to determine the effects of these control devices on the flow by calculating the loss coefficient, the flow coefficient and the cavitation number (although this was calculated differently to the equation used in this thesis). The author reported observing vortical

structures in the flow field whose size was proportional to the pressure drop occurring across the model (Chern & Wang, 2004).

An interesting paper investigated the cavitation behaviour of cone valves (referred to as poppet valves) in hydraulic oils. Steady-state testing was carried out to compare flow rates at different valve lifts whilst exposed to a range of CN's. Thought-provoking conclusions were drawn with the aim of estimating cavitation intensity in order to reduce or even prevent cavitation erosion. These include determination of a critical CN, the use of smooth flow passages which avoid discontinuities and the use of multi-stage orifices to prevent the static pressure dropping below the vapour pressure of the fluid (Koivula & Ellman, 1998). These conclusions may be equally applicable within FIE systems as with the hydraulic systems for which they were intended.

A paper which leans towards automotive Anti-lock Braking Systems (ABS) compared experimental testing with CFD data for differing ball check valve designs (Leventhal, 2003). The designs were operated across different pumping frequencies and assessed for efficiency, pressure oscillations, resonance and leakage. Due to the low feed pressures and the low transient operational frequencies, it is likely that the conclusions would not be applicable to dynamic FIE applications where pressure gradients and movement velocities are much higher.

An interesting paper used CFD simulation and experimental visualisation to assess the cavitation phenomena across the seats of two valves used commonly within hydraulic systems. These were a sprung cone check valve with a flat seat (referred to a poppet valve in the paper) and a sprung ball check valve with a conical seat. High speed imaging was carried out whilst the valve lift was measured as the cone valve was allowed to undergo sustained 2D self-excited oscillations (or check valve clatter). The effects of outlet area, inlet velocity and outlet pressure were examined as a means to supress cavitation across the valve seat (Gao, et al., 2006). A second paper by the same author focused on ball check valve experimental testing and in particular concentrated on cavitating flows and the effect they have on the 3D motion of the ball. The author indicated that cavitation around the valve seat occurs periodically with a very high frequency as the ball vibrated periodically in a lateral direction. It was also found that cavitation not only occurred at the valve seat but also around the entire surface of the ball. Experimental tests were again compared with

numerical tests which also investigated the effects of a non-axis-symmetric location of the ball (Gao, 2003).

4.1.2. Cone Check Valves

It is well known that sprung cone check valves can exhibit unstable behaviour as a result of the interaction between the dynamics of the downstream volume and the dynamics of the valve (Potter, et al., 2008) (Stone, 1960). However, apart from a sprung cone check valve with a flat seat (Gao, 2003), very little research of relevance to diesel FIE has been published. Perhaps this is explained by most FIE investigations having focused on the needle valve which admittedly is quite close in terms of its design to a cone check valve although actuated entirely differently.

One exception to the lack of relevant research into check vales within FIE systems was a 1961 unpublished internal report from CAV ltd.[19] which showed that the delivery valve of a distributor pump undergoes very erratic behaviour due to unloading and decompression of the fuel between the valve and the pump plungers in a Rotary diesel fuel pump. Figure 37 is a replication of this data showing the effects of engine speed on ball lift and line pressure.

[19] A previous incarnation of Delphi Diesel Systems

Engine Speed	Ball Lift	Line Pressure
100 rpm	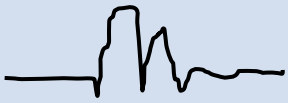	
200 rpm		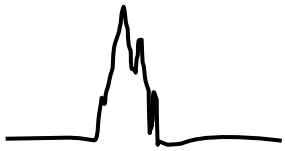
400 rpm		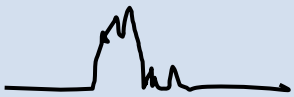
800 rpm		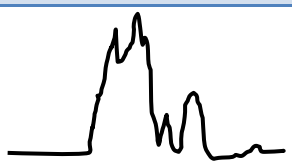
1200 rpm	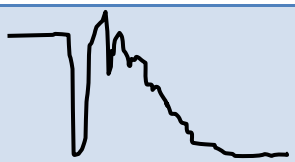	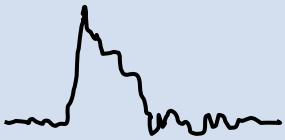

Figure 37 - Ball check valve lift with increasing RPM (Knight, 1961)

The report suggested that the effects of secondary waves set up in the system, should be minimised to prevent these residual waves from re-opening the nozzle. It concluded that the behaviour of both sprung and free-floating ball delivery valves are too dependent on the wave phenomena in the injection pipe and where ball check valves appear attractive in a design, then that specific application should be made and tested.

The reason for the commissioning of this report was that sprung ball check valves could offer a cheap substitute for mitre valves which were used at the time. Additionally it was thought that sprung ball check valves when fitted with unloading collars might have offered advantages over free-floating balls, although the absence of a spring would be more desirable as it would allow the clearance to be increased.

4.2. Needle Valve Review

Within the engine cylinder, before the effects of the ambient environment become dominant, it is the upstream fluid dynamics that are known to have the greatest influence on the initial spray plume development. The upstream fluid dynamics are determined by parameters such as fuel injector nozzle geometry, injection hole orifice diameter and the needle valve lift characteristics. These parameters all influence the characteristics of the injected fuel which in turn affects engine performance and exhaust emissions (Ramirez, et al., 2009). For this reason and in contrast with both ball and cone check valves, the perceived importance of the needle valve has led to it being extensively researched by FIE and engine manufacturers alike. Experimentally, there are two main approaches to investigating the needle valve, **Real size study** and **Large Scale Models**.

4.2.1. Real Size Study

Spray Plume Imaging

The simplest method of assessing needle valve performance on real-size components is through study of the spray plumes momentarily after the SOI Obviously this is not directly evaluating the needle valve itself, but looking for an effect that the needle has induced on the fuel prior to it passing through the injection holes. Where a needle lift sensor is not fitted, spray plume imaging can be supplemented with simulation data so that needle lift can be associated with plume development. The following passage discusses some key published papers that have used this approach in order to identify needle behaviour and its effects on the flow.

Using a high-speed camera, imaging of the spray plumes has been used to compare the sprays between a solenoid and a piezo-driven injector fitted with a mini-sac nozzle (Lee, et al., 2006). It was concluded that the faster needle opening rate with the piezo-driven injector, resulted in approximately 10% increased fuel delivery and higher levels of cavitation within the nozzle, although this was determined from CFD analysis. Optical observations of the plumes indicated that the increased flow and cavitation with the piezo-driven injector had a profound effect on spray plume development.

This same approach of spray plume imaging has also been used extensively to investigate VCO nozzle designs, where at low lift the needle valve entry-throttles the injection holes, often leading to a significant spray imbalance (Soteriou, et al., 1993). Placing the needle valve eccentrically on the large scale model was observed to generate the same sprays as witnessed on real size VCO nozzles, thus indicating that needle valve eccentricity is the mechanism for spray in-balance within real size nozzles.

Internal Nozzle Flow

In order to visualise the flow within the nozzle and injection holes of real size diesel injectors, early attempts focused on optically accessible components with much simplified geometries and then equating these findings to the actual components. Whereas most reviewed literature has primarily focused on using this technique for the purpose of studying the flow within the nozzle sac and/or the injection holes, occasionally this technique has provided useful data regarding the movement of the needle valve and/or the flow across its seat. This is of interest as at low needle lift, the restriction across the valve seat is critical to the low lift performance of the nozzle. Furthermore, cavitation bubble collapse not only has the potential to damage the sealing capacity of the needle valve but shed cavitation from this region creates a two-phase flow, thus complicating the downstream flow as it attempts to enter the injection holes. There exist two substantially more accurate approaches to providing optical access to the injector nozzle tip, these are:

1. **Removal of part of the nozzle tip and its replacement with a transparent insert or window.**

   Approximately one sixth of the sac of a 6-hole CR multi-hole nozzle was replaced with a quartz window providing optical access to a single injection hole whilst resulting in only minimal interference to the adjacent injection holes (Arcoumanis, et al., 2000) (Gavaises, et al., 2002). The injector body was also modified so that the needle valve could be held at a fixed lift in order to allow direct comparison with a steady-state enlarged transparent model of the same internal geometry. Although this technique did not allow visualisation of the flow past the seat at low needle lift, cavitation was observed upstream of the injection holes and is therefore likely to have been generated in the vicinity of the seat due to

the pressure drop and turbulence created across this restriction. The papers concluded that the CN is the most critical parameter controlling the cavitating flow structure and whilst complications exist between scaling of individual bubble dynamics, the cavitating structures inside the injection holes are comparable for both real size components and scalar models. In effect the findings of these two papers were used to validate the large scale modelling methodology.

2. **Removal of the entire nozzle tip and its replacement with a transparent replication of the removed geometry.**

   This second approach was used to study the flow in the injection holes and across the needle seat of a transparent VCO nozzle (Chaves & Schuhbauer, 2006). Optical access was provided by replacing the nozzle tip with a glass prism and fixing the needle at a large lift to prevent damage to the prism upon needle closing. Using RIM to prevent optical distortion and through back-lighting, cavitation bubbles appearing as black regions provided evidence of the internal flow structure. Strong 3D velocity components were observed in the flow within the injection holes at a range of cavitation numbers equivalent to those occurring in a CR equipped diesel engine. However, due to the large lift adopted for testing, no cavitation was observed across the needle seat. In an associated paper, the same glass nozzle arrangement was used albeit with a needle incorporating a glass tip (Miranda, et al., 2003). With this arrangement, testing was performed over a range of realistic cavitation numbers with the needle again set at a fixed lift but in an eccentric position. Images taken of the emerging plume at the exit of the injection holes appeared to show a vortex structure within the cavitating region itself.

   This same approach was used on a HD nozzle by removing the tip and clamping an identical geometry acrylic tip in its place. Internal nozzle flow was visualised for two differing needle opening rates which were produced by operating the injector dynamically using either a CR or a PLN system (Blessing, et al., 2003). At 800 bar rail pressure, the CR system resulted in a much slower needle opening compared to the PLN system. This has the effect of throttling the fuel during the early phase of the injection process leading to high local seat velocities. When

compared with the PLN tests, this resulted in greater turbulence, more uneven sac pressure distribution and a more unstable flow within the injection holes which persisted for a longer period of time. Differences in spray plume development and atomization between the CR and PLN systems were attributed to the observed dissimilarities in the internal nozzle flow. It was concluded that the rate of needle movement, particularly at the start (and probably also the end) of injection was proven to be decisive in the overall performance of the nozzle.

X-ray Analysis

In recent years a method has developed to assess the movement of the needle valve during dynamic operation by utilising very high energy X-rays which are capable of penetrating the nozzle tip, thus ensuring no modifications are required to the fuel injector nozzle. This unique approach allows direct comparisons to be drawn between the movement dynamics of the needle and the observed dynamics of the spray plumes as well as providing quantitative information regarding needle lift, necessary for accurate CFD simulation. Published literature has identified two X-ray techniques, radiography which has been used to provide density and structure detail from within the spray plumes and phase contrast imaging which has been used as a non-intrusive method to visualise internal machining and finishing defects within a fuel injection hole (Lee, et al., 2005). It is the most recent advances with this phase contrast technique that now permit measurement of needle movement both axially and laterally (wander) during an injection event. An example of this was a paper outlining the use of this technique to dynamically investigate two variants of the same single-hole axial nozzle with differing amounts of honing at 1000 bar injection pressure (Powell, et al., 2011). Phase-enhanced imaging indicated that significant eccentricity of the needle valve occurred during testing which correlated to oscillations in the fuel density observed near the outer surface of the emerging plume. CFD simulation to investigate this finding indicated that needle eccentricity can significantly affect the flow patterns inside the nozzle sac yet produce no significant changes in the nozzle exit flow structure. Non-published information has indicated that more recently this technique has been applied successfully on modern multi-hole CR nozzles to quantify needle lift and wander.

Ignoring X-ray analysis which requires a huge capital involvement, real size studies tend to be challenging as the fitting of a transparent insert, be it a window or a whole section, can affect the sealing and robustness of the nozzle. Often this places limits on the number of test injections possible, the maximum permissible injection pressure and habitually the injector cannot even be operated dynamically. Additionally, due to the small dimensions involved, when modifying real size components to make them optically accessible, it is difficult to avoid the creation of flow disturbances at the interface between the original component and the replacement transparent section(s). To avoid these limitations, the large Scale modelling technique is often adopted which allows the manufacture of scaled whole components or at least the regions of interest.

4.2.2. Large Scale Models

The use of Large Scale Models (LSMs) is a well-established technique widely used in fluid dynamics for the study of flow encountering complex geometries. Complicated models with intricate internal geometries can be manufactured to a precision that would not be possible with actual size transparent components. Testing of these models at equivalent REs to the real components requires much lower velocities and hence pressures, due to the increased dimensions as given by Equation 5. Owing to these reduced upstream pressures and by applying a high vacuum downstream, it is possible to obtain similar CNs to the real size components, as is evident from Equation 4. Often acrylic is chosen for the manufacture of these models due to its low cost and ease of fabrication, however, quartz or sapphire has been used where scaling factors are low and pressures are necessarily high. Due to the sheer size or even mass of most LSMs and owing to the complexities with scaling a dynamic event, testing is normally steady-state with in the case of a nozzle model, the needle valve held at a pre-set lift. Using high-speed cameras and high intensity lighting, uncompromised visualisation of these models is possible to provide a detailed understanding of the internal flow structure. Additionally, pressure tapings may easily be incorporated into these models and are able to provide quantitative information to assist with flow analysis or for the validation of simulation data.

As with the real size studies, the simplest LSMs have merely been basic 2D approximations of the real size geometry. In one example of this, high speed camera imaging was used to study the effects of asymmetric flow, needle lift and injection hole orientation (relative to the upstream flow) on in-hole cavitation and the emerging spray plumes (Sou, et al., 2011). Although the experimental test piece featured a much simplified geometry, it was concluded that at small needle lifts the increased thickness of the separated region at hole entry promoted inception and development of cavitation as well as deformation of the emerging spray plume. The latter finding was most interesting, with plume deformation appearing to coincide with the location of cavitation within the injection hole, possibly indicating the influence of shed cavitation on the spray plume structure.

Another interesting paper used a 10x scale model of a VCO diesel nozzle to assess the effects of needle eccentricity on internal cavitating flow and primary atomisation (Oda, et al., 2010). At 50µm real size lift, moving the needle eccentrically towards an injection hole was observed to produce three different cavitating structures within this injection hole when compared to the flow structure with the needle set concentrically. This eccentricity of the needle valve was also associated with the occurrence of a hollow-cone spray and the degree of needle eccentricity was linked to a change in the jet angle of the spray plume.

20x scale models of both a VCO and a sac-type nozzle were used to investigate cavitation erosion that had been observed to occur within real size components. CFD simulation along with instantaneous and time-averaged high speed camera images from both LSMs indicated that geometrically-induced in-hole cavitation, string cavitation and needle seat cavitation were occurring at low needle lift (Gavaises, et al., 2007). These cavitating regions were found to coincide with the location of cavitation erosion observed on the real size nozzles. LSM modifications were carried out on the sac-type nozzle design to reduce sac volume and allow a faster exit of the cavitation bubbles formed at the seat by way of a new needle design. Likewise, the VCO needle was redesigned to allow an easier flow into the injection holes at low needle lift. Both CFD and LSM tests indicated that the modified designs resulted in less likelihood of cavitation erosion.

The same author was also involved with a study of cavitation initiation and flow turbulence within the sac and injection holes of both a Mini-Sac and a VCO acrylic LSM. Adopting the principals of RIM, high speed imaging was compared with LDA data at two valve lifts equating to the 1st and 2nd stages of a production two-stage lift injector (Roth, et al., 2002). It was found that the Root Mean Square (RMS) values are higher at low needle lift, due to the reduced seat area causing the flow to be locally accelerated which slightly increased the turbulence levels from this point onwards. The link between cavitation and flow turbulence in the nozzle sac and the injection holes was quantified through LDV measurements. It was also found that higher turbulence levels at low lift led to more frequent string cavitation and at higher lift the cavitating flow patterns appeared to exhibit a more stable structure. These cavitation strings appeared mostly to be connected to the needle surface and were observed to extend to the hole exit.

A quite similar paper studied the effects of needle eccentricity at two lift conditions on a 20x scale LSM of a six-hole conical Sac-type nozzle both experimentally and through CFD simulation. Adopting the principals of RIM with high speed camera imaging and LDV, the flow and cavitation structure was observed at two eccentric needle conditions (Arcoumanis, et al., 1998). It was found that the flow initially entering the top of the injection hole with the needle concentric, would switch to flow below the needle tip and enter the opposite injection hole from below resulting in cavitation at the bottom of hole inlet when the needle was re-positioned eccentrically. Results also indicated that the eccentric needle generated swirling motion inside the nozzle sac which progressed through the injection holes and persisted until the hole exit, giving rise to different flow patterns at their exit. This could have ramifications for manufacturing as even minor variations from the design geometry could result in slight needle eccentricity and therefore unequal flow distribution between successive holes.

A paper which looked at the emerging spray plumes from a LSM as opposed to the internal nozzle flow, confirmed that not only is a hollow cone spray induced by an element of swirl as the fuel enters the injection hole but also by eccentricity of the needle valve (Soteriou, et al., 1995). It was observed that the two mechanisms producing unequal sprays on VCO nozzles at low needle lift is partial hydraulic flip or eccentricity of the needle valve.

Another paper by the same author investigated the flow and emerging plume from a transparent, entry-throttled, circular orifice adopting the principals of RIM (Soteriou, et al., 2000). At partial entry-throttling it was observed that the flow consisted of two parts, the mainstream core sometimes appearing to spiral slightly in the first half of the hole-length and a secondary flow from the sides of the opening which merged together and producing a flow that entwined the main flow. The resulting spray plume exhibited a wide variation in spray angle and the plume targeting[20] was unstable at most running conditions. Although this testing was on a simplified, single-hole orifice model, it is clear that this could indicate a mechanism for of the formation of poor and unequal sprays in multi-hole nozzles due to needle eccentricity effectively causing entry-throttled holes.

High speed imaging and PIV measurements were taken of the flow through a transparent axial single-hole (Ø8mm) acrylic model in order to investigate the relationship between cavitation (cavity) length and turbulence (Cameron, et al., 2008). High speed imaging indicated that the divergence of the liquid jet upon exit depended strongly on the cavity length along with orifice wall, whilst shed cavitation bubbles from hole entry inflicted a significant influence on the structure of the exiting spray resulting in rapid jet divergence and atomisation. PIV results were only possible at the least cavitating conditions but indicated that turbulent kinetic energy was highly dependent on the cavity length and less so on the RE.

4.2.3. Limitations of Large Scale Modelling

Whilst it is difficult to accurately replicate the highly transient conditions found within real size components, perhaps the most challenging issue is with the small scale of the actual components. For instance, with LSMs it is possible to accurately set such parameters as needle lift, upstream and downstream conditions or even maintain constant fluid properties. With real size components, however, these parameters cannot be set and often they are unknown and have to be assumed. Taking for example a LSM of an injector nozzle with the needle valve positioned concentrically. In a real size component

[20] Plume targeting is a term used to describe the positioning of the injected fuel spray plumes to ensure they interact with the cylinder and piston geometry optimally

the needle valve is guided some distance from its tip such that the valve might spend a large proportion of its non-seated operation in an axially eccentric position. Thus the LSM is not accurately replicating the actual operation of the real size component. Additionally, the formation of cavitation bubbles is thought to originate from either nuclei present within the bulk fluid (homogeneous nucleation), or from nucleation sites along the walls of the nozzle (heterogeneous nucleation). Whereas real size nozzles will contain numerous tooling marks and indentations, the interior surfaces of the LSMs are highly polished to ensure a high degree of optical clarity. Therefore the latter mechanism of nucleation is expected to prevail in real size nozzles, which exemplifies the importance of parameters such as wall surface roughness when comparing between real size and LSM data. Moreover regarding cavitation in real-size nozzles, cavitation bubbles have been observed to collapse within the nozzle hole, whereas in the corresponding LSMs they tended to survive to the hole exit suggesting a different bubble life and collapse time (Arcoumanis, et al., 2000).

Whilst the cavitating structures inside the injection holes having been found to be comparable for both real size components and LSMs, it has to be stressed that it remains absolutely necessary to give appropriate consideration to the concerns outlined above when comparing between any real size and LSM data.

4.3. Scaling Between Real Size & Large Scale Models

The scaling methodology between real size and LSM adopted in this thesis is derived from assuming that the model (and the real size component) behaves as a single orifice. In light of this it is only strictly correct to use this scaling at full needle lift where the restriction across the valve seat can be assumed to be negligible. Ideally for all other lifts it is necessary to consider the nozzle as being two orifices in series, firstly the valve seat and then the injection holes, which further complicates the scaling as the properties within the nozzle sac are not usually known and have to be assumed. However, at full needle lift the influence of the needle valve on the flow is relatively insignificant; therefore the needle valve can usually be neglected allowing the nozzle to be treated as a

single orifice. Consequently at full needle lift the following scaling is applicable (Equations 12 and 13).

4.3.1. Deriving Scaling Equations

The scaling is derived by rearranging the C_d equation (Equation 8) and inserting this into the equation for flow (Equation 6). Taking this new equation and substituting this into the Reynolds number equation, we derive the following equation for Re (Equation 11).

$$\boldsymbol{Re} = \frac{\boldsymbol{C_d} \cdot \sqrt{\frac{2\Delta P}{\rho}} \cdot d}{\nu}$$

Equation 11

Equating Equation 11 between a real size orifice and a scalar model of this orifice, C_d can be cancelled as it will remain constant. By multiplying this out, the following equation can be obtained for model pressure drop (Equation 12) and model flow (Equation 13), with the $_r$ and $_m$ subscripts referring to real size and model respectively.

$$\Delta \boldsymbol{P_m} = \Delta \boldsymbol{P_r} \cdot \left[\frac{\boldsymbol{d_r}}{\boldsymbol{d_m}}\right]^2 \cdot \left[\frac{\boldsymbol{\nu_m}}{\boldsymbol{\nu_r}}\right]^2 \cdot \left[\frac{\boldsymbol{\rho_m}}{\boldsymbol{\rho_r}}\right]$$

Equation 12

$$\boldsymbol{Q_m} = \boldsymbol{Q_r} \cdot \frac{\boldsymbol{d_r}}{\boldsymbol{d_m}} \cdot \frac{\boldsymbol{A_m}}{\boldsymbol{A_r}} \cdot \frac{\boldsymbol{\nu_m}}{\boldsymbol{\nu_r}}$$

Equation 13

It can easily be seen from Equation 12 that if the fluid properties are the same between model and real size, the viscosity and density terms cancel leaving real size ΔP_r greater than model ΔP_m by the square of the scale factor. This is a scaling assumption that has been adopted in the past when scaling between the

LPR and real size components, but not with the LBFR due to the vastly different working fluid adopted with this rig. However, in recent years, higher injection pressures (and hence fluid temperatures) have altered the fluid properties within the real size components such that density and viscosity can no longer be neglected during scaling.

4.4. Summary of Literature Review

As was mentioned in section 4.1, it was found difficult to obtain past research of relevance to check valves in FIE applications or even regarding check valves experiencing similar operational conditions. Perhaps this indicates that (at least within the FIE sector) up until now, check valves have not been considered worthy of investigation or that their performance was too difficult to accurately study. Whatever the reasons, the author has identified a distinct lack of past research in high pressure applications. Some of the reviewed papers from the power generation sector in particular did however suggest interesting methods of improving the transient performance of check valves, but mostly owing to the small scale of the FIE components these methods would not be possible or would prove cost prohibitive to implement.

Section 4.2 detailed published literature which investigated the flow entering the nozzle sac and in doing so encountering the needle valve. In contrast to check valves, this region has been heavily studied both experimentally and through simulation as the flow within this region is known to be extremely influential on the combustion process. The two principal approaches to investigating this region involve either optically accessible real size components or enlarged scale steady-state models. Real size study of accurate internal geometries is remarkably difficult at modern CR fuel injection pressures owing to manufacturing, robustness and sealing issues, therefore not much published literature exists concerning this approach. Furthermore with future trends suggesting higher injection pressures alongside further reductions in sac volume and injection hole sizes, these difficulties are likely to be exuberated. The technique of enlarged scale models as adopted within this thesis is a well-established approach often used in the study of fluid mechanics. Owing to the large amount of literature which exists in the public domain, only research which

focused on diesel FIE components of accurate geometry (as opposed to 2D approximations) was included in this thesis. The x-ray technique is a an interesting method allowing study of needle motion without any modification to the injector nozzle, however this requires specialised facilities and techniques not readily available. Therefore not much published literature currently exists on this method but the author anticipates even further development and optimisation of this technique in the coming years.

5. CHAPTER 5 – EXPERIMENTAL PROJECTS

This chapter details four main experimental projects that have been investigated during the course of this PhD. The findings or conclusions are included for each project in turn, with a final discussion in Chapter 6 having the purpose of colligating and comparing all the respective findings. Details regarding the experimental test rigs mentioned here may be found earlier within Chapter 2.

5.1. Ball Delivery Valve LSM

Within Delphi's DFP3 CR fuel pump, the high pressure outlet or delivery valve is a 60° conically seated ball valve. To investigate this component with the aim of improving its operational performance, a 10x scale acrylic LSM was commissioned with square external geometry to limit refraction at the air/model interface. The interior geometry featured a Ø25mm upstream bore, a Ø40mm downstream bore and the valve element itself was a Ø35mm acrylic ball. Mounting flanges and O-ring grooves allowed the model to be connected to the LBFR downstream of a long straight section of pipe with the purpose of acting as a flow straightener.

Background

Initial plans to investigate the steady-state flow over an unsupported ball were rejected owning to the destructive and even violent interaction between the ball and the valve seat. Flowing in the opening direction with the ball lift fixed by means of a concentrically located lift-stop, the ball appeared to be spinning around its own axis whilst following a circular motion around the axis of the flow. Such 3D motion made it exceedingly difficult to analyse the flow with simple 2D LLS and PIV techniques. Furthermore at sufficiently high flow rates, the ball would often be moving laterally around the axis of flow with such velocity that repeated impact with the edge of the valve body would cause the acrylic ball to crack and eventually shatter. Early attempts to prevent this destructive motion with the ball supported by means of a rigid rod, unfortunately resulted in a situation removed from the real life operation of the valve.

5.1.1. Eccentric Flow Insert – LLS Analysis

A solution was reached to the destructive ball motion through a lift-stop with an eccentric flow opening to trap the ball element to one side of the model when flowing in the opening direction. Figure 38 is a solid model of the side and end views of this assembly with the ball at rest at the bottom of the model (identified in blue) and a red dashed box to indicate the target area for the LLS and PIV techniques. Normal flow direction is left to right to represent the valve in the opening or positive direction.

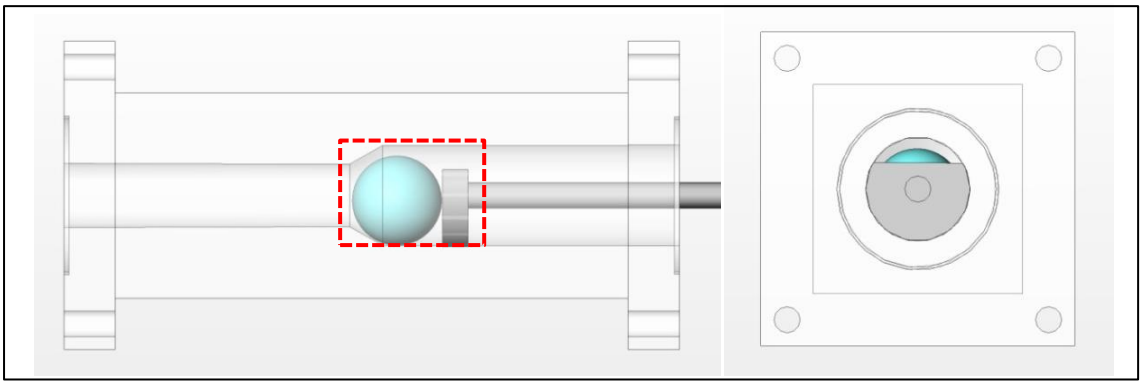

Figure 38 - Side and end views of the CAD model assembly

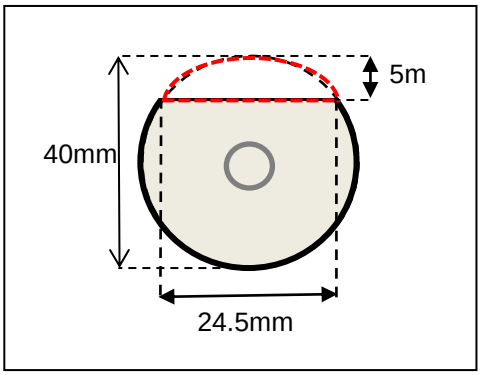

Figure 39 - Eccentric flow insert

Figure 39 is a schematic indicating the dimensions of the eccentric insert with a red dashed area indicating the flow opening.

LLS images are shown in Figure 40 with the insert orientated so that the flow opening is at the top of the model and the laser light sheet located at the model's central axis.

5mm Ball Valve lift

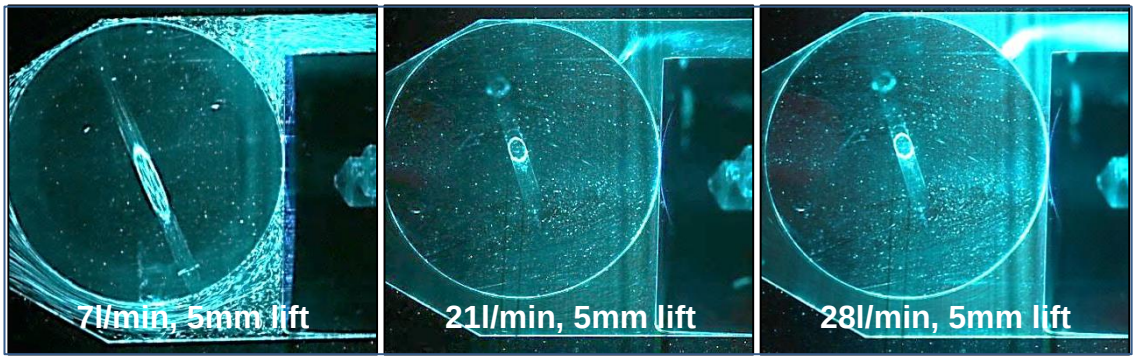

Figure 40 - LLS images with insert at 5mm lift – Stable behaviour

Observations – Figure 40

The ball initially at rest at the bottom of the model with a density of 1190 kg/m³ is 33% more-dense and therefore has a third greater mass than the working fluid (896 kg/m³) it displaces. However, as the flow was increased, it was observed that the ball lifted against the gravitational forces and moved upwards towards the flow outlet where the ball remained stationary. This behaviour is likely the result of the highest fluid velocities occurring in the regions above the ball and therefore producing the lowest static pressure. This movement although not likely beneficial to the fully opened flow characteristics of the valve, has at least resulted in stabilizing the ball motion. In Figure 40, the first image was captured at a flow rate of 7 l/min in the opening direction with the insert setting the ball lift at 5mm (full lift or 500µm real size). The second image, again at the same lift but at 21 l/min, appears slightly darker as the higher fluid velocities required a shorter camera exposure than at 7 l/min. This flow rate was detected as being the onset of cavitation which occurred at the centre of a vortex, formed where the flow which had split to travel different directions around the obstruction (ball), has recombined. Close to the centre of this vortex where the velocities are sufficiently high, the static pressure has dropped below the vapour pressure and cavitation has occurred. The third image in Figure 40 was captured again at 5mm lift but at an increased flow of 28 l/min. The vortex, initially seen at 21 l/min has now grown in strength so that intense cavitation is occurring at its centre and overpowering the scattered light from the seeding, thus making it difficult to detect the path lines.

Generally speaking at 5mm ball lift it was observed that with successively higher flow rates and even after the onset of cavitation, the ball remained in a stable position at the top of the model.

2.5mm Ball Valve Lift

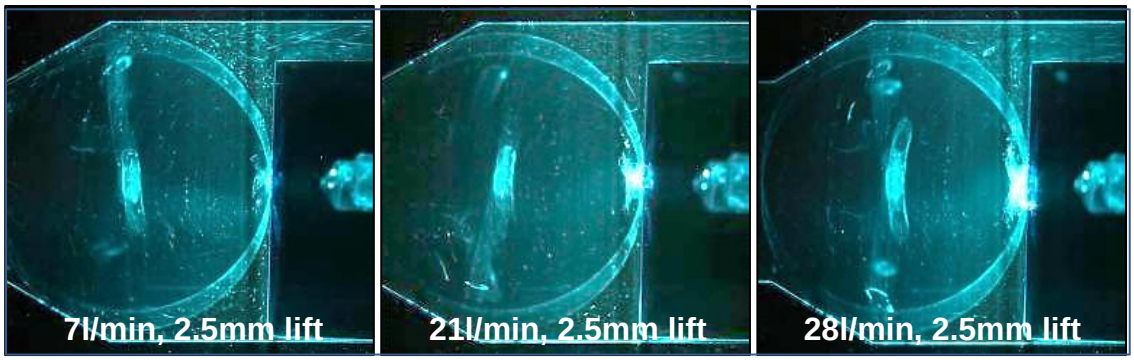

Figure 41 - LLS images with insert at 2.5mm lift – Unstable behaviour

Observations - Figure 41

Figure 41 contains images taken at the same flow rate as before but at a reduced lift of 2.5mm. Unlike at 5mm lift, the ball was no longer stable but rapidly rotated around the axis of flow whilst apparently revolving around its own axis in quite the same manner as was described in the background section. It is this rapid ball motion which has resulted in the apparently double exposed camera images with the rate of movement of the ball appearing to grow with increasing flow rate. Possible evidence of weak vortices were also detected like those witnessed at 5mm lift, however, these were less defined as quite likely the ball motion was interrupting their development. After running at 28 l/min for only a short period of time (~60 seconds), contact between the insert and the ball was observed to cause localized surface damage to the ball. This is apparent in the image as a high intensity region where the two parts touch. It is evident that unlike at 5mm lift, the ball is no longer in a stable condition at 2.5mm lift.

0.8mm Ball Valve Lift

Attempts to run the model at 0.8mm lift and the same range of flow rates as at 2.5 & 5mm lift were halted due to a much more violent motion of the ball with an associated loud contact or grinding noise. It was likely that this noise was the

result of forceful contact between the ball and the insert and possibly also the valve seat. In light of this, the 0.8mm lift testing was not completed.

5.1.2. Eccentric Flow Insert – PIV Analysis

Due to the erratic nature of the ball motion at 2.5mm & 0.8mm lift, it was chosen to perform PIV at 5mm lift & 10 l/min in the opening direction which is a non-cavitating condition as cavitation could compromise the quality of the PIV data. This equated to a Re of 5000 in the upstream (Ø 25mm) circular bore which indicates that that flow should be turbulent (Munson, et al., 2006). Where the flow velocity varies substantially across the PIV camera's target area or field-of-view, it is often difficult to select a single optimum 'dt' value '(the time interval between successive laser pulses) for the entire region. Therefore in an attempt to increase PIV accuracy, the PIV camera was moved closer to the model to separately encompass four distinct regions, thus allowing optimum 'dt' values to be chosen for each region. These four regions are displayed in Figure 42. For the PIV testing, as with the LLS images the light sheet was located at the model's central axis.

These measurement regions were:

Region 1 - Upstream of the valve seat
Region 2 - Across the valve seat
Region 3 - Between seat and the restriction
Region 4 - Across eccentric flow restriction

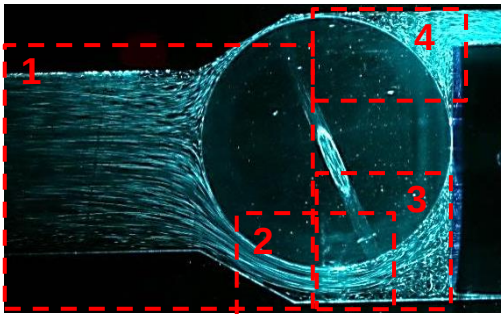

Figure 42 - Ball valve PIV measurement locations

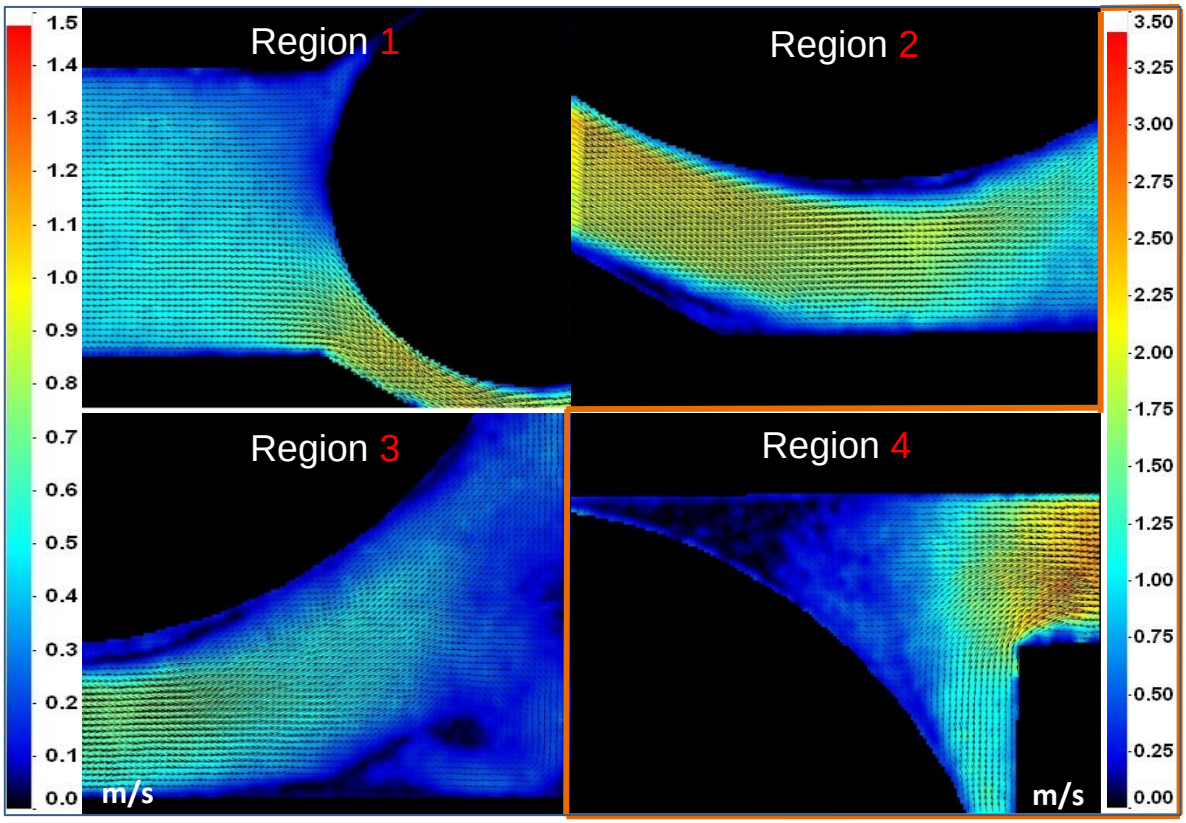

Figure 43 - Mean PIV velocity contours regions 1 – 4

Figure 43 contains mean PIV velocity contour plots for each of the four regions. Due to the larger velocities found to occur at region 4 compared to the other three regions, a different velocity scaling range had to be adopted. Therefore regions 1, 2 & 3 all use the LHS scale with a maximum velocity of 1.5m/s whereas region 4 uses the RHS scale (surrounded with an orange box) with a maximum velocity of 3.5m/s.

Observations- Figure 43

1. Not overlooking the likely 3D nature of the flow in this model, the flow in **Region 1** is seen to accelerate from the upstream bore into the seat region between the ball element and the valve body.
2. In **Region 2** the flow is seen to diminish in velocity as it expands through the restriction formed between the ball and the valve body. A gradual thickening was observed of the separated or detached flow along the ball's surface which at 5mm lift remained stationary.

3. In **Region 3** the flow is forced to move upwards towards the flow opening in the insert and in doing so, a vortex is observed to develop which shears against the main body of the flow resulting in a 'finger' of low velocity flow where these interact.
4. In **Region 4** the flow is observed to travel up the surface of the insert and accelerate as it passes through the eccentric flow opening with the flow detaching from the sharp leading edge. This increase in velocity is likely to be due to the flow being funnelled into the light sheet plane due to the geometry of the insert.
5. A general observation was that no high velocity flow was seen above the ball when looking at regions 1 or 4. Therefore the presumed high velocity flow that has resulted in the low pressure region (to lift the ball element against gravity), must exist either side of the model's central axis.

5.1.3. Project Conclusions

The LLS and PIV techniques have shown that it is possible to stabilize or control damaging or undesirable valve behaviour with the addition of a novel design of lift-stop, at least during steady-state operation and 5mm lift. Taking this forward, it is highly likely that a lift-stop with a suitably designed eccentric flow opening could result in a ball valve which is stable across the whole operational lift range. However, further testing is necessary to determine whether a lift-stop such as this would potentially affect the valve's performance such as to result in a design with an unacceptable head loss or even a poor opening and closing behaviour. Whereas the experimental testing in this project has been steady-state, due to the highly transient nature of this component within a fuel injection pump, transient testing is necessary to evaluate these findings further. Furthermore, due to complications with instrumentation of real size components and with the previously mentioned difficulties with real size transparent components, simulation would likely be the best route to obtaining an optimum design of lift-stop with experimental study better suited to validate any findings.

5.2. 120° Seat Nozzle Project

Whereas typically the needle valve inside a fuel injector nozzle features a 60° conical valve seat, the 120° seat design was a new concept intended to provide a larger seat area and therefore a larger flow at low needle lift. This is advantageous for modern multiple injection strategies comprising pilot, split-main and post injections, where the needle valve is spending an increasing duration at low lift. Depending on the nozzle design, maximum needle lift varies; however, in this thesis low needle lift shall be regarded as being the first 15% of needle opening, or until 30µm for a design which lifts to 200µm. A concern with this 120° design when compared against nozzles with 60° or even 90° valve seats is that the fuel is required to undergo a large flow turn when attempting to enter the injection holes. Large flow turns have been associated with instability and boundary layer detachment possibly leading to cavitation and ultimately poor injector transient performance. Therefore this project is of specific interest within DDS to determine the effect a 120° seat design would have on the flow entering the injection holes.

5.2.1. LSM Design & Manufacture

A 20x scale LSM was designed and manufactured to evaluate the 120° seat design. The model was based on a real-size production nozzle with a full lift flow of 0.86 l/min at a pressure drop of 100 bar. This production nozzle incorporated seven tapered injection holes of Ø 139µm and set at a cone angle of 155°. To aid optical access on the LSM, the number of holes was reduced to 6 requiring that the hole sizing be increased to ensure the same flow area. Additionally, a reduced nozzle C_d of 0.8 was assumed due to the LSM being designed with parallel or cylindrical holes which would likely result in greater amounts of in-hole cavitation. This also required an increased hole sizing to ensure the same effective C_d as given the following equation:

$$\boldsymbol{C_{d1} \cdot A_1 = C_{d2} \cdot A_2}$$

Equation 14

where A is the flow area of the injection holes. The parallel holes were a necessity owing to previous unsatisfactory results when attempting to accurately and repeatedly manufacture tapered injection holes in acrylic. With a scale factor of 20, this equated to six equispaced injection holes of Ø 3.1mm on the LSM.

Stanley Plastic Ltd, a specialized firm with over 50 years' experience of acrylic manufacturing was chosen to fabricate both the 120° nozzle model and its associated needle valve. The needle valve shall henceforth be referred to as the 120° Reference needle for reasons that will become clear later. Post manufacturing the LSM was then honed using the Abrasive Flow Machining (AFM) process to create hole inlet radii comparable with those found on the real size nozzle. This resulted in average inlet radii of 0.11 and 0.16mm at the top and bottom (or 12 and 6 o'clock) of the inlet to the injection holes as is indicated in Figure 44.

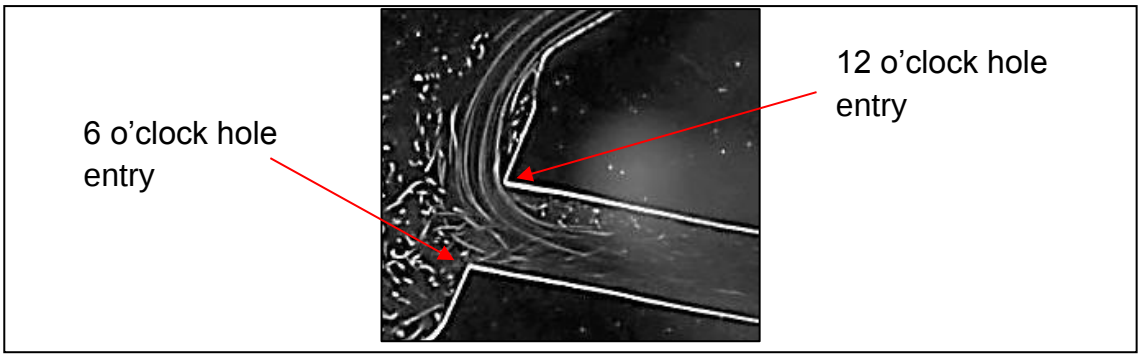

Figure 44 - Hole entry rounding

An additional advantage of the AFM process is that it removes machining marks from within the nozzle sac and particularly the injection holes which obviously benefits optical imaging. The AFM process used to create the inlet hole conditions on the LSMs differs from that described previously for the real size nozzles. The methodology is described below.

5.2.2. AFM Method for Nozzle LSMs

A honing media containing 10µm abrasive cutting particles is forced through the model at a ∆P of 25 bar. Being a trial-and-error process which is sensitive to parameters such as model geometry and media temperature, periodically the model needs to be removed from the AFM machine and assessed by taking and measuring silicone impressions of each of the injection hole bores. The LSM is then successively honed a number of times, each for a short period of time until the correct hole inlet rounding geometry has been generated. Often it is not possible to generate the same degree of inlet rounding as found on the real size components, due to the LSM's holes 'barrelling' which is where the media begins to miss-shape the injection hole bore instead of generating an inlet radii. Once 'barrelling' begins to occur it is accepted that the maximum hole entry radii has been generated.

Figure 45 contains side and plan views of CAD models for the 120° seat nozzle model alongside the Reference needle. Attached to the nozzle model are 6 black 1½'' BSP pipe fittings which have the purpose of returning the injected rig fluid back to the tank and also to allow the incorporation of pressure tapings. Owing to confidentiality reasons it has not been possible to include the LSM drawings in this thesis.

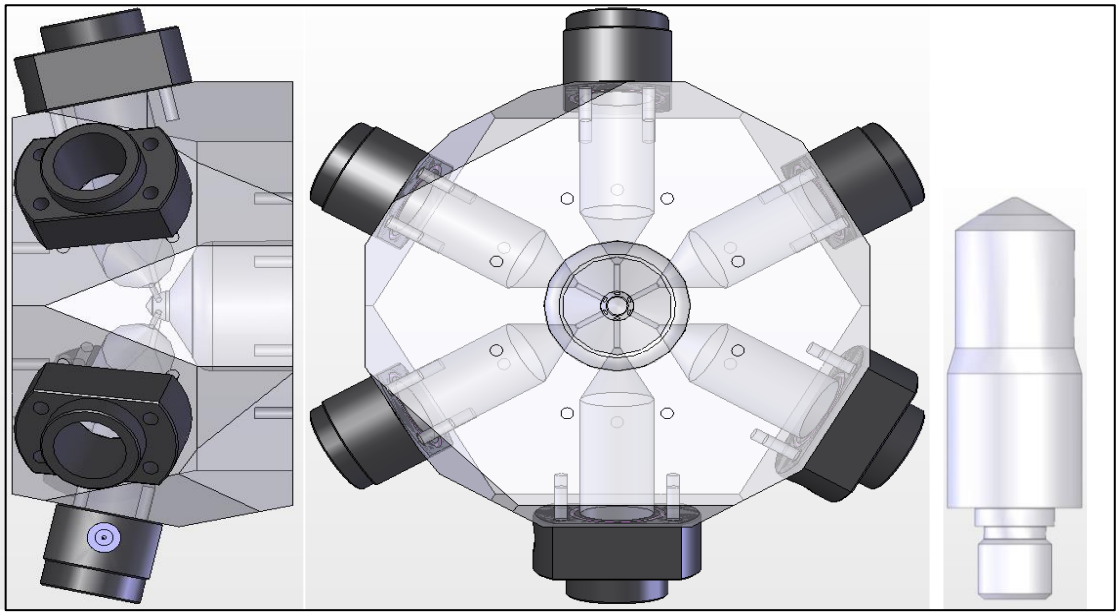

Figure 45 - 120° seat nozzle LSM nozzle and needle valve

Areas of Maximum Restriction

Most nozzles feature four possible areas of maximum restriction (or minimum flow), three of which are dependent on the needle geometry and its lift, whereas the fourth occurs at the injection holes. These four areas are:

1. Valve seat - the area between the needle valve's seat and the nozzle body
2. Truncation - the area between the start of the needle truncation and the nozzle body. Sometime the truncation location is also referred as the tip-change angle location.
3. Sac entry - the area between the needle valve and the start of the parallel section on the nozzle body at the entry to the sac volume.
4. Injection holes - the sum of the cross-sectional areas of the injection holes. For converging tapered injection holes this is taken at hole exit which is the minimum hole area.

This 120° Reference needle design is what is referred to an un-truncated needle and therefore only has three possible areas of maximum restriction. Figure 46 is a section-view of the tip of the 120° seat nozzle with the Reference needle coloured green and the locations of the three areas of maximum restriction identified by the (red) numbers, 1, 3 & 4.

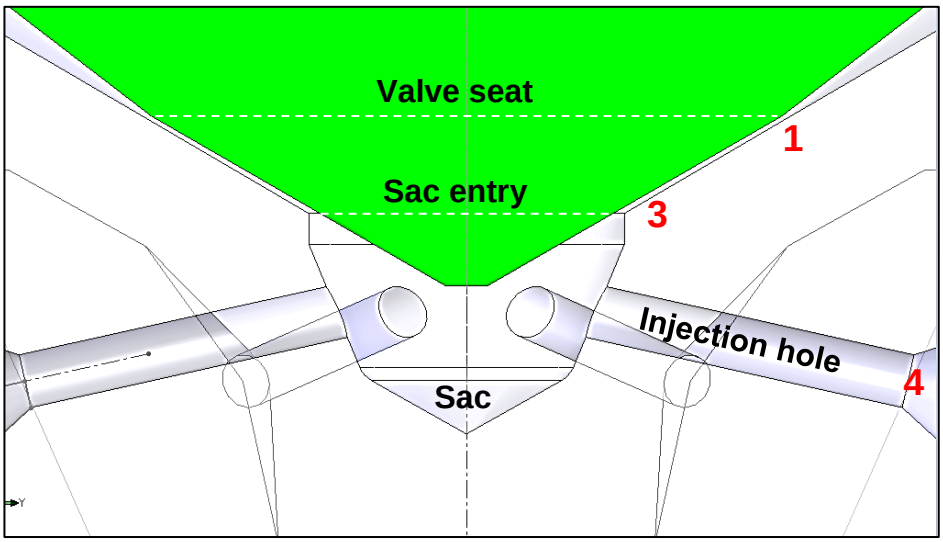

Figure 46 - CAD section view of 120° seat nozzle LSM with Reference needle

The three areas of maximum restriction have been calculated and are graphically displayed in Figure 47. It is evident that with this design as the lift is increased the maximum restriction initially at the seat moves to the sac entry location after only 0.14mm lift. The maximum restriction then persists at this location until 0.8mm lift where the injection holes dictate the minimum flow area.

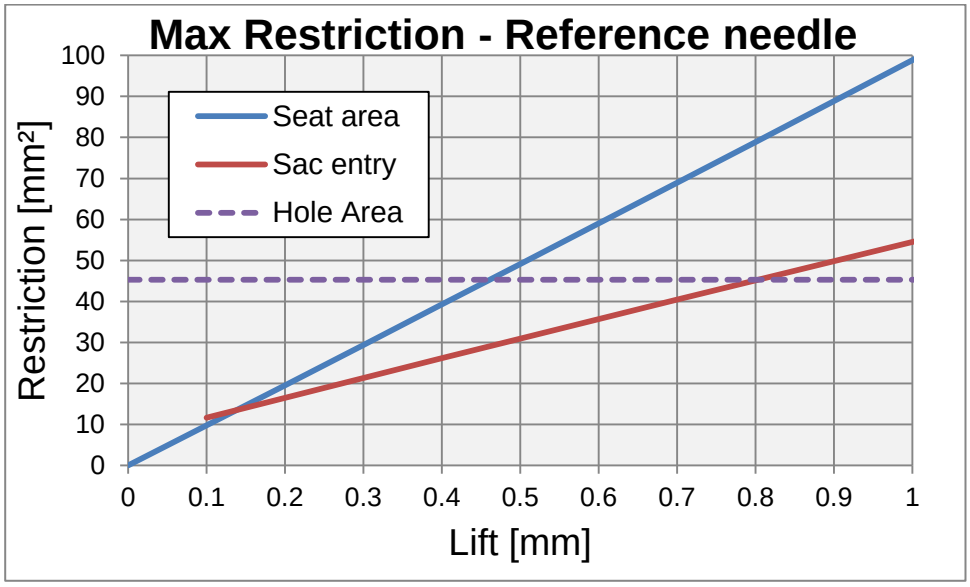

Figure 47 - 120° Reference needle flow areas

As a means of evaluating the performance of the 120° seat LSM with the Reference needle, a flow versus lift plot was produced. This is displayed in Figure 48 containing experimental data at 1.0 and 2.0 bar. The LSM data has been separated into opening and closing directions to identify any hysteresis and ranges up to 4.0mm needle lift, which is full lift for this design (200µm real size).

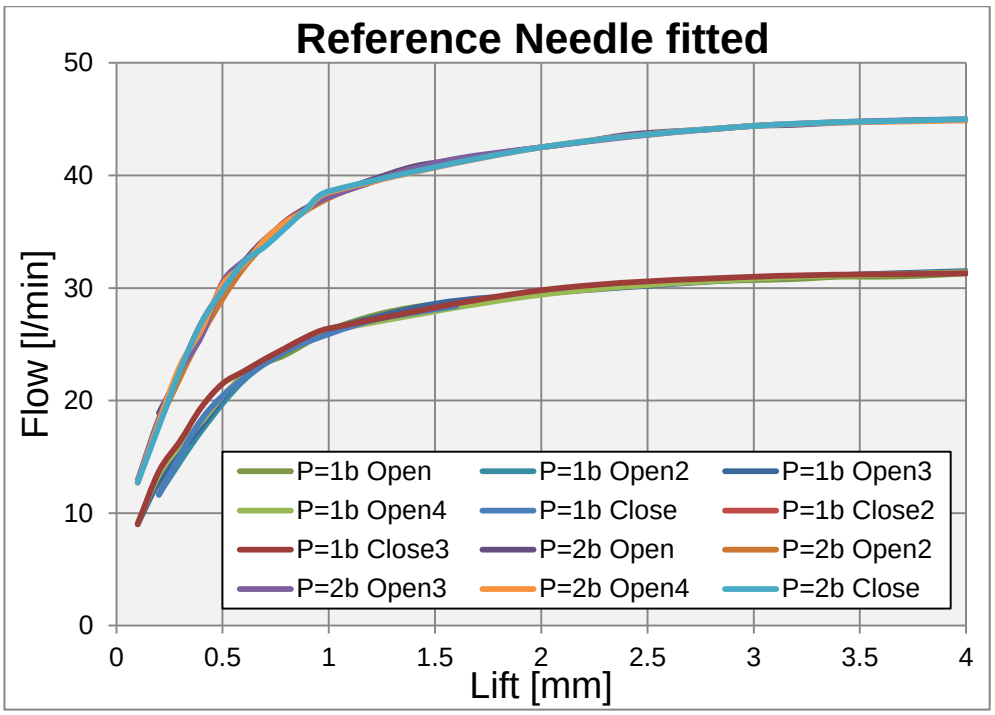

Figure 48 - Reference Needle Flow versus Lift

The LSM experimental plots do not indicate any obvious hysteresis however, both the 1.0 and 2.0 bar ΔP LSM plots appear to show an increase in flow with lift until ~3.0mm, where the flow begins to plateau and is seen to increase only very slightly during the remaining 25% of lift. This is in all likelihood due to the influence of the needle valve on the flow diminishing as the lift is increased.

5.2.3. Flow Transition

Previous unpublished research within DDS (Torres, n.d.) has indicated that with some injector nozzle designs a transition occurs with the flow entering the sac choosing to flow either along the surface of the nozzle body or along the surface of the needle valve. With the needle valve at low lift and moving in the opening direction, it is believed that the flow follows the surface of the needle before transitioning to follow the nozzle body once the needle has reached a predetermined lift. Additionally, experimental evidence has indicated hysteresis with this transition occurring at a different lift position when the valve is moving in the closing direction. Furthermore, CFD simulation and real size experimental data has indicated that this flow transition could be associated with performance instability and a change in the hydraulic lifting force on the needle. This change in lifting force could obviously be detrimental to the lifting

(and closing) behaviour of the needle valve and therefore the performance of the injector itself. Unfortunately it is not possible to measure needle lift force with any of the LSM test rigs described earlier, hence only flow velocity data shall be analysed regarding this flow transition.

5.2.4. Flow Overshoot

The aforementioned unpublished research within DDS has also identified a flow phenomenon linked to the flow transition which has been referred to as a 'flow overshoot'. This is where the flow entering the nozzle sac and following the surface of the needle valve penetrates too deep into the sac and overshoots the entrance to the injection holes. Because of this the flow has to undergo and large flow turn to enter the injection holes from below.

5.2.5. LBFR Reference Needle - Opening CN 3

In an attempt to fully understand the development of this flow transition, the LSM was assessed with the valve nominally concentric and moving between 0.2 and 0.7mm lift, which is within the range of lifts where the flow transition was expected to occur. Due to a combination of rig and LSM limitations, the range of cavitation numbers that are possible when using the Laser Based Flow Rig (LBFR) is limited. Whereas the inherent weakness of the acrylic model limits the maximum permissible upstream pressure, the sealing of the rigs vacuum tank restricts the minimum downstream pressure obtainable. Therefore CN 3 was realistically the maximum cavitation number permissible and consequently was adopted for study of cavitating flows.

Figure 49 consists of PIV velocity contour plots which were collected in the opening direction with the upstream and downstream pressures set at 0 & -0.75 bar respectively which equates to CN 3. A scale of between 0 and 6.5m/s has been adopted. Each image is the average of 30 individual PIV frames captured at a frequency of 5Hz with LIF seeding and a suitable camera edge filter, thus permitting greater laser intensities than are possible with conventional PIV. With the laser light sheet positioned at the central axis of the model, the camera was orientated perpendicular to this for optimum PIV accuracy in determining the V_X and V_Y components whilst minimising any V_Z component of the flow.

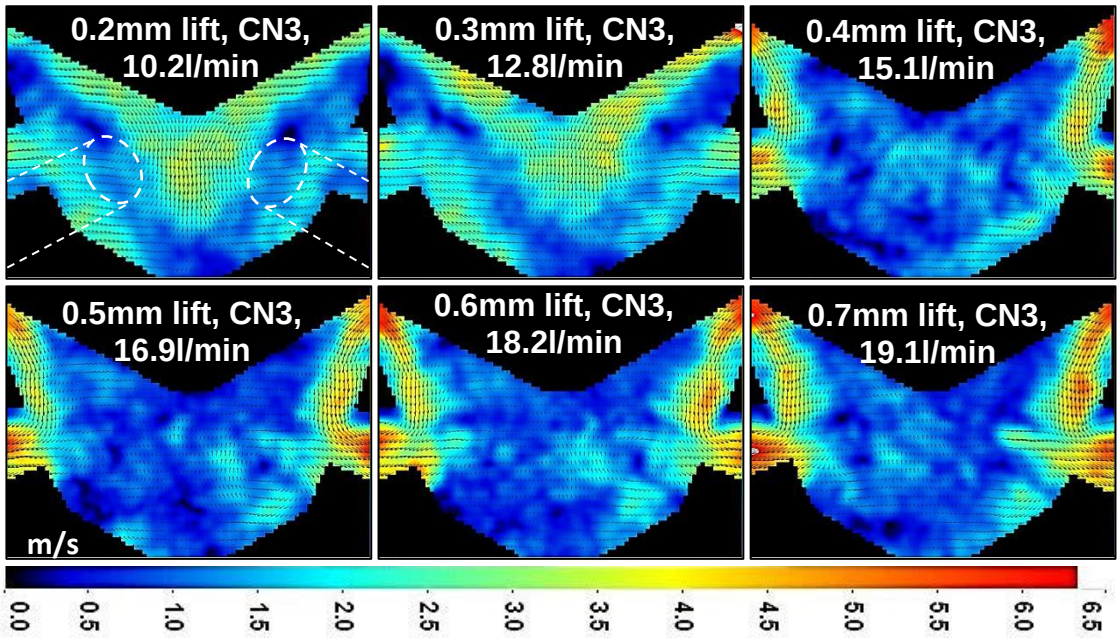

Figure 49 - PIV velocity contours - Reference needle opening – CN 3

Observations – Figure 49

1. At 0.2 & 0.3mm lift it is evident that the main flow is travelling along or near the surface of the needle valve and progressing deep into the nozzle sac. It is not altogether clear how this occurs, but in all likelihood the flow then moves momentarily out of the light sheet plane before returning to travel up the nozzle body to enter the injection hole from below. Although only the inlet of the two visualised holes is visible, the high velocity or bulk flow appears to be confined to the top of the injection hole with a significant sized separated flow at the bottom.
2. By 0.4mm lift the flow has transitioned to flow within a narrow band close to the surface of the nozzle body. It also appears to enter the injection hole from above resulting in a separated flow at the top of the injection hole with the bulk flow confined to the region below this.
3. At 0.6 & 0.7mm lift, alongside the main flow entering the hole from above, a secondary flow is seen to enter the injection hole from below. This could be the result of flow moving into the light sheet plane in an attempt to enter the injection holes. Perhaps this was not seen at 0.4 & 0.5mm lift as the flow rate was lower being more heavily throttled by the restriction at the valve seat.
4. Superimposed on the 0.2mm lift images are dashed lines indicating the position of the two injection holes located between the light sheet and the

PIV camera. Intense cavitation in either of these holes may prevent light emitted by (as light is technically not scattered by fluorescent seeding) the LIF seeding from reaching the PIV camera, potentially leading to areas with poor quality or even inaccurate vectors. This could be another mechanism for the observation of the secondary flow entering the holes from below at 0.6 & 0.7mm lift. This is an example of one of the complexities of using PIV to analyse two-phase flows.

5.2.6. Spray Visualisation – Real Size Nozzle

In an attempt to assess what effect the observed flow transition may have on the spray plume development, the real size 120° nozzles were tested on the Spray Visualisation Rig which is designed to represent in-cylinder engine conditions except at non-evaporating conditions. Further details about this rig can be found in the Spray Visualisation Rig section earlier in this thesis. The real size nozzle geometry is not identical to the LSM hole geometry as the real size nozzle contains 7 tapered injection holes, although this difference is accounted for during the model design as mentioned in the LSM Design & Manufacture section.

Figure 50 consists of sequential side and front images of the developing spray plumes at running conditions of 400 bar upstream (rail pressure) and 60 bar downstream (chamber pressure). This equates to a CN of 5.7 which although is higher than CN 3, allows an approximate comparison with the PIV internal flow data in Figure 49.

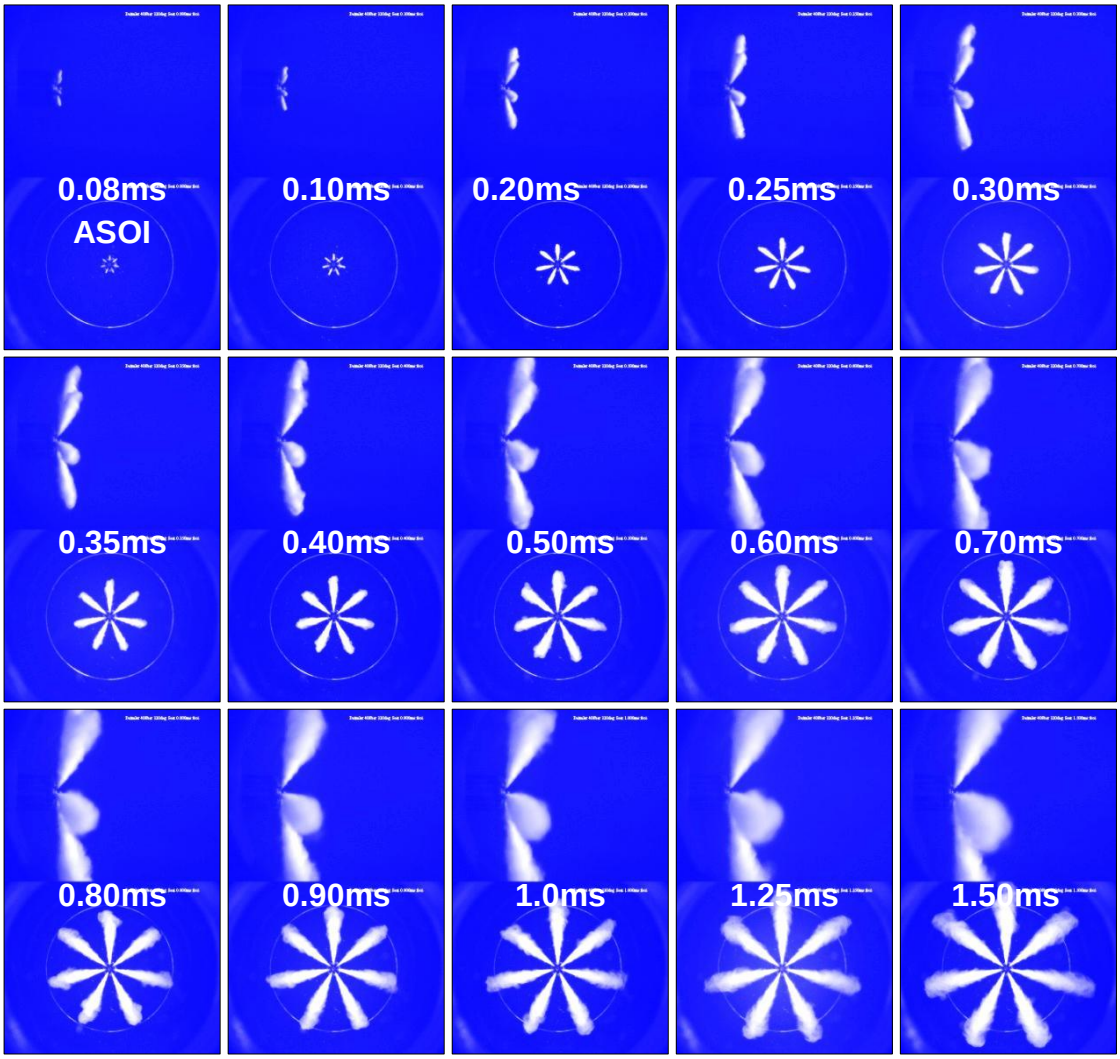

Figure 50 – 400 bar Spray Visualisation Images (Images obtained by colleague in DDS)

Observations - Figure 50

As the nozzle was not instrumented, no data relating to needle lift was available. Therefore the images are labelled in terms of time ASOI (After Start of Injection) rather than needle lift. The notable observations are:

1. The plume development rate is quite fast for such a low injection pressure, which is a feature of the 120° seat design having a relatively large flow area at low needle lifts.
2. Although the interval between successive images is not constant, the plume development and bushiness seems to be reasonably consistent with no evidence of irregular plumes which could indicate instability.
3. Regarding the side images, there did not appear to be any change in the plume targeting although this is difficult to detect from these images due to the bushiness of the spray plumes.

4. All plumes appear to have developed symmetrically suggesting that the flow in the sac is relatively uniform and the needle has not moved laterally to throttle any of the injection holes which is usually indicative at low lift of a poorly performing nozzle design.

5.2.7. FEATS Needle Design Variant

A new needle valve has been designed within the Simulation and Physical Modelling department of the Advanced Engineering Group at DDS. The intention of this design is to improve the fuel flow into the injection holes whilst diminishing the effects of any flow transition in the flow arriving into the nozzle sac. This design is referred to by the acronym FEATS which stands for 'Flow Enhancer and Transition Stabiliser'. As mentioned previously, the occurrence of a flow transition and the resulting overshoot can potentially lead to unstable injector transient performance. A needle design which improves the fuel flow into the injection holes would likely allow for nozzles to be designed with a higher C_d to increase fuel spray plume penetration and to aid air/fuel mixing, particularly at low needle lift. A further advantage of the FEATS design is that it penetrates deeper into the nozzle sac than the Reference needle; this brings an additional benefit in sac volume reduction when the valve is seated. This is a recent trend that is emerging amongst FIE manufacturers as a large sac volume has been associated with increased UBHC emissions.

In order to evaluate this new FEATS design, a 20x scale needle valve of this geometry was commissioned for comparing against the 120° Reference needle. Whilst both designs share the same seat angle and diameter, principal differences exist between their respective areas of maximum restriction. This is illustrated for the FEATS design in Figure 51 and also Figure 47 for the Reference needle. In comparing these plots, the FEATS design features a much increased area at sac entry when compared to the Reference needle. The result of this is that unlike the un-truncated Reference needle, the area of maximum restriction with the FEATS needle moves rapidly from the seat to the truncation location until 0.66 mm lift, upon which it moves to the injection holes, slightly earlier than occurs with the Reference needle. Due to the unusual FEATS design, the previous description of the truncation location is perhaps no longer valid. Therefore in the case of the FEATS needle, the truncation is

regarded as being at the end of the needle's 120.75° conical section and the start of its unusual tip geometry.

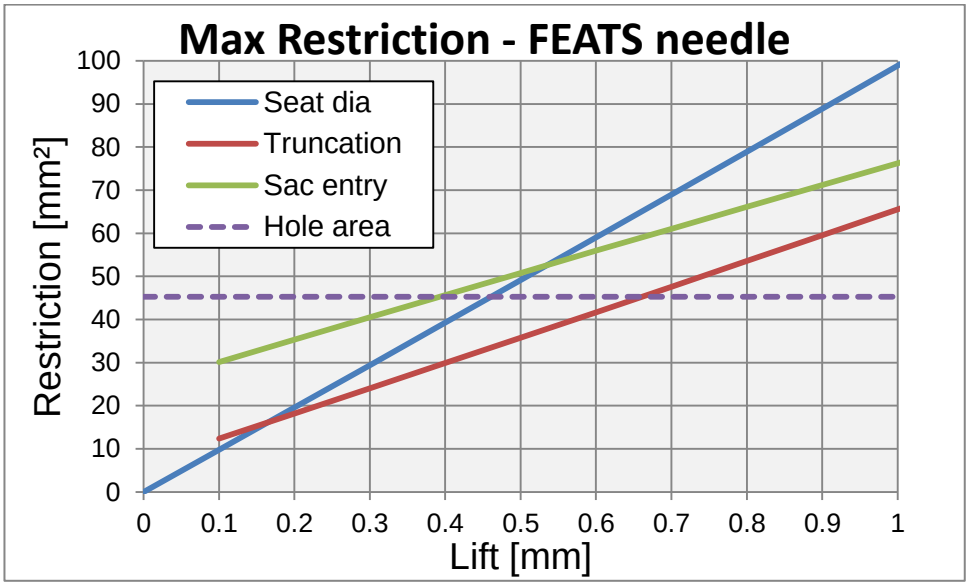

Figure 51 - 120° FEATS needle flow areas

As with the 120° Reference needle, the performance of the FEATS needle was evaluated by means of a flow versus lift plot. Figure 52 contains data from the 120° seat nozzle LSM fitted with the FEATS needle on the LBFR at 1.0 and 2.0 bar ΔP. This data has been separated into opening and closing directions to assist the identification of any hysteresis.

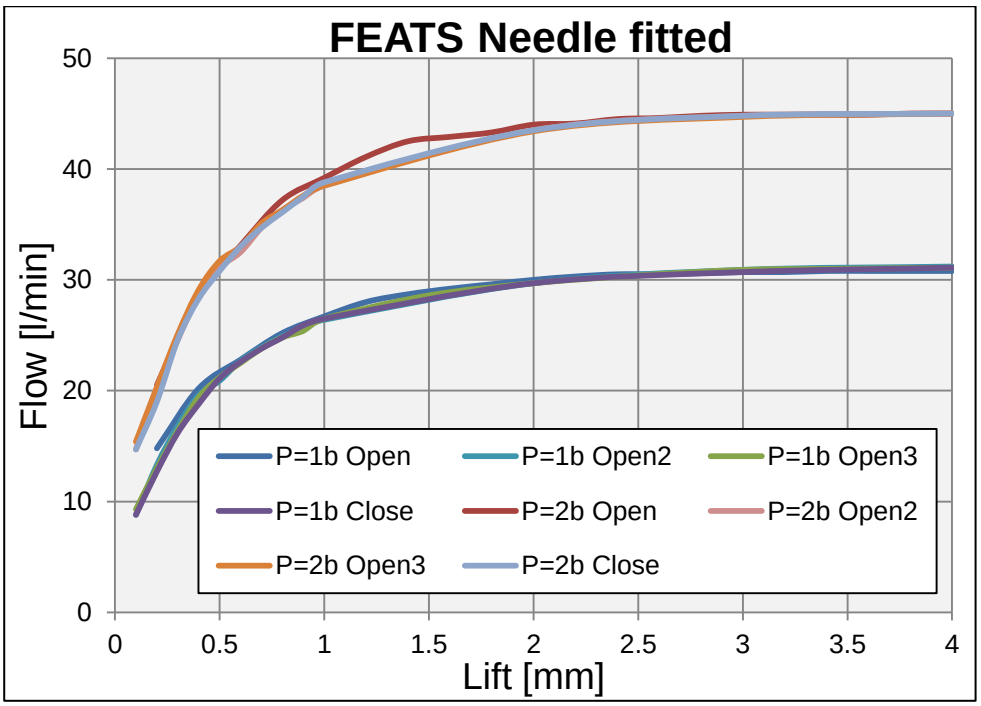

Figure 52 - FEATS needle Flow versus Lift

The LSM experimental plots do not indicate any obvious hysteresis however, the *P=2b Open* case does contain some outlying points more likely accountable for by experimental error. Overall the data appears to show an increase in flow with lift up until ~2.5mm, where the flow begins to plateau and is seen to increase only very slightly during the remaining increase in lift up to 4.0mm.

In order to evaluate the performance of the FEATS needle against the Reference needle, their internal nozzle flows were compared across a range of lifts and at two differing running conditions. These conditions were a (mostly non-cavitating) constant flow rate of 20 l/min and a (cavitating) constant pressure condition of CN 3. Both LLS and PIV techniques were adopted.

5.2.7. LBFR Reference needle – Opening 20 l/min

Laser Light Sheet (LLS) images are able to assist with determination of the flow structure by providing qualitative information within the nozzle sac and the injection holes. Details of the methodology for capturing these images may be found in the Laser Light Sheet Illumination section earlier in this thesis. Figure 53 comprises a sequence of LLS images taken in the opening direction between 0.2 mm and 4.0 mm needle lift (10 µm to 200 µm on real size components) at a constant flow rate of 20 l/min which equates to a Reynolds

number of 14,000 within the injection holes. Atmospheric pressure was applied downstream and although 20 l/min was chosen as a non-cavitating condition, cavitation did occur but only at the very lowest lift. The needle valve was set nominally concentrically with a vertical laser light sheet illuminating the model from below at the central axis of two of the injection holes, effectively intersecting the six-hole model in half. Although taken at mostly non-cavitating conditions, it is common practice to angle the camera downwards 15° from the horizontal in order to prevent any cavitation within the holes in front of the light sheet plane from obscuring the flow in the illuminated plane. It is for this reason that the remaining injection holes illuminated by cavitation at 0.2 mm lift do not appear to fall on the same PCD as the two holes intersected by the light sheet. The red path-lines apparent in the first six images are from fluorescence of the LIF seeding which was mixed with the conventional seeding within the LBFR working fluid. This seeding was filtered out prior to capturing the remaining nine images, hence in these images the only path-lines present are a result of the hollow glass spheres reflecting the green 532nm laser light.

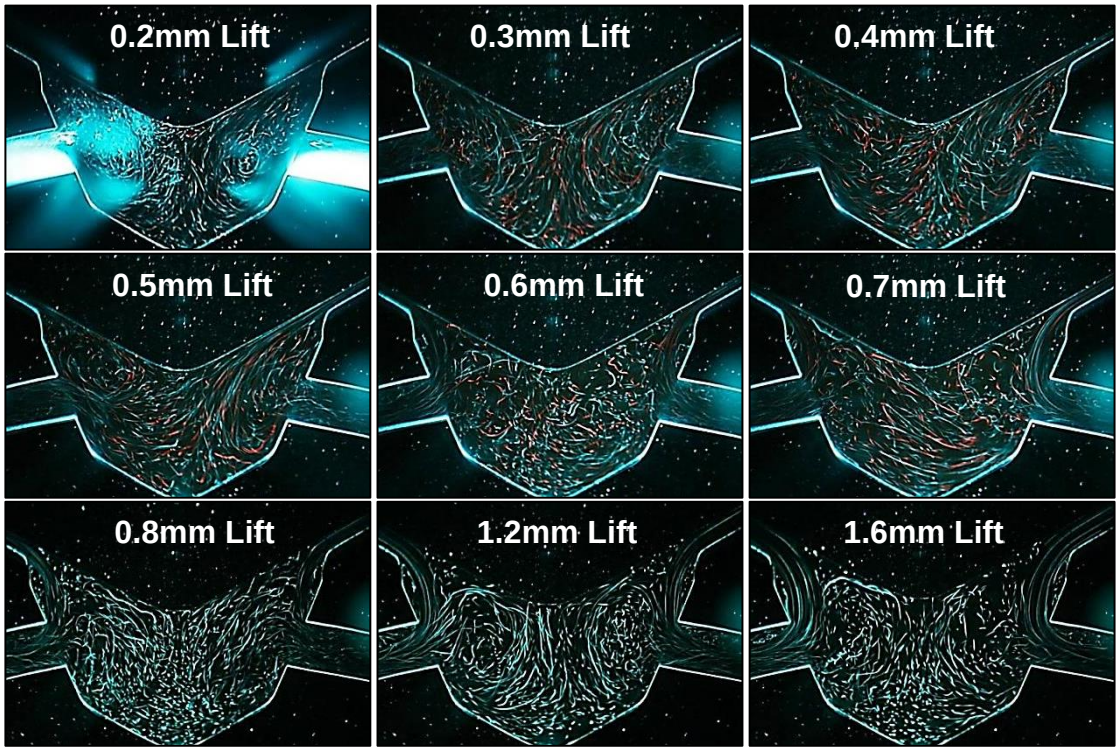

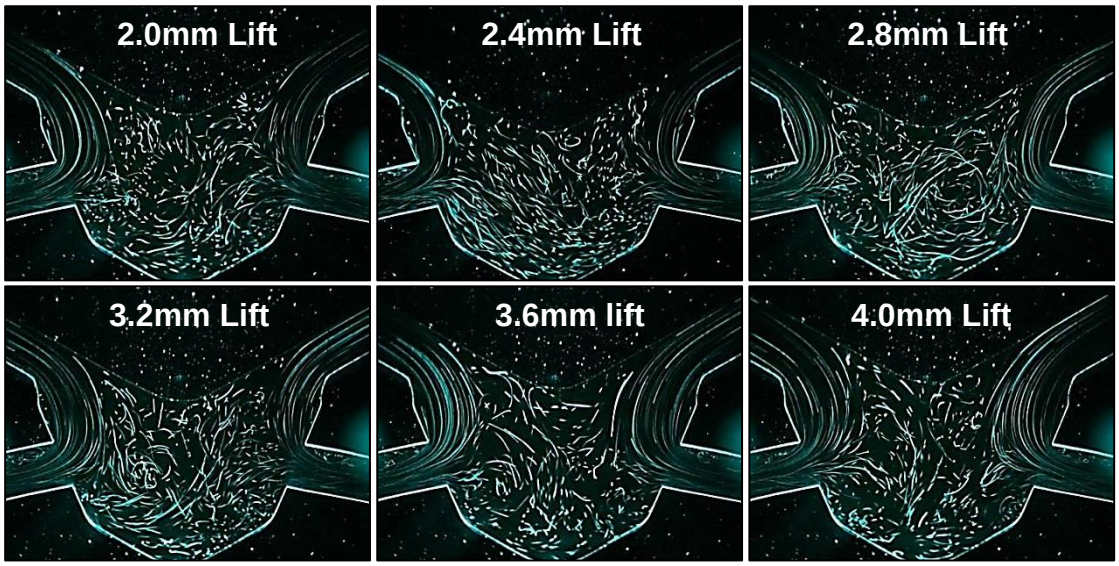

Figure 53 - LLS images with Reference needle opening – 20 l/min

Observations - Figure 53

1. It is apparent from the LLS images that the flow, initially attached to the needle valve has transitioned to follow the nozzle body between 0.5 & 0.6mm lift. The flow then continues to follow the nozzle body throughout the remainder of the lifting range.
2. Between 0.2 & 0.5mm lift with the flow following the needle valve, the flow penetrates deep into the sac and over-shoots the injection holes. In doing so the flow is noted to be turning sharply and travelling back up the sac and entering the injection holes from below. In the 0.2mm lift case this is associated with hole-entry cavitation which is confined to the bottom of the hole at entry.
3. Eccentricity is detected in the flow at 0.5mm lift but this was not clearly evident at other lifts.
4. If these tests had been captured at a cavitating condition, it is likely that at lifts ≥0.6mm cavitation would be present at the top of the injection holes as the flow entered the injection holes from above. This is potentially important as a change in the location of this hole entry cavitation will affect the spray plume development and potentially its targeting and penetration.
5. Between 0.8 & 1.6mm lift a reverse flow is visible in the region below the needle valve tip. It would appear that flow from deep within the sac is moving upwards along the needle surface before encountering the

arriving main flow and being drawn out of the injection holes. Owing to the opposite direction of this flow compared to the overshoot observed at lower valve lifts, this has been referred to as a 'reverse overshoot'. As the origin of this flow cannot be discerned it is possible that this is flow moving into the light sheet plane and/or a precursor for vortex motion within the holes in-front (or behind) the light sheet plane.

PIV Images

The LLS images are only able to provide qualitative information regarding the flow structure. In order to provide quantitative information, PIV testing was carried out at the same running conditions, in the same valve opening direction and the same light sheet plane orientation. Due to difficulties keeping the LIF seeding in suspension within the LBFR's working fluid, unlike the previous testing at CN 3, only normal PIV was used for these tests. Like the CN 3 PIV tests, the camera was positioned perpendicular to a laser light sheet and unless stated to the contrary, this arrangement is adopted during all PIV experimentation as this is optimum for vector quality. Each PIV vector image in Figure 54 is the average of 20 individual images and all are scaled with a velocity scale of between 0 & 18m/s.

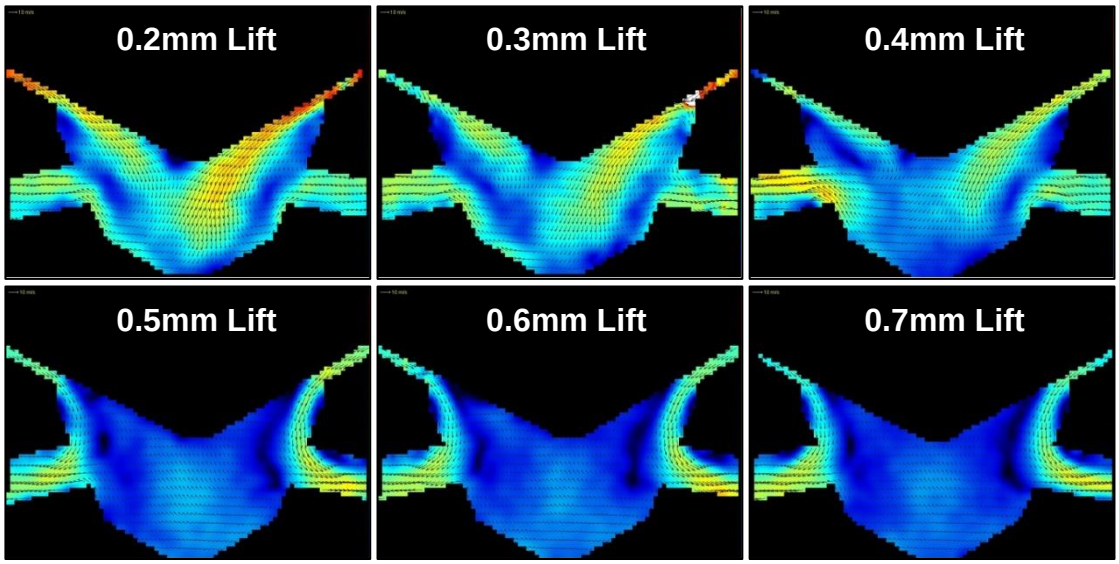

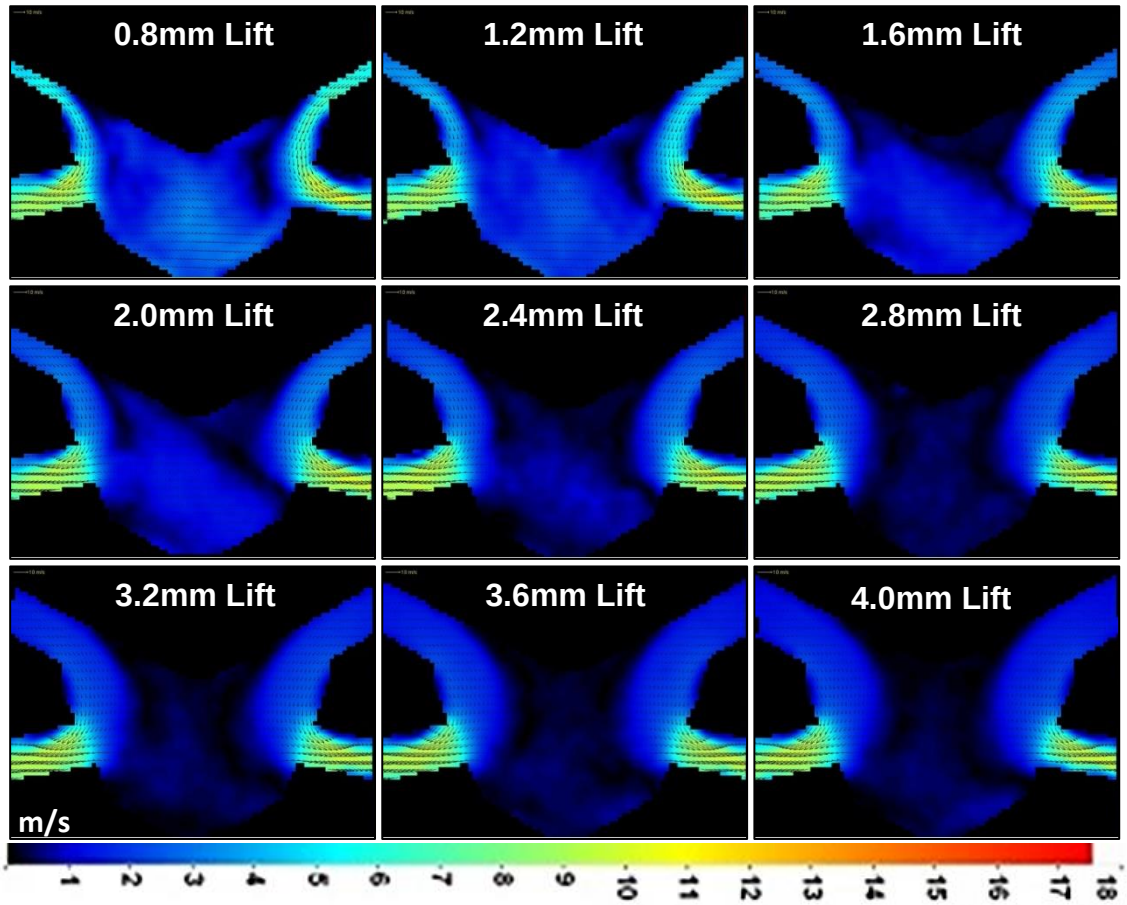

Figure 54 - PIV velocity contours - Reference needle opening – 20 l/min

Observations - Figure 54

1. The most striking observation from the above images is that the flow appears highly eccentric especially up to and including 0.4mm lift. Perhaps indicating that the needle is slightly eccentric at this lift.
2. The PIV results indicate that the flow transition occurred between 0.4 and 0.5mm. This is slightly different to the LLS images where it appeared that the transition occurs 0.1mm in lift earlier. Considering that the experimental conditions were identical, this just goes to exemplify how chaotic and unstable the flow (and transition) is at low needle lift.
3. At 0.2mm & 0.3mm lift, large velocities are seen directly below the needle tip as fluid flowing down opposite sides of the needle valve combines and directs itself towards the very bottom of the sac. As manufacturing tolerances are known to be loose at the bottom of the sac, it is highly likely that geometry variations between successive production nozzles could affect the plume development at low needle

lifts. Furthermore, interaction and shearing between these two high velocity flows could potentially lead to increased vortex activity within the sac.

4. At lifts ≤0.4mm, the flow velocity close to the needle surface is almost five times greater than the velocity at this location for lifts ≥0.5mm. This undoubtedly will affect the local static pressure and possibly the needle lifting force.
5. At lifts ≥0.4mm, there appears to be a very low velocity migration across the sac from right to left mainly along the bottom and diagonally up through the centre. This is most likely due to slight geometric imperfections in the model and/or the injection holes.

5.2.8. LBFR Reference needle - Closing 20 l/min

In order to test for the effects of hysteresis, the 20 l/min LLS testing was repeated but with the needle being moved between 0.7 and 0.2mm (35µm and 10µm real size) in the closing direction. The results can be seen in Figure 55. Only this range of lift was re-assessed as this is the interesting region where any flow transition might be expected to occur. In an attempt to increase the intensity of the illumination and allow for a shorter camera exposure, the laser light sheet generating lens was moved closer to the model. A disadvantage of this is that only half of the nozzle was visualised, however, any highly eccentric flow as with the opening direction tests still remained evident.

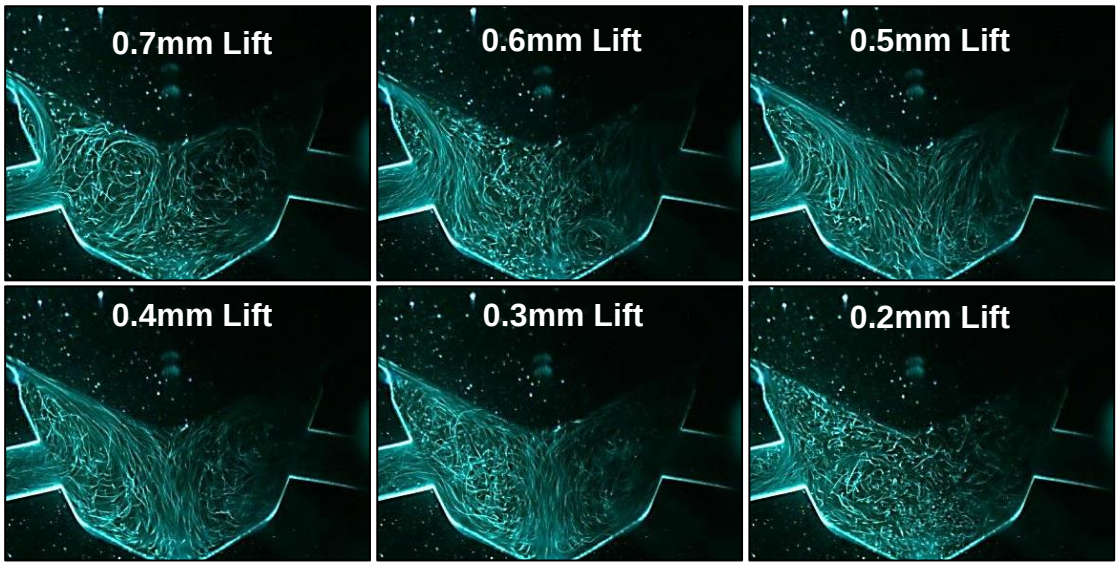

Figure 55 - LLS images with Reference needle closing – 20 l/min

Observations – Figure 55

1. At 0.7mm lift, the main body of flow is flowing along or at least close to the nozzle body before entering the injection hole from above. Other observations include a lesser secondary flow seen to enter the injection hole from below and a reverse flow upwards from the bottom of the sac towards the needle tip, similar to that witnessed in the opening direction LLS images.
2. At 0.6mm lift, the image appears to have captured the flow midway through a transition as the flow is neither following the nozzle body, not the needle valve. Therefore 0.6mm lift is the flow transition point.
3. At 0.5mm lift, the flow following the needle valve appears to penetrate deep into the sac and overshoot the injection hole. This is even more apparent at 0.4 & 0.3mm lift where the flow is clearly seen to reach the bottom of the sac before turning to flow up along the sac wall and enter the injection hole from below.
4. At 0.2mm lift, it is difficult to discern any dominant flow structure probably due to the higher sac velocities and increased turbulence induced by the restriction across the valve seat. However, unlike with the opening direction (where cavitation was constant), there was only intermittent bottom hole cavitation which indicates a degree of hysteresis.

As with the opening direction tests, the 20 l/min closing direction LLS tests were repeated between 0.7mm and 0.2mm lift for PIV. Again each vector image in Figure 56 was produced from the average of 20 individual PIV images and each has the same scaling range as the opening direction tests.

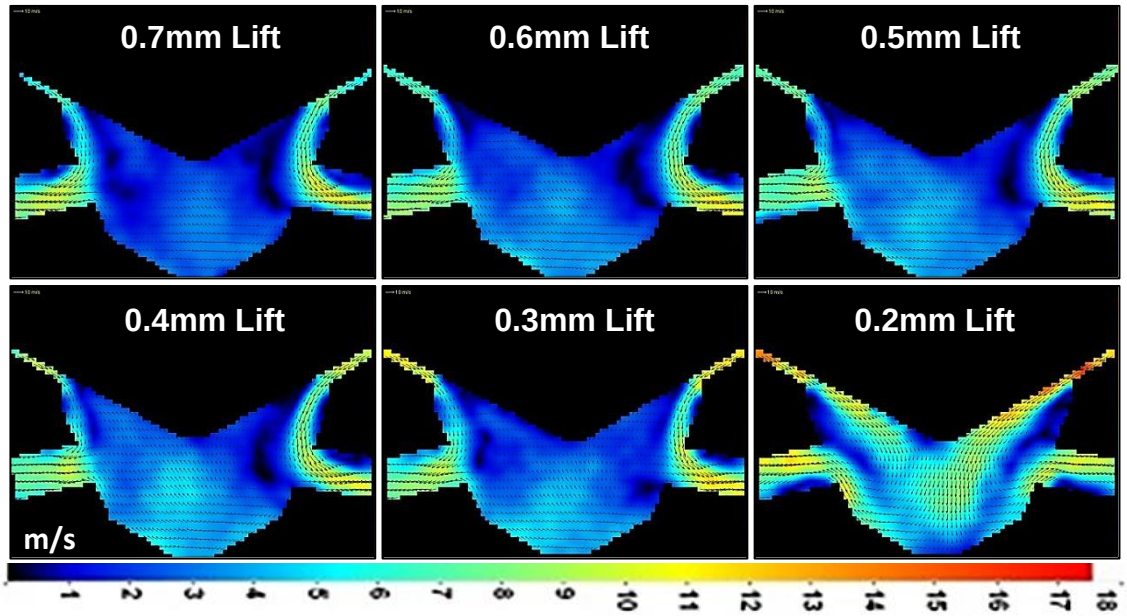

Figure 56 - PIV velocity contours - Reference needle closing – 20 l/min

Observations - Figure 56

1. The PIV images indicate that the transition occurred between 0.3 and 0.2mm, with the flow following the needle valve and overshooting the injection holes only at the lowest lift.
2. Between 0.7 and 0.3mm lift, the highest velocities within the sac (~9m/s) were found in the flow following the nozzle body with the velocities in the centre of the sac comparably much lower (~3m/s). The dark, low velocity regions within the sac and close to the vicinity of the injection holes could be associated with the reverse flow that was evident in both the opening and closing LLS images.
3. With the flow following the needle valve, the same low velocity migration or dominance from right to left across the sac was detected as in the opening direction PIV results.
4. Similar to the opening direction results, the closing direction PIV data indicates that with the flow following the needle valve, the velocity in the

region close to the surface of the needle has increased almost five fold compared to when the flow was following the nozzle body.

To complement the mean vector data, the RMS velocity contours were created from the same 20 individual PIV frames but without vector arrows having been superimposed. Adopting a smaller scaling range of between 0 and 8m/s, the RMS values are an excellent way of identifying any variability within the flow.

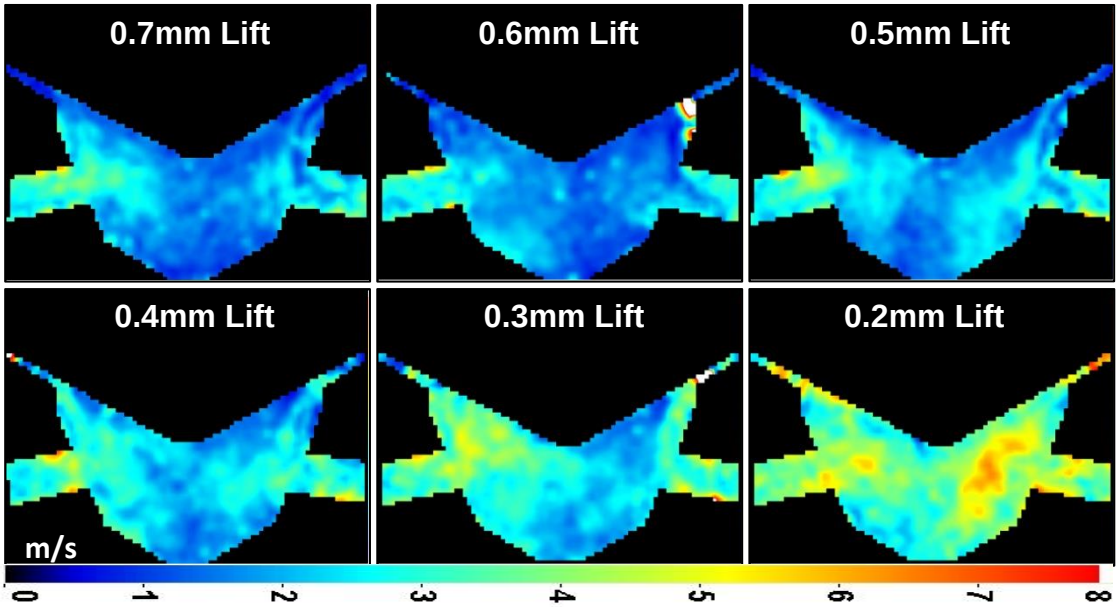

Figure 57 - RMS velocity contours - Reference needle closing – 20 l/min

Observations- Figure 57

1. With the exception of 0.2 & 0.3mm mm lift, the highest RMS magnitudes occur within the injection holes rather than the nozzle sac, indicating this is where the max flow variability occurs.
2. At 0.3mm lift, much greater RMS magnitudes were observed within the nozzle sac in the region between the left hand side injection hole and the needle valve tip. It is likely that this is due to instability where the flow is momentarily switching to follow the needle valve although not for any significant duration as to afflict the mean velocity vectors.
3. At 0.2mm lift, large variations in the flow exist across the majority of the nozzle sac at least in this light sheet plane. This indicates that the flow overshoot results in significant variations in the in-nozzle flow which is conceivable as having a (likely negative) influence on the spray plumes development, targeting and penetration.

5.2.9. LBFR FEATS needle - Opening CN 3

To offer a direct comparison, the FEATS needle design was tested using the LLS imaging and PIV techniques at the same running conditions as the Reference needle. Again these were CN 3 in the opening direction and 20 l/min in both the opening and closing directions.

The PIV results from the CN 3 testing with the FEATS needle between 0.2 & 0.7mm lift are displayed in Figure 58. The upstream and downstream running conditions were -0.19 and -0.8 bar respectively (which equates to CN 3). Unlike the case with the Reference needle, the raw PIV images have been included below each vector image to help identify the location of any in-hole cavitation.

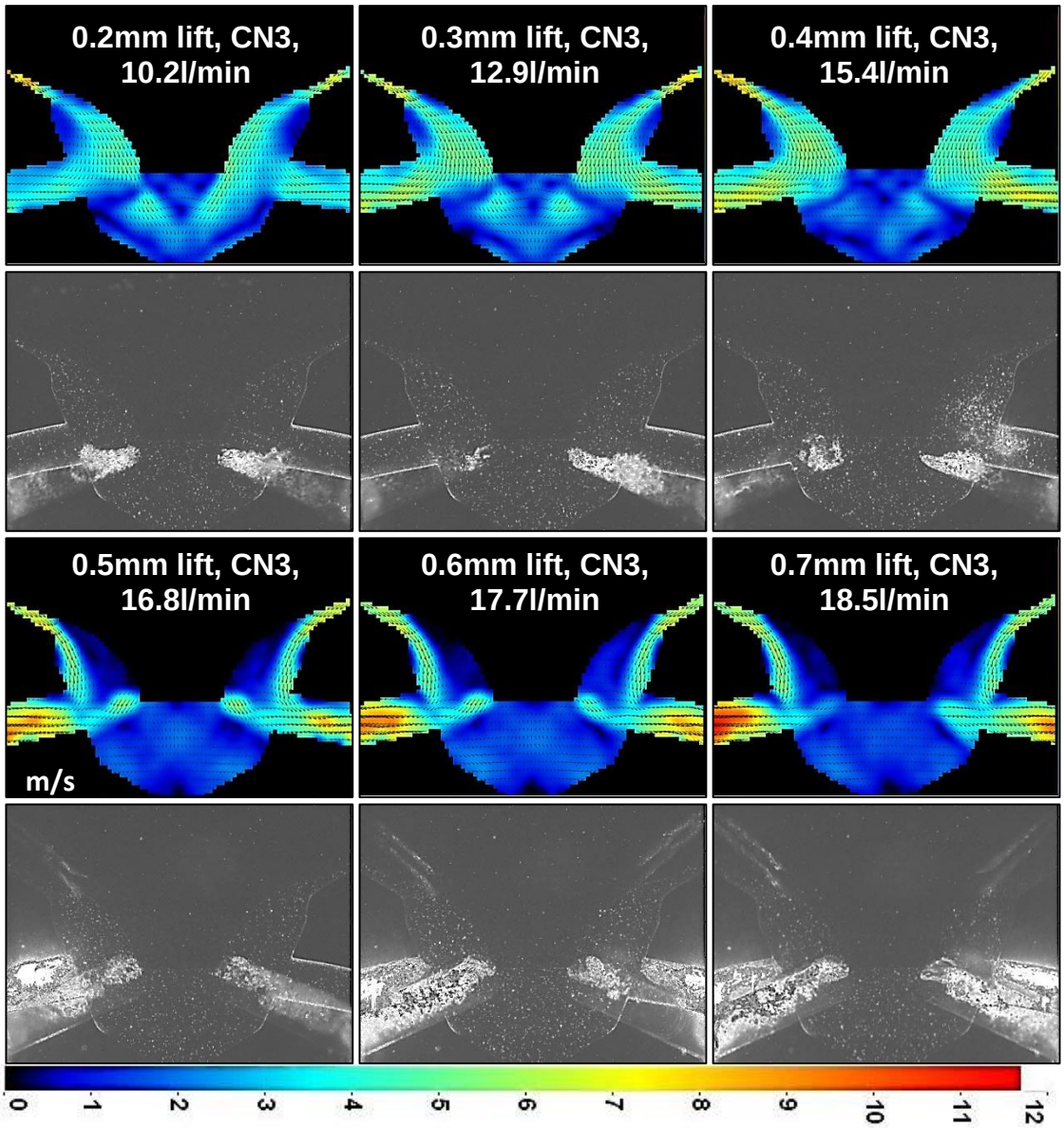

Figure 58 - Mean PIV and raw images - FEATS needle opening - CN 3

Observations – Figure 58

In the raw images the seeding is quite clear as well as is the geometry of the FEATS needle tip within the nozzle sac. It is also quite clear that due to its opacity, it is not possible to determine any flow information from the regions in the vicinity of cavitation; hence these regions in the PIV vector images should be treated with suspicion.

1. The adopted velocity scale of between 0 & 12 m/s is in contrast to the scale of between 0 & 6.5 m/s used at CN 3 with the Reference needle. At first glance this appears odd however, the CN 3 PIV data collected with the Reference needle had the camera situated closer to the model and therefore the higher velocity flow entering the sac from the seat region was outside the camera's field-of-view. This makes the comparison somewhat trickier but upon closer inspection, the velocities within the sac are comparable.
2. Between 0.2 & 0.4mm lift, although the flow entering the sac fills the majority of the area constrained between the needle valve and the nozzle body (in this light sheet plane anyway), it can be considered to be following the needle valve. A small proportion of the flow is seen to overshoot the injection holes and penetrate deep into the nozzle sac; however, this is largely insignificant compared to the much larger flow overshoot with the Reference needle.
3. With the flow following the needle valve (≤ 0.4 mm lift), the raw images indicate that cavitation in the holes between the camera and the light sheet plane occurs at the bottom of these injections holes. This suggests flow entering these holes from below, which disagrees with the PIV vectors from within the light sheet plane, perhaps indicating a different flow structure in this part of the sac for these two holes.
4. An additional observation with the flow following the needle valve is the formation of three small, regular and interlocking vortices immediately below the needle valve tip. The location of these vortices, removed from the injection holes and the main flow entering the sac, likely ensures that they are insignificant to the nozzle's performance.
5. Between 0.4 & 0.5mm lift, the flow has undergone a slight transition to follow the nozzle body.

6. Between 0.5 and 0.7mm lift with the flow following the nozzle body, significant hole entry cavitation is observed at the top of the illuminated injection holes which did not occur when the flow was following the needle valve at lifts < 0.5mm. Furthermore, the hole entry cavitation witnessed in the two holes between the camera and the light sheet plane has now switched from the bottom to the top of the injection holes indicating a different flow structure within the nozzle sac.
7. An additional observation from the PIV vector images between 0.5 & 0.7mm lift is a secondary flow apparently originating from the bottom edge of the needle valve and moving towards the injection holes. The fact that these vectors are in the vicinity of a cavitating region (due to the holes in front of the light sheet plane), indicates this data should be treated with suspicion.

5.2.10. LBFR FEATS needle - Opening 20l/min

The LLS images for the 20l/min tests are shown below in Figure 59. As with the Reference needle in the opening direction, it was desirable to assess the performance of the FEATS needle across the whole operational lift range, i.e. up to full lift or 4.0mm.

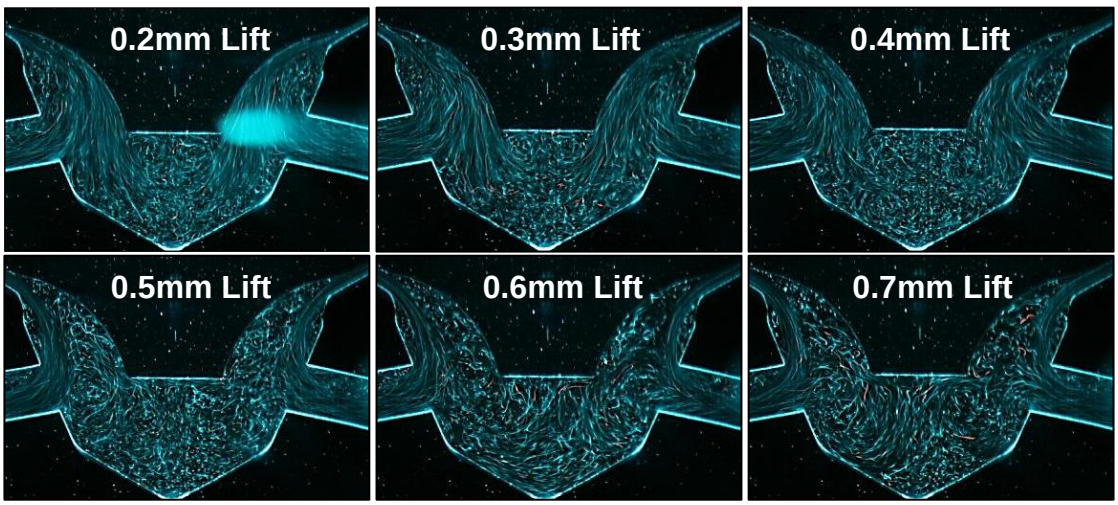

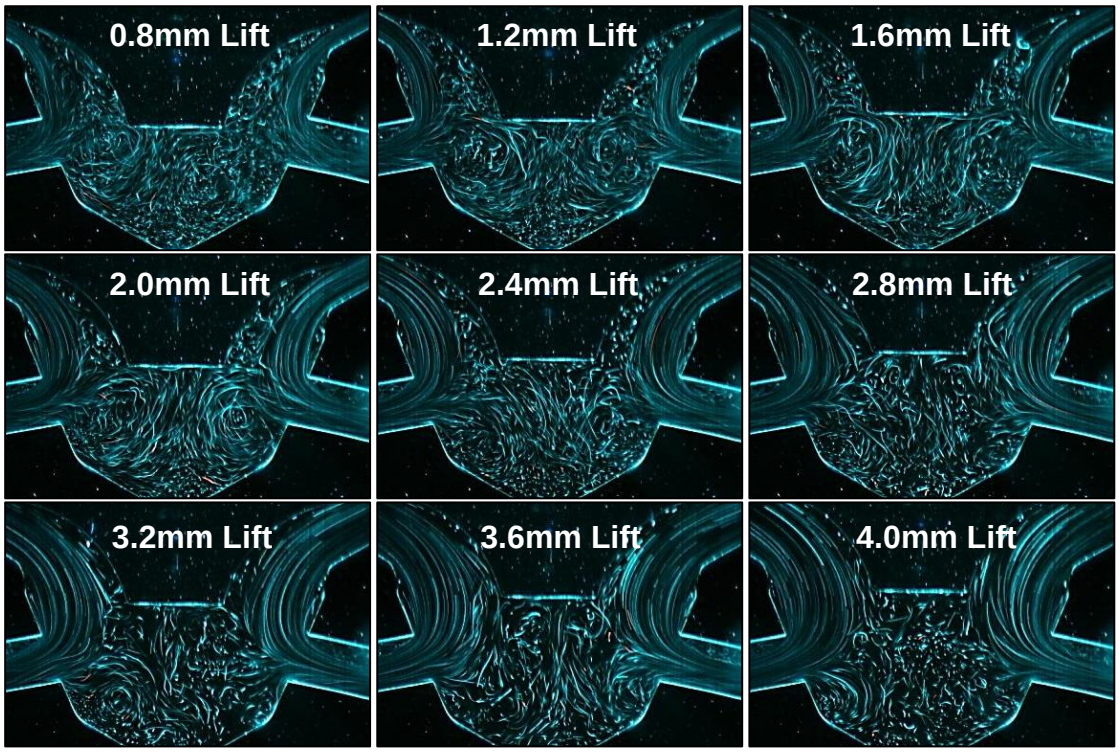

Figure 59 - LLS images - FEATS needle opening - 20l/min

Observations – Figure 59

1. It is clear that the flow, initially following the needle valve transitions to follow the nozzle body between 0.4 & 0.5mm lift.
2. Unlike the Reference needle, with the flow following the needle valve the prominence of the FEATS needle in the sac appears to minimise any flow overshoot so that the majority of the flow is able to enter the injection hole from above with no significant flow entering from below (at least in this light sheet plane).
3. At 0.2 & 0.3mm lift, a very small proportion of the flow is seen progressing deep into the bottom of the sac. By 0.4mm lift this flow was no longer evident even though the flow had yet to transition to follow the nozzle body.
4. As with the Reference needle, what appears to be a reverse overshoot was detected in the flow below the needle tip. This was especially apparent between 1.2 & 2.0mm lift.
5. Across the whole needle lifting range no cavitation was present in the visualised injection holes with only one of the holes behind the light sheet plane containing hole entry cavitation at 0.2mm lift.

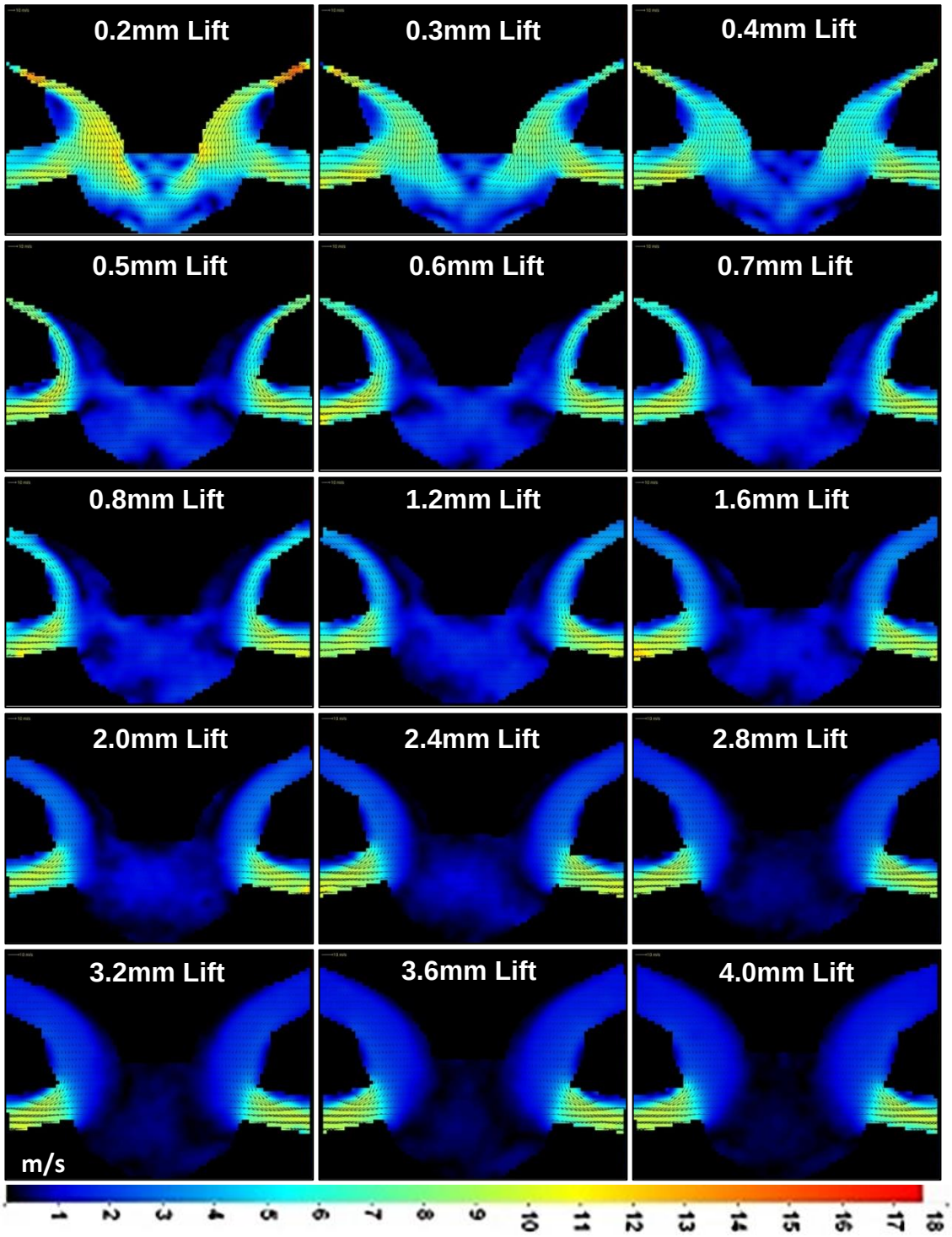

Figure 60 - PIV velocity contours - FEATS needle opening - 20l/min

Observations - Figure 60

1. The flow follows the FEATS needle valve until transitioning to follow the nozzle body between 0.4 & 0.5mm.
2. Especially at low lift, the flow entering the injection holes appears to be much more symmetrical when compared to the PIV results with the Reference needle.

3. As with the CN 3 data, with the flow following the FEATS needle valve, three small, regular vortices were detected directly below the valve tip.
4. The secondary flow seen linking the tip of the needle to the injection holes at CN 3 was not replicated at the non-cavitating condition of 20l/min. This suggests that at CN3 this was a false result linked to the occurrence of cavitation in the holes between the camera and the lights sheet plane.
5. Once the flow has transitioned to follow the nozzle body, the velocities within the sac appear to be comparatively lower than with the Reference needle and any low velocity regions appear to develop symmetrically.
6. The reverse overshoot that was evident in the LLS images between 1.2 & 2.0mm lift was not identified in the PIV vector images. The most likely explanation for this is due to the large scaling range adopted and owing to the velocities being relatively low.

5.2.11. LBFR FEATS needle - Closing 20l/min

In order to check for the occurrence of hysteresis, the experimentation was repeated in the closing direction with the light sheet fitting again moved closer to the model to increase the illumination intensity. As before only the lifting range of most interest was assessed, between 0.7 & 0.2mm lift.

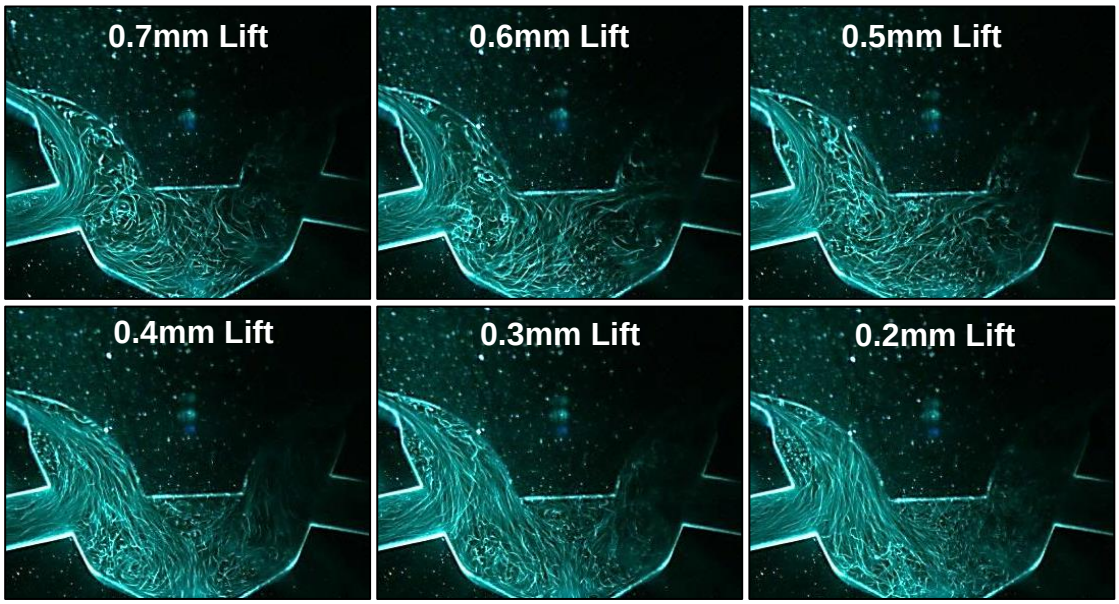

Figure 61 - LLS images - FEATS needle closing - 20l/min

Observations - Figure 61

1. In the closing direction the flow transition has occurred between 0.5 & 0.4mm lift.
2. With the flow following the FEATS needle a small proportion of the flow is seen overshooting the injection holes and arriving at the bottom of the sac. This flow does not appear to enter the injection hole from below as it does with the Reference needle.
3. No cavitation was present in any of the six injection holes even at 0.2mm lift.

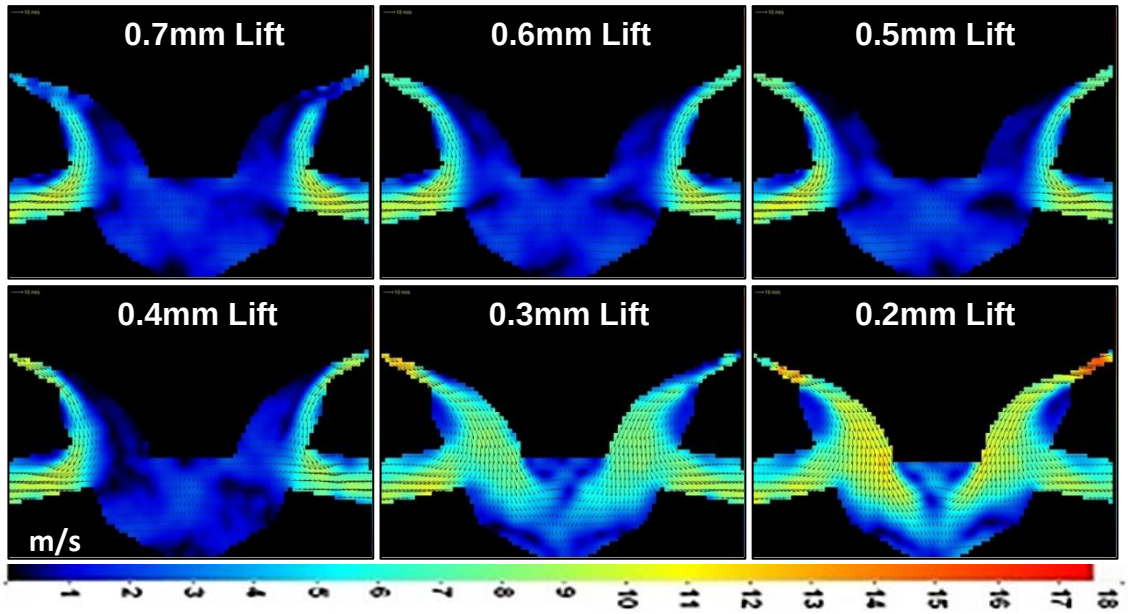

Figure 62 - PIV velocity contours - FEATS needle closing - 20l/min

Observations - Figure 62

1. In the PIV results the flow transition was noted to occur between 0.4 & 0.3mm lift.
2. The observations from the opening direction are in the most part valid for the closing direction too.

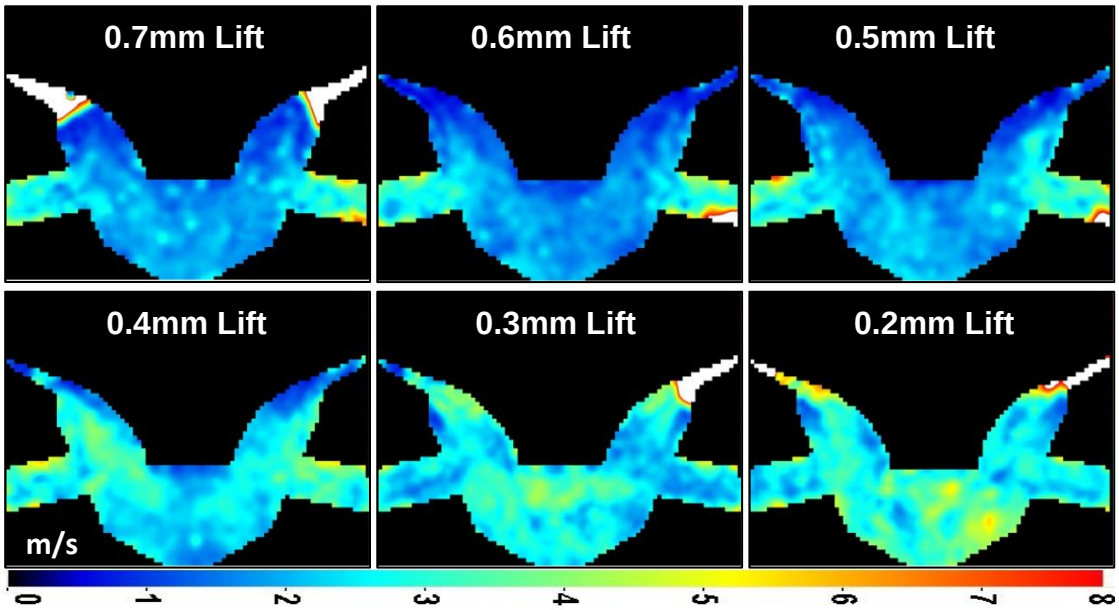

Figure 63 - RMS velocity contours - FEATS needle closing - 20l/min

Observations - Figure 63

1. The white regions upstream of sac entry at 0.7, 0.3 & 0.2mm lifts are beyond the adopted scaling range and indicate that there are significant variations in the flow at this location. The fact this is not observed with the reference needle suggests that this is likely due to the FEATS needle geometry and the sudden expansion in flow area immediately downstream of the seat which allows the flow to be momentarily unguided (and open to variability).
2. Inside the sac and within the injection holes the RMS magnitudes with are comparable with those of the Reference needle design when the flow was following the nozzle body.
3. Compared to the RMS data with the Reference needle (Figure 57), there are significantly lower RMS magnitudes with the FEATS design particularly when the flow is following the needle valve. This indicates less variability in the flow with the FEATS design (ignoring of course at sac entry).

5.2.12. Flow Transition Plots - 20l/min

Although informative, PIV vector plots often make it difficult to identify the changing flow structure as the needle valve opens or closes. For this reason it is sometimes beneficial to compare flow velocities graphically. This was performed by extracting the data from each PIV computational cell along an arbitrary line and importing this into Excel for manipulation. Figure 64 indicates the position of this arbitrary line (red dashed) which connects the top of the two illuminated and opposite injection holes. Also superimposed is a depiction of the adopted sign convention.

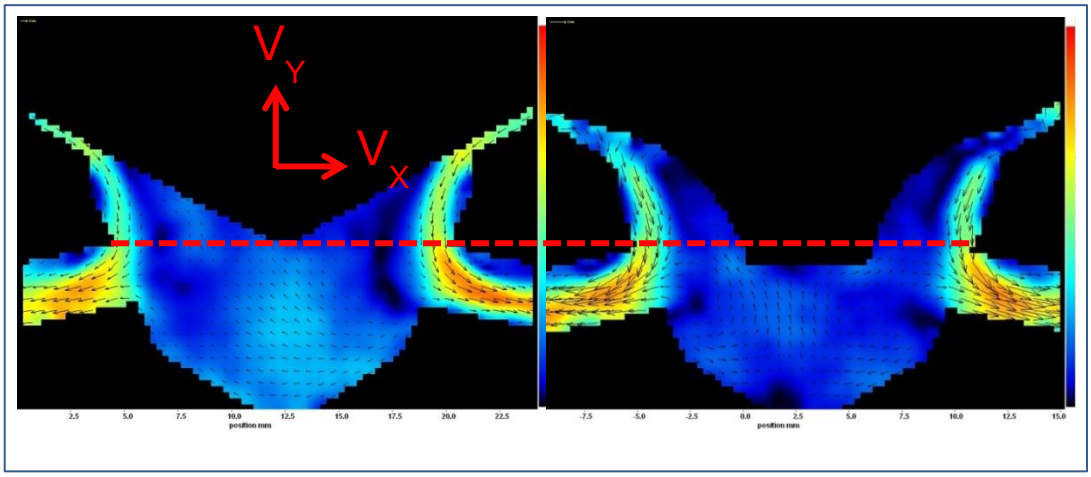

Figure 64 - Transition plots measurement location

Figure 65 contains plots of V_X & V_Y (velocity components) for the Reference and FEATS needles in both the opening and closing directions between 0.2 and 0.7mm lift (10 and 35µm real size) and at 20 l/min. With the data presented in this manner the flow transition is much more evident than in the PIV vector images. The dashed lines indicate the velocity in the x-direction and the solid lines indicate the velocity in the y-direction, however, the scaling interval on both vertical axes is the same so the separate plots are easily comparable. Due to model symmetry and the adopted sign convention, the highest V_Y values are negative whilst the V_X values are opposite in sign either side of the nozzle central axis. The zero velocity values between the -3 & 3mm positions with the FEATS needle are accountable due to the FEATS needle penetrating deeper into the sac than the Reference needle, and therefore intersecting the measurement line.

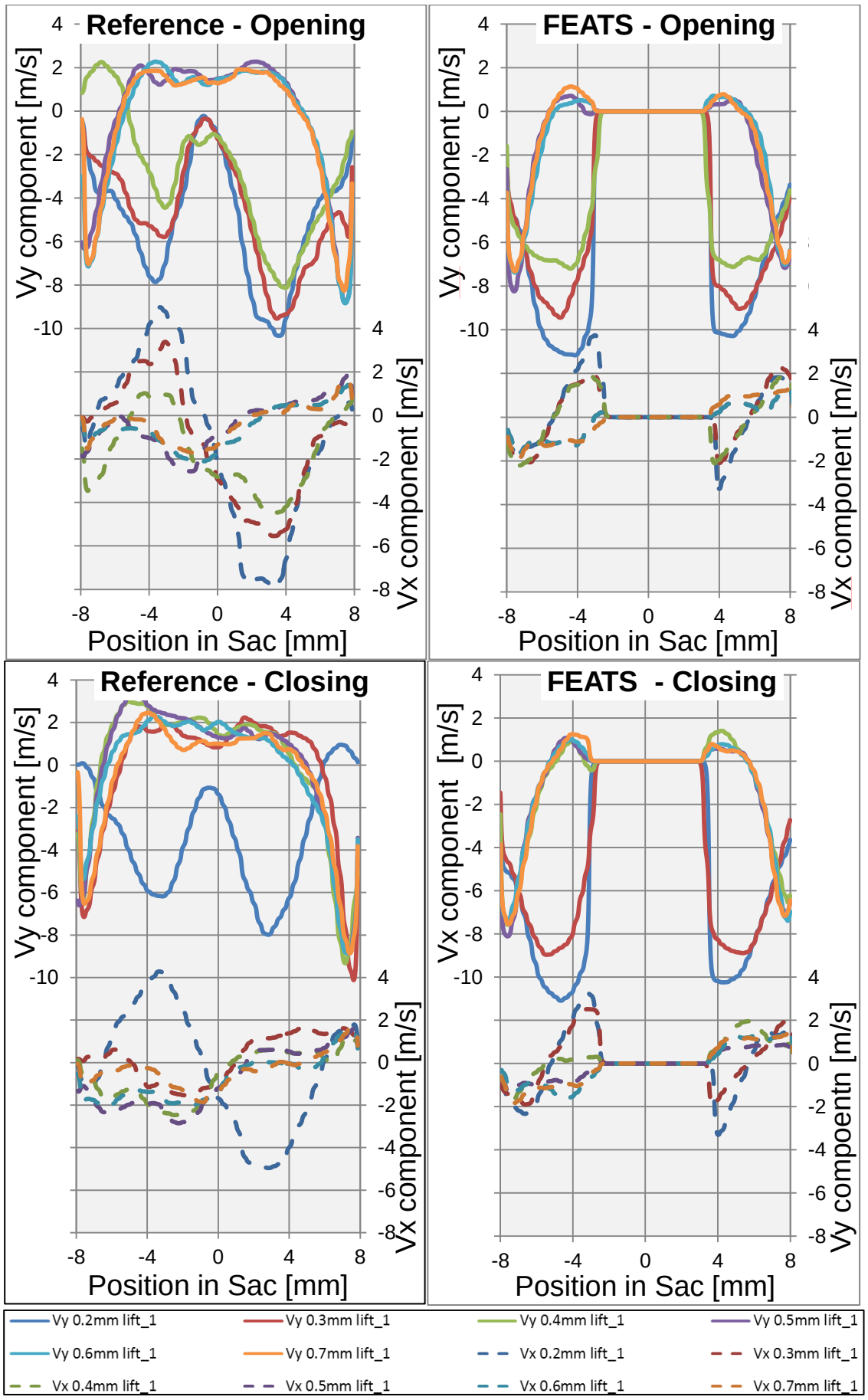

Figure 65 - Mean V_X & V_Y component plots

Opening Direction - Reference Needle

The flow is quite clearly following the needle valve at 0.2, 0.3 & 0.4mm lift. This is detected by w-shaped V_Y plots, indicating that the highest velocities (negative due to sign convention) are occurring towards the centre of the nozzle but not actually at the centre where the flow is in the lee of the needle's tip. Furthermore at these low needle lifts, peak velocity magnitudes are identified in the V_X direction, probably due to the flow which was following the needle in a direction towards the centre of the sac, having to undergo a large flow turn to enter the injection holes. At lifts ≥ 0.5mm, the V_Y plot has changed to identify what is obviously nozzle body flow. Here the highest V_Y components are found in the flow near the nozzle wall (but obviously not at the wall itself), with a low velocity yet opposite direction flow in the centre of the sac, possibly the reverse overshoot that has been identified earlier in the LLS images. With the flow following the nozzle body the V_X component does not vary much across the nozzle cross-section.

Opening Direction - FEATS Needle

With the FEATS needle it is clear that the flow transitions from following the needle valve to follow the nozzle body between 0.4 & 0.5mm lift. Below 0.5mm lift, with the flow following the needle valve, the V_Y component magnitudes are larger whilst the V_X components are smaller than those with the Reference needle. This is accountable due to the shape of the FEATS needle which is forcing the flow to move almost vertically at the measurement location so maximising the V_Y component. At lifts ≥0.5mm, with the flow following the nozzle body the flow structure is very similar to that of the Reference needle, especially in the V_Y direction but with the obvious exception of the centre of the nozzle. This is expected as the FEATS needle should not influence the flow when it is following the nozzle body. Slight asymmetry is detected in the flow for both needles but to a lesser degree with the FEATS needle.

Closing Direction- Reference Needle

In the closing direction the flow follows the nozzle body until between 0.3 & 0.2mm lift where it transitions to follow the needle valve. This is the only significant difference detectable between the opening and closing direction plots as the observations made in the opening direction remain applicable.

Closing Direction - FEATS Needle

The FEATS needle in the closing direction also differs from the opening direction as the flow initially following the nozzle body, transitions to follow the needle valve between 0.4 & 0.3mm lift. Other than this hysteresis, the flow structure is comparable with the opening direction.

5.2.13. Summary of Flow Transition & Hysteresis

Table 2 summarises the lifts at which the flow transition was observed to occur for both the LLS images and the PIV data.

Design	Needle Movement Direction	Transition lift – LLS images [mm]	Transition lift - PIV data [mm]
Reference needle	Opening CN 3	n/a	0.3 – 0.4
	Opening 20l/min	0.5 – 0.6	0.4 – 0.5
	Closing 20l/min	0.6	0.3 – 0.2
FEATS needle	Opening CN 3	n/a	0.4 – 0.5
	Opening 20l/min	0.4 – 0.5	0.4 – 0.5
	Closing 20l/min	0.5 – 0.4	0.4 – 0.3

Table 2 - Observed flow transition lift location

Observations – Table 2

1. Whereas, the LLS images indicated no hysteresis between opening and closing for both needle designs, the PIV results indicated that there is hysteresis especially apparent with the Reference needle.
2. The differences between the LLS and PIV results may not be too alarming, as there is a good agreement for the FEATS needle in the opening direction. Admittedly the large discrepancy in the closing direction for the Reference needle was unexpected; however, this could be accounted for by the fact that the PIV results are averaged and therefore a truer representation of the flow as they are captured over typically a four second interval. The LLS images have an exposure of ~5ms and may therefore be capturing an abnormal flow event.
3. The 20l/min PIV results imply that in the closing direction, both needle designs would undergo a flow transition at a lower lift than when moving in the opening direction. This may not be altogether unexpected and

could possibility be associated with the flow phenomena known as the Coandă Effect[21]. Therefore in the case of the needle valve moving in the opening direction, the flow attempts to remain attached to the needle until a relatively large lift has been reached before undergoing a transition to follow the nozzle body. However, with the valve moving in the closing direction, the flow already following the nozzle body resists transitioning to follow the needle valve until a much lower lift.

4. The PIV results indicated that the difference between opening and closing, or hysteresis is greater with the Reference needle compared to the FEATS design. This is possibly due to the geometry of the Reference needle where the flow has to 'swing' or turn through a large flow angle during a flow transition. Due to the proximity of the FEATS needle to the nozzle body upstream of the injection holes, the flow needs only undergo a small flow angle turn when transitioning, therefore the flow is more 'willing' and likely to do so.

5.2.14. Reference Needle PIV - Eccentric Light Sheet Positions

The previous PIV data has all been obtained with the laser light sheet plane located at the central axis of the model. With the PIV laser mounted on a traverse table, the light sheet plane was moved at successive intervals further away from the PIV camera to provide a better understanding of the flow structure within the remainder of the nozzle sac. Inspired by Magnetic Resonance Imaging (MRI) techniques, this approach effectively provides a series of sections through the nozzle sac to create a 3D picture of the flow structure.

Figure 66 shows a side view of the nozzle sac alongside a plan view with the eight light sheet planes superimposed as green lines. The needle valve is not shown but each line represents a plane starting at the central axis and up to 7mm of eccentricity in 1mm intervals.

[21] Coanda Effect is the tendency of a fluid jet to be attracted to a nearby surface

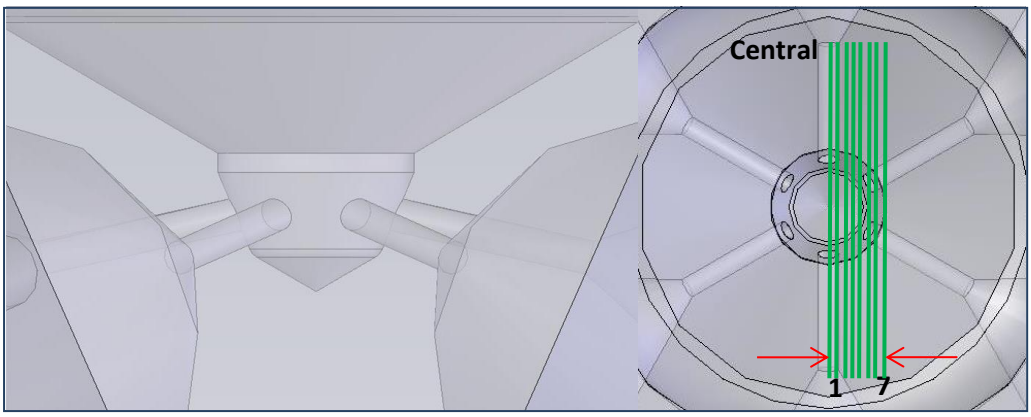

Figure 66 - Eccentric laser light sheet positions

0.2mm needle lift and CN3

A needle lift of 0.2mm at CN 3 was chosen to allow study of the 3D flow structure with the flow following the needle valve and overshooting the injection holes at cavitating conditions. Figure 67 contains the PIV vector images for the central and seven eccentric light sheet positions.

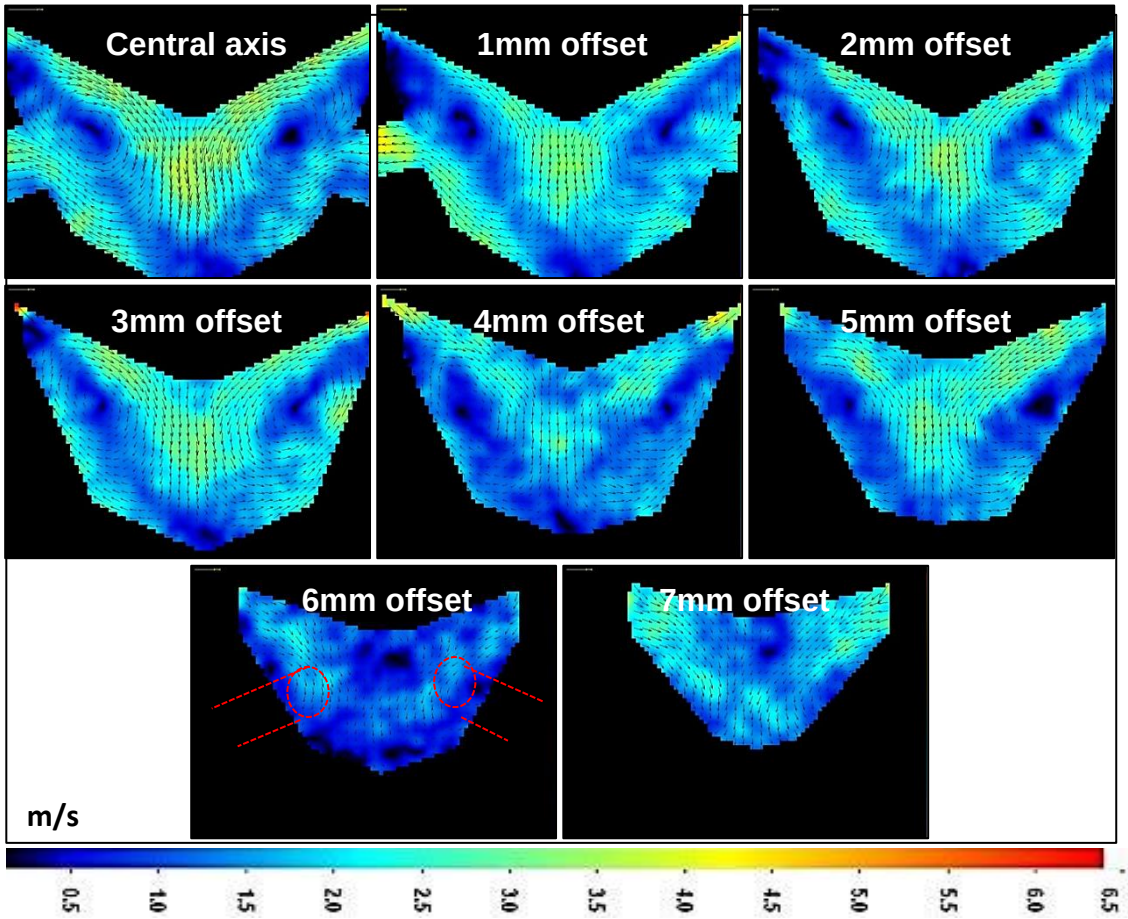

Figure 67 - PIV velocity contours, 0.2mm lift - CN 3

Each image is the average of 20 individual frames which were captured at a frequency of 5Hz with a pressure drop equivalent to CN3 (P_{up} = 0 bar and P_{dn} = -0.75 bar). The vector image at 6mm offset has had the positions of the two holes closest to the camera highlighted in the event that their proximity to the light sheet plane may influence the flow at this location.

Observations - Figure 67

- The highest velocities were found to occur at the central axis where the flow likely contains the lowest V_Z component. This is due to symmetry in this light sheet plane with the flow confined between likely identical flow structures on either side.
- At 1mm offset, the flow within the sac is almost identical to that at the central axis except for slightly lower velocities. However, as the flow enters the injection hole it appears to have uniform velocity across its whole cross-section indicating that no separated flow exists at the bottom of the hole.
- The overshoot was evident up to and including 5mm of light sheet eccentricity until at which point the light sheet plane was too far removed from the needle valve to likely encounter the flow following it. Also beyond 5mm of offset, the effect of other injection holes and the proximity of the nozzle wall is likely to have a significant influence on the flow.
- At 6mm offset, the vectors indicate that the flow is moving into the light sheet plane from under the needle valve tip. The effect of the two injection holes which lie near this plane is also noticed as the flow turns seemingly to enter these holes.
- At 7mm offset the flow is quite uniform perhaps due to the proximity of the sac wall which channels the flow and suppresses any 3D nature.
- Vortices have been suggested as a potential mechanism for the formation of string cavitation observed within the injection holes in both large scale and real size studies. However, between the centreline and until the 5mm offset position, the twin vortices remain centred at the same position, (approximately level with the top of the injection holes) yet do not appear to engage with any of the injection holes. By 0.6mm offset

these vortices appear to have merged to form a central low velocity region, perhaps indicative of a flow with a large V_Z component. It was initially considered that the above evidence could indicate a large vortex ring (toroid) structure within the sac and being sustained by the overshooting flow, however, the apparently fixed location of the centre of these vortices does not appear to support this.

0.4mm lift and CN3

The previous testing was repeated but with the needle valve set to a larger lift to assess the 3D flow structure when the flow was following the nozzle body. Earlier research with the Reference needle has indicated that at CN 3 for both opening and closing directions, the flow follows the nozzle body at 0.4mm lift (equivalent to 20µm real size). Therefore this still low lift condition was chosen to compare with the data collected at 0.2mm lift. As before the light sheet was moved away from the PIV camera in 1mm intervals up to 7mm of eccentricity.

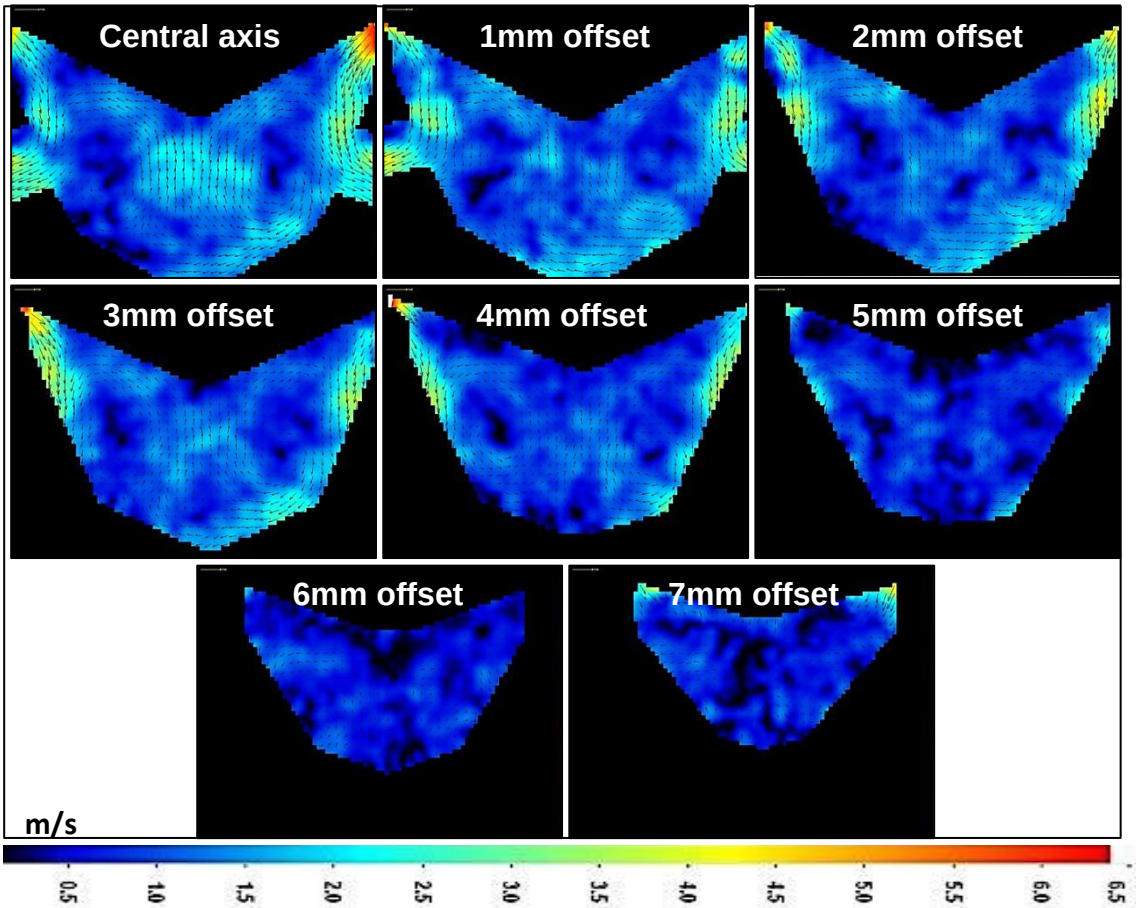

Figure 68 - PIV velocity contours, 0.4mm lift - CN 3

Observations – Figure 68

- The first observation is that compared to at 0.2mm lift, the vectors are generally of lower magnitude and considering the fact that the images are averages, they also appear to be more chaotic with a less discernible flow structure.
- At the model central axis the flow is quite symmetrical with the majority of the flow following the nozzle body and entering the injection holes from above. The same reverse flow that was seen at 20l/min is seen in the middle of the sac, flowing upwards and along the needle surface to combine with the main flow and eventually pass out through the injection holes. This flow appears to be the driving mechanism for the formation of weak vortices either side of the model with their centres approximately level with the bottom of injection hole entry.
- At 1mm offset, although the vector magnitudes are slightly lower, the flow is quite similar to that which was observed at the central axis.
- At 2, 3 & 4mm of offset, the highest velocities are observed in regions where the flow was possibly being accelerated as it is 'funnelled' towards the injection hole, although having to leave the light sheet plane to do so. Additionally, the vortex structures noted at the central axis appear to be less clearly defined, perhaps because their velocities have diminished in magnitude.
- At 6 & 7mm of offset, the vector field contains multiple low velocity regions. These could indicate either the influence of the other injection holes, flows with a large V_Z component or simply numerous vortex structures interacting with each other.

Comparison of the eccentric PIV results at 0.2 & 0.4mm lift

At the central axis, significant differences were known to exist between the flow structures at 0.2 and 0.4mm lifts. By moving the light sheet eccentrically it has been found that these differences perpetuate across the whole cross section of the nozzle. Comparison of the PIV results has identified two possibly significant findings regarding vortex activity within the nozzle:

1. At 0.2mm lift, the higher velocities associated with the overshoot resulted in twin, intense vortices centred approximately level with the top of the injection holes. These vortices appeared to dominate the surrounding flow resulting in a more stable flow structure across the remainder of the sac. In contrast, at 0.4mm lift the flow appeared to be much more chaotic and consisted of multiple low velocity regions which may indicate the presence of numerous small vortices.
2. At 0.4mm lift with the flow following the nozzle body, the vortex structures were centred approximately 3mm lower than those which occurred at 0.2mm lift. Additionally these vortices appeared to be rotating in the opposite direction and of significantly lower intensity. As vortex structures inside the nozzle sac have been associated with in-hole vorticity and string cavitation, this could indicate a significant differences in the injection hole flow between 0.2 & 0.4mm lift.

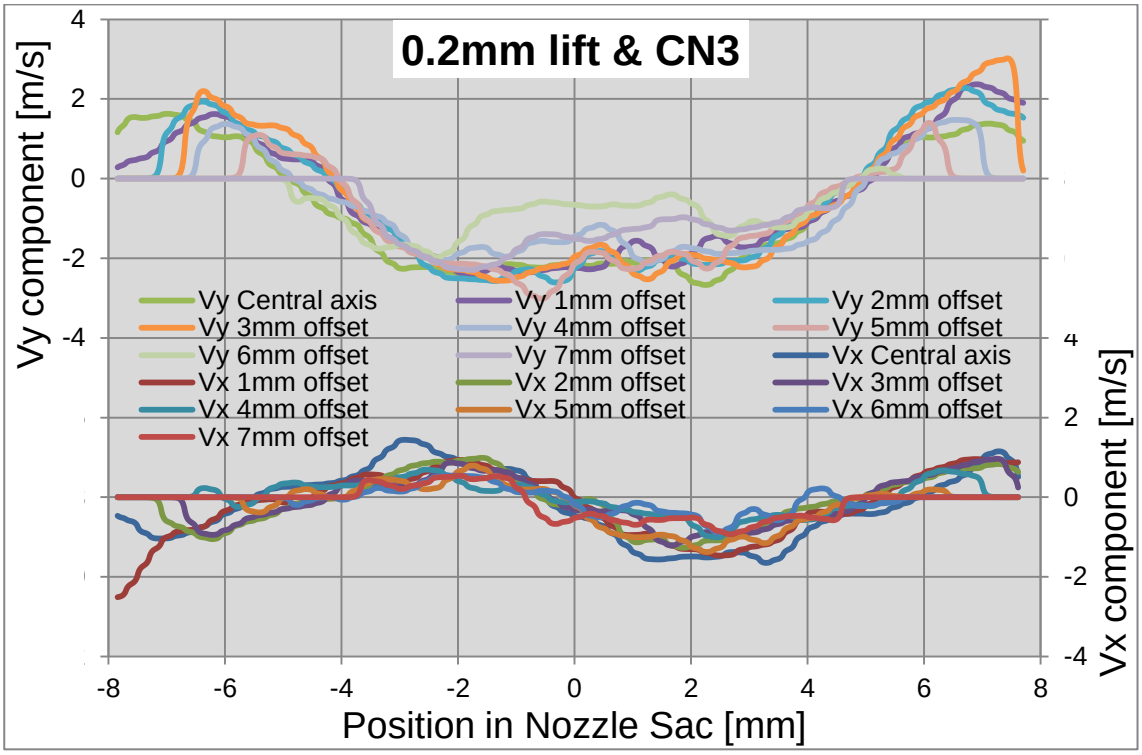

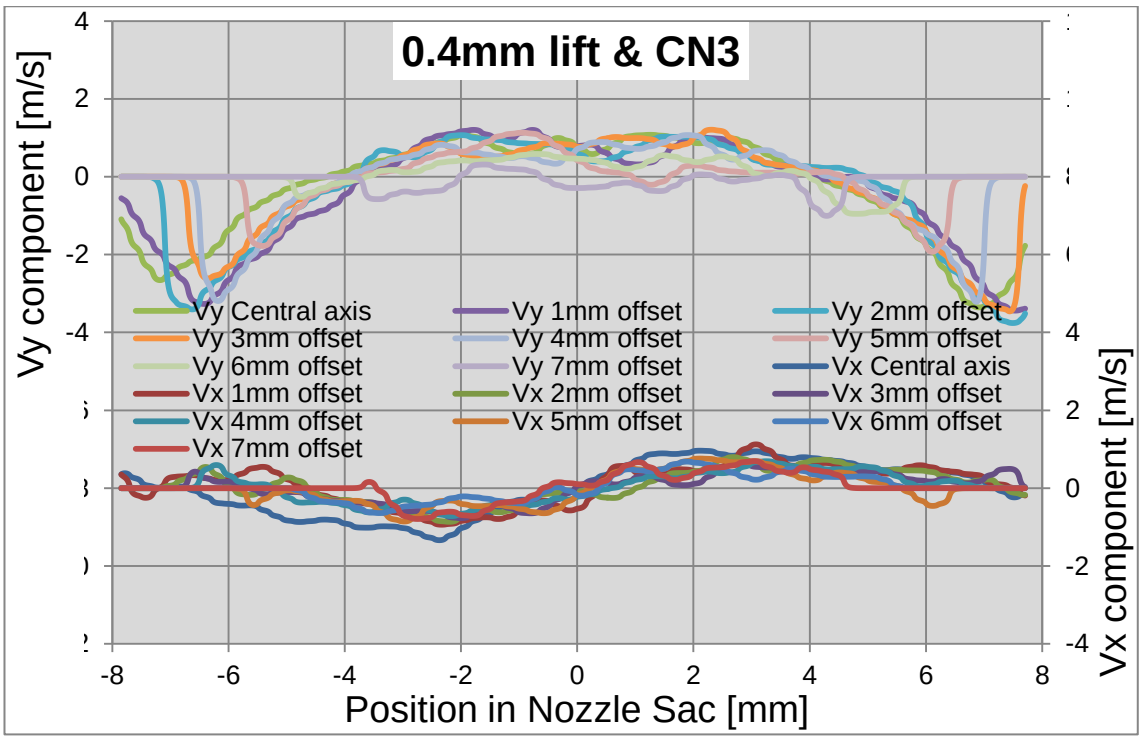

Figure 69 - V_X and V_Y component plots - CN 3

Observations - Figure 69

Figure 69 consists of CN 3 velocity plots for the eccentric light sheet positions. As with the flow transition plots at 20l/min, the data has been extracted from the PIV images along an arbitrary line positioned at the top of the two injection holes when at the model central axis. Although both plots identify a different flow structure before and after the flow transition, they do not as was hoped assist with illustrating any 3D flow structure within the nozzle sac. At 0.2mm lift, although the V_Y components at 6 & 7mm of eccentricity indicate a differing flow structure within the centre of the nozzle sac, the difference is not significant enough to prove the existence of a separate flow structure. In fact it is likely that this difference could be accounted for by the proximity of the nozzle wall and/or the two injection holes in this vicinity. In fact a similar observation but to a lesser degree was made at the same eccentric positions at 0.4mm lift. Interpretation of the V_X component data was less clear but as anticipated the peak velocities where largely found to occur at the model centreline.

5.2.15. Project Conclusions

The flow transition and flow overshoot have been extensively studied for both cavitating and non-cavitating conditions through the use of a 20x scale transparent nozzle LSM. Additionally two needle design variants have been evaluated and the observations from the LSM have been compared against data from real size components.

Flow Transition

Initially when conceiving possible driving factors, it was considered that the onset of hole entry cavitation could initiate the observed flow transition. It was supposed that in order to enter the injection hole as efficiently as possible, the flow may choose to approach the hole from a preferable direction to avoid any cavitating region. However, this theory was soon rejected owing to the fact that the flow transition was observed to occur for both cavitating and non-cavitating conditions, hence cavitation cannot be a driving factor.

The PIV and LLS data for both the Reference and the FEATS needle designs has produced the following findings in regard to the 120° seat design of nozzle:

1. The needle lift discrepancy between opening and closing where the flow transition was observed to occur could possibly be explained by the flow phenomena known as the Coandă effect. Thereby the flow entering the nozzle sac choosing to attract/attach itself to either the nozzle body or the needle valve. Further investigation is however, necessary to determine if this is indeed the mechanism governing this apparent hysteresis.
2. The hysteresis identified between opening and closing in the PIV vector images and summarised in Table 2, was not replicated in the LSM constant pressure Flow versus Lift plots. Therefore the occurrence of the flow transition does not appear to affect the nozzle flow rate (and therefore not the C_d), or at least to an extent that is detectable on the LBFR.
3. The discrepancy in lift between opening and closing where the flow transition was observed was much more pronounced with the Reference needle. This is probably owing to the fact that with the Reference needle the flow is less confined than with the FEATS needle and therefore has

to undergo a much larger flow turn when transitioning. This large flow turn is likely to result in instability making the performance of the injector less predictable and more difficult to control.

4. With the flow following the nozzle body, the velocities within the majority of the sac appear to be comparatively lower with the FEATS needle compared to the Reference needle. Low pressure regions also appear to develop symmetrically with the FEATS needle suggesting that the flow within (supposed) non-critical parts of the nozzle are more stable than with the Reference needle.
5. The final observation with the Reference needle is that the flow following the needle valve (and overshooting the injection hole) appears to be associated with a degree of flow eccentricity, perhaps indicating that the needle was slightly eccentric even though care was taken to position the needle as concentrically as possible. It is therefore not possible to state whether this flow eccentricity arose as a result of the flow following the needle valve or the possible needle eccentricity.

Extensive investigation would be required to investigate if the effects of the flow transition are in fact damaging to the transient performance of the nozzle. Fuel injector nozzle design involves closely guarded intellectual property of which FIE manufacturers have amassed over numerous years of research and product development. In this respect research to assess the effect of any flow transition would be best carried out by the FIE manufacturers and likely not be in the public domain.

Flow Overshoot

The flow overshoot only occurred to any significance with the Reference needle and at low needle valve lift, which for a modern fast-acting injector would be for a small period at the start and the very end of an injection. However, due to modern multiple injection strategies where the needle valve is spending an increasing amount of time at these low-lift conditions, the effects of the flow overshoot are potentially becoming more significant.

In regards the flow overshoot, analysis of the Reference needle data has produced the following observations:

1. With the flow overshooting the injection holes and penetrating deep into the sac, the flow is likely to come into contact with a region where nozzle manufacturing tolerances are known to be loose. This potentially may result in significant variation between nominally identical nozzles which could prove problematic for multi-cylinder engine calibration.
2. Separate overshooting flows travelling down opposite sides of the needle valve were observed to jostle each other as they interacted and combined below the valve tip. The interaction of these two flows could potentially be a source of instability or even vorticity. This is a concern as high levels of sac vorticity have been associated with the occurrence of string cavitation which has itself been associated with poor spray plume development.
3. Compared to the Reference needle, the FEATS needle having a slightly larger flow area at low lift should have a slightly higher sac pressure as the flow is being less throttled prior to entering the sac. However, interpretation of the real size force versus lift data (from within DDS but not included in this thesis) indicated an increased sac pressure at low lift with the Reference needle. As this was found to occur at the range of lifts where the overshoot was observed, it is likely that the increased sac pressure is an effect of the flow overshoot. A plausible explanation for this is that the flow is being arrested at the bottom of the sac thus resulting in a greater stagnation pressure. This is not necessary a negative aspect as the greater sac pressure would contrive to suppress any cavitation formed across the seat and produce a larger lifting force to move the needle rapidly away from the low lift condition. In effect, the occurrence of the overshoot could well serve to limit its effects.
4. The effect of the flow entering the injection hole from below when the flow is overshooting, as opposed to more typically from above, may result in minor changes to the plume targeting so that the spray plume does not interact optimally with the piston bowl. Potentially this could contribute to poor combustion efficiency or increased wall-wetting.

Reverse Overshoot

Whilst the existence of the flow transition and flow overshoot have been confirmed and scrutinised over, a secondary and much lower velocity flow was discovered within the nozzle sac when the flow was following the nozzle body. This has been referred to as the 'reverse overshoot' and in all likelihood it is a mechanism for allowing flow from outside the light sheet plane to combine with the flow arriving into the sac to pass through the injection holes. Although this reverse overshoot does not appear to directly interact with or impair the flow entering the visualised injection holes, its approximate location could indicate that it is a precursor for vortex activity within the holes in-front of (or behind) the light sheet plane.

5.2.16. Summary of FEATS Needle Concept

The Flow Enhancer and Transition Stabiliser (FEATS) design of needle was directly compared against the Reference needle. Table 3 weighs up the relative advantages and disadvantages found through study of the LSM.

Pros	Cons
Limited flow overshoot, flow guided into injection hole with most flow entering from above, potentially less effect on plume targeting	Increased complexity and cost of manufacture
Reduced hysteresis with flow transition between opening and closing direction	FEATS tip geometry needs to be matched to nozzle design and flow rate
Reduced instability within nozzle sac	
Reduced low lift flow eccentricity	
Reduced sac volume – UBHC benefit	
Possible retro-fit solution to meet future stringent emission standards	

Table 3 - Observations from FEATS needle testing

Pros

With the majority of the flow able to enter the injection holes from above, any cavitation should be confined to the top (12 o'clock) of the injection holes. Unlike with the Reference needle, this should result in a more consistent flow within the injection holes and therefore provide a stable spray plume development across the whole valve lifting range. The FEATS geometry confined the flow arriving into the nozzle sac within a much narrower band or flow area. This appears to have limited the large directional flow changes and the resulting instability that they bring. The PIV data and LLS images indicated that at low needle lift the FEATS needle exhibited less apparent flow-eccentricity than the Reference design, which could indicate an additional (negative) effect that the overshoot has on the flow within the sac. An additional benefit of the FEATS variant over the Reference needle is the fact that when seated the FEATS needle penetrates deeper into and occupies a larger region of the nozzle sac. This serves to reduce sac volume which in recent years has seen a reduction in order to limit UBHC emissions. Further combustive studies are clearly necessary to determine whether the seemingly advantageous observations from the FEATS needle LSM are favourable within an actual engine installation; however, this new needle design could potentially offer a retrofit solution to existing FIE systems to satisfy increasingly stringent future exhaust emission standards.

Cons

The more complicated geometry of the FEATS needle will likely prove more costly to manufacture. Furthermore, for optimum benefit the tip geometry needs to be tailored or matched for a particular application in terms of injector nozzle flow, seat angle and injection hole cone angle. More development time (and cost) is therefore required at the design and validation stage to select the optimum values for each application.

5.3. 60° Seat Nozzle Project

The principal aim of this project was to allow for enhanced visualisation of the entire length of one or more of the nozzle's injection holes. The following sections detail the design of the real size test nozzle to facilitate this, the design of the representative LSM and finally the LSM experimental testing.

5.3.1. Research Visualisation Nozzle (RVN)

Initially a 0.5l/min[22] µSac nozzle was chosen with seven Ø108µm tapered injection holes. For experimental simplicity, the number of holes was reduced to six which required an increased injection hole diameter to provide the same nozzle flow. The reasoning behind initially selecting a low-flow original nozzle design was that a reduction in the number of holes still resulted in a nozzle with a hole size comparable to higher flow nozzles of 7 or even 8 injection holes. This resulted in a nozzle design with six equispaced Ø117µm holes which shall be referred to as **Design A**. Figure 70 is CAD model of this with representative spray plumes attached. The included angle between each hole is 60° and the cone angle is 162°.

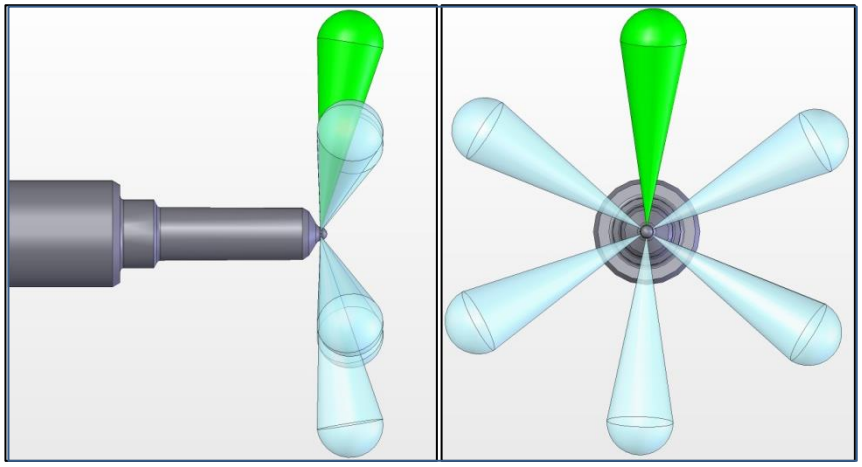

Figure 70 - Design A nozzle with plumes attached

With a conventionally designed multi-hole nozzle such as Design A, when attempting to scrutinise the flow within a single injection hole bore, the proximity of the neighbouring injection holes partially obstructs the view. This can normally be avoided by angling the visualising camera, however, optimum PIV

[22] Steady-state flow at 100 bar ΔP and full needle lift

accuracy is achieved when visualising at 90° to the flow which would be along the injection hole's axis. A simple solution to this problem would be to vastly reduce the number of injection holes to perhaps 4; however, this would result in a design of nozzle which was removed from that found on modern HSDEs. To avoid having to pursue this approach, a novel solution was reached within Delphi Diesel Systems which will be used in a future research project. This approach involved a modification of the two injection holes adjacent to the hole dedicated for flow visualisation. These two holes were effectively raked back, away from the dedicated hole and manufactured with a smaller included cone angle of 132°. This raking back of the two injection holes was accomplished by laterally moving their intersection point relative to the remaining four holes. By ensuring that the hole entry of all six holes remained at the same PCD, all holes remain at the same depth within the sac so therefore will experience the same flow. These modifications resulted in a nozzle which shall be referred to the Research Visualisation Nozzle (RVN). Figure 71 is a CAD model of this with representative plumes attached. The dedicated visualisation hole (or alternately hole 1) is shown with a green spray plume attached and unlike with design A, is visible when viewing from the side perpendicular to the axis.

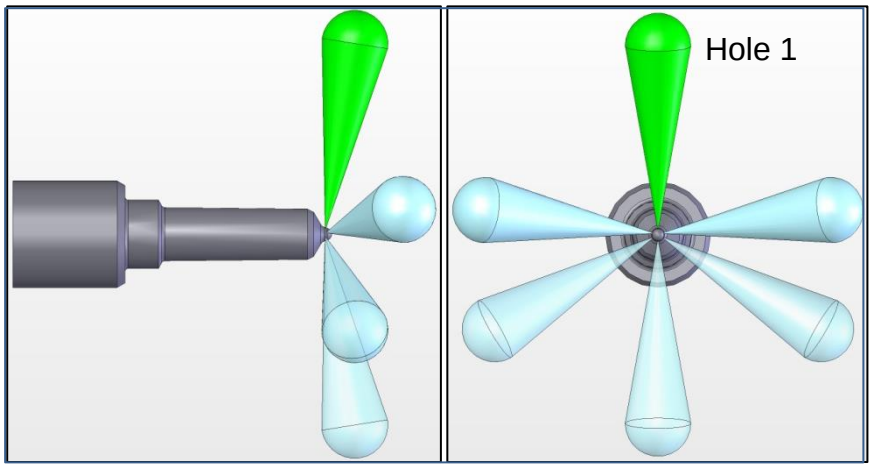

Figure 71 - RVN design with plumes attached

Summary of RVN design

1. Six Ø 0.117mm holes
2. 0.62mm hole length
3. 1.5 taper or K- factor
4. Flow rate of 0.5l/min at 100 bar ΔP
5. Four holes at a cone angle of 162° and two at 132°

5.3.2. RVN Real Size Nozzle testing

Spray Visualisation

Batches of nozzles of Design A and the RVN design were manufactured and their internal geometry was assessed from measurement of silicone impressions. For each design a nozzle found to be closest to the actual design specifications was chosen and these two nozzles were fitted to a solenoid injector and tested on the Spray Visualisation Rig. This is standard practice with any new nozzle design and is essential to check for any detrimental behaviour resulting from the design modifications mentioned previously. With the injector firing into an optically accessible non-evaporating chamber at 30 bar back pressure, front and side images of the spray plumes were captured. Figure 72 comprises single spray visualization images of design A and the RVN design at 2000 bar injection pressure and 0.4 ms after the SOI, where the needle valve is expected to have obtained full lift. Hole 1 is located at 12 o'clock and the silver ring evident in the background of the right hand image is exactly 50 mm in diameter. This is a necessary dimension to derive a scale when measuring plume penetration.

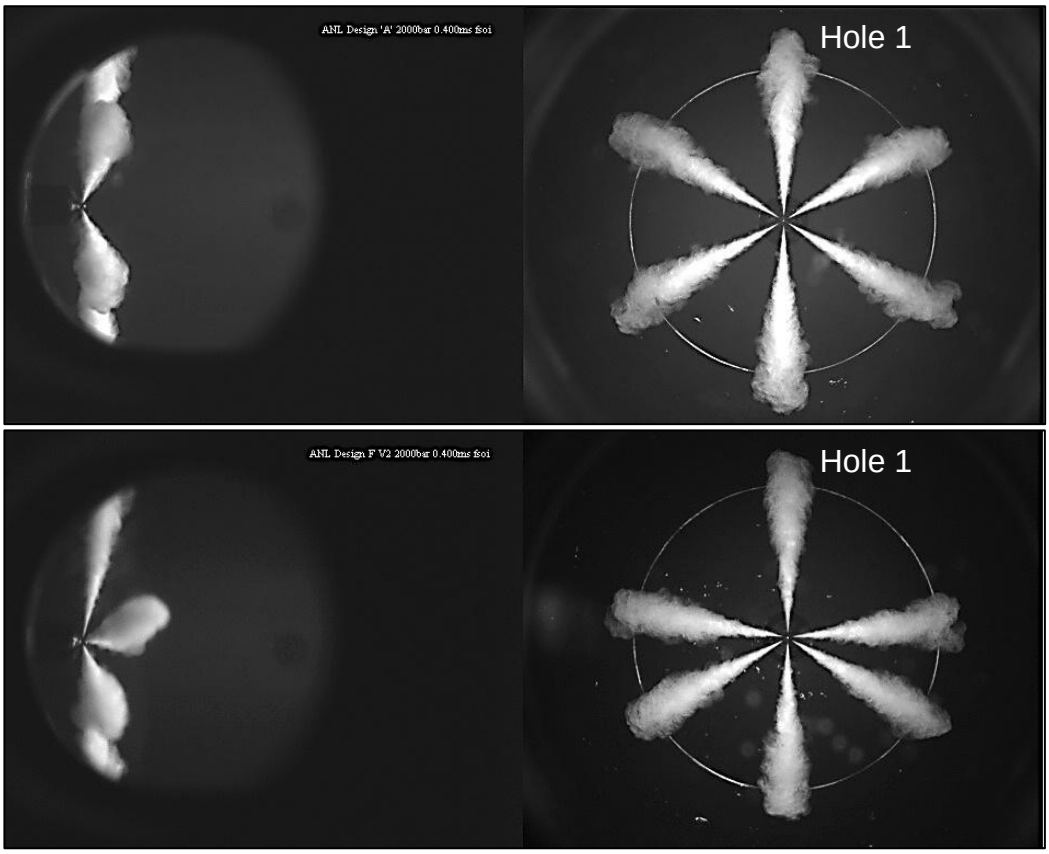

Figure 72 – 2000 bar Spray visualisation - Design A and RVN at full lift (Images obtained by colleague in DDS)

A poorly performing nozzle might be expected to have plumes of unequal length or bushiness which within an engine would likely result in unsatisfactory fuel-air mixing and hence poor combustion efficiency. Regarding the front images (right hand side) in Figure 72, Design A appears to have six plumes of equal length and bushiness; however, the RVN appears to have the two plumes either side of hole 1 with a slightly lower penetration than the remaining four. This effect is due to these plumes having a smaller cone angle and therefore being directed more towards the camera, which is clearly evident from the side image. To take account of this, actual plume penetration is calculated using the following:

$$\boldsymbol{Penetration} = \frac{\boldsymbol{Optical\ measurement}}{\boldsymbol{Cos\left(\frac{\theta}{2}\right)}}$$

Equation 15

where θ is the cone angle of the nozzle. Within DDS the individual spray plume images were measured through imaging software and this data has been used to create penetration plots, which can be seen in Figure 73. The plot denoted plume 1 is obviously from hole 1 and contains line markers to facilitate comparing this result against the remaining 5 injection holes. During spray visualisation, at each time step a minimum of four still images are captured to check for any unusual plume development. These plots are therefore averages and provide a useful means of identifying any unusual features or peculiarity which is not always apparent from the individual images. It is immediately clear that not only does the higher injection pressure result in the plumes having a higher velocity, but being servo-actuated the needle motion is increased so that the plumes reach maximum penetration[23] considerably faster than at the 1000 bar pressure tests. As needle lift data was not available, the penetration plots are labelled in terms of time ASOI (After Start of Injection).

[23] Maximum penetration is limited by the field of view of the camera

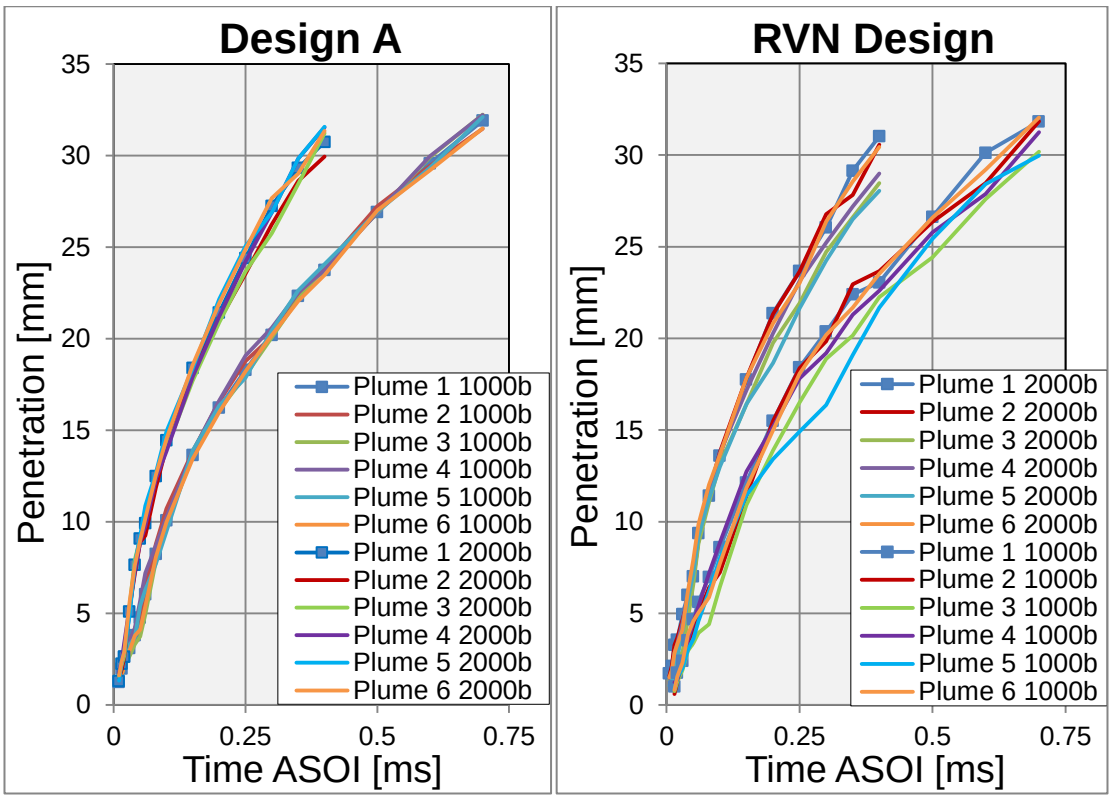

Figure 73 - 60° Seat Nozzle - Average plume penetration

The penetrations from all plumes of Design A are very similar with only a slight deviation apparent at 2000 bar perhaps due to small geometric differences between individual injection holes having a more discernible effect as the injection event progresses. With the RVN design, holes 3 & 5 have a lower penetration across the whole range at both injection pressures yet the remaining four holes appear to be reasonably consistent. This could be a result of these holes being starved of fuel due to the proximity of the two modified holes 2 & 6, although oddly enough this seems more apparent at 1000 bar than at 2000 bar.

CFD - Individual Hole Mass Flow Rates

In order to build upon the findings from the penetration plots, CFD simulation was carried out by a colleague within DDS to assess the individual mass flows for design A and the RVN design. At full needle lift (300 µm) with 30 bar of downstream pressure and at 200 bar and 2000 bar injection pressures, the individual flow rates for each of the injection holes was determined. The results from this are not included in this thesis however, they indicated that at both injection pressures, the two modified holes (holes 2 & 6) would likely experience

~1% greater mass flow than the remaining four unmodified holes. A plausible explanation for this could be explained by the 15° reduced change in direction that the main flow would have to undergo to enter these holes. This increased flow was not detected in the penetration plots however, plume penetration is considered to be governed by many factors of which flow rate is just one. For instance, a bushy spray plume will penetrate less far than a thin plume of the same flow rate, for this reason it is often difficult to draw conclusions between hole flow rate and plume penetration.

CFD - Liquid Phase Volume Fraction

To ensure that the behaviour of holes 2 & 6 was not hugely dissimilar to the four un-modified injection holes, on the request of the author CFD simulation was performed within DDS on the full 360° geometry of the RVN design using the LBFR's working fluid properties. Figure 74 shows the CFD results for the liquid phase volume fraction at 200 and 2000 bar with the needle valve set to full lift and a downstream pressure of 30 bar. Due to the symmetry of the nozzle about the axis of hole 1, cavitation will therefore be symmetrical; hence only a side view of the nozzle is sufficient to identify any cavitating regions.

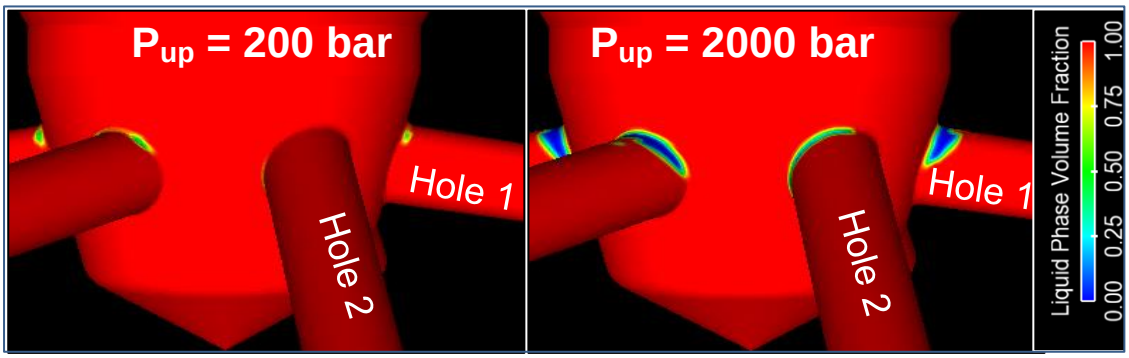

Figure 74 - Liquid Phase Volume Fraction (LPVF) for RVN design (simulation carried out by colleague in DDS)

Observations - Figure 74

1. At 200 bar injection pressure the CFD indicates that there is only a very small likelihood of vapour phase (cavitation) within the injection holes, although for holes 1, 3 & 4 this appears to be not at the hole central axis but just either side of this. Within hole 2 the cavitation is almost negligible (in fact difficult to distinguish in the image) yet oddly eccentric,

being confined between 9 and 10 o'clock at entry when viewed from the hole exit.

2. Similar to the 200 bar case, at 2000 bar injection pressure the cavitation is again confined to the top of hole entry for holes 1, 3 & 4, yet is found to peak in distinct regions either side of the holes central axes. A potential reasoning for this could be the effect of twin, close-coupled vortices at the top of the injection hole as has been identified at hole entry (Soteriou, et al., 2000) (Soteriou, et al., 2001). Any cavitation occurring at the centre of these vortices would therefore appear slightly off the central axis of the hole. Within hole 2, the cavitation is eccentric and located between 8 and 1 o'clock again when viewed from the hole exit. This is likely due to the unusual positioning of this hole and indicates that the flow is entering this hole eccentrically.

5.3.3. LBFR RVN - LSM Design & Manufacture

Whereas the real size RVN provided useful spray plume development data, this is not beneficial in determining the interior flow structure and the interaction this has with the needle valve and the injection holes. This information is desirable as knowledge of how the flow behaves and interacts within the injection hole could enhance understanding of spray plume formation which is key to air/fuel mixing and thus the combustion process.

Having validated and proven the injection hole positioning modifications made to create the RVN design, an acrylic 20x scale LSM was manufactured for testing on the LBFR but featuring parallel injection holes for the same reasons as given with the 120° seat nozzle project. Like the 120° seat nozzle, a lower C_d was assumed which necessitated slightly enlarged injection holes to provide the same flow as the six tapered holes of Ø0.117mm. This resulted in holes of Ø0.121mm equivalent to Ø2.42mm when scaled to LSM values.

Figure 75 is a CAD model of the RVN LSM in both side and plan views with pipe fittings. Also included in Figure 75 is the acrylic needle valve which can be regarded as being lightly truncated owing to the low flow nature of the base nozzle design. The numbering system for each of the holes is representative to that of real size nozzle manufacturing, clockwise when viewing from an upstream position. The external geometry of the LSM was shaped to provide

enhanced optical access with flat polished surfaces angled perpendicular to the intended regions of interest, thus preventing camera glare and unwarranted internal reflections. The outstanding feature of this model however, is the optical access to the full length of injection hole 1 when looking perpendicularly through a viewing face just above the pipe fitting of hole 2. This provides unprecedented LLS and PIV image quality and is a unique feature for a nozzle model with four or more equispaced injection holes. Compared to the 120° seat nozzle model, it is therefore much simpler to perform PIV within cavitating flows as cavitation from the adjacent injection holes does not obstruct optical access to the flow within hole 1. The same specialist firm who made the 120° seat nozzle LSM was again used to manufacture this model.

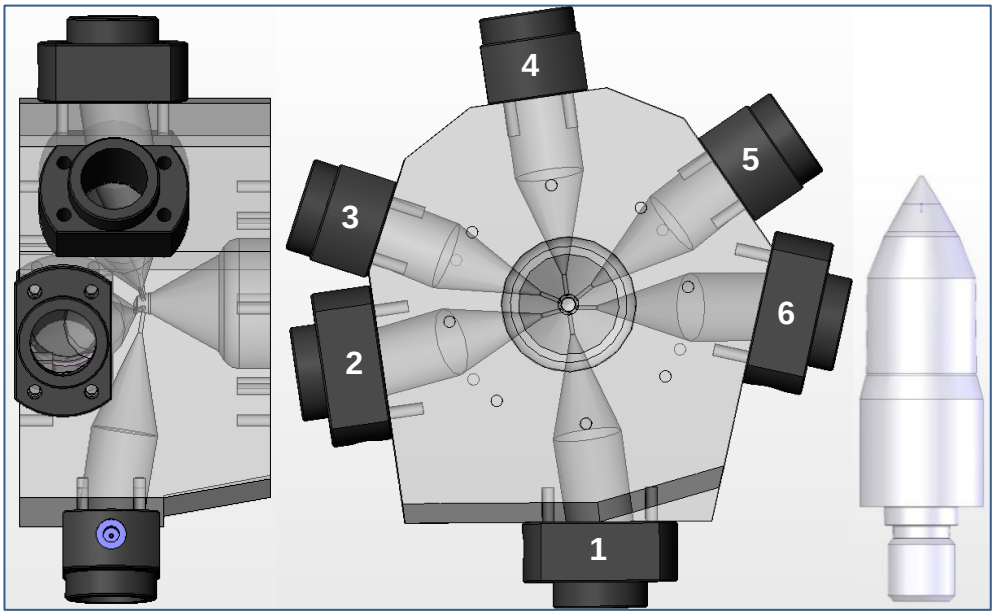

Figure 75 - RVN LBFR nozzle LSM and needle valve

To create the same inlet radius conditions as the real size components, post manufacture the nozzle LSM was honed using the AFM process in the same manner as with the 120° seat nozzle project. Owing to the modified geometry of holes 2 & 6, measurement of the real size RVN nozzles indicated that these holes should feature slightly larger inlet radii than the four remaining holes. This somewhat complicated the honing process but the results from this are summarised in Table 4.

5.3.4. LPR RVN - LSM Design & Manufacture

In addition to the model for the LBFR, a second much smaller LSM of the RVN design was manufactured but for the purpose of being ran on the LPR. Whilst the LPR model features the same internal geometry as the LBFR model, it was shaped externally like the real size nozzle. The reasoning behind this was to ensure that the hole exit shape was representative of the real size nozzle so that the spray plume development would be accurate. This results in distortion when looking through the curved external surface, making it difficult to observe the internal flow structure. Hence the main purpose of the LPR model is for visualisation of the emerging spray plumes, however, with adequate lighting cavitation within the injection holes may still be distinguishable.

The RVN LPR model is shown in Figure 76 in side and plan views with representative plumes attached and alongside the needle valve of representative scale. Unlike the LBFR model, as the LPR model is not designed for internal flow visualisation, the needle can be fabricated from aluminium (for ease of manufacture) instead of acrylic.

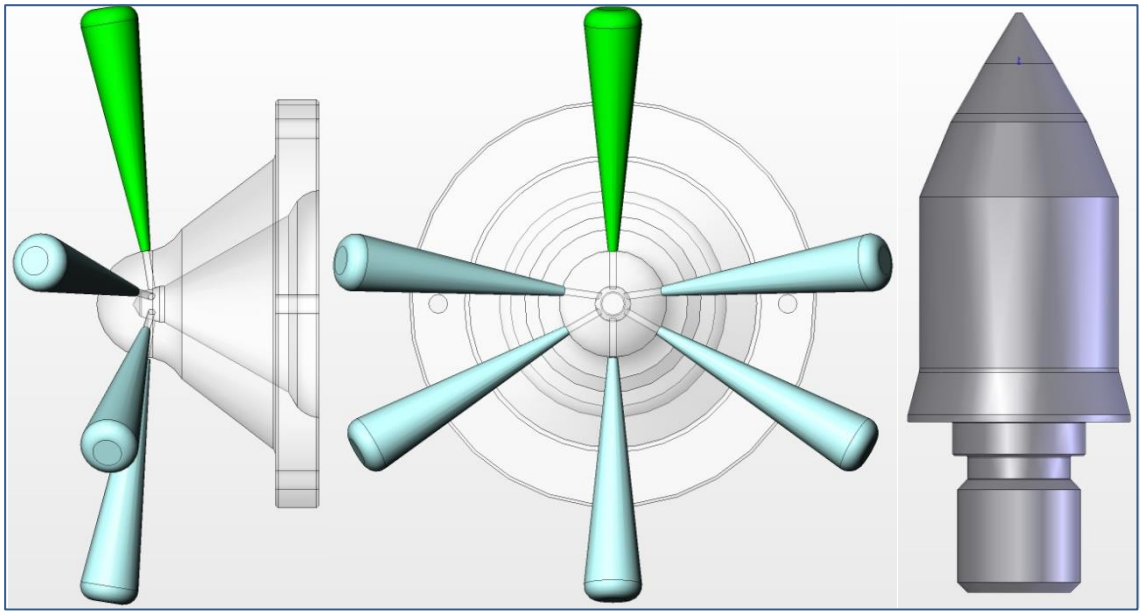

Figure 76 - RVN LPR nozzle model and needle valve

As with the LBFR model, the LPR model was honing using the AFM process to create the required hole inlet radius conditions. Owing to the variability of this process, whilst the internal dimensions were nominally identical between the

two models, slightly different inlet conditions were created compared to the LBFR model. These are summarised in Table 4.

Hole number(s)	Desired Real Size Radii's (scaled x 20) [mm]		LBFR model Radii's [mm]		LPR model Radii's [mm]	
Location	Top hole	Bottom hole	Top hole	Bottom hole	Top hole	Bottom hole
1,3,4,& 6	0.26	0.22	0.23	0.10	0.17	0.17
2 & 6	0.34	0.15	0.26	0.08	0.22	0.15

Table 4 - Injection hole inlet edge conditions

For both models it is quite evident that the honing process has not created hole inlet edge conditions of the same magnitude as the real size nozzles, especially at the downstream edge (6 o'clock). This is an observation that has been reached with previous LSMs as the relative weakness and softness of acrylic limits the maximum permissible honing pressure and duration. It was expected that having the same internal geometry, the LPR and the LBFR models would have resulted in the same hole inlet conditions if honed for the same duration and at the same pressure. However, the honing media had to be renewed prior to the LPR model honing and a possible slight difference in the viscosity of the new media may have contributed to create a different hole inlet geometry. With hindsight it is likely that the large differences between the upstream and downstream radii on the LBFR model is due to the viscosity of the cutting media being too high.

In Figure 77 the four areas of maximum restriction have been calculated and are displayed graphically up to 1mm lift which is the most interesting lifting region. It is evident that as the needle lifts the area of maximum restriction moves from the seat to the truncation location after 0.29mm lift and remains there for a short period before moving to the sac entry location. Finally at 0.72mm lift, the injection holes become the maximum restriction or minimum flow area. Having a 60° seat and being based on a low flow nozzle (0.5l/min

real size), the RVN design has a much reduced flow area for a given needle lift compared to the 120° seat design in the earlier project.

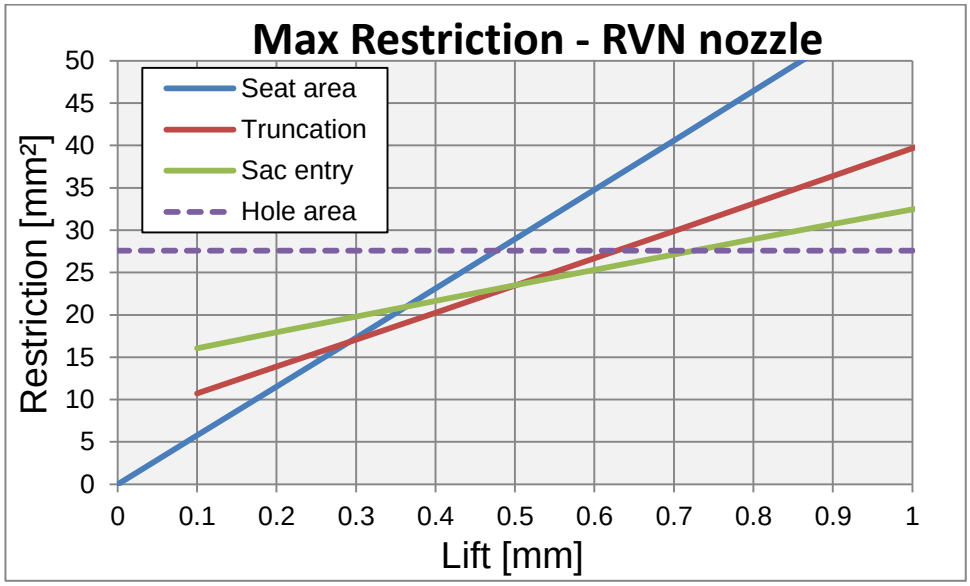

Figure 77 - RVN LSM flow areas

5.3.5. Scaling Between LSM & Real Size

In order to draw comparisons between the observations from the real size nozzle and both the LPR and LBFR models, it was necessary to equate between each to ensure identical test conditions. Unfortunately due to the different fluid properties between the working fluids of the LPR and LBFR, this was a more difficult task than initially envisioned. Whilst the LBFR uses a blend of liquids to create 'laser rig fluid', the LPR and the real size experimentation both use calibration oil.

Fluid Properties

As both the LPR and LBFR operate at relatively low pressures and at a fixed temperature, the fluid properties can be assumed to remain constant. However, with both simulation and real size nozzle experimentation this is not the case as fluid properties are known to vary significantly with changes in pressure and temperature. Table 5 summarises the constant LPR and LBFR values alongside the assumed CFD upstream values which were derived from previous laboratory investigations within DDS.

Test	Density [kg/m³]	Viscosity [m²/s]	P_{Vapour} [bar abs.]
CFD [200 bar]	802.98	$1.46e^{-06}$	0.01
CFD [2000 bar]	800.61	$1.86e^{-06}$	0.01
LPR [35 °C]	816.15	$2.77e^{-06}$	0.013
LBFR [25 °C]	896	$1.63e^{-06}$	0.01

Table 5 - Fluid properties for model scaling

Scaling From Real Size

When scaling between real size components and LSMs, the significantly different fluid properties need be taken into account as indicated from the equations within the Scaling Between Real Size & Large Scale Models section earlier in this thesis. Also it is worth at this stage reaffirming that this scaling relationship is only strictly correct to use at full needle lift where the restriction across the valve seat can be assumed to be negligible.

An example of the difference that the fluid properties make when scaling pressure drop of 500 bar and a flow of 0.98l/min on a real size to both the LBFR and LPR is given in Table 6.

Parameter	Real size	LBFR	LPR
Pressure Drop [Bar]	500	0.87	2.27
Flow [l/min]	0.98	20	34

Table 6 - Scaling of pressure and flow

A 500 bar pressure drop across a real size nozzle equates to a 0.87 bar pressure drop across the LBFR when scaled using the laser rig fluid properties. However, scaling this 500 bar pressure drop to the LPR using calibration oil fluid properties, equates to a pressure drop of 2.27 bar. Therefore even adopting the same scaling factor between models, a pressure drop of 0.87 bar on the LBFR is comparable to a pressure drop of 2.27 bar on the LPR, owing to the different working fluids. Alternately when scaling in terms of flow, a flow rate of 20l/min on the LBFR, is equivalent to a flow rate of 34l/min on the LPR.

Flow versus Lift

In order to validate the scaling process, Figure 78 consists of plots of Flow versus Lift comparing the LSM and scaled real size experimental data. The LHS plot consists of LPR experimental data at a constant ΔP of 2.27 bar (P_{up} = 2.02 & P_{dn} = - 0.25 bar, CN 3.0). The RHS plot consists of LBFR experimental data at a constant ΔP of 0.87 bar (P_{dn} = 0 bar, CN 0.86). Both plots have purple lines superimposed relating to the scaled real size data from the Curtis rig at a ΔP of 500bar (P_{up} = 500 & P_{dn} = 0 bar). This Curtis rig data has been supplied by colleagues within DDS.

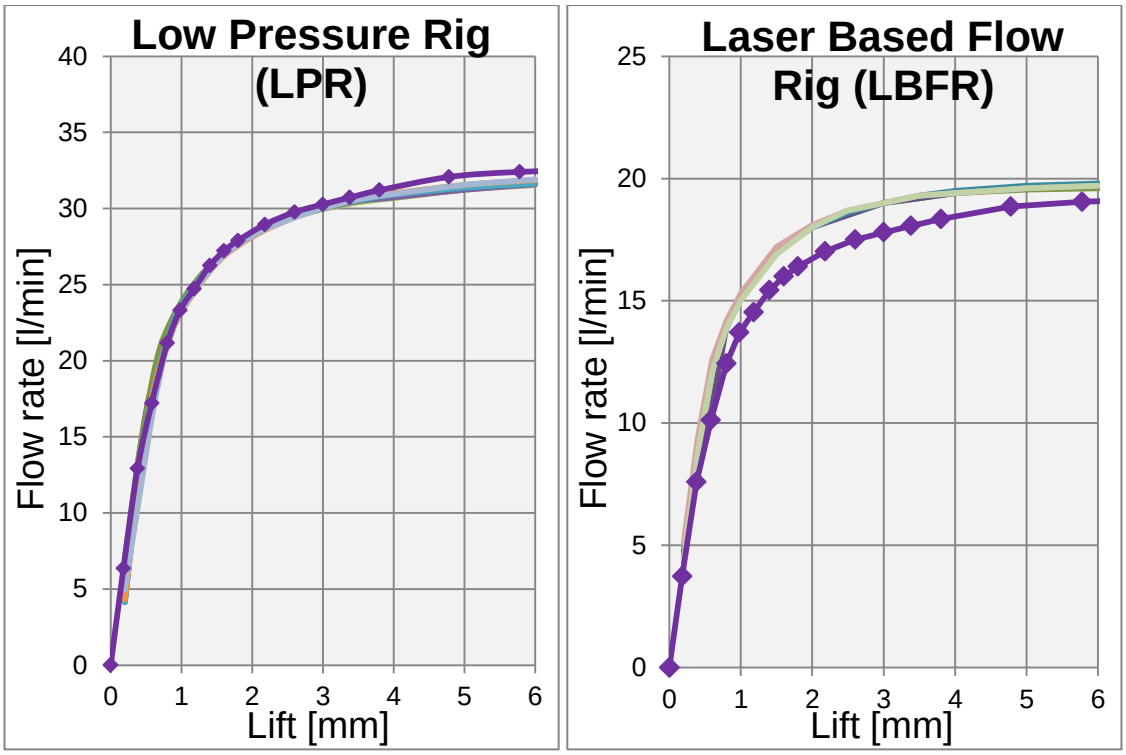

Figure 78 - LSM and Real Size - Flow versus Lift plots

The LPR plot shows a good correlation between the LSM data and the scaled Curtis rig data. The slight difference seen above 3.5mm valve lift could be accounted for by the hole taper present on the real size nozzles which may prevent in-hole cavitation and account for the slightly higher flow at full lift. The LBFR plot is not so agreeable. Although a good following is noted at low lift, from approximately 0.6mm lift the scaled results diverge from the LSM data and remain significantly lower throughout the remainder of the lifting range. As the scaling assumes that the influence of the needle valve on the flow is

insignificant, the results should be closer at large lifts where this is perhaps justifiable. The vast difference in fluid properties (especially density) is the most likely cause of the difference in the LBFR plot. As both the LPR and the Curtis rig use calibration oil (although properties are temperature compensated), scaling is relatively straightforward. Even though the vastly different fluid properties are accounted for within the scaling equations, the microscopic effects of the different fluid properties on the flow (such as within the boundary layer) may be having an influence and perhaps warrants further investigation.

Experimental LSM Testing

The two LSMs were investigated to observe the internal nozzle flow within the LBFR model and the emerging spray plumes from the LPR model. The following section details this experimentation.

5.3.6. LBFR Hole 1 Internal Flow at CN 3

As has been mentioned, having the entirety of hole 1 visible from a 90° orientation without needing to look through or past another injection hole, is a unique advantage of this model. Not only is there a reduced likelihood of cavitation or optical distortion from adjacent injection holes, but having the camera mounted perpendicular to the illuminating light sheet plane ensures optimum PIV data accuracy.

Figure 79 contains both mean PIV velocity contours and raw unprocessed PIV camera images, collected at CN 3 with the light sheet orientated along the central axis of hole 1. The running conditions were 0.17 bar upstream, -0.8 bar downstream with the needle moving in the opening direction between 0.2 & 6.0mm lift (full lift) or 10µm and 300µm in real size component terms. The raw images have been included to indicate the location and intensity of any cavitation within the injection hole. LLS images have not been compared at this running condition as intense laser light scattered from the cavitation bubbles at CN 3 makes it almost impossible to visualise the path lines from the seeding.

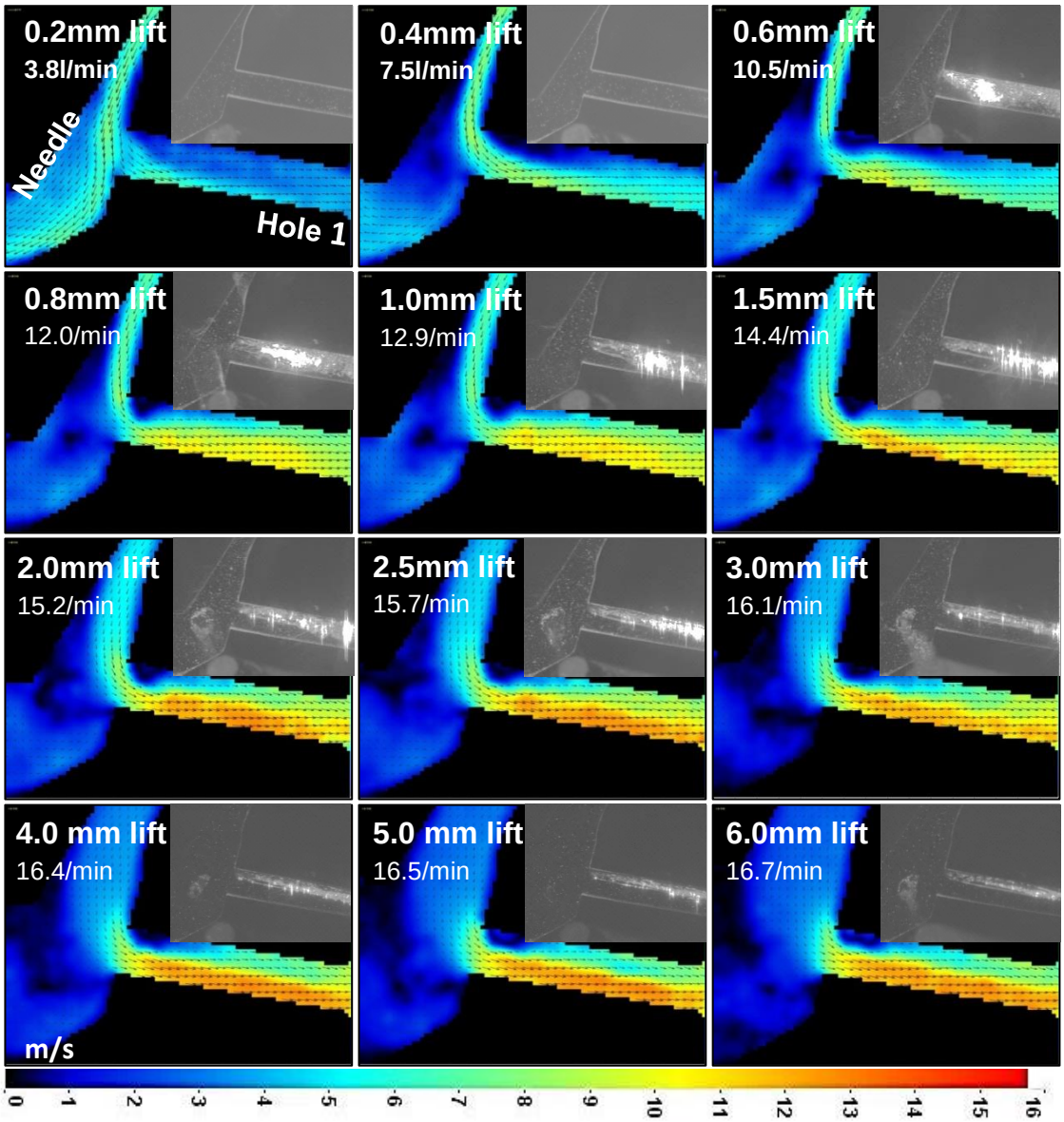

Figure 79 - Hole 1 PIV velocity contours - CN 3

Observations - Figure 79

1. At 0.2mm lift the majority of the flow appears to be passing the inlet to the injection hole and flowing under the needle valve's tip, which perhaps indicates a degree of needle eccentricity at this very low lift.
2. At 0.4mm lift the majority of the flow from the seat is seen entering the injection hole from above resulting in a large separated region at the top of the hole with the bulk flow confined below this. The velocities in the bottom of the sac although not as large in magnitude as at 0.2mm lift, still remain reasonably high.
3. At 0.6mm lift the separated region exhibits a noticeable change in its shape owing to the occurrence of cavitation at the top inlet of the

injection hole. Additionally, a vortex structure is seen to develop centred about level with the bottom of the injection hole and approximately midway between the nozzle body and needle valve.

4. By 1.5mm lift the cavitating region in the raw PIV camera image appears to be thinner and more confined to the top of the injection hole whilst taking on a more glass-like appearance.
5. The stationary vortex structure observed since 0.6mm lift appears to have started to migrate towards the needle valve tip at 1.5mm lift. By 2.0mm lift it would appear that the vortex structure has become a low velocity region extending towards the needle tip. However, on closer inspection of the raw image, this is in all likelihood due to cavitation in hole 2 between the camera and the light sheet plane manipulating the vectors in this vicinity.
6. As the lift is further increased to 6.0mm, both the PIV vectors and the raw images indicate that the separated region at the top of hole 1 continues to reduce in thickness with the shed cavitation bubbles eventually appearing to form a region occupying the top approx. 40% and extending the whole visible length of the hole.

In addition to the mean PIV vector images in Figure 79, Root Mean Square (RMS) data was also extracted and this is displayed in Figure 80. RMS data provides an excellent method of identifying the variation in a particular flow, which may not be immediately obvious from the mean vectors. The RMS images have adopted a scaling range of between 0 and 6m/s and for ease of clarity only contain the velocity contours.

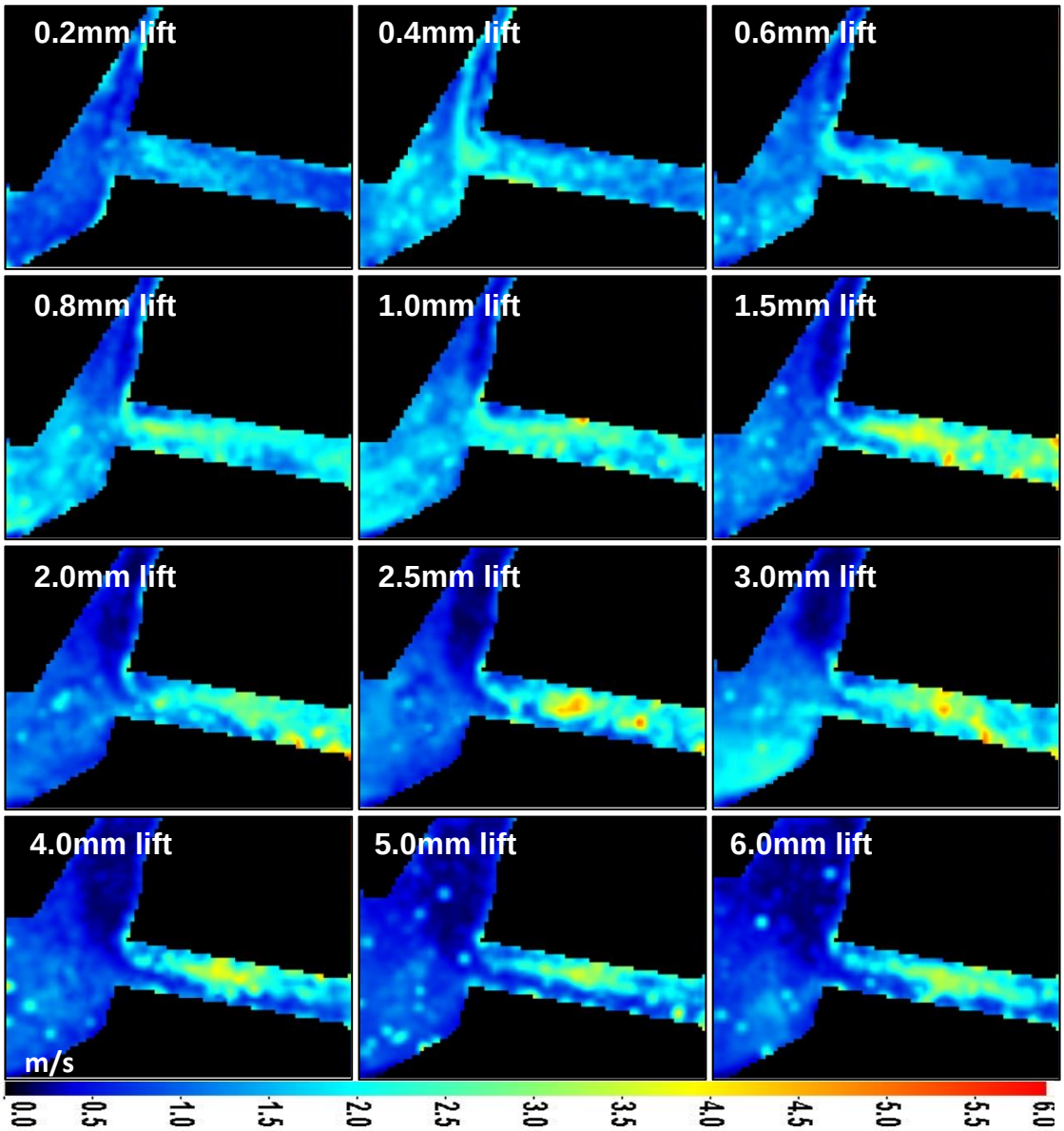

Figure 80 - Hole 1 RMS PIV velocity contours - CN3

Observations - Figure 80

1. The onset of hole entry cavitation at 0.6mm lift has a marked effect on the magnitude of the in-hole RMS values. This is possibly due to either a reduction in effective flow area at entry due to the growth of the cavitating boundary layer, or through increased 'jostling' between the travelling bulk flow and the shed cavitation bubbles. However, the fact that peak RMS values are found to occur roughly midway along the visualised hole length and not towards the entrance, indicates that it is likely the shed cavitation which is inducing the variation in the flow.

2. One interesting observation is the region of consistently low RMS values at the topmost entrance to the injection hole where cavitation inception is most likely to occur. This indicates a degree of uniformity in that the velocities in this area are relatively stable. This assuming the PIV data collected within this cavitating region is accurate, suggests the mechanism governing the growth and period shedding of cavitation is constant and stable.
3. Clearly identifiable at lifts above 3.0mm is a large relatively stable region that is confined to the bottom of the injection hole and extending along its entire length. Clearly this indicates the bulk flow which is able to pass through the injection hole without encountering and being influenced by the cavitating region at the top of the bore.

Detached Boundary Layer Thickness

In an attempt to investigate the separated region and a possible change in the thickness of the detached boundary layer with increasing needle lift, the mean PIV velocity component data at CN 3 was extracted along an arbitrary line positioned perpendicular to the injection hole axis and located just inside the entry to the injection hole.

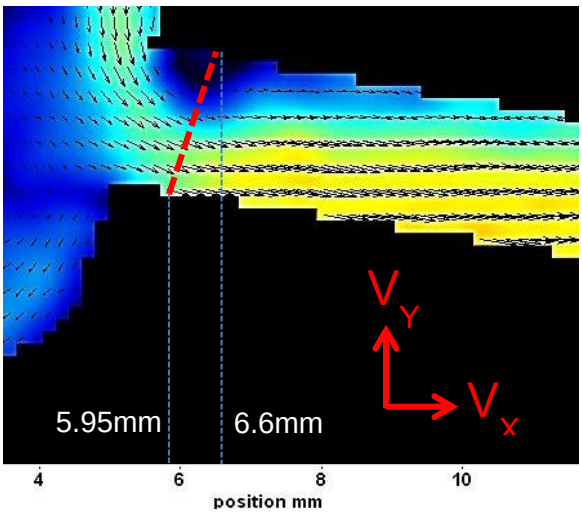

Figure 81 - Boundary layer measurement location

Due to the orientation of the camera relative to the visualised injection hole, the flow consists of a large V_X and a much smaller V_Y component. Figure 81 shows the location of this line with the velocity data being extracted in relation to the PIV image x-axis location and not the distance along the line.

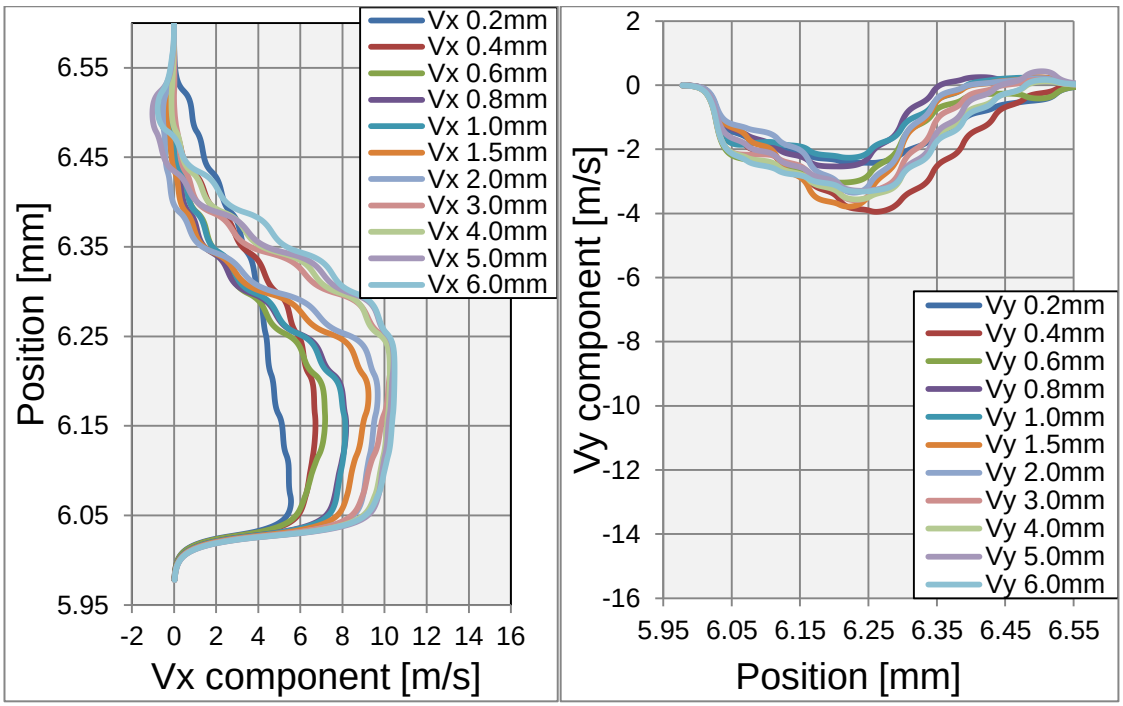

Figure 82 - V_X and V_Y components - CN 3

In Figure 82, both velocity plots have the same scaling range although the V_Y plot has had its scales reversed to assist with interpretation of the data. The same sign convention has been adopted as with the 120° seat angle project - to the right and upwards being positive in the V_X and V_Y directions respectively.

Observations - Figure 82

1. V_X component
    a. The highest velocities and the majority of the flow is found to be in the bottom half of the injection hole.
    b. Except at 0.2mm lift, the shape of the individual plots appear to show the classical separated boundary layer velocity profile with a slight reverse flow close to the upper surface of the injection hole.
    c. At 0.2mm lift, a gradual almost linear decrease is seen in the velocity from the bottom to the top of the injection hole. This is not replicated at higher lifts and flow rates.
    d. A step change is detected in the plots between 2.0 & 3.0mm lift with a much reduced thickness in the separated region at 3.0mm lift and above. Ignoring the 0.2 & 0.4mm plots which are non-

cavitating, two distinct profiles are detected within the cavitating flows. In an attempt to better demonstrate this apparent reduction in separated region thickness, the V_X data for 1.5 - 2.0mm lifts and 3.0 - 6.0mm lifts were grouped together, averaged and then plotted. Figure 83 illustrates this with dashed red lines indicating the apparent velocity profiles. The arrows indicate a marked reduction in the separated regions thickness (b_1 & b_2) as the needle valve lift was increased.

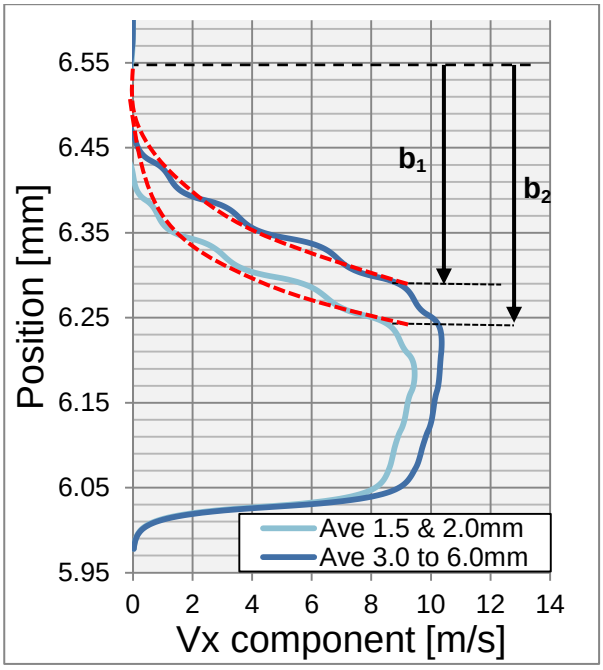

Figure 83 - Separated region reduction with lift - CN 3

1. V_Y component
   a. As with the V_X component, the highest velocities were found to occur within the bottom half of the injection hole.
   b. A very slight positive (upwards) flow was seen at the top of the injection hole in the V_Y direction for lifts of 0.8mm and above. This likely indicates significant recirculation associated with the detachment of the boundary layer.

5.3.7. LBFR Hole 1 Internal Flow at ΔP = 0.87 bar

As has been demonstrated in Table 6, a pressure drop of 0.87 bar on the LBFR is comparable to a pressure drop of 500 bar on the real size component when scaling and the different fluid properties are taken into account. With the PIV camera and light sheet nominally located at the same position as during the CN 3 testing, the needle valve was again moved in the opening direction between 0.2 and 6.0 mm lift. Unlike the CN 3 testing however, both LLS and PIV vector images were captured and these are shown in Figure 84. The experimental conditions for these tests were a P_{up} of 0.87 bar and a P_{dn} of 0 bar (or atmospheric conditions). Owing to the presence of the LLS images it was deemed not beneficial to include the raw PIV images.

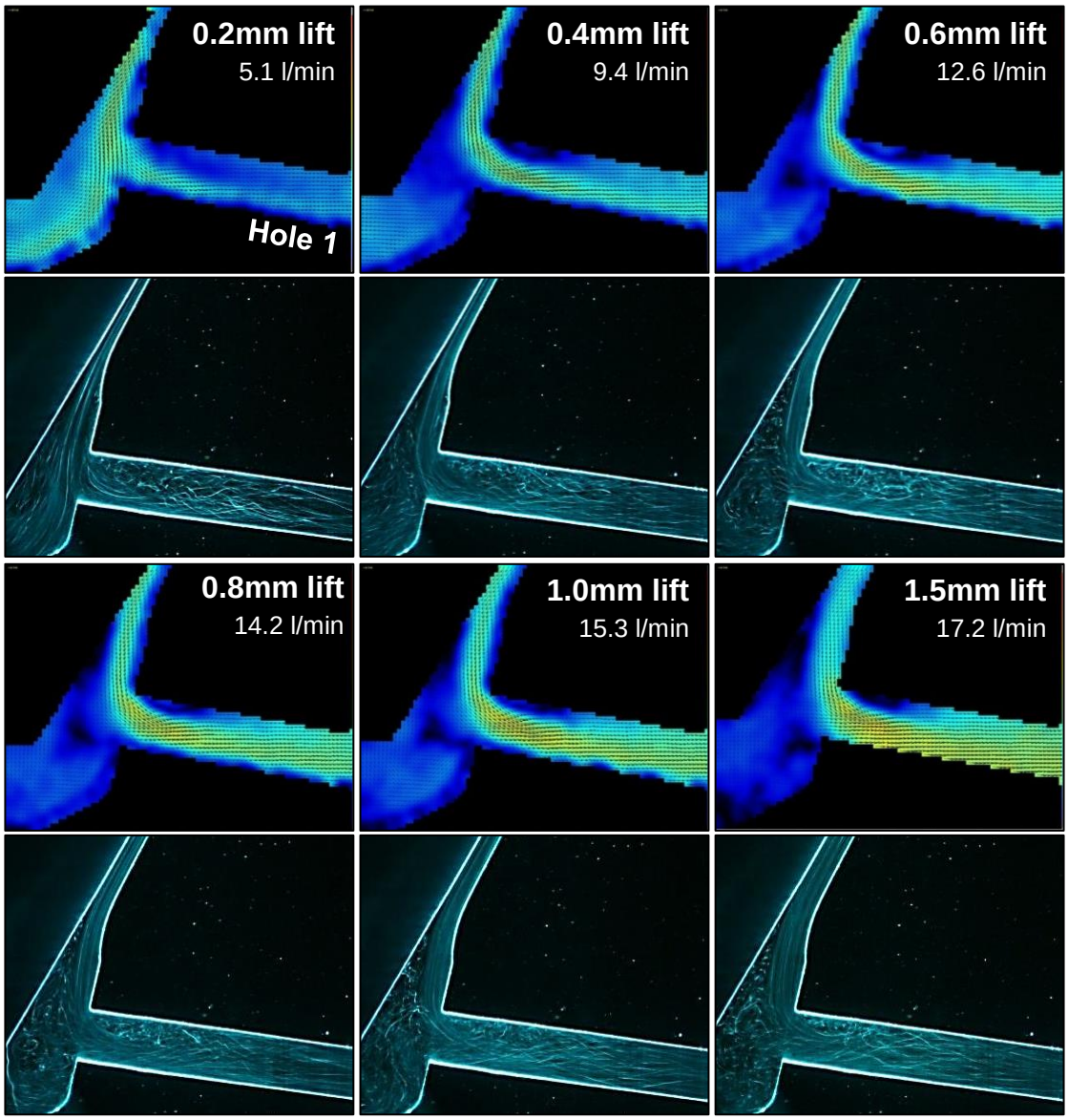

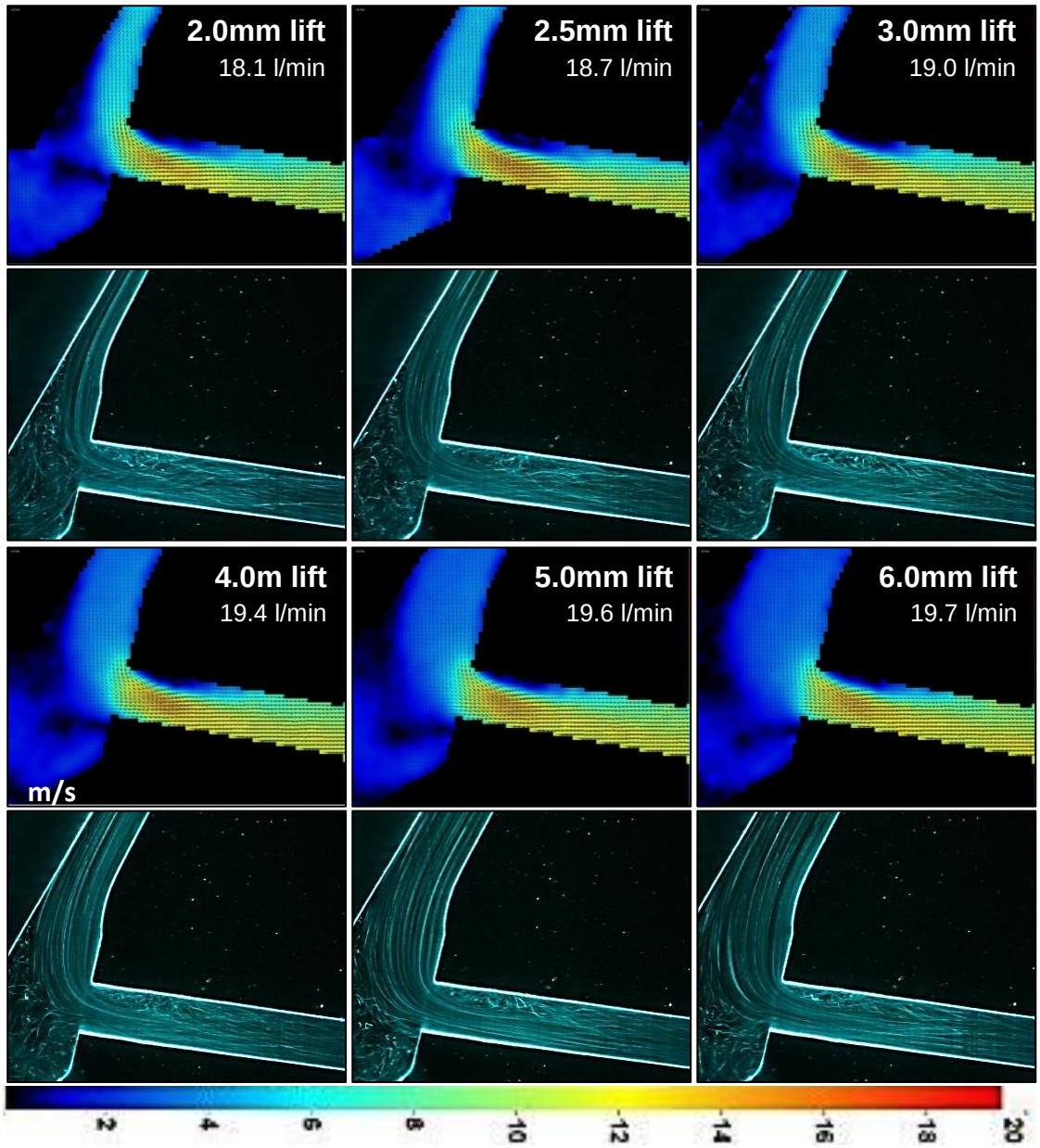

Figure 84 - Hole 1 PIV velocity contours and LLS images - 0.87 bar ΔP

Observations -Figure 84

At this pressure drop it is apparent that the flow is non-cavitating which is beneficial to not only improve the optical quality of the LLS images but also to increase PIV vector accuracy. When comparing between the LLS and PIV images, it is worth remembering that the PIV results are averaged whereas the LLS images are individual images subject to fluctuations and possibly short-lived and erratic flow phenomena.

The findings are as follows:

1. Like what was observed at CN 3, at 0.2mm lift it is evident that the majority of the flow is passing the entry to hole 1 and progressing into the

bottom of the sac. As only half the nozzle is being visualised, it is impossible to state whether there exists a cross-flow within the sac.

2. At 0.4mm lift the main body of flow is now entering injection hole 1 from above, however, at the bottom of the sac in the PIV image, somewhat high velocities still remain.
3. At 0.6mm lift a vortex structure is seen in the PIV images with a substantial sized low-velocity 'eye', centred approx. level with the bottom of the inlet to hole 1. This vortex continues at this location until 2.5mm lift where it begins to interact with a large low velocity region developing below the needle tip. In all likelihood this structure is associated with the flow moving to enter hole 2, which is the hole situated between the camera and the light sheet plane. The reasoning behind this is that at this location the flow is expected to have a large V_Z component and therefore smaller V_X & V_Y components.
4. An interesting observation with the separated region's thickness is that it appears to grow and peak at 0.4mm lift, before diminishing as lift further increases to retain approx. 50% of its original thickness by full lift. This is likely explained by the flow being able to undergo a wider flow turn into the injection hole at larger lifts where it is less confined between the needle valve and the nozzle body. Overall the separated region's thickness appears much reduced compared to the CN 3 data.

As with at CN 3, RMS data was also extracted at 0.87 bar to compliment the mean PIV vectors. These RMS images are displayed in Figure 85 and again use a scaling range of between 0 and 6m/s.

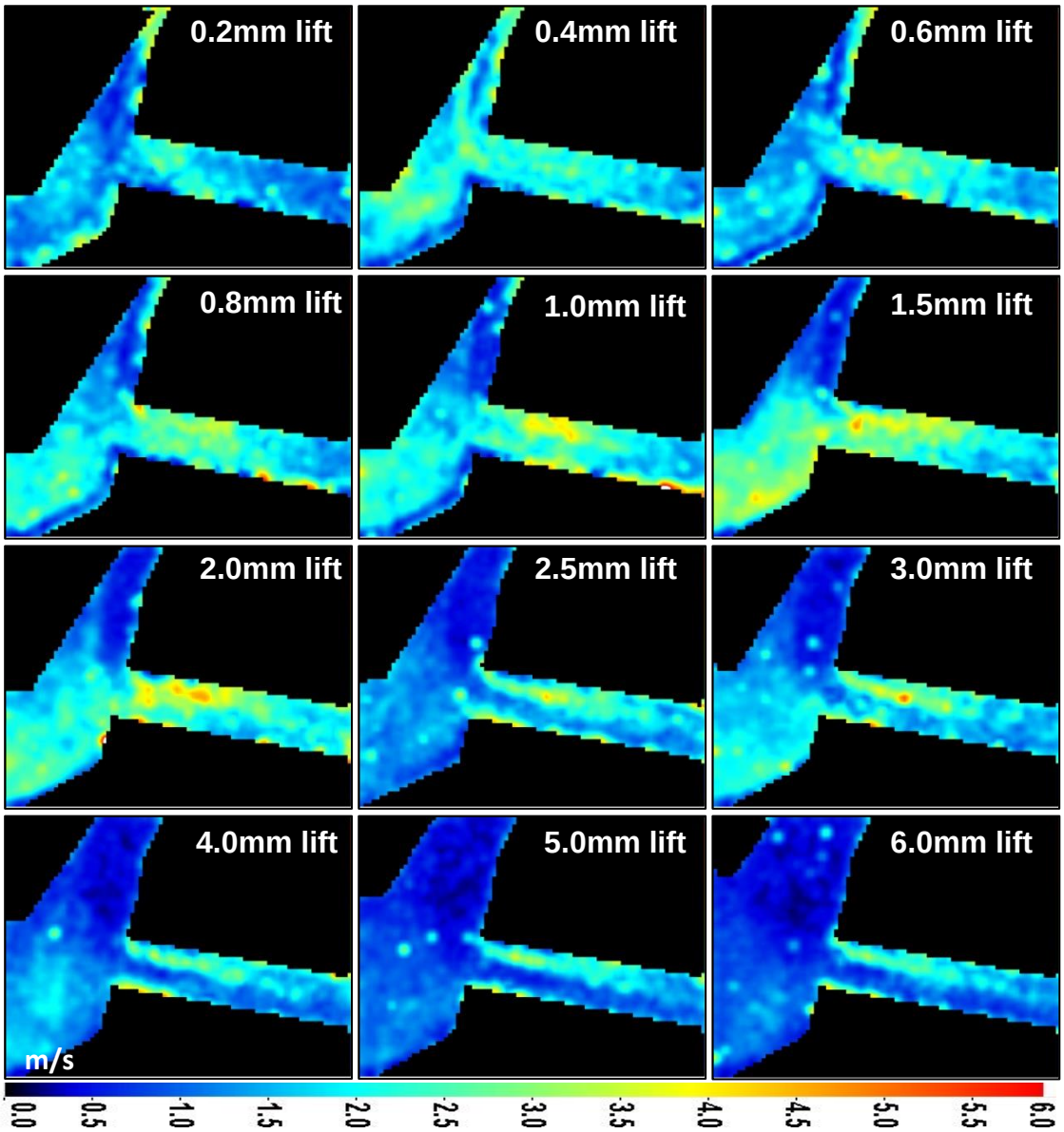

Figure 85 - Hole 1 RMS PIV velocity contours - 0.87 bar

Observations - Figure 85

1. It may not be fair to directly compare the CN 3 RMS (Figure 80) and 0.87 bar data as the running conditions vastly differ with a greater flow rate, velocity and hence RE within the injection hole at 0.87 bar. This is also perhaps the reasoning for the somewhat higher sac RMS magnitudes at 0.87 bar.
2. The greatest variations in the flow are detected in the first half of the injection hole near the vicinity of its entrance. This is to be expected owing to the flow turning sharply and then redistributing itself to continue through the remainder of the hole where it can do so unobstructed. This

is in contrast to the CN 3 case where shed cavitating was thought to interfere with the flow in this part of the hole.

3. Especially at lifts above 2.0mm, the RMS values within the hole and the nozzle sac are much reduced indicating lower variability in the flow. Quite like at CN 3, a region of low magnitude has developed at the bottom of the injection hole, however, at 0.87 bar this appears to extend over a greater cross-sectional area of the hole.

Detached Boundary Layer Thickness

Similar to at CN 3, V_X & V_Y data was extracted from the ΔP = 0.87 bar tests along an arbitrary line just inside the entrance of hole 1 and situated perpendicular to the hole's axis. While nominally the same setup and measurement location was used as at CN 3, the PIV camera's distance from the LSM and hence the scaling differed slightly so the values for position within the nozzle sac do not correspond with the CN 3 plots. Figure 86 contains the extracted V_X & V_Y data plotted against the horizontal measurement location. The legend on the V_Y plot applies to the V_X plot also and the same velocity scaling range was used for both plots with the sign convention of right & upwards being positive in the V_X and V_Y directions respectively.

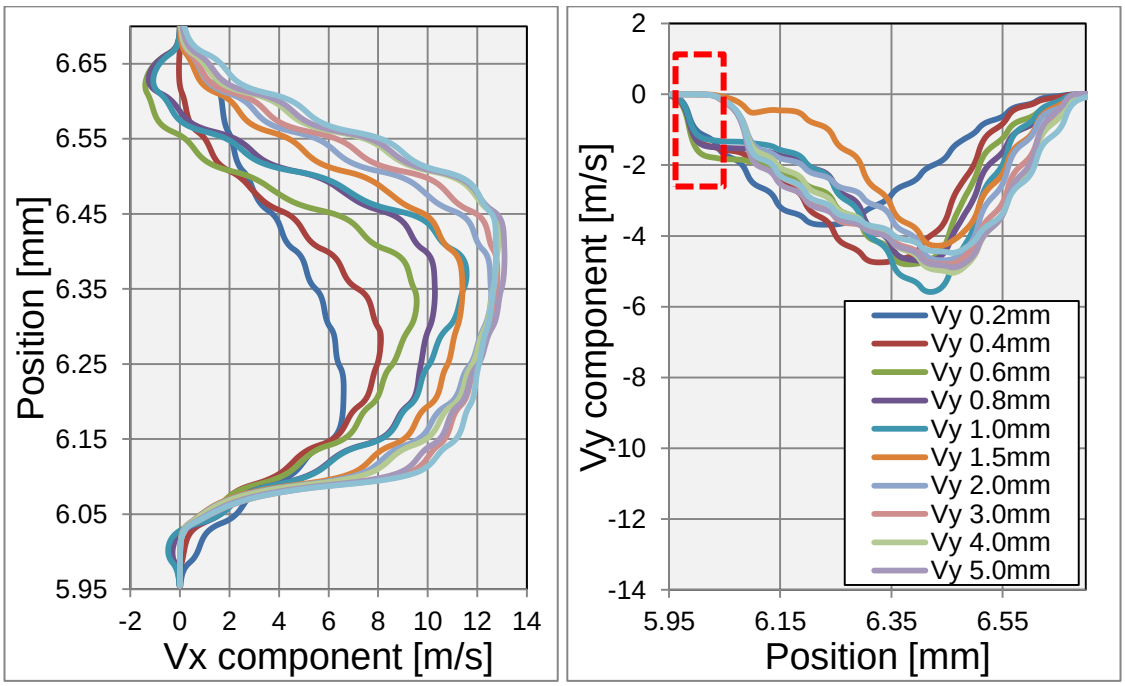

Figure 86 - V_X and V_Y component plots - 0.87 bar ΔP

Observations - Figure 86

1. V_X component
    a. Towards the centre of hole 1 the velocities are consistent with the highest velocities occurring slightly towards the top of the hole at lifts ≥ 0.8mm lift.
    b. The lowest four lifts all appear to exhibit some degree of reverse flow near the top of the injection hole. The path lines in the LLS images support this as they appear to be highly confused within this part of the injection hole.
2. V_Y component
    a. The peak V_Y magnitudes appears to coincide with the location of the peak V_X data by occurring slightly towards the top of the injection hole. This is reasonable as the injection hole is not aligned with the x-axis therefore for flow moving parallel to the hole axis, a large V_X value would result in a large V_Y value.
    b. At 1.5mm lift the data shows a significantly reduced magnitude across the lower half of the injection hole, indicating a different flow structure than the remaining ten lifts. No obvious evidence for this was observed in the LLS and PIV images.
    c. At 1.5mm lift and above, the flow at the bottom 10% of the hole cross-section (area indicated by a red dashed rectangle on the V_Y plot) contains zero V_Y magnitudes, however, at lifts below 1.5mm the flow in this region consists of significant (~30% of peak) velocities. This appears to be linked to the mask that was applied prior to PIV processing which seems to have clipped the vector image slightly thus affecting the velocities at this location.

Although measured at the same position and within the same injection hole, there exists a very different velocity profile at 0.87 bar than at CN 3. In the V_X direction at 0.2 & 0.4mm lift, the velocities were similar (both being cavitation free) and much more consistent within the injection hole at both running conditions. However, above 0.6mm lift the effect of cavitation at CN 3 was to confine the highest velocities to the lower approx. 60% of the injection hole. At 0.87 bar there appeared an almost linear increase in velocity and an apparent linear reduction in the separated region's thickness with increasing needle lift,

whereas at CN 3 there appeared to be two distinct velocity profiles to this separated region. The comparison between CN 3 and 0.87 bar results is less clear in the V_Y direction.

Ignoring the odd results that have already been mentioned, the different velocity profile of the 0.87 bar results is likely explained by the greater V_X velocities during these tests, the reduced separated region thickness and/or the lack of shed cavitation jostling the travelling flow.

5.3.8. LPR Hole 1 Plume Structure

The LBFR is designed for the purpose of studying the internal nozzle flow and is therefore not optimised for study of the emerging spray plume structure. For this reason the analysis of the plume structure was carried out on the RVN LPR model whose design and manufacture was discussed earlier in this project section.

In order to compare like-for-like between the LBFR and the LPR, equivalent running conditions are essential. Due to the vastly different working fluids between the rigs, the scaling resulted in a much higher ΔP for the LPR compared to the LBFR. A fuller explanation of this was given earlier, however, simply put a ΔP of 0.87 bar on the LBFR equates to a ΔP of 2.27 bar on the LPR.

The test conditions for LPR testing were chosen to satisfy both the required pressure drop and the necessary CN with the needle again being moved in the opening direction. This resulted in pressures of P_{up} = 2.02 and P_{dn} = - 0.25 bar (CN 3) un-submerged.

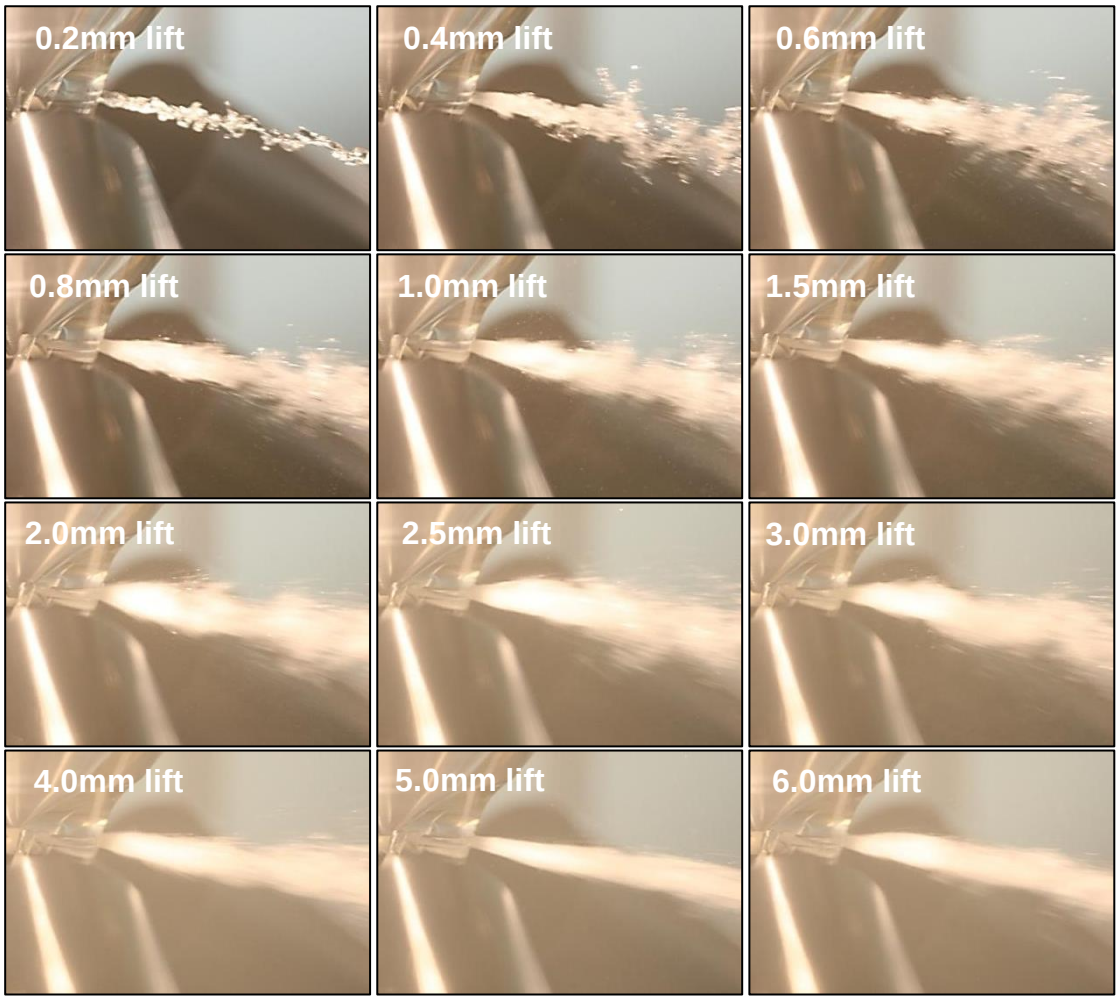

Figure 87 - Emerging spray plume un-submerged - 2.27 bar ΔP

Figure 87 contains images taken in the opening direction with the camera positioned perpendicular to the axis of hole 1. The camera was fitted with a macro lens and set to a shutter speed of 1/4000 s (250 µs) with illumination provided by a 1000W flood light. Between the relatively small injection holes (for a 20x scale LSM) and injecting into un-submerged downstream conditions, the inside of the LPR's vacuum chamber rapidly filled with atomised fuel resulting in poor optical clarity. In an attempt to curtail this, six black metal pipes of 40mm internal bore were installed within the LPR chamber and orientated in an attempt to direct the injected fuel away from the windows and allow it to return to tank. These pipes can be seen in the images and although they somewhat improved the image quality, the chamber still filled with atomised fuel, particularly as the flow rate rose with increasing needle valve lift.

Observations - Figure 87

1. It is difficult to determine any spray detail from these images with the possible exception of the image at 1.5mm lift which appears to show the plume of hole 1 consisting of an anticlockwise vortex coiling around its core or axis (when viewing from the hole exit).
2. The only other noteworthy observation is that with increasing lift, the jet angle of the plume from hole 1 increases to a maximum value at 0.6m lift and then remains relatively constant before diminishing again but not until 5.0mm lift. This is likely associated with the observed reduction in the thickness of the separated region within the injection hole bore as lift increases.

To improve upon the spray plume images, the tests were repeated but in this instance injecting into a submerged downstream chamber.

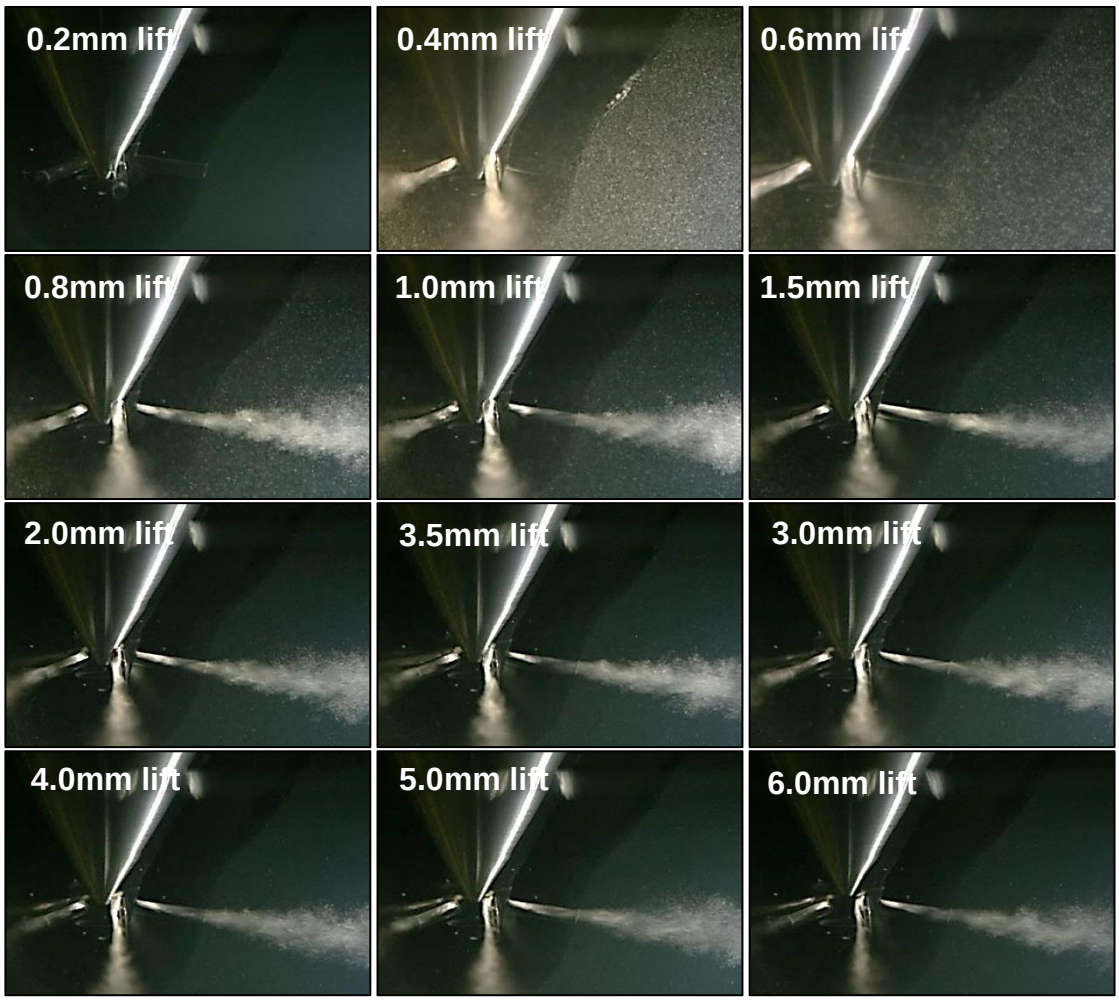

Figure 88 - Emerging spray plumes submerged - 2.27 bar ΔP

It is worth mentioning that although the running conditions were the same, injecting into liquid results in a much higher density than when injecting into air, which will likely affect the plume penetration and possibly the plume development also.

The arrangement with the submerged chamber had the beneficial effect of allowing more direct lighting via an LED light source as opposed to the 1000w flood light used when un-submerged. The different light source explains the difference in colour saturation and also allowed the adoption of a faster camera shutter speed of 1/8000s (125 µs). Whilst the running conditions were initially set at a ΔP of 2.27 bar, in order to improve the imaging it was necessary to suppress the cavitation by slightly throttling the submerged chamber's exit. This would have resulted in a slightly higher P_{dn} value than the intended -0.25 bar.

Observations - Figure 88

1. Although hole 1 did not cavitate until 0.8mm lift, the visible remaining holes all appeared to be cavitating from just 0.4mm lift. This is most likely due to very slight geometric differences between each of the six holes.
2. In agreement with the un-submerged images, the jet angle from hole 1 is seen to increase and then reduce as the needle valve is lifted.
3. The emerging plume of hole 1 appears to show a helix structure. This is especially evident in the images at 0.8, 1.0, 3.0 & 6.0mm lifts.
4. Although it is difficult to identify the flow structure within hole 1 itself, the cavitation is clearly confined to the top of the injection hole and the separated region (containing the shed cavitation) undeniably reduces in thickness and possibly elongates as the needle valve is lifted.
5. With hole 2 situated in front of hole 1 and with the camera looking along its length, a unique perspective is provided of the flow structure within this injection hole. Not only is it evidently clear that the cavitation is confined to the side of the bore furthest from hole 1, but the cavitation is also seen to follow a helical flow pattern immediately as it exits the hole and even possibly within the hole itself. Figure 89 is an enlarged image of the 3.0mm lift case with the brightness and contrast altered to better illuminate the in-hole flow. Lines have been superimposed to identify the geometry of the needle valve and that of holes 1 & 2.

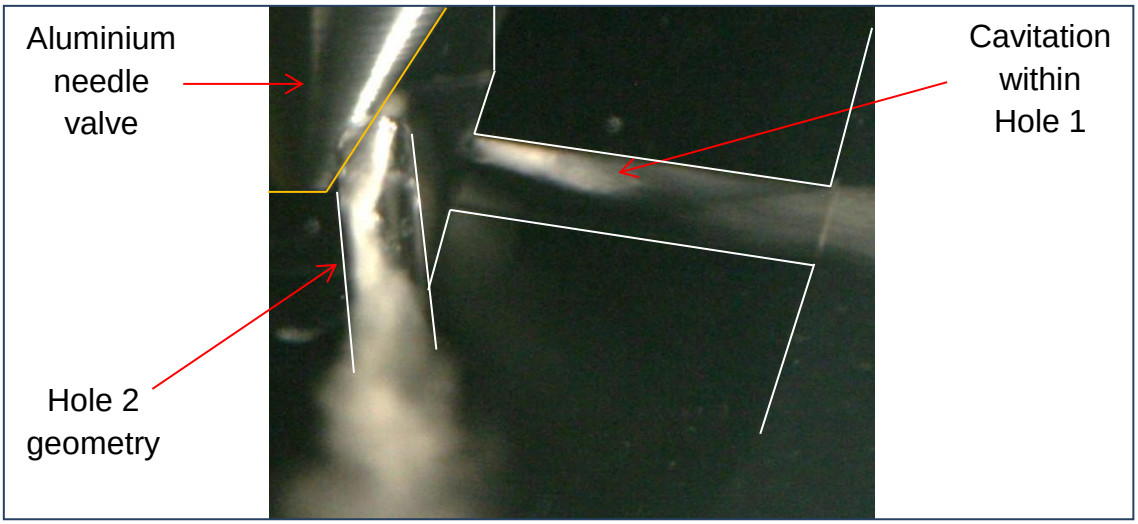

Figure 89 - Enlarged image at 3.0mm lift submerged - 2.27bar ΔP

5.3.9. LBFR Hole 2 Internal Flow at CN 3

In order to compare the observed in-hole flow variability between holes 1 and 2, the light sheet plane was repositioned to assess the flow within hole 2 through PIV and LLS analysis. Although the LSM had been designed primarily for optical access to hole 1, it also allowed for hole 2 to be imaged through a model face orientated perpendicular to this hole's axis, albeit looking downwards at 10° from the horizontal.

Figure 90 consists of a series of PIV velocity contours of the flow within hole 2, alongside the raw images to identify the location of any cavitation. Once again as it is difficult to visualise the path lines in cavitating LLS images, hence only PIV data is included. As with the CN 3 testing of hole 1, the running conditions were 0.17 bar upstream and -0.8 bar downstream.

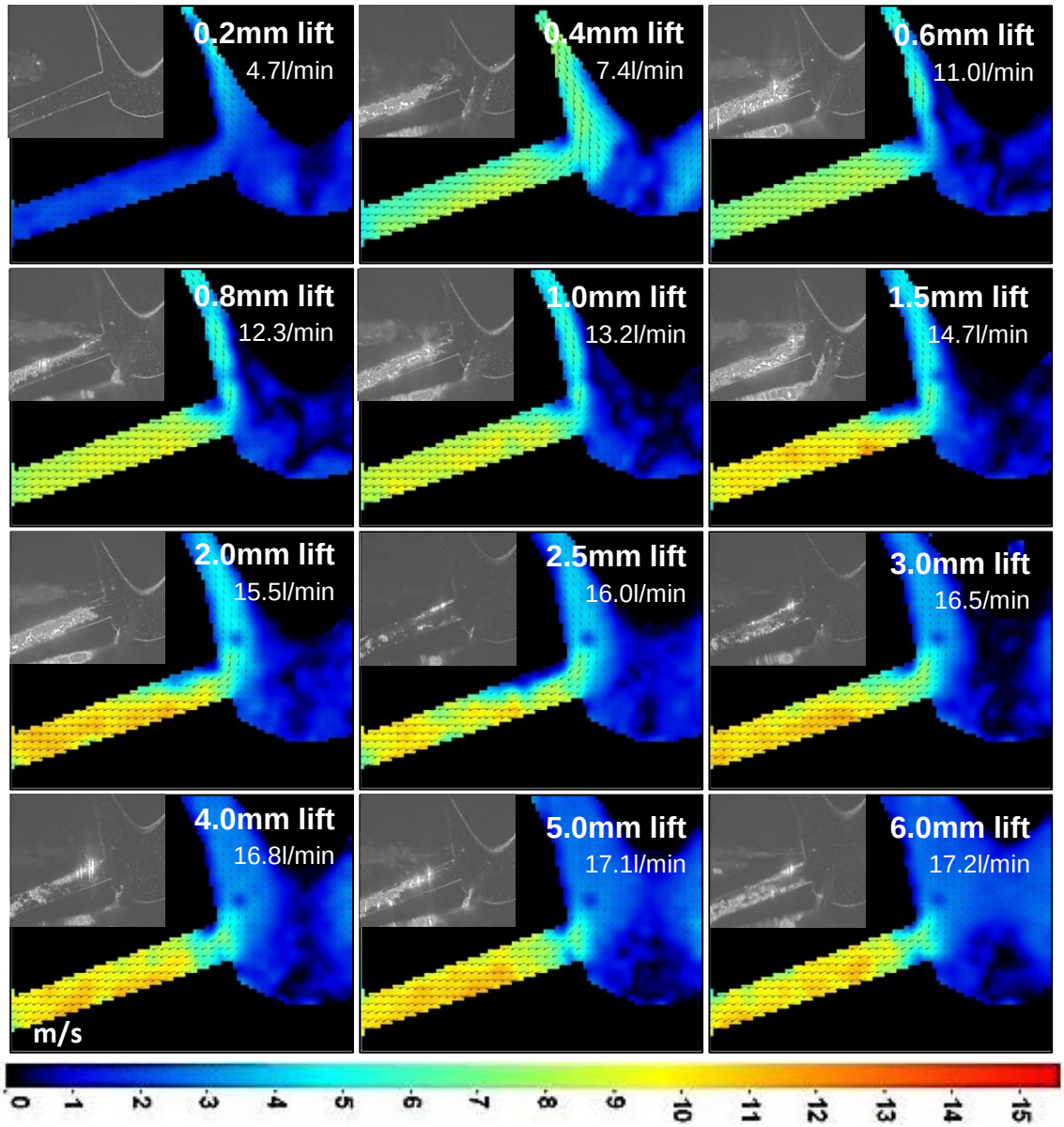

Figure 90 - Hole 2 PIV velocity contours - CN 3

The first point to note is the very different shape of the needle valve compared to the data captured at hole 1. This is due to the location of hole 2 within the nozzle sac, being one of the holes modified in the creation of the RVN design. With the light sheet plane positioned along the axis of this hole, the light sheet does not intersect the centre of the needle valve, resulting in the needle appearing much smaller than when looking at hole 1. With this new light sheet and camera arrangement it is necessary when interpreting the PIV vector images to take note of any cavitation within hole 1 (now situated between the light sheet and the PIV camera). Additionally it is worth pointing out a circular region of lower velocity, just above the inlet of injection hole 2 at 1.5mm lift and above. On further inspection this is detectable on the raw images as a bright

pinprick, likely due to an inclusion within the acrylic model through contamination during manufacture when the model was first cast. This inclusion is close to the light sheet plane and scattering laser light with such intensity as to overpower light from seeding in its vicinity. It is likely that overlapping the cells during processing has resulted in this appearing as a circular region in the PIV vector images.

Observations - Figure 90

1. The difference in the recorded flow rates between the testing of hole 1 and hole 2 is especially noticeable at 0.2mm lift. At low lifts the flow area is highly sensitive to needle lift, therefore even a very slight inaccuracy in setting the lift will result in a different flow for a given pressure drop.
2. The flow structure entering hole 2 appears to be similar to the flow entering hole 1 across all lifts; however, the results differ inside the injection hole. This is because within hole 2 there does not appear to be a clearly defined separated region at the top of the injection hole bore. In fact looking at the raw images it appears that shortly after hole entry, the entire cross-section of hole 2 is full of cavitation bubbles. To investigate this further, the raw PIV images at CN 3 with the camera orientated to view hole 1 were re-assessed. Although not optimised for this purpose, these images can provide a 3D perspective of the cavitation within hole 2. Two example images are shown in Figure 91 and both show that hole 2 has a ring of cavitation at hole entry around approximately 60% of its circumference. Shed cavitation from this region then appears to be confined to the side of the injection hole furthest from hole 1 as it is carried away with the bulk flow. This evidence therefore indicates that the entire cross-section of hole 2 is not in fact full of cavitation bubbles as was indicated from viewing this hole from the side as in Figure 90.

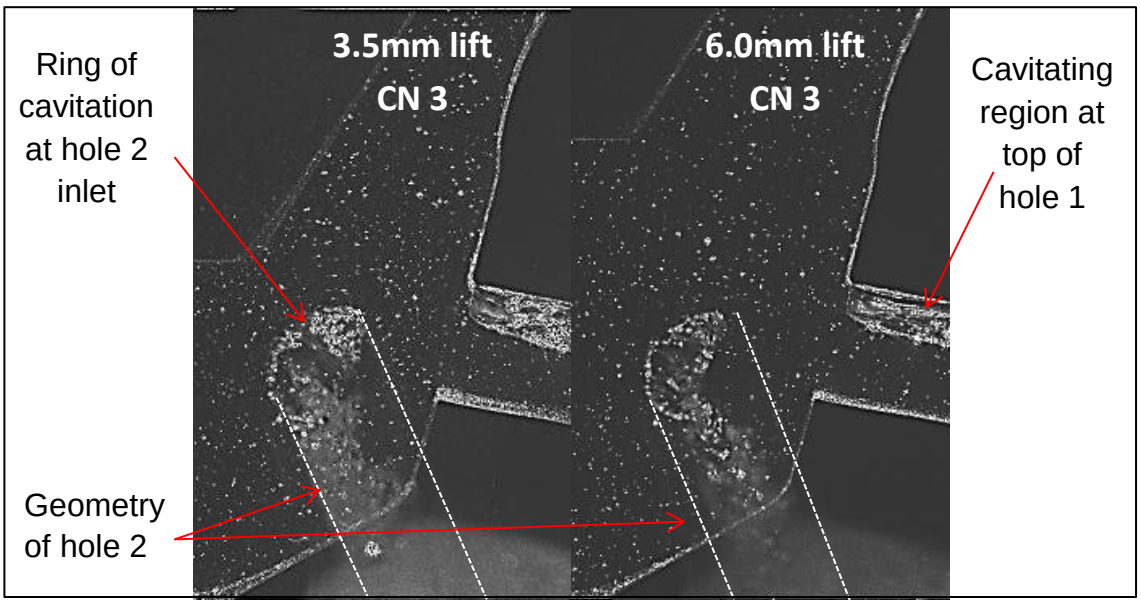

Figure 91 - PIV raw images of cavitation within hole 2

3. The final observation from the images in Figure 90 is the formation of a cavitating region at the bottom entry of hole 2 at 3.0mm lift and above. This indicates a secondary flow entering the hole from below which is detected in the PIV velocity contours as a vena-contracta just inside the entry to the injection hole.

In summary, the behaviour of the flow passing through hole 2 is very different to that through hole 1. This is likely not only due to the eccentric position of hole 2 within the sac relative to the needle but also due to the fact that the hole is set at a reduced cone angle. Therefore in order to enter hole 2, the flow has to undergo a 15° less flow turn than the flow entering hole 1.

5.3.10. LBFR Hole 2 Internal Flow at ΔP = 0.87 bar

As with hole 1, the flow structure of hole 2 was investigated at a non-cavitating pressure drop of 0.87 bar. Not only does the lack of cavitation improve the quality of the collected data but it also removes doubts that may exist over the accuracy of the vectors directly behind hole 1. Figure 92 consists of both PIV velocity contours and LLS images captured with the needle valve being moved in the opening direction between 0.2 & 6.0 mm lift.

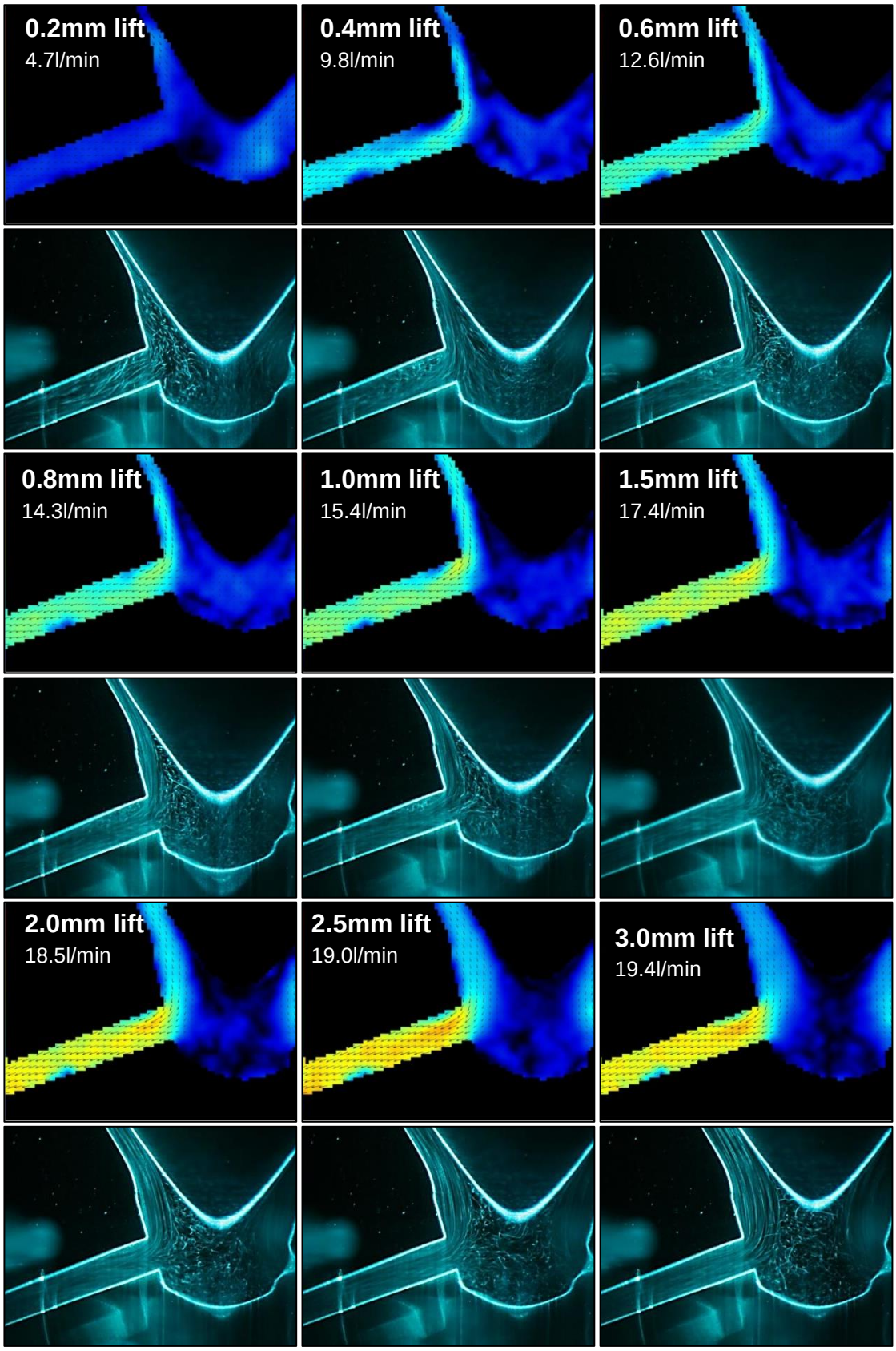
0.2mm lift
4.7l/min
0.4mm lift
9.8l/min
0.6mm lift
12.6l/min
0.8mm lift
14.3l/min
1.0mm lift
15.4l/min
1.5mm lift
17.4l/min
2.0mm lift
18.5l/min
2.5mm lift
19.0l/min
3.0mm lift
19.4l/min

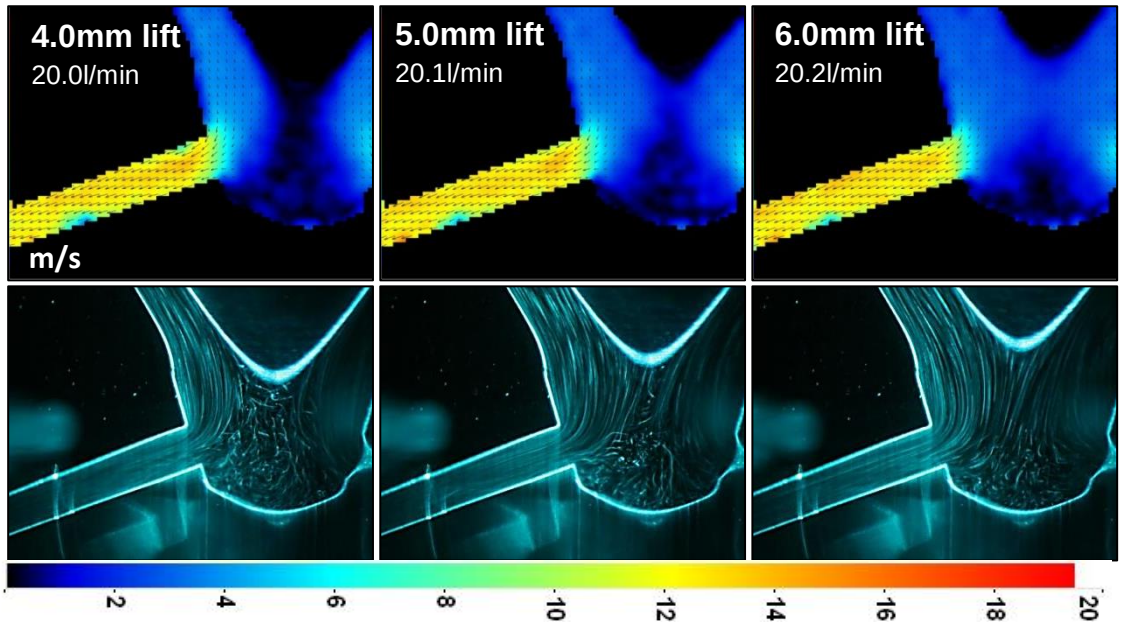

Figure 92 - Hole 2 PIV velocity contour and LLS images - 0.87 bar ΔP

In Figure 92, it is necessary to mention what appears to be the effect of an inclusion within the acrylic model which has resulted in a corrupted region at the bottom of hole 2 at an length/diameter (l/d) location of approximately 4. It is not known why this inclusion was not detected at CN 3, or why the inclusion detected at CN 3 does not appear in the 0.87 bar data but the most plausible explanation is that the light sheet is positioned ever so slightly differently to that of the CN 3 tests.

Observations - Figure 92

1. There is a good agreement between the bulk flow in the PIV velocity contours and the path lines in the LLS images.
2. Similarity is detected with the testing at CN 3 for both the flow upstream of hole 2 and the velocities at the bottom of the sac. These velocities indicate a growing low velocity region as the needle lifts.
3. Inside the injection hole the lack of cavitation has resulted in a very different flow structure to that at CN 3. Unlike at CN 3, where hole entry cavitation jostles with the flow attempting to enter hole 2, at 0.87 bar ΔP the flow is able to take a more direct route into the injection hole and therefore appears to flow more smoothly through it.
4. Observed at the top of the injection hole is a small separated region which appears to diminish in thickness between 0.4mm and 3.0mm lift. This is contrast to the results from hole 1 at 0.87 bar which indicated a

much larger separated region which existed throughout the entire lifting range. This difference is likely explained by the flow entering hole 2 undergoing a 15° less flow turn than the flow entering hole 1 owing to the difference in cone angles.

5.3.11. LBFR Hole 2 Vortex Activity

It has been established that within hole 2 the cavitation and hence the flow is eccentric, likely due to the unusual position of this hole relative to the needle valve tip. To investigate this eccentric flow in more detail, the light sheet was moved either side of hole 2's central axis, with the expectation that one side of the central axis would consist of cavitating flow whereas the other would not. At these two positions, the previous CN 3 and 0.87 bar ΔP tests were repeated. Figure 93 contains both side and bottom views of the location of these light sheet positions which are referred to as Position A and Position B. These equate to +0.36mm from the centreline for Position A and -0.64mm for Position B with the negative sign indicating towards the PIV camera.

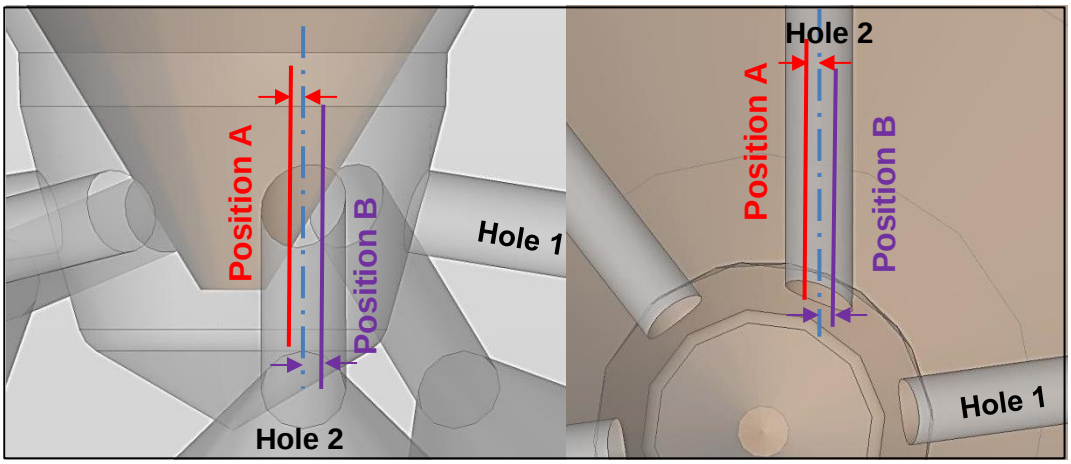

Figure 93 - Hole 2 eccentric laser light sheet positions

Section views of the CAD model at positions A & B in Figure 94 exemplifies the influence that the needle valve is likely to have on the flow entering hole 2. When compared to light sheet Position B, the needle valve is significantly closer to injection hole inlet at Position A. Therefore at Position A the flow is more tightly constrained between the needle and the nozzle body as it attempts to enter the injection hole. This potentially could result in greater levels in-hole

vorticity as detected with entry-throttled injection holes within previous research (Soteriou, et al., 2000).

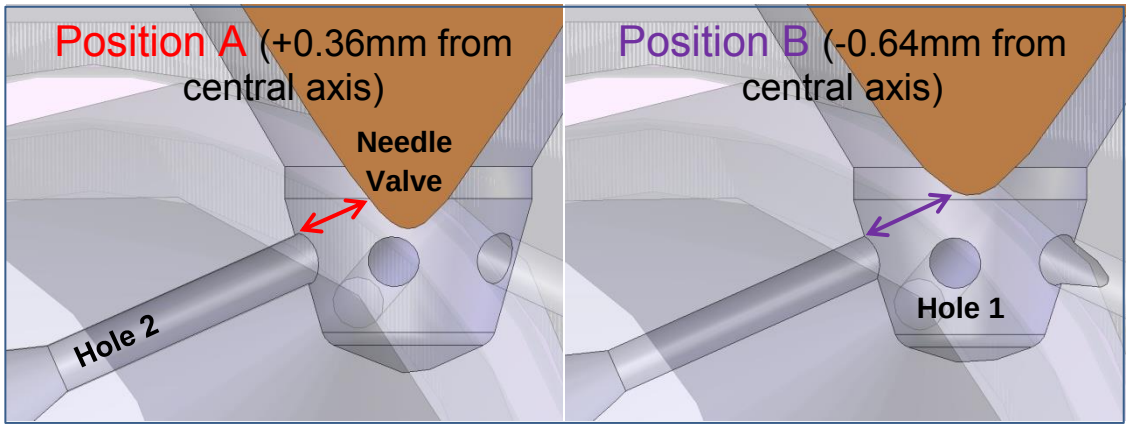

Figure 94 - Hole 2 position A & B section views

Hole 2 - CN 3 Positions A & B

Figure 95 & Figure 96 consist of CN 3 mean PIV velocity contours at Position A and Position B respectively. As before the running conditions were 0.17 bar upstream and -0.8 bar downstream.

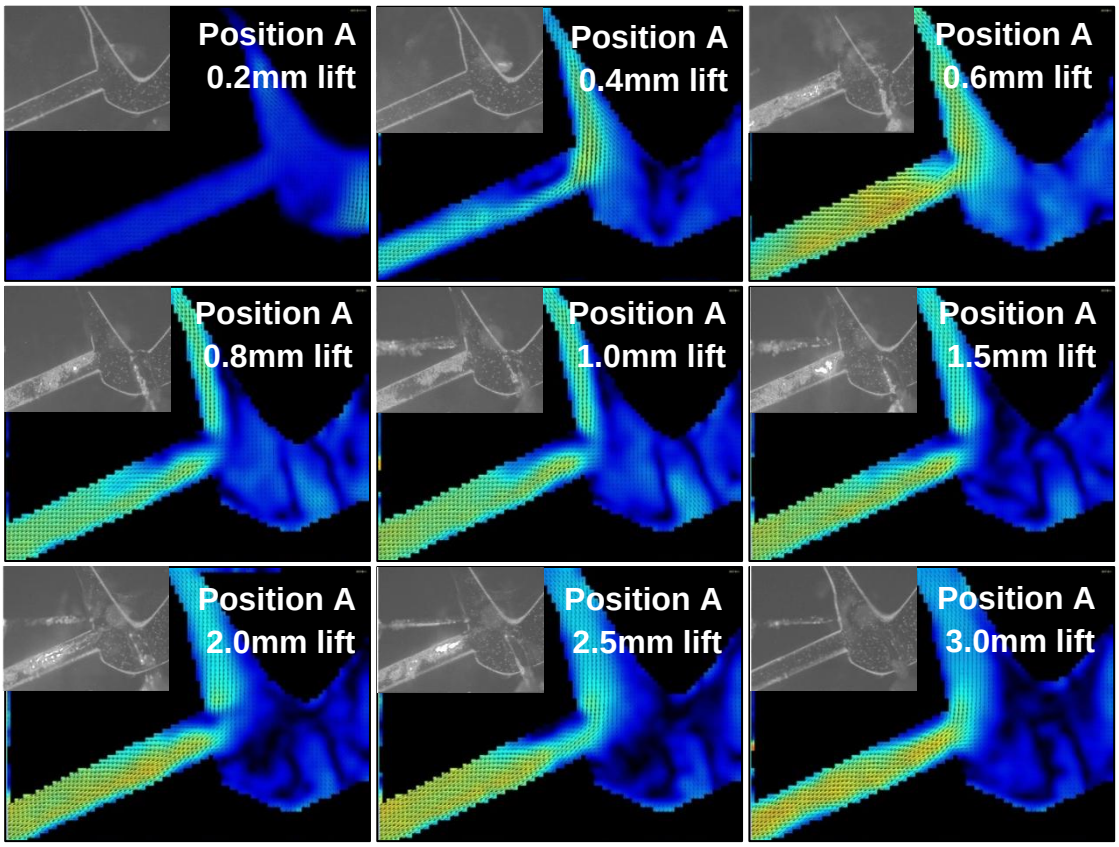

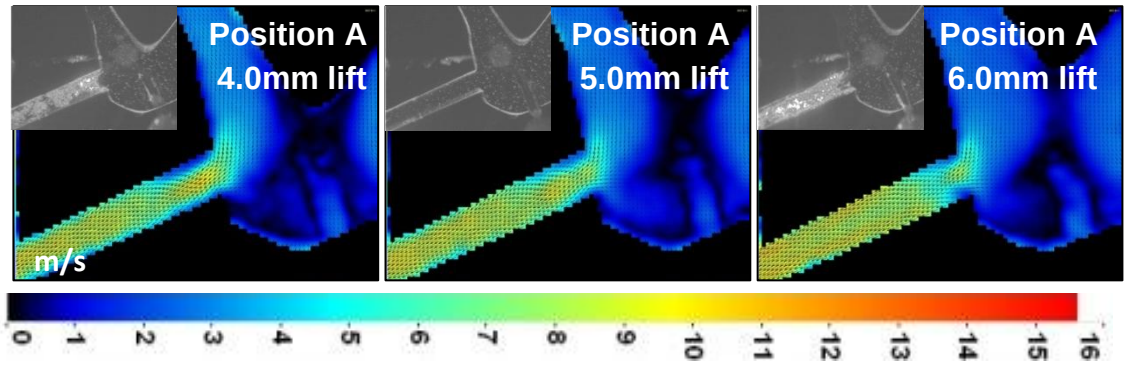

Figure 95 - Position A - mean PIV vector images at CN 3

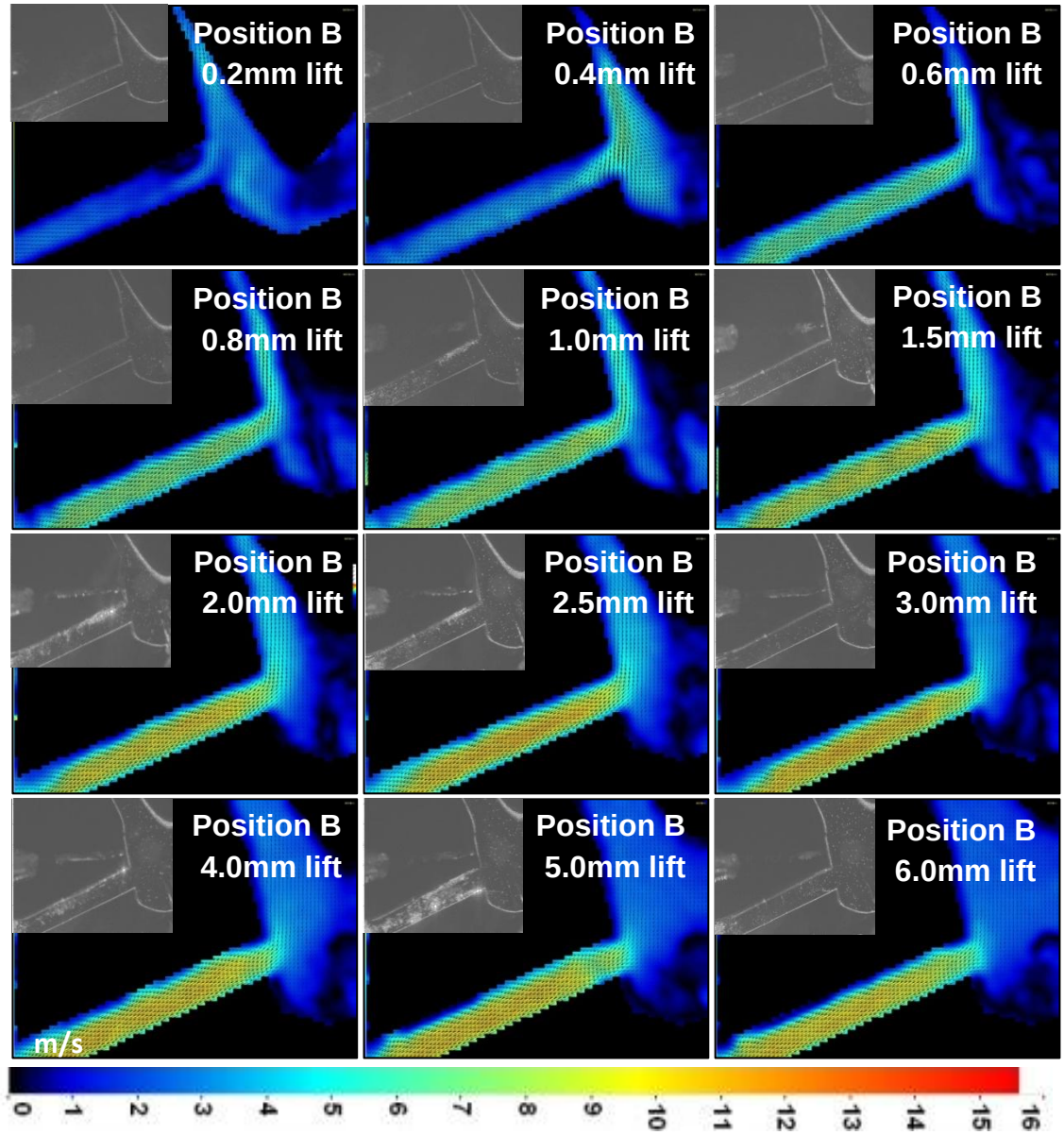

Figure 96 - Position B – mean PIV vector images at CN 3

Observations - Figure 95 & Figure 96

1. At CN 3, the PIV data confirms the assumption that Position A would be cavitating whereas Position B would not, was largely correct. Whereas

Position A was seen to always cavitate at lifts above 0.4mm (with the exception of 3.0 and 5.0mm lift), Position B was only observed to cavitate intermittently. This resulted in a rather different flow structure between the two positions. This is especially apparent in the vicinity of hole entry with Position A having a large separated region.

2. At position A between 0.8 and 2.0mm lift, probable evidence of a flow across the light sheet plane just prior to hole entry was detected.

Hole 2 – 0.87 bar ΔP Positions A & B

Figure 97 & Figure 98 consist of 0.87 bar ΔP mean PIV velocity contours at Position A and Position B respectively.

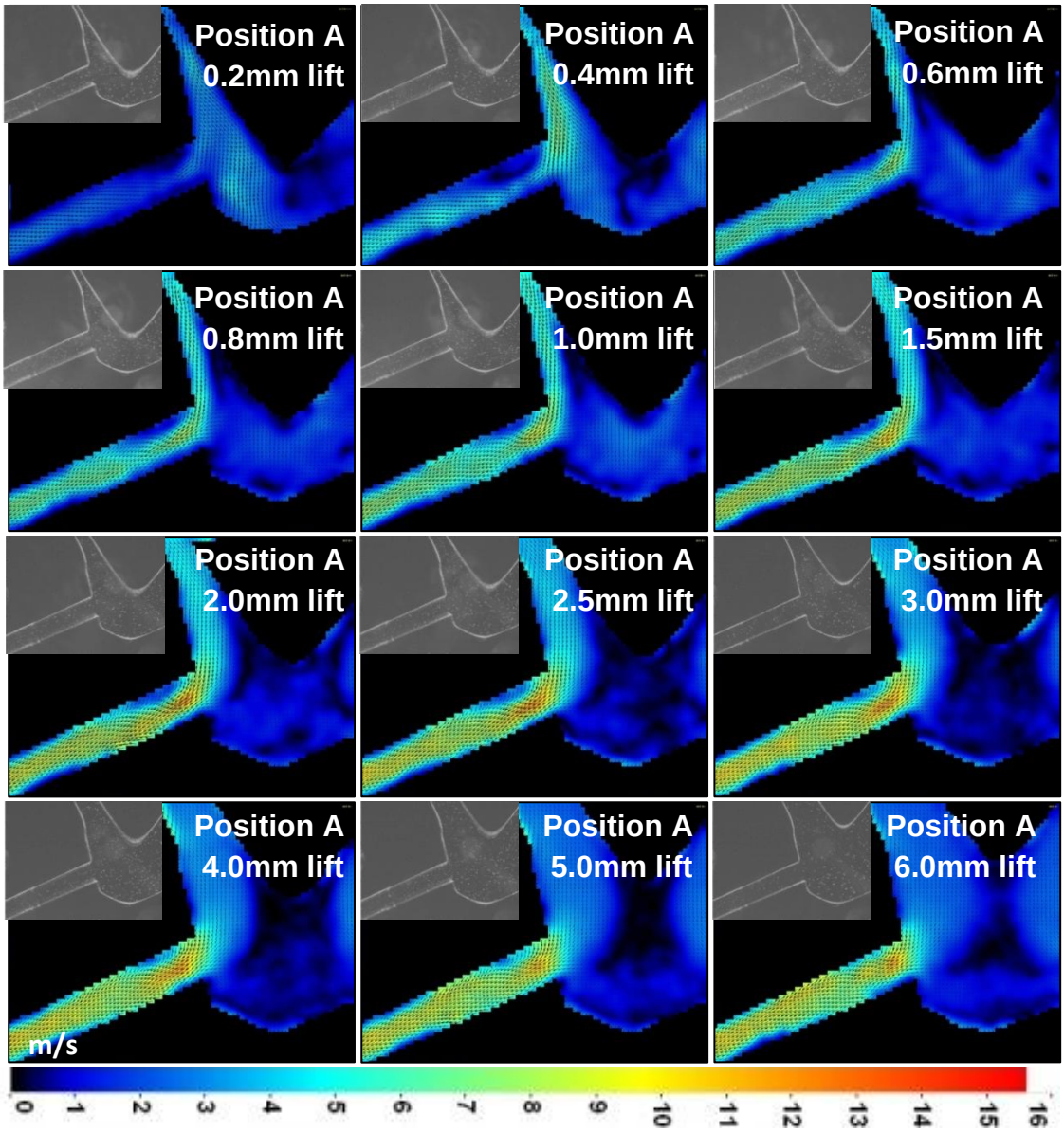

Figure 97 - Position A - mean PIV vector images at 0.87 bar

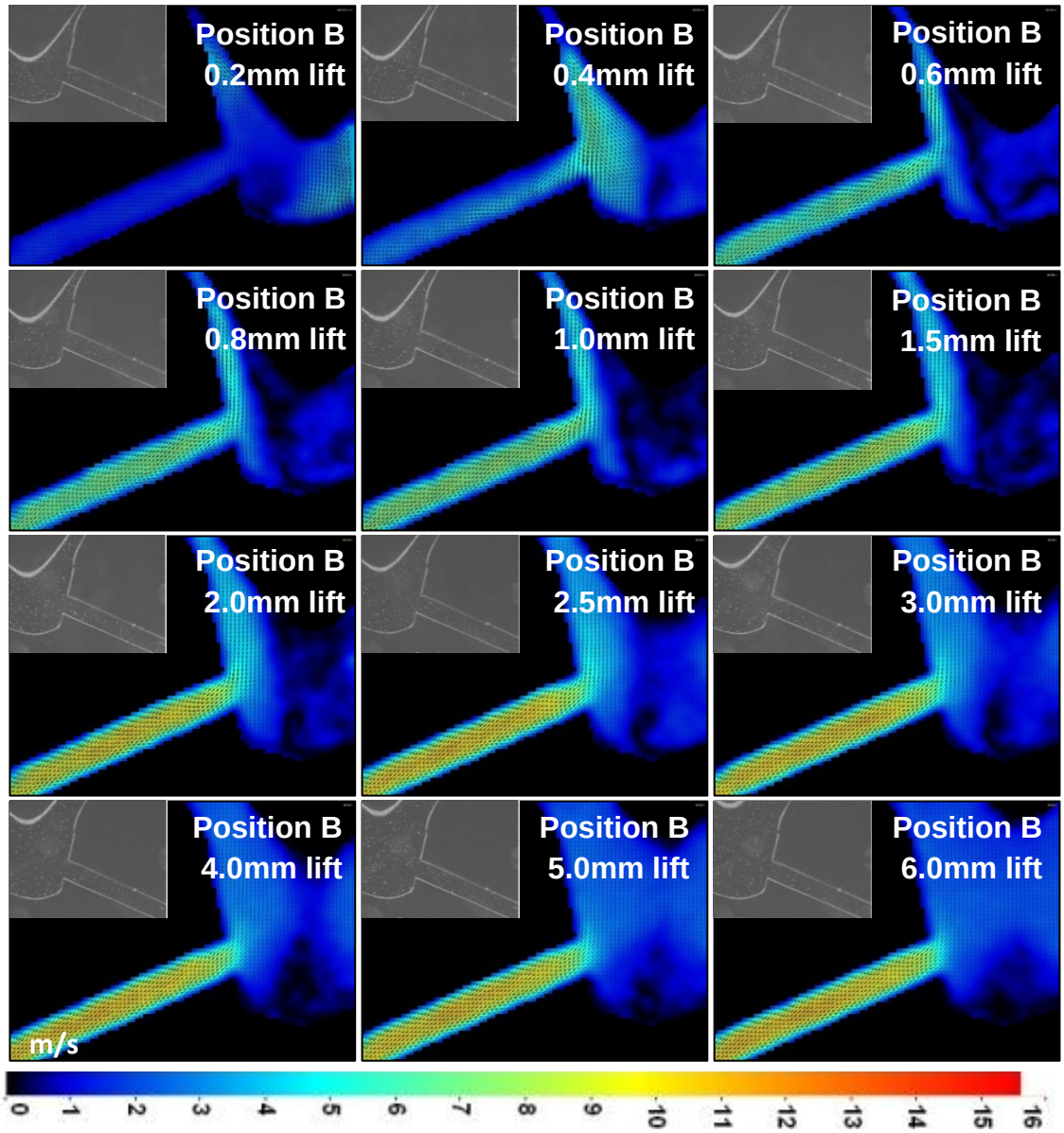

Figure 98 - Position B – mean PIV vector images at 0.87 bar

Observations – Figure 97 & Figure 98

1. At 0.87 bar ΔP, the PIV vectors indicate that at Position A the flow is less uniform than at Position B and appears to undulate much more as it passes through the injection hole.
2. Position A appears to have a relatively large separated region located slightly inside the entry to the injection hole whereas at position B this was much reduced in size and located closer to hole entry. Indeed at Position A this separated region exists at all lifts and appears to extend until an l/d ratio of at least 2.

The PIV velocity contour images within hole 2 have indicated a distinct difference in the in-hole flow structure and the appearance of the separated region between the two eccentric light sheet positions, A and B. A secondary observation is the apparent vortex activity at the entry to hole 2 with the light sheet at position A. The most likely explanation for this is the proximity of the needle valve at Position A and the flow asymmetry that it induces at hole entry. As the PIV images have thus far been averaged, potentially short-lived phenomenon such as vortex motion could effectively be filtered out. To overcome this, the individual PIV frames were scrutinized to search for any possible vortex motion within injection hole 2.

Individual PIV frames from Position A

Selected PIV frames which best identify apparent vortex motion within hole 2 at position A have been selected and are presented in order of increasing lift in firstly Figure 99 at CN 3 and then in Figure 100 at a ΔP of 0.87 bar. When studying these individual PIV frames, it is worth remembered that using only a 2D PIV system it is not possible to track flow in the z-direction, therefore the vector arrows only indicate the flow that occurred within the light sheet plane. For this reason it is perhaps beneficial to ignore the vector arrows and pay attention solely to the velocity contour colours. Lines have been superimposed to identify the hole geometry.

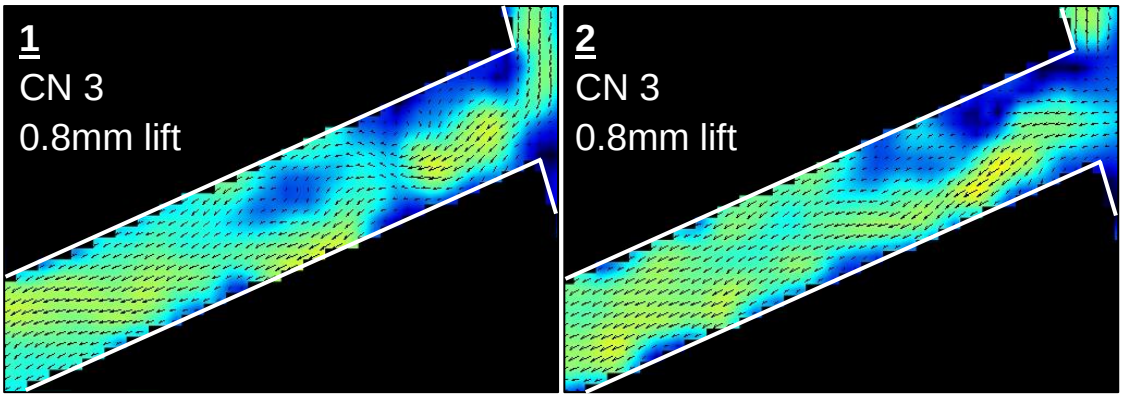

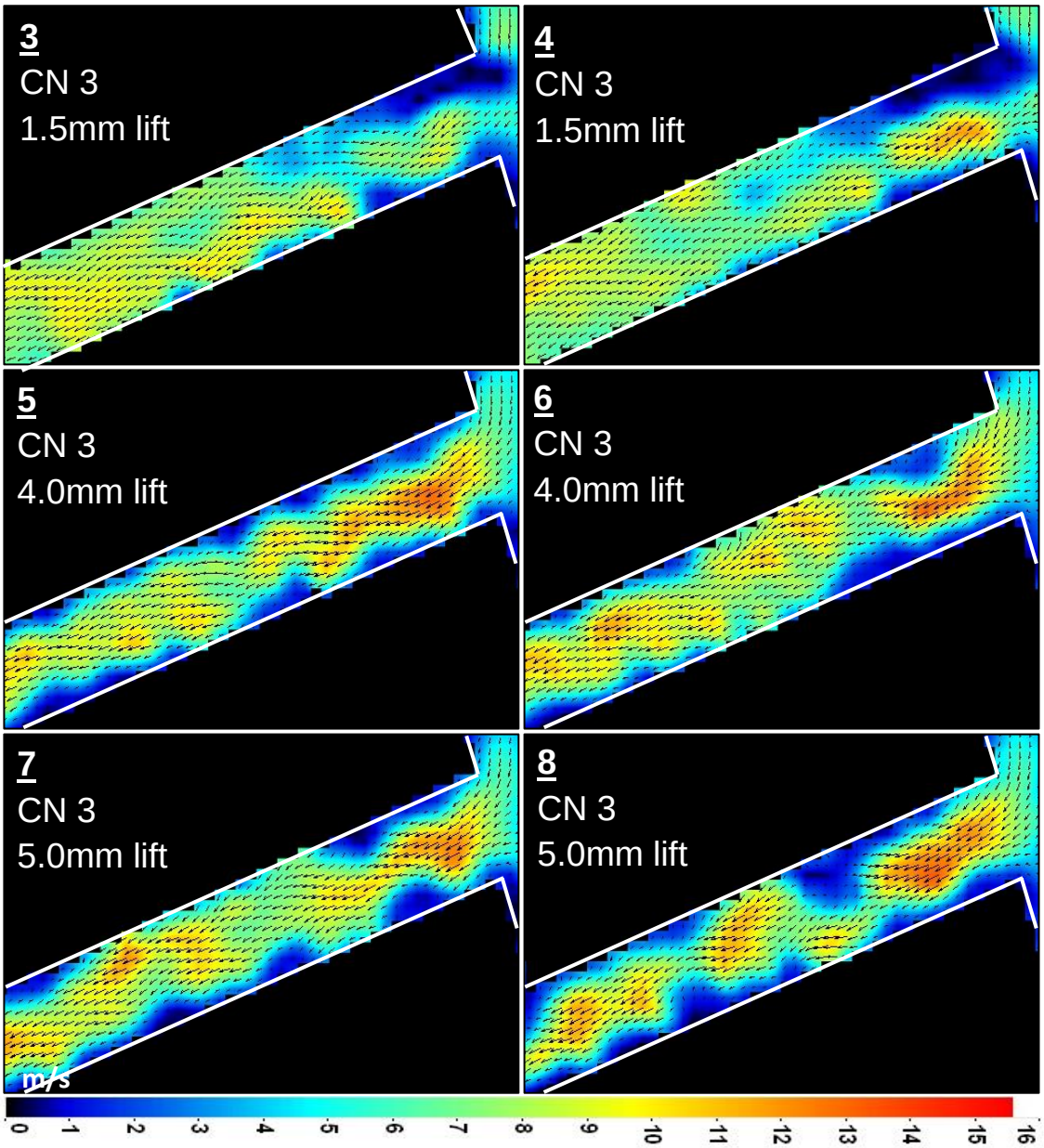

Figure 99 - Hole 2 possible vortex activity - CN 3

Observations - Figure 99

1. The velocity contours at CN 3 appear to be quite confused, perhaps due to the likely complicated interaction between the apparent vortex activity and hole entry cavitation. This seems to be more prolific towards the first half of the injection hole particularly at low lifts where the (cavitating) separated region would be thicker therefore constraining any vortices to a smaller flow area. A prime example of this is image 4 where the high velocity flow appears to be confined to the bottom approx. 60% of the hole cross-section until an l/d ratio of ~3.

2. An unusual low velocity region was seen in the flow entering the injection hole at 0.8 & 1.5mm lifts (images 1 – 4). This could indicate a large flow crossing the light sheet plane and therefore resulting in reduced V_X and V_Y components. This could signify the origin of vortex motion within the remainder of the injection hole.
3. At 4 & 5mm lift (images 5 – 8) the high velocity flow appears to utilise more of the hole cross-section which is plausible as the (cavitating) separated region would have been much reduced by this lift.

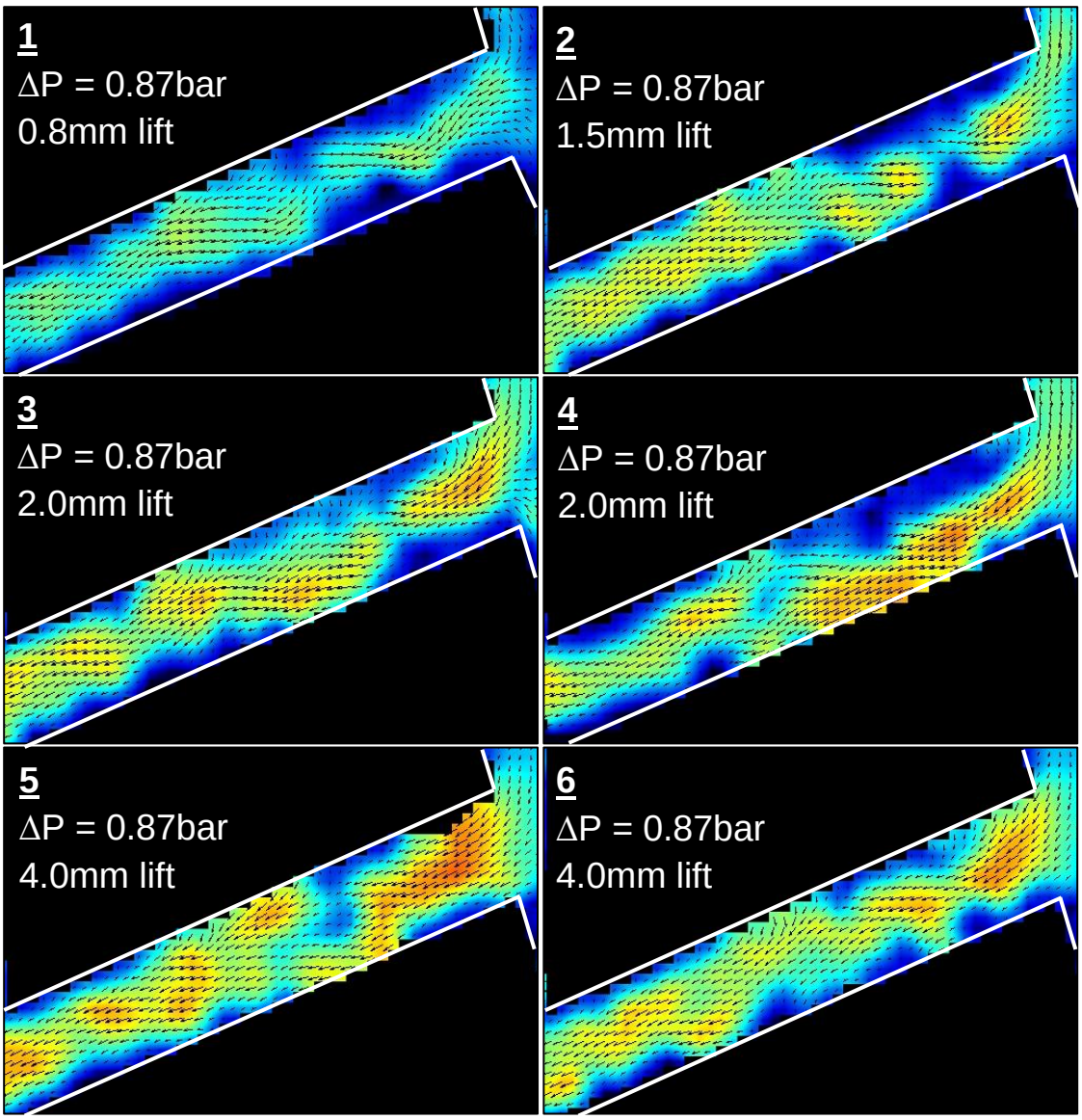

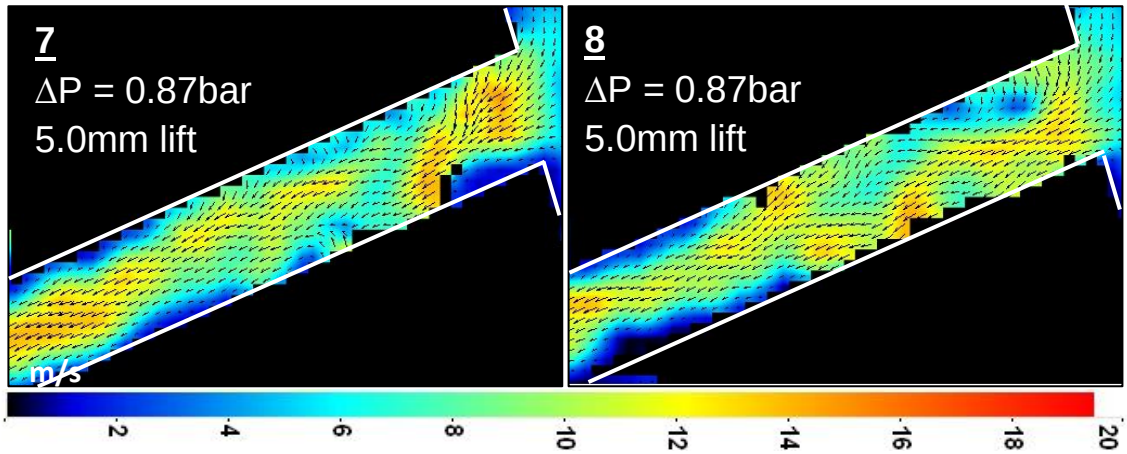

Figure 100 - Hole 2 possible vortex activity - 0.87 bar ΔP

Observations - Figure 100

1. Note the different scale used than at CN 3. At lifts ≤ 1.5mm (images 1 & 2), the high velocity flow appears to consist of a tightly wound vortex evident by a saw tooth external profile. This appears to be travelling down the centre of the injection hole or at least along the light sheet plane at Position A.
2. At larger lifts the high velocity flow appears to be less uniform and hence more difficult to identify perhaps indicating either the prominence of multiple structures (vortices) present within this flow or that the vortex structure is itself following a circular path as it travels along the injection hole bore. The latter suggestion is supported by images 4, 5 & 7 where the high velocity flow appears to move out of the light sheet plane near the bottom of the injection hole before reappearing momentarily later near the top.

In summary, although possible vortex structures have been identified within the PIV vector individual frames, as the results are only along a 2D light sheet plane, it is difficult to identify a highly 3D structure with just this data. Therefore PIV data may not be the best technique to identify vortex structures within the internal nozzle flow.

5.3.12. Project Conclusions

The unique design of the RVN LSM has provided exceptional access to allow study of the flow within a single injection hole of a multi-hole nozzle. Although the necessary design modification required the movement of two of the injection holes, any alteration in the performance of the nozzle has been kept to an absolute minimum, thus validating this technique or approach for future projects. This view is supported by extensive testing of the real size components through spray visualisation, plume penetration measurement and CFD simulation.

Analysis of the data from both the LPR and the LBFR LSMs has produced the following outcomes:

Vortex Activity

- Large low pressure regions have been observed to develop within the sac midway between the needle valve and the nozzle body, outside the entry to injection hole 1. These regions have been associated with flow moving to enter the injection holes situated outside the light sheet plane and have been postulated as a mechanism for vortex activity within these holes.
- With the light sheet at Position A, the mean PIV velocity contours indicated a large flow across the light sheet plane just outside the entry to hole 2. This likely indicates vortical behaviour in the flow entering this injection hole which supports understanding that in-hole vortex motion originates within the nozzle sac and is highly influenced by the proximity of the needle valve.
- A complicated interaction was observed between the apparent vortex activity and hole entry cavitation with the cavitation appearing to confine any vortex activity to the bottom of the injection hole at least for the first half of the hole's length.
- At higher lifts where the separated region has been observed to diminish in thickness, the apparent vortex activity appears to be able to utilise more of the hole cross-section resulting in a less uniform shape and possibly even following a circular path along the hole axis.

- In agreement with DDS published work (Soteriou, et al., 2001), the emerging plumes from holes 1 and 2 appear to consist of a helical structure. This is particularly evident in the submerged LPR images and is likely a continuation of the vortex activity that has been observed within the injection holes and/or the nozzle sac.

In-Hole Separated Flow / Boundary Layer

- At non-cavitating conditions the flow is able to take a more direct route into the injection hole without being 'jostled' by hole entry cavitation. This appeared to coincide with the flow through the injection hole appearing less chaotic.
- At cavitating conditions and with increasing needle lift, the PIV and LLS images indicated a noticeable change in the shape of the separated region at the top of the injection hole. After initially growing, this region was observed to become thinner and more confined to the top of the hole whilst taking on a 'glass-like' appearance which was an observation found during the literature search to be a common discovery with cavitating voids within LSMs. As this region reduces the effective flow area (especially owing to shed cavitation from the inlet) for the bulk flow, this observation indicates that the effective hole area increases slightly as the needle lifts and the area occupied by the separated region wanes.
- The V_X component data extracted at the inlet to the injection hole at non-cavitating conditions indicates a linear increase in velocity and an apparent linear reduction in the separated region's thickness with increasing needle lift.
- The V_X component data at cavitating conditions indicated a sudden step change in the separated region's thickness between 2.0 & 3.0mm lift. This reduction in thickness perhaps indicates a significant change in the flow structure.
- For both cavitating and non-cavitation conditions, the apparent separated region at the top of hole 2 and at the central axis appears vastly smaller than at hole 1. This difference is likely explained by the different cone angles with the flow undergoing a 15° less flow turn to enter hole 2 than the flow entering hole 1.

- Changes in the separated region's thickness within hole 1 were observed whilst variations were detected in the jet angle of the emerging spray plume. This could suggest an effect this region is having on the bulk flow within the injection hole and ultimately on the emerging spray plume(s).
- Although Positions A and B were not equidistance either side of the central axis of hole 2, significant differences were observed between their respective flows which are likely not accounted for by their asymmetry. This has been proposed as being due to the greater proximity of the needle valve tip at Position A. In light of this the influence that the needle valve may have on the flow entering the injection hole cannot be underestimated as not only may needle eccentricity throttle some of the injection holes but also adversely disturb the flow entering them. In a worst-case scenario this could result in poor plume penetration and/or abnormal in-hole flows resulting in asymmetrically shaped fuel spray plumes.

Hole Entry Cavitation

- Significant differences were detected in the hole entry cavitation of hole 2 between the two eccentric light sheet positions. At CN 3, light sheet Position A was seen to cavitate at most lifts whereas Position B was only observed to cavitate intermittently. This resulted in position A having a large separated region and the flow here appearing less uniform or well-ordered that at position B.
- At large lift a vena-contracta was detected at the central axis and just inside injection hole 2, this indicates that the flow must be entering the hole from below as well as above. This is more common on single-hole axial injectors so was a surprise observation.
- The CFD liquid phase volume fraction data was based on the real size RVN design which has tapered injection holes of k-factor 1.5. Therefore cavitation is likely to be reduced on the CFD results when compared to the LSM experimental results. In spite of this, the indicated inception location of hole entry cavitation at the edge of hole 2 in the CFD, agrees well with LSM experimental data.

5.4. Real Size Transparent Nozzle Tip

A collaboration was initiated between DDS and City University to investigate the flow within a real-size transparent fuel injection nozzle running at actual CR injection pressures. A requirement for the project was that the transparent nozzle design remained as close as possible to a production multi-hole nozzle without adopting the common approach of simplifying the nozzle design until it becomes unrealistic.

5.4.1. Transparent Tip Design

In order to aid manufacture of a transparent nozzle tip, DDS designed and manufactured real nozzles with a heavy duty sac design but injection holes of typical light duty sizing and flow rate. This equated to a design with six holes of Ø160µm, a nozzle flow of 0.94l/min and a 60° needle seat angle. The injection holes were designed parallel or cylindrical to facilitate the manufacture of the transparent tips due to anticipated difficulties with accurately creating tapered injection holes. The reasoning behind the choice of a HD sac design was to provide a larger sac volume to not only assist with transparent tip manufacture but also to aid alignment with a modified nozzle body during the experimentation. In the same manner as with the previous experimental projects disclosed in this thesis, the areas of maximum restriction have been calculated but are obviously much reduced in magnitude owing to this being a real size nozzle. These areas have been illustrated in Figure 101; however, it was not possible to calculate the area of restriction formed between the needle truncation and the seat at lifts below 90µm. This is explained by the large sac diameter allowing the truncated part of the needle to penetrate inside the sac at lifts below 90µm.

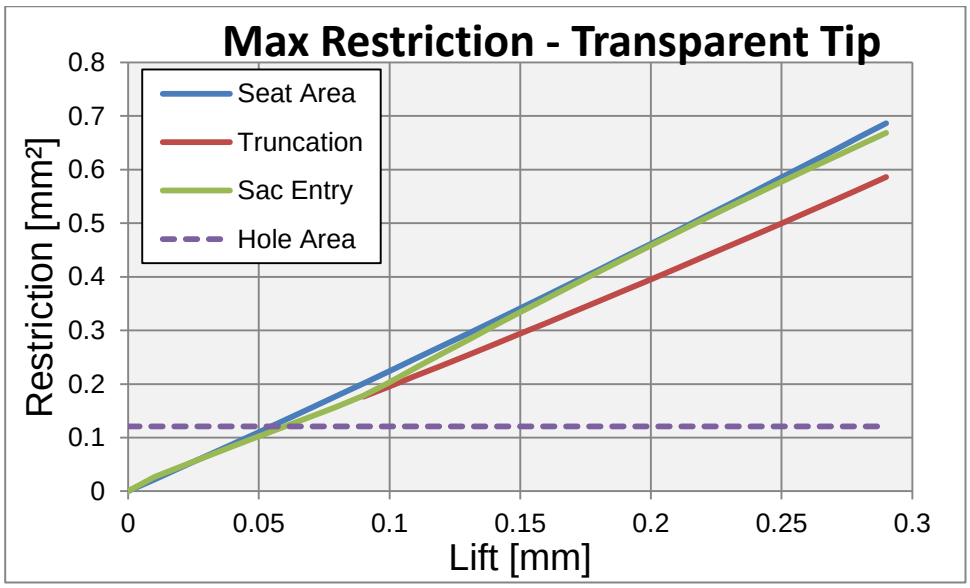

Figure 101 - Transparent tip geometry flow areas

The research team at City University incorporated DDS internal nozzle geometry with an external geometry utilising their past experiences with the internal visualisation of real size transparent (acrylic) nozzle components. This involved the design of larger external dimensions for increased robustness, ease of handling and to allow for the incorporation of polished viewing faces to limit optical distortion when visualising the internal fluid flow. A secondary requirement of the project was to visualise the emerging spray plumes in the near nozzle region. This required that the acrylic tips have the correct hole exit shape which is regarded as being an essential requirement for producing representative spray plumes. This was solved by the addition of a small chamfer at the exit of the injection holes. This feature has been identified on the CAD models of the acrylic tips in Figure 102.

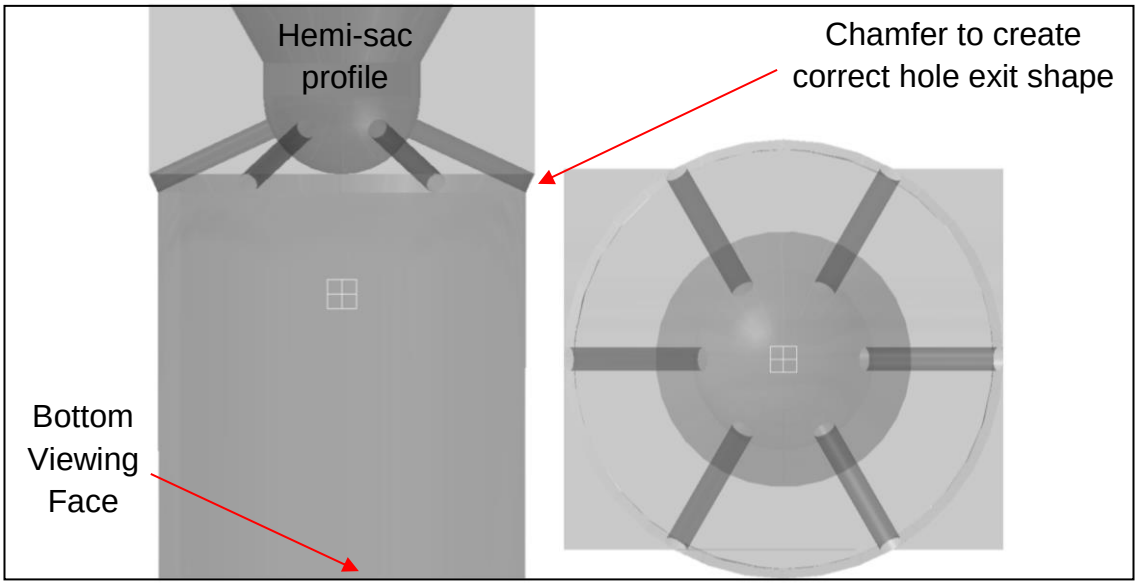

Figure 102 - CAD side and plan views of transparent nozzle tip (Mitroglou & Gavaises, n.d.)

5.4.2. Real Nozzle Modification

The experimental method to test these acrylic tips at actual CR injection pressures required that the tips be clamped onto a modified nozzle body as part of an injector assembly. With input from DDS, City University derived the method of grinding off the tip of one of the real (metal) nozzles and the addition of a recess to facilitate concentric tip alignment. This recess was created using an Electro Discharge Machining (EDM) process. Figure 103 shows this modified nozzle with the tip noticeably removed, alongside the matched needle valve.

Figure 103 - Modified nozzle body

5.4.3. Acrylic Tip Manufacture

For the experimental testing a batch of 30 tips were manufactured by City University. This large number was required as at 300 bar injection pressure the tips have an experimental test life of approx. 100 injections. This was believed to be due to localised thermal effects which with repeated testing would lead to minor geometry changes before eventual tip failure. As the acrylic tips were hand manufactured, to ensure consistency it was necessary to accurately measure the internal geometry of each prior to testing. Besides project managing this collaboration from the DDS perspective, this is a role that was undertaken by the author. To take account for any elastic deformation that may occur during testing, apparatus was designed and constructed to apply an axial compressive load to the tip similar to the clamping force exerted during actual testing. With the tips then loaded axially, silicone impressions were taken of the internal geometry, measured, and then compared against the original design specification. The 20 best tips were then selected for testing and these had their external viewing faces polished to improve optical access.

Realistic Hole Entry Conditions

As part of the manufacturing process, real production nozzles are honed using the AFM process to remove internal burrs and sharp edges. Details about this honing process can be found in the Nozzle Manufacture section earlier in this thesis. Arguably the most important end result of this honing process is the creation of a variable radius at injection hole entry, which is impossible to accurately replicate with machine tooling. The real (metal) nozzle design was specified as having a post-honing 10% increase in flow which equates to the generation of an average hole inlet radius of 30µm. To produce a similar hole inlet condition on the acrylic tips, they were honed using the AFM process but with a thinner cutting media at a reduced pressure, owing to the relative softness of the acrylic. After a trial and error process it was determined that honing the acrylic tips for three seconds at a pressure of 100 bar was sufficient to create a 30µm inlet radius. An additional benefit of the honing process was an improvement in the surface finish of the injection holes through the removal of machining marks, which is an aid to internal flow visualisation.

5.4.4. Experimental Testing

The actual experimental testing of the transparent nozzle tips was carried out at City University by Dr Nicholas Mitroglou. A 1600 bar CR FIE system and controller was provided by DDS but the rail pressure was limited to < 400 bar due to safety concerns over the robustness of the acrylic tips. The images of the internal flow and cavitation inside the transparent tips were recorded using a high-speed camera, a long-distance microscope and high intensity back lighting.

Figure 104 is an image sequence with Image 2 showing start of injection (SOI) and the final image some 1729 µs later, with the needle at full lift (300 µm). The recording was at 30,000 fps with only every forth image displayed here which equates to a period of 133 µs between the successive images. The injection pressure was 300 bar with atmospheric conditions downstream. The profile of the needle valve, the sac and a single injection hole (orientated perpendicularly to the camera) are all clearly visible whilst the opaque cavitation bubbles appear as darks regions. Also distinguishable towards the top left corner of each image is the emerging spray plume.

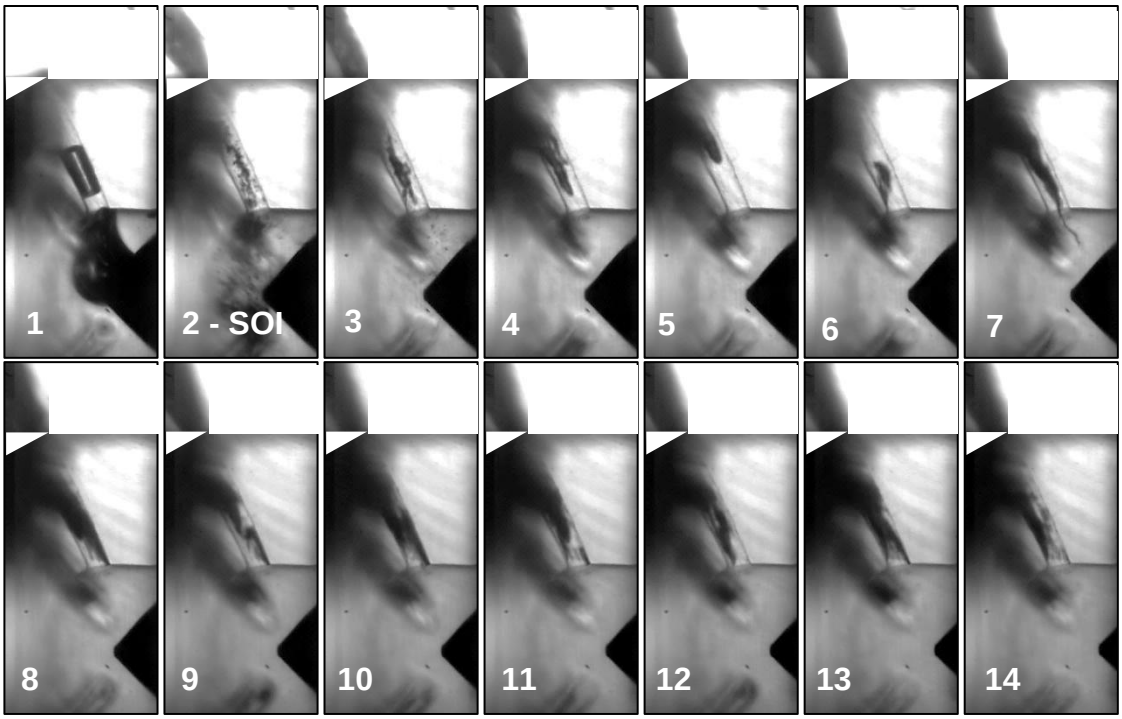

Figure 104 - Transient nozzle cavitation and flow – 300 bar (Mitroglou & Gavaises, n.d.)

Observations – Figure 104

1. In images 2 & 3, small cavitation bubbles are detectable in the sac and within the visualised injection hole. These are undoubtedly shed cavitation from the seat region. This apparent shed cavitation has ceased to exist by image 4 (266 µs after SOI), with the likely reasoning being that the valve lift is sufficiently large to no longer be throttling the flow enough to introduce cavitation.
2. In image 6, cavitation can be seen at the bottom of the entry to the injection hole, whereas image 7 just 133 µs later, has what appears to be a 'cavitation string' originating near the needle's surface. Previous literature has suggested that this 'string' is likely the result of strong vortex motion resulting in the formation of cavitation along its central axis. It is possible that this lift condition indicates an unstable point as the image immediately afterwards (image 8) appears to show geometrically induced cavitation at the top of the hole where there had only been cavitation at the bottom of the hole previous to this (image 6).
3. Images 10 to 14 with the exception of image 12 appear to have both top and bottom hole entry cavitation, although to differing degrees. This is unexpected as only cavitation at the top of the injection hole would be expected at high needle lift; however, this could be accounted for by the design having a non-standard large sac volume.

5.4.5. Project Conclusions

High-speed camera imaging has been used to study the internal flow and cavitation within a real size nozzle operating dynamically at actual CR injection pressures. This has provided detailed knowledge of the internal nozzle flow and the location of cavitation within the nozzle sac and the visualised injection hole. However, looking back, there exist a few enhancements that could have been made to improve this project or at least have made the experimentation easier. Firstly and perhaps the most obvious of these is the effect of the chamfer on the external face of the tip. Although necessary for accurate hole exit shape and therefore to ensure realistic spray plumes, the addition of this chamfer has compromised the optical clarity of the latter half of the injection hole. If it had been manufactured to a higher degree of accuracy or if it had

been omitted (with obvious effect on the emerging spray plume), the optical quality within the latter part of the injection hole could have been enhanced. Secondly, an improvement could have been made with the design of the tip to facilitate easier alignment with the modified nozzle body. This is critical to the internal nozzle flow as any misalignment in this region will significantly affect the flow, possibly resulting in a flow in-balance within the sac. Finally, if the decision had been made to manufacture the tips from a material such as quartz, more resilient to the suspected thermal failures that beleaguered the acrylic tips, a single tip may have allowed for the entire experimental testing. Although quartz would be much more difficult to manufacture, the resources used in manufacturing and measuring a batch of 30 acrylic tips could be redistributed into making a single high quality quartz tip.

The high-speed camera images have highlighted the chaotic nature of cavitation under transient operation with a combination of apparently dynamically and geometry induced cavitation. As it is not possible to accurately replicate dynamically induced cavitation with steady state large scale testing, the need for transient testing of real size components has been emphasised.

6. CHAPTER 6 – CONCLUSIONS & RECOMMENDATIONS

6.1. Thesis Overview

Owing to the broad title of this thesis, it was initially decided to encompass the range of different valve designs found within diesel FIE. For this reason an extensive literature review was carried out paying special attention to ball and cone check valves, as these were considered to be of special interest particularly for the purposes of cost reduction. However, during the course of this PhD, the rapid increase in the cost of crude oil in 2008 resulted in market forces which placed increased emphasis on a reduction in specific fuel consumption. As this research was financed and based within Delphi Diesel Systems, the research direction moved to accommodate this market shift. This resulted in the research focusing more heavily on the needle valve as its location within the nozzle sac ensures that it is critical to the combustion process and therefore the fuel economy. Therefore, alongside an investigation of a ball check valve model, the needle valve was investigated through two nozzle models and a real size nozzle fitted with a transparent tip.

Refractive index matching has allowed the use of both LLS and PIV techniques to study the internal fluid flow within suitably designed scalar models of FIE components. Both these techniques have been proven to be a useful way of investigating complicated flow phenomena and the effects of relatively simple geometric changes on the internal flow field. Whereas LLS images are only qualitative, PIV provides quantitative information which has the advantage of being easily manipulated both visually and numerically, especially useful for comparison with simulation data. Being aware of the associated costs and longer time-scales required for experimental study, the author is fully aware that these techniques will likely be used as an aid to, or for the validation of simulation data in regards to product development and optimisation.

The author supported a challenging parallel activity or project utilising real size transparent components of realistic geometry to visualise the internal flow within a multi-hole nozzle during transient operation and actual CR injection

pressures. The advantages of a project such as this are obvious to the other experimental LSM projects disclosed in this thesis to alleviate any doubts that may exist over the scalability of cavitation or bubble transit durations with the LSMs. The findings from this project confirm some of the observations made with the LSM's, in particular the location of hole entry cavitation.

6.2. Statement of Findings

The most significant outcome of this research has been the implementation of the PIV flow measurement technique to analyse some complicated flow phenomena inside enlarged multi-hole injector nozzle models of realistic geometry. This approach has not previously been attempted in such geometries perhaps owing to the difficult experimental setup, the complexities of the PIV technique itself and possibly a lack of knowledge in the open literature about actual nozzle designs. In the author's opinion, the findings of particular importance within this thesis are the mean and RMS velocity data showing growth of the separated region within the injection hole and development of hole entry cavitation. This data has the potential to contribute to understanding of the spray plume development, the fuel/air mixing process and assisting with the validation of RANS and emerging LES CFD models. Additional outcomes of these findings could be the development of improved FIE components, especially fuel injector nozzles with a higher C_d at low needle lift and ball check valves with a more stable operational behaviour.

The fact that this research was conceptualised and funded by a leading FIE manufacturer, exemplifies that the direction of this research is in close agreement with future development within the Diesel powertrain sector. Therefore the findings and the techniques detailed herein have the potential to assist with future product development and optimisation.

6.3. Project Synopsis

The major findings from each of the four experimental projects are detailed below:

1. **Ball Delivery Valve LSM**

   A relatively simple 10x scale transparent model of a ball check valve has been used to assess a newly conceived and novel design of lift-stop with an eccentric flow opening in an attempt to overcome some undesirable opening performance. During steady-state testing across a range of flow rates and ball valve lifts, the performance of the check valve has been assessed through LLS analysis. It was discovered that this simple design of lift-stop was able to suppress the destructive behaviour of the ball element by moving and trapping the ball at an eccentric position. The LLS findings were further scrutinised through PIV analysis of the flow structure at four separate positions within the model to allow the PIV data to be optimised for enhanced accuracy. Significant further investigation is necessary to determine if these findings could be replicated during transient operation as a precursor for product optimisation.

2. **120° Seat Nozzle Project**

   Analysis of the internal flow within the sac of a LSM featuring a 120° seat has confirmed the existence of two interesting flow phenomena, the 'flow transition', the 'flow overshoot' and also identified a third which has been referred to as the 'reverse overshoot'. A new DDS design of needle valve referred to as the 'FEATS' has been compared against the existing design with the FEATS design being proven to reduce the effects of both the flow transition and the flow overshoot. This is an interesting observation as only a slight modification to the needle valve design seemingly improved the performance of the flow within the nozzle sac with the potential to enhance the combustion process and reduce engine exhaust emissions.

3. **60° Seat Nozzle Project**

   The unique geometry of DDS RVN design has allowed the manufacture of a LSM with enhanced visualisation of the flow within the sac and more importantly within the injection holes of a fuel injector nozzle. This has provided high quality PIV data and LLS images of the growth of the separated region at the top of the hole and apparent in-hole vortex activity during both cavitating and non-cavitating conditions. Furthermore,

comparison between similar internal geometry LSM's on two vastly different test rigs, each optimised for either internal or external flow visualisation, has in agreement with previous research, connected vortex activity in the injection hole with helical structures observed within the emerging spray plumes. Moreover, testing with the light sheet at two eccentric positions has demonstrated the effect of the proximity of the needle valve on hole entry cavitation and the in-hole flow.

4. Real Size Transparent Nozzle Tip

This parallel activity has proven the possibility of internal flow visualisation on a real size nozzle tip of realistic geometry at actual CR injection pressures. By adopting the same honing approach as used with the actual metal components, similarity of hole inlet geometry is achieved which is known to be highly influential on producing 'accurate' in-hole flow conditions. The approach of only replacing the nozzle tip ensured that the nozzle remained robust enough to be operated dynamically, which a limitation often found within real size visualisation attempts found in published literature. The location of hole-entry cavitation and the structure of the internal fluid flow has been derived from analysis of the high-speed camera images to assist with the understanding of the dynamic fuel injection event. Additionally, shed cavitation from the seat, geometrically-induced cavitation at hole-entry and string cavitation within the nozzle sac were all identified, helping confirm that these occur in both real size and LSMs alike.

6.4. Recommendations for Future Work

It is said that 'hindsight is a wonderful thing' and with a long-term experimental project such as outlined in this thesis, it would be difficult to disagree. In respect to the experimental projects that constitute this thesis, the following suggestions for future work have been put forward:

- Whereas the 2D PIV system has quantified vortex activity within the nozzle sac and the injection holes, it is likely that a second PIV camera as part of a 3D system could improve upon this data, being able to account for the likely large V_Z component within these flows.

- Whilst vortex structures were observed in the spray plumes of hole 1 on the RVN model, no vortex activity was detected in the PIV data at the central axis of this hole. Assuming this vortex activity originates inside the injection hole or even within the nozzle sac, this should be detectable by moving the light sheet eccentrically away from the central axis. Taking this further, assuming a certain degree of stability with this vortex activity, it should be possible by moving the light sheet in very small successive steps to obtain a 3D image of the flow structure within an injection hole in the same manner as the operation of a MRI scanner.
- The difficulties and limitations of performing PIV within cavitating flows have been discussed at length within this thesis. However, it would be beneficial to perform a sensitivity analysis to determine the influence that the two-phase flow is having on the calculated vectors to remove any uncertainty.
- By rotating the PIV camera slightly so that its x-axis is aligned with the injection hole axis, the V_X and V_Y components of the flow through the hole would be better separated and hence this data would be easier to interpret.
- Recent advances in miniature sensors for measuring local pressures and flow may allow for their incorporation within the LSMs to compliment the PIV velocity data. In particular local measurement of sac pressure could assist with understanding of the hydraulic force acting on the needle valve.
- Although both used the same 120° seat nozzle body, the FEATS needle had marginally a greater flow area for a given lift than the Reference needle. Therefore these two designs are not quite like-for-like, hence differences observed between the two designs may not actually be solely attributed to the FEATS needle geometry.
- The advantage of having two separate LSMs of the same internal geometry, with one optimised for internal flow visualisation and the other for visualisation of the spray plumes, has been detailed. This offers the significant advantage of allowing connections to be drawn between the internal nozzle flow and the emerging spray plumes. However, a major stumbling block remains the scaling process owing to the vastly different

working fluids between the LPR and the LBFR, in particular their respective differences in density. To limit this uncertainty it should be possible to modify the LPR to use the LBFR's working fluid, thus removing the fluid properties from the scaling process. This is technically feasible whereas it is not possible to use the LPR's calibration oil on the LBFR without compromising refractive index matching and therefore the optical quality of the data.

- During the course of this PhD the LSM design has gone through a number of improvements and iterations to improve or optimise the optical access with numerous polished and angled external faces designed to limit refraction at the air/model interface. This has resulted in cost escalation and increased manufacturing time so much so that a redesign of the LBFR may be advantageous to utilise smaller and cheaper models. In response to this and at the time of writing, the author has designed and is currently implementing a submerged chamber for this test rig. There is optimisation within DDS that this will facilitate the testing of lower cost models more akin to real size production components with converging tapered injection holes.

REFERENCES

Andrews R.J., S. S., 2004. *The Application of large Scale Modelling in the Development of Fuel Injection Equipment,* s.l.: Delphi Diesel Systems Internal Report.

Andriotis, A. & Gavaises, M., 2009. Influence of Vortex Flow and Cavitation on Near-Nozzle Diesel Spray Dispersion Angle. *Atomization and Sprays,* Volume 19, pp. 247-261.

Arcoumanis, C., Flora, H. & Gavaises, M., 2000. *Cavitation in Real-Size Multi-Hole Diesel Injector Nozzles 2000-01-1249.* Detroit, Michigan, US, SAE World Congress.

Arcoumanis, C., Gavaises, M. & Nouri, J., 1998. Analysis of the Flow in the Nozzle of a Vertical Multi Hole Diesel Engine Injector 980811. *Journal of Engines,* Volume 107-3.

Arcoumanis, C., Gavaises, M. & Nouri, J., 2008. *The role of Cavitation in Fuel Injection Systems.* Baden-Baden, 8th AVL International Symposium on Internal Combustion Diagonostics.

Arcoumanis, C., Nouri, J. & Andrews, R., 1992. Application of Refractive Index Matching to a Diesel Nozzle Internal Flow. *6th International Symposium on Applications of Laser Techniques to Fluid Mechanics and Workshop on Computers in Flow Measurements,* pp. 10.4.1 - 10.4.7.

Arcoumanis, C., Nouri, J. & Andrews, R. J., 1992. *Measurement of the Internal Fluid Flow in a Diesel Injector using Refractive Index Matching,* Birmingham: IMechE.

Balin, M., 2004. *CFD Analysis of the DFP Pressure Limiting Valve,* s.l.: Unpublished Delphi internal report.

Blessing, M. et al., 2003. *Analysis of Flow and Cavitation phenomena in Diesel Injection Nozzles and its Effects on Spray and Mixture Formation 2003-01-1358.* Detroit, Michigan, US, SAE 2003 World Congress & Exhibition.

Bosch, R., 2004. *Diesel-Engine Management: Systems and Components.* 4th ed. s.l.:Bosch Automotive Technology.

Breenan, C. E., 1995. *Cavitation and Bubble Dynamics.* s.l.:Oxford University Press.

Brogan, M., 2011. *'Advanced Diesel Emission Control' Presentation.* Ford Dunton Technical Centre: Ford motor Company.

Burman, P. & DeLuca, F., 1962. *Fuel Injection and Controls for Internal Conbustion Engines.* s.l.:Simmons-Boardman.

Cameron, S., Rosengarten, G., Milton, B. & Barber, T., 2008. *Investigation of Cavitation in a Large-Scale Transparent Nozzle,* Munich, Germany: FISITA.

Caprotti, R., Bhatti, N. & Balfour, G., 2010. *Deposit Control in Modern Diesel Fuel Injection Systems SAE 2010-01-2250.* San Diego, California, US, SAE 2010 PowertrasinsFuel & ubricants Meeting.

Chaves, H. & Schuhbauer, I., 2006. *Cavitation in an Asymmetric Transparent Real Size VCO Nozzle.* Freiberg Germany, Technische Universität Bergakademie.

Chern, M.-J. & Wang, C.-C., 2004. Control Of Volumetric Flow-Rate Of Ball Valve Using V-Port. *Journal of Fluids Engineering ASME,* Volume 126, pp. 471 - 481.

Chern, M.-J., Wang, C.-C. & Ma, C.-H., 2007. Performance Test And Flow Visualisation Of Ball Valve. *Experimental Thermal and Fluid Science,* Volume 31, pp. 505 - 512.

Clemens, S. et al., 2007. *Advanced Technology for HFO Injection Systems Developed for Medium Speed Engines.* Vienna, Austria, International Council on Combustion Engines.

Delphi.com, 2012. *Delphi F2 Distributed Pump Common Rail System.* [Online]
Available at: http://delphi.com/shared/pdf/ppd/cv/pwrtrn/f2-distributed-pump-diesel-common-rail-system.pdf
[Accessed 27 10 2012].

Delphi, 2011. *Worldwide Emissions Standards - Heavy Duty and Off-road Vehicles,* s.l.: s.n.

Delphi, 2012. *Delphi Diesel Systems.* [Online]
Available at: www.delphi.com
[Accessed 11 11 2012].

DeLuca, F., n.d. *History of Fuel Injection.* s.l.:American Bosch Arma Corporation.

Dingle, P. J. & Lia, M.-C. D., 2005. *Diesel Common Rail and Advanced Fuel Injection Systems.* s.l.:SAE International.

Ellis, J. & Mualla, W., 1986. *Selection of Check Valves.* Hanover, Germany, BHRA.

Environmental Protection Agency, 2012. [Online]
Available at: http://www.epa.gov/otaq/regs/nonroad/nrcycles.htm

European Union, 2012. *Reducing CO2 emissions from passenger cars.* [Online]
Available at: http://ec.europa.eu/clima/policies/transport/vehicles/cars/index_en.htm
[Accessed 1 11 2012].

Fuller John E., 1989. *Electrical Discharge Machining,.* ASM Handbook Vol 16 ed. s.l.:Rockwell International.

Gamba, M., Clemens, N. & Ezekoye, O., 2013. *Volumetric PIV and 2D OH PLIF imaging in the far-field of a low Reynolds number nonpremixed jet flame,* s.l.: Measurements Science and technology Volume 24.

Gao, H., 2003. *Numerical and Experimental Investigation of Cavitating Flow in Oil Hydraulic Dall Valve,* Zhejiang University: China Mechanical Engineering.

Gao, H., Lin, W. & Tsukiji, T., 2006. *Investigation of Cavitation near the Orifice of Hydraulic Valves,* Shanghai Jiao Tong University, Shanghai: IMechE Journal of Aerospace Engineering.

Gavaises, M. et al., 2009. Characterization of String cavitation in Large-Scale Diesel Nozzles with Tapered Holes. *American Institiute of Physics; Physics of Fluids,,* 21(10).

Gavaises, M. et al., 2002. *Nozzle Flow and Spray Characteristics from VCO Diesel Injector Nozzles.* Valencia, Spain, THIESEL 2002 Conference on Thermo- and Fluid- Dynamic Processes in Diesel Engines.

Gavaises, M. et al., 2002. Nozzle Flow and Spray Characteristics from VCO Diesel Injector Nozzles. *Thermo- and Fluid Dynamic Processes in Diesel Engines 2,* Volume 2.

Gavaises, M., Papoulias, D., Andriotis, A. & Giannadakis, E., 2007. *Link Between Cavitation Development and Erosion Damage in Diesel Injector Nozzles 2007-01-0246,* Detroit, Michigan: SAE World Congress & Exhibition.

Gilkin, P. E., 1985. *Fuel Injection in Diesel Engines - Chairman's Address,* London: IMechE Automobile Division.

Goodwin, R. & Jenkins, K., 2000. *Anti-Pressure Surge Developments on Dual Plate Check Valves.* The Hague, The Netherlands, 8th International Conference on Pressure Surges.

Greeves, G., Tullis, S. & Barker, B., 2003. *Advanced Two-Actuator EUI and Emission Reduction for Heavy-Duty Diesel Engines 2003-01-0698.* Detroit, Michigan, US, SAE 2003 World Congress & Exhibition.

Hart, D. P., 1998. *PIV Error Correction.* Lisbon, Portugal, Experiments in Fluids- 9th International Symposium on Applications of Laser Techniques to Fluid Mechanics.

Heywood, J. B., 1988. *Internal Combustion Engine Fundamentals.* s.l.:McGraw-Hill International Editions.

Hilliard, J. & Wheeler, R., 1979. *Nitrogen Dioxide In Engine Exhaust SAE 790691,* s.l.: SAE International.

How cars work, n.d. *How cars work.* [Online]
Available at: http://www.howcarswork.co.uk/modules/articles/article.php?id=7
[Accessed 01 April 2013].

iAV, n.d. *iAV Injection Analyser.* [Online]
Available at: http://www.iav.com/sites/default/files/120509_injectionanalyzer_en_web.pdf
[Accessed 30 10 2012].

Johnson, T. V., 2008. *Diesel Emission Control in Review SAE 2008-01-0069.* Detroit, Michigan, US, SAE International.

Keane, R. D. & Adrian, R. J., 1992. Theory of cross-correlation analysis of PIV images. *Applied Scientific Research,* 49(3), pp. 191-215.

Kennametal Inc., 2012. *Kennametal Inc..* [Online]
Available at: http://www.kennametal.com/en/home.html
[Accessed 29 10 2012].

Kimura, S., Aoki, O., Ogawa, H. & Muranaka, S., 1999. *New Combustion Concept for Ultra-Clean and High-Efficiency Small DI Diesel Engines 1999-01-3681,* s.l.: SAE Technical Paper.

Knecht, W., 2004. *Some Historical Steps in the Development of the Common Rail Injection System,* s.l.: The Newcomen Society.

Knight, B. E., 1952. *Distributor Pump Research - Part 1,* s.l.: C.A.V Limited (unpublished).

Knight, B. E., 1960. *Fuel - Injection System Calculations.* London, IMechE - Automobile Division.

Knight, B. E., 1961. *The Unloading of Ball Valves,* s.l.: C.A.V Limited (unpublished).

Koetzier, H., Kruisbrink, A. C. H. & Lavooij, .. S. W., 1986. *Dynamic Behaviour of Large Non-Return Valves.* Hannover, Germany, 5th International Conference on Pressure Surges.

Koivula, T. S. & Ellman, A. U., 1998. *Cavitation Behaviour of Hydraulic Orifices and Valves 982038,* Milwaukee, Wisconsin, US: International Off-Highway & Powerplant Congress & Exposition.

Kontoulis, P., Chryssakis, C. & Kaiktsis, L., 2008. *Evaluation of Pilot Injections in a Large Two-Stroke Marine Diesel Engine, Using CFD.* Athens, Greece, National Technical University of Athens.

Kruisbrink, A. C. H., 1996. *The Dynamic Behaviour of Check Valves in Pipeline Systems,* London: City University PhD Thesis.

Lacey, P. et al., 2011. Internal Fuel Injector Deposits SAE 2011-01-1925. *SAE.*

Lacey, P., Gail, S., Kientz, J. & Milovanovic, N., 2012. Internal Fuel Injector Deposits SAE 2011-01-1925. *Journal of Fluels Lubrication,* 5(1), pp. 132-145.

LaVision, 2012. *LaVision PIV.* [Online]
Available at: http://www.lavision.de/en/techniques/piv.php
[Accessed 2012].

Lee, J. W. et al., 2006. Effect of Piezo-driven and Solenoid-driven Needle Opeing of Common-rail Diesel Injectors on Internal Nozzle Flow and Spray Development. *IMechE Journal of International Engine Research,* 7(6), pp. 489-502.

Lee, W.-K., Fezzaa, K. & Wang, J., 2005. Metrology of Steel Micronozzles using X-ray Progagation-based Phase-enhanced Microimaging. *Aplied Physics Letters,* 87(8).

Leventhal, L., 2003. *CAE Applications in Hydraulics - Experimental and Analytical Study of a Check-Valve 2003-01-1605.* Grand Traverse, Michigan, US, SAE Noise & Vibration Conference and Exhibition.

Lüders, H. B. R., Hüthwohl, G. & Ketcher, D. e. a., 1995. *A Urea Lean NOx Catalyst System for Light Duty Diesel Vehicles SAE 952493.* s.l., SAE technical paper series.

Mahn B., 2002. *Future and Potential of Diesel Injection Systems,* Stuttgart, Germany: Robert Bosch GmbH.

Mardell, J. E., 2003. *Getting fun out of Diesel, in IMechE AD chairmans Address. 2003.* London, IMechE.

Miranda, R., Chaves, H., Martin, U. & Obermeier, F., 2003. *Cavitation in a Transparent Real Size VCO Injection Nozzle.* Sorrento, Italy, 9th International Conference on Liquid Atomization and Spray Systems ICLASS.

Mitroglou, N. & Gavaises, M., n.d. *Diesel Real-Size Imaging,* s.l.: s.n.

Mitroglou, N., Gavaises, M. & Theodorakakos, A., 2011. *Cavitation Simulation and Experimental Verification using a new Diesel Nozzle Design Concept.* Thessaloniki, Greece, 4th ANSA & µETA International Conference.

Moujaes, S. & Jagan, R., 2008. 3D CFD Predictions And Experimental Comparisons Of Pressure Drop In A Ball Valve At Different Partial Openings In Turbulent Flow. *ASCE Energy Engineering.*

Munson, B., Young, D. & Okiishi, T., 2006. *Fundamentals of Fluid Mechanics 5th Edition.* s.l.:John Wiley & Sons Inc..

National Toxicology Program, Department of Health and Human Sciences, 2011. *Diesel Exhaust Particlates 2011/12.* [Online]
Available at: http://ntp.niehs.nih.gov/go/roc12

Oda, T. et al., 2010. *Experimental and Numerical Investigation about intrenal Cavitating Flow and Primary Atomisation of a Large-Scaled VCO Diesel Injector with Eccentric Needle.* Brno, Czech Republic, 23rd Annual Conference on Liquid Atomization and Spray Systems ILASS.

Payri, R., Salvador, F., Gimeno, J. & De la Morena, J., 2011. *Influence of injector technology on injection and combustion development: Part 2: Combustion analysis,* s.l.: Applied Energy pp 1130–1139.

Payri, R., Salvador, F., Gimeno, J. & Venegas, O., 2012. *Study of Cavitation Phenomenon Using Different Fuels in a Transparent Nozzle by Hydraulic Characterization and Visualization,* s.l.: Experimental Thermal and Fluid Science.

Perko, H. D., 1986. *Check Valve Dynamics In Pressure Transient Analysis.* Hannover, Germany, 5th International Conference on Pressure Surges.

Potter, M., Bacic, M., Ligrani, P. & Plackett, M., 2008. Instabilities of Nonreturn Valves in Low-Speed Air Systems. *ASME Journal of Fluids Engineering,* Volume 130.

Powell, C. F. et al., 2004. *X-ray Absorption Measurements of Diesel Sprays and the Effects of Nozzle Geometry 2004-01-2011,* Toulouse, France: SAE Fuels & Lubricants Meeting & Exhibition.

Powell, C. F., Kastengren, A., Liu, Z. & Fezzaa, K., 2011. The Effects of Diesel Injector Needle Motion on Spray Structure. *Journal of Engineering for Gas Turbines and Power,* Volume 133.

Provoost, G. A., 1982. *The Dynamic Characteristic of Non-Return Valves.* Amsterdam, The Netherlands, Operating Problems of Pump Stations and Power Plants. 11th symposium IAHR(AIRH).

Provoost, G. A., 1983. *Theoretical Approach to a Check Valve Response in the Cooling Water Circuit of a Power Plant.* s.l., 6th Symposium on Hydraulic Transients in Power Stations IAHR.

Quigley, R. et al., 2011. *A Study of the Internal Diesel Deposit Phenomenon,* s.l.: Lubrizol Limited, UK.

Raffel, M., Willert, C., Wereley, S. & Kompenhans, J., 2007. *Particle Image Velocimetry - A practical guide.* 2nd ed. s.l.:Springer.

Ramirez, A. et al., 2009. *Characterizing Spray Behaviour of Diesel Injection Systems Using X-ray Radiography 2009-01-0846.* Detroit, Michigan, US, SAE World Congress & Exhibition.

Roth, H., Gavaises, M. & Acroumanis, C., 2002. *Cavitation Initiation, its Development and Link with Flow Turbulence in Diesel Injector Nozzles 2002-01-0214.* Detroit, Michigan, US, SAE World Congress & Exhibition.

Scarano, F., 2013. *Tomographic PIV: principles and practice,* s.l.: Measurement Science and Technology, Volume 24, number 1.

Schoppe, D., Hardy, M., Zulch, S. & Guerts, D., 2008. *Exceeding Customer Expectations with the Innovative Direct Acting Diesel Fuel Injection System: Unique Advantages of a Breakthrough Technology.* Vienna, Austria, 29th International Vienna Motor Symposium.

Schoppe, D., Kruger, G., Weigand, A. & Dian, V., 2012. *The New Diesel Servo-Piezo Common Rail System - the efficient solution for euro 6 and above.* Rouen, France, SIA Societe Des Ingenieurs De L'Automobile.

Shervani-Tabar, M. T., Mahmoudi, S. M. S., Amir-Kamvar, B. & Rezaee-Barmi, A., 2003. *Collapse Behaviour of Two Parts of a Cavitation Bubble after its Splitting.* Osaka, Japan, 5th International Symposium on Cavitation CAV.

Soteriou, C., Andrews, R. & Smith, M., 1995. *Direct Injection Diesel Sprays and the Effect of Cavitation and Hydraulic Flip on Atomization SAE 950080.* Detroit, Michigan, US, SAE World Congress.

Soteriou, C. et al., 2000. *The Flow Patterns and Sprays of Variable Orifice Nozzle Geometries for Diesel Injection 2000-01-0943.* Detroit, Michigan, SAE World Congress .

Soteriou, C. et al., 2001. *Through the Diesel Nozzle Hole - A Journey of Discovery.* Dearborn, Michigan, US, 14th Conference on Liquid Atomisation and Spray Systems ILASS.

Soteriou, C., Lambert, M., Zuelch, S. & Passerel, D., 2006. *The Flow Characteristics of High Efficiency Diesel Nozzles with Enhanced Geometry Holes.* Valencia, Spain, THIESEL International Conference on Thermo- and Fluid Dynamic Processes in Diesel Engines.

Soteriou, C., Smith, M. & Andrews, A., 1998. *Diesel injection: Laser light sheet illumination of the development of cavitation in orifices.* London, IMechE International conference on combustion engines and hybrid vehicles.

Soteriou, C., Smith, M. & Andrews, R., 1993. *Cavitation Hydraulic Flip and Atomization in Direct Injection Diesel Sprays.* Birmingham, IMechE.

Sou, A., Pratama, R., Ohashi, R. & Sugimura, R., 2011. *Cavitation in a Nozzle with Asymmetric Inflow and its Effects on liquid Jet.* Estoril, Portugal, 24th European Conference on Liquid Atomization and Spray Systems ILASS.

Stone, J., 1960. Discharge Coefficients and Steady-State Flow Forces for Hydraulic Poppet Valves. *Journal of Fluids Engineering,* 82(1), pp. 144 - 154.

Tang, J. et al., 2009. *Coking Phenomena in Nozzle Orifices of DI-Diesel Engines 2009-01-0837.* Detroit, Michigan, SAE World Congress & Exhibition.

Thorley, A. R. D., 1989. Check Valve Behaviour Under Transient Flow Conditions: A state-of the-Art Review. *Journal of Fluids Engineering,* 111(2), pp. 178-183.

Torres, N., n.d. *Sac Type Nozzle Tip Study – Visualisation of Flow Transition, Cavitation and Flow & Spray Structure,* s.l.: Delphi (unpublished).

Val-Matic Valve and Manufacturing Corp., 2003. *Dynamic Characteristics of Check Valves,* s.l.: s.n.

Wanga, X. et al., 2011. *Effects of ultra-high injection pressure and micro-hole nozzle on flame structure and soot formation of impinging diesel spray,* s.l.: Applied Energy, Volume 88, Issue 5, Pages 1620–1628.

WHO, World Health Organisation, 2112. *(IARC) International Agency for Research on Cancer-Press Release No. 213,* s.l.: s.n.

Wilczynski, L., 2003. *Stoichastic Modelling of Cavitation Erosion Based on the Concept of Resonant Energy Absorption.* Osaka, Japan, 5th International Symposium on Cavitation.

Yanagihara, H., Sato, Y. & Minuta, J., 1996. *A simultaneous reduction in NOx and soot in diesel engines under a new combustion system (Uniform Bulky Combustion System -UNIBUS),* s.l.: 17th International Vienna Motor Symposium, pp 303-314.

Zhiming, Z. & Yujian, D., 2003. *On Standardization of Cavitation Inception Testing Technique.* Osaka, Japan, 5th International Symposium on Cavitation.

Zülch, S., Schöppe, D., Jorach, R. W. & Judge, R., 2006. *The new delphi common rail injection system for medium duty diesel engines.* Aachen, Germany: 15. Aachener Kolloquium 'Fahrzeug- und Motorentechnik'.

APPENDIX

1. **Scanned original experimental data of ball lift for a distribution pump** (Knight, 1961)**. This has been re-drawn in Figure 37.**

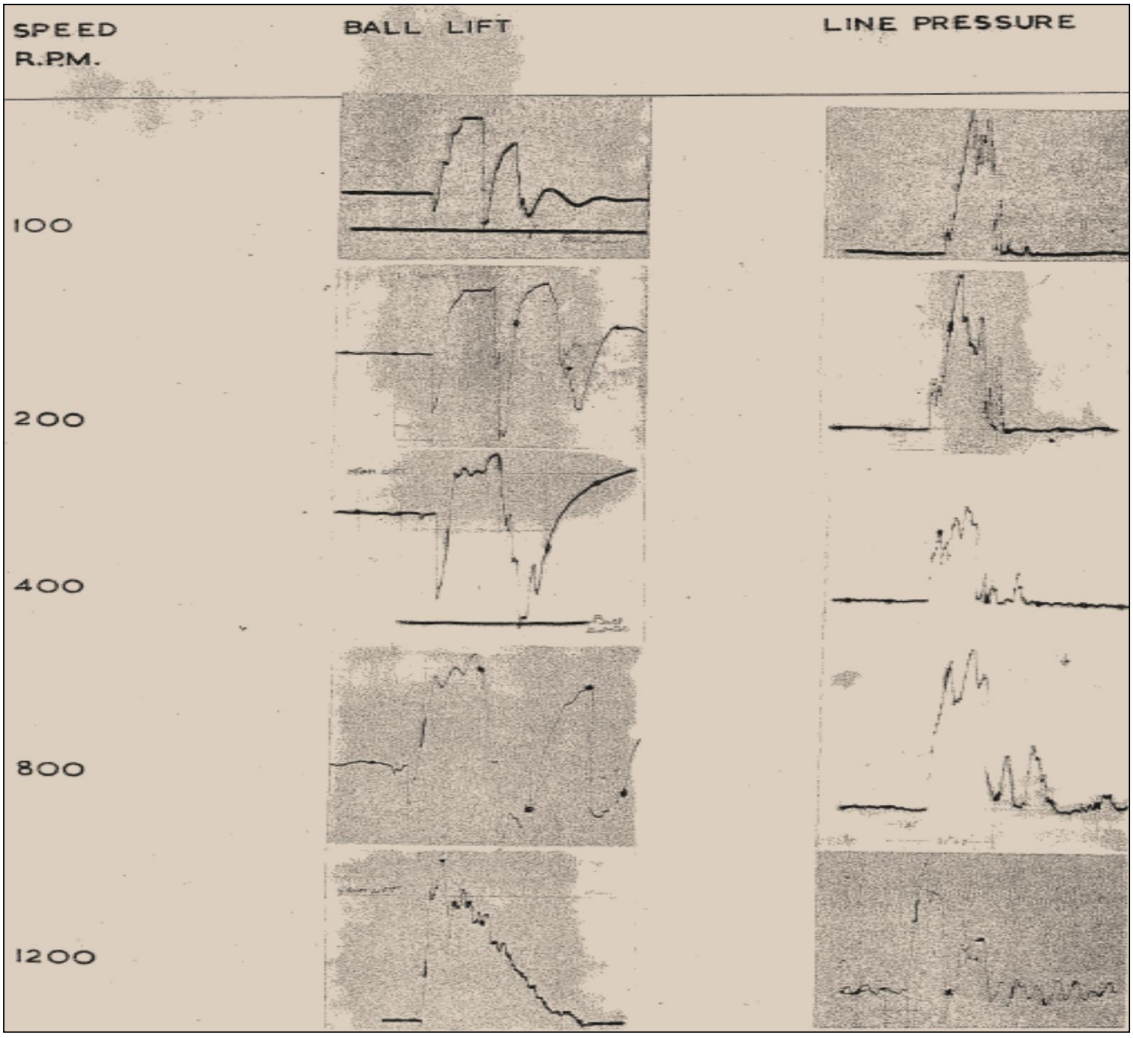

2. **MD Duty Cycles for a tractor and a back-hoe** (Environmental **Protection Agency, 2012).**

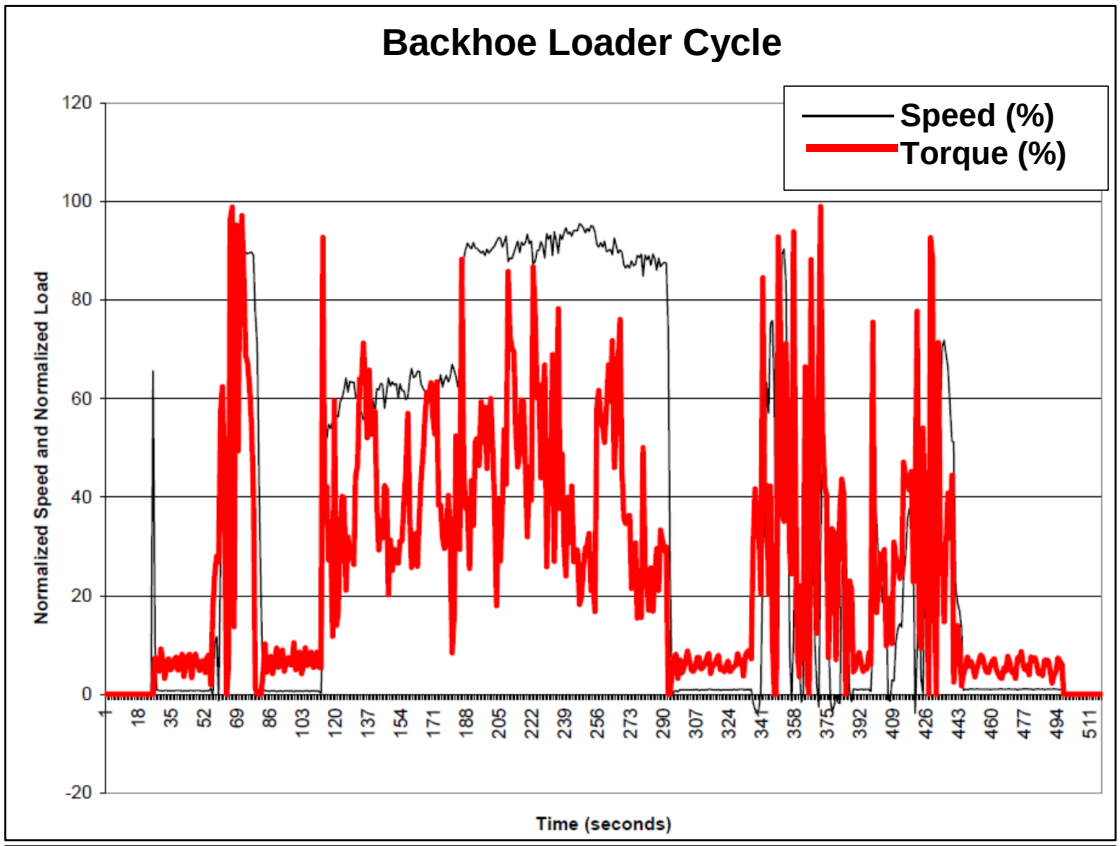

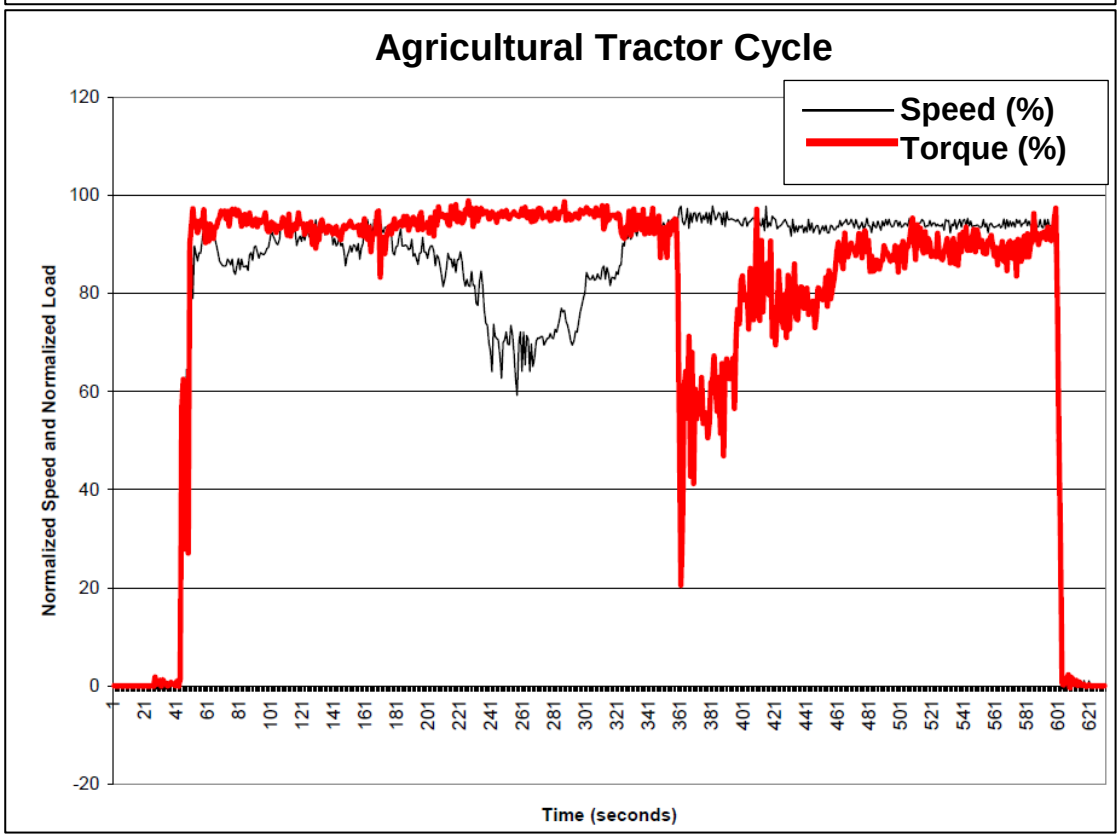

3. Castrol Calibration oil ISO4113 spec sheet

Calibration Oil 4113

Diesel Injector Test Fluid

Description

Castrol Calibration Oil 4113 is a low viscosity mineral oil based test fluid.

Application

Calibration Oil 4113 is a calibration and storage oil for diesel fuel injectors, conforming fully with ISO 4113 and Lucas CAV 7-10-106 (now obsolete) specifications. The rust preventative properties of this oil are such that, without cleaning of the equipment after calibration, proper functioning of the equipment is ensured after one years storage in normal conditions. Whilst Calibration Oil 4113 contains no harmful additives it is a light mineral oil and will have a de-fatting effect upon unprotected skin. Use of a barrier cream or otherprotection is recommended when in contact with this product.

Typical Characteristics

Name	Method	Units	4113
Appearance	Visual	-	Clear off-white liquid
Density @ 15°C	ISO 12185/ASTM D4052	g/ml	0.825
Viscosity, Kinematic 40C	ISO 3104/ASTM D445	mm^2/s	2.53
Colour	ASTM D1500	-	0.5
Foam Sequence I, Tendency/Stability	ISO 6247/ASTM D892	ml/ml	20/0
Flash Point, PMC	ISO 2719/ASTM D93	°C/°F	84/183
Pour Point	ISO 3016/ASTM D97	°C/°F	<-30/<-22
Rust Test, Procedure A	ISO 7210/ASTM D665A	-	Pass
Rust Test	ASTM D1748	-	Pass
Copper Corrosion, 3hrs @ 100C	ASTM D130	-	1a
4 Ball wear test 300N 1450rpm/10s	ASTM D4172	mm	0.3
Lubricity HFRR	ISO 12156-1	microns	410

Subject to usual manufacturing tolerances

4. Vehicle classification and comparison of EURO 5/Euro V exhaust emission standards

Class	Description	GVW [kg]	RW [kg]	Seats	PM	NO_x	CO
M1[24]	Passenger car	n/a	n/a	≤8	5.0 mg/km	180 mg/km	500 mg/km
M2	Minibus	≤5t	n/a	>8	*0.02 g/kWh*	*2.0 g/kWh*	*1.5 g/kWh*
M3	Buses & coaches	>5t	n/a	>8	*0.02 g/kWh*	*2.0 g/kWh*	*1.5 g/kWh*
N1[25] **CI1**	Light commercial vehicle(LCV)	≤3.5t	≤1.305t	n/a	5.0 mg/km	180 mg/km	500 mg/km
N1 CI2	Light commercial vehicle(LCV)	≤3.5t	1.305 to 1.760t	n/a	5.0 mg/km	235 mg/km	630 mg/km
N1 CI3	Light commercial vehicle(LCV)	≤3.5t	>1.760t	n/a	5.0 mg/km	280 mg/km	740 mg/km
N2	Large goods vehicle(LGV)[26]	3.5t to 12t	n/a	n/a	5.0 mg/km	280 mg/km	740 mg/km
N3	Large goods vehicle(LGV)	>12t	n/a	n/a	*0.02 g/kWh*	*2.0 g/kWh*	*1.5 g/kWh*

[24] Class M is denoted for vehicles intended for carrying passengers
[25] Class N is for vehicles intended for transporting goods
[26] Large goods vehicles were previously known as heavy goods vehicle (HGV)

5. Stanley Plastic - acrylic spec sheet

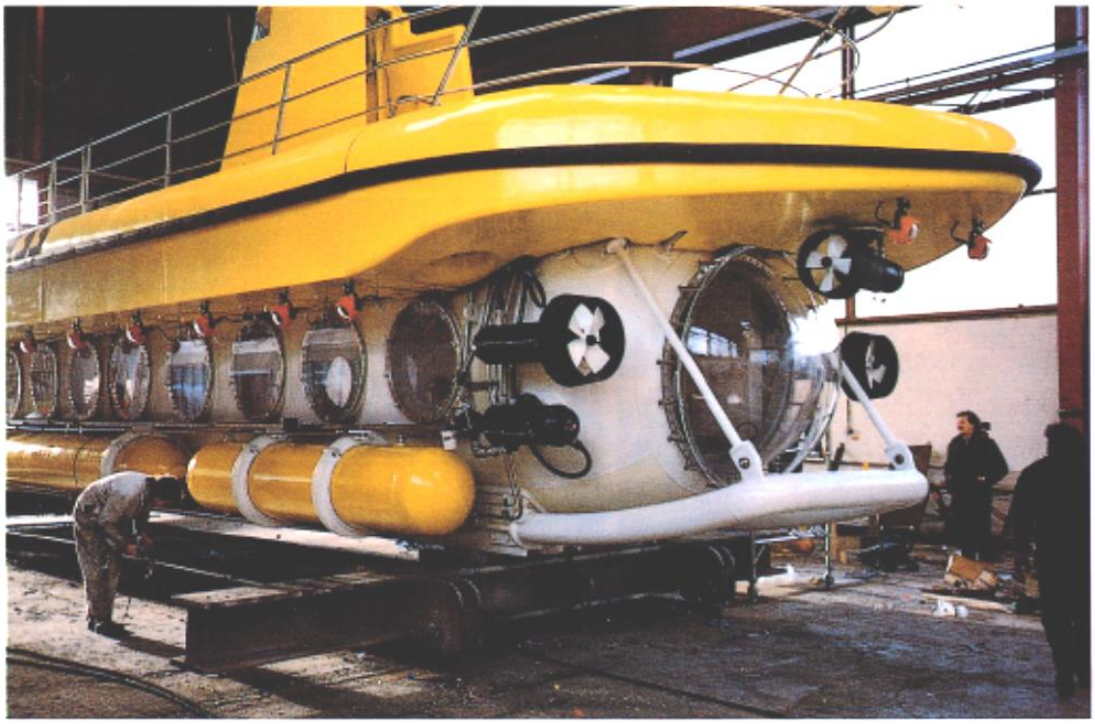

Manufactured in
"TRANSPALITE® SS" acrylic to exceed the ASME specifications for certification by:

Lloyds Register of Shipping
American Bureau of Shipping
Det Norske Veritas
Registro Italiano Navale

"TRANSPALITE® SS":
YOUR WINDOW TO THE WORLD BENEATH THE SEA

"TRANSPALITE® SS" PROPERTIES			ANSI/ASME/ PVHO-1 Specification
Test Procedure ASTM	Physical Properties	Average Value	Minimum Value
D256	Izod Notch	22 J/m	133 J/m
D542	Refractive Index	1.49	1.49
D570	Water absorption 24 hr	0.25%	0.25%
D732	Shear ultimate strength	79 MPA	55 MPA
D785	Rockwell hardness	M Scale 108	M Scale 90
D792	Specific gravity Poissons ratio	1.19 0.38	1.19
D696	Coefficient of linear expansion @ 26°C	10^{-5} (per/per °C) 8.48	10^{-5} (per/per °C) 7.74
D638*	Tensile ultimate strength Elongation at break Modulus of elasticity	77 MPA 5% 3540 MPA	62 MPA 2% 2758 MPA
D695*	Compressive yield strength Modulus of elasticity	125 MPA 4400 MPA	103 MPA 2758 MPA
D621*	Compressive deformation at 275 MPA and 50°C	≤0.56%	≤1%
E398*	UV Transmission	≤0.08%	≤5%
B5*	Residual methyl methacrylate monomer	≤0.025%	≤1.5%
B5*	Residual ethylacrylate monomer	≤0.00%	≤0.01%
D702	Visual clarity	passes read-ability test	passes read-ability test

*Mandatory tests which must be verified by specimen testing of a casting batch
1 MPA = 1 N/mm² = 145.04 PSI

Stanley
PLASTICS LTD

HOLMBUSH INDUSTRIAL ESTATE MIDHURST
WEST SUSSEX GU29 9HX ENGLAND
Telephone: MIDHURST (01730) 816221
Telefax: MIDHURST (01730) 812877

6. List of Possible Experimental Errors

Experimentation is often affected by measurement errors which need be confidently predicted and taken into account when analysing data. Ideally any experimental uncertainty should be of the order of a few per cent of the measured quantity, however this is often not the case and in these instances the data must be handled with care and presented alongside the potential sources of error. The following section attempts to disclose any potential sources of experimental error that could have influenced the results presented in this thesis.

LPR and LBFR Experimental Flow rigs

- The flow meters (turbine type) used during the experimentation described in this thesis read in litres/min and to 2 decimal places. However owing to occasional fluctuations on these readings, the flow rates were typically only recorded to the nearest to ±0.1l/min. These flow meters were calibrated through DDS's internal gauge control.
- The LBFR and the LPR are maintained at a constant 25 and 35°C respectively. These temperatures are set by closed loop control systems and owing to the large volumes of working fluids contained within each rig, these temperatures are stable. The temperature measurement accuracy is to ±0.1°C.
- As both the LBFR and the LPR are steady-state, pressure measurement was by way of analogue test gauges. On each test rig separate gauges were located for measurement of upstream, downstream and vacuum tank pressures. The range of these gauges was between -1 & 9 bar with a minimum division or error of ±0.05 bar. Within DDS, gauges are maintained within calibration through an internal gauge control.
- The LBFR requires that the working fluid be refractive index matched (at 25°C) to that of the acrylic model adopted for testing. The working fluid was periodically checked by way of a SPER Scientific 300034 digital refractometer to ensure its refractive index was maintained at 1.49.
- The LPR working fluid is high quality calibration oil (ISO4113). This was replaced on an annual basis.

Real Size Nozzle Study

Owing to the reasonably high injection pressure and being operated dynamically, pressure measurement on this project was performed by way of a kistler pressure gauge which was situated at the location where the injector is connected to the high pressure pipe linking it to the common rail. This design of gauge has a working range of up to 2000bar and an accuracy of ±50bar. As the actual experimental testing was performed by Dr Mitroglou and no actual quantitative measurements were obtained, the other possible errors in this project shall not be discussed further.

Particle Image Velocimetry (PIV)

Requiring a statistical correlation of images to determine local flow velocities, PIV is subjective to inherent errors that arise from the finite tracer particle numbers, the sample volume size, and the resolution of the image. Velocity vectors determined by correlating finite sub-regions of images of tracer particles are often biased to varying degrees by out-of plane motion, correlations occurring between unmatched particle pairs, particle overlap, non-uniform particle distribution and variations in image intensities. Such errors along with the errors associated with excessive velocity gradients and the finite sample volume size necessary to image a statistically meaningful number of tracer particles, limits the accuracy and hence the usefulness of the PIV technique (Hart, 1998). Some of the major sources of error are detailed below:

- **Correlation errors.** These errors occur primarily from insufficient data, be it a lack of imaged tracer particles, poor image quality, and/or unmatched tracer particles within the sample volume. These errors can be minimised by using a high resolution imaging camera and by carefully controlling the seeding density and interrogation window size (Hart, 1998).
- **Seeding size.** Tracer particles ideally should be neutrally buoyant and small compared with the fine flow structures being studied whilst not interfering with the bulk fluid flow (Quantitative flow analysis around aquatic animals using laser sheet particle image velocimetry). Additionally, the tracer particles need to be sufficiently large as to sufficiently scatter the laser light whilst not undergoing interactions or jostling with each other. On the recorded images, the tracer particle

diameter depends not only on the particle size but also on the magnification of the camera's acquiring optics. It is recommended that the imaged particle diameter should be more than 2 pixels to provide a good correlation (Raffel, et al., 2007).

- **Seeding density**. The probability of obtaining an accurate measure of the displacement of a set of particles using correlation increases as the number of particles increases. Excessive seeding may however cause sampling rate drop, poor signal to noise ratio, window (or surface) fouling and even alteration to the characteristics of the flow being measured. Insufficient seeding on the other hand is also likely to result in a poor signal-to-noise ratio. Optimum seeding density is considered to be an average of 10 particles per interrogation window (Keane & Adrian, 1992).
- **Gravitationally Induced velocity**. A primary source of error can exist if the density of the tracer particles differs sufficiently from that of the working fluid. This gravitational induced velocity is more apparent at lower flow velocities and can be derived from the Stokes drag law (Raffel, et al., 2007).
- **Interrogation (window) size.** The interrogation size can be optimised for the particular application. Large velocity gradients however limit the maximum permissible interrogation size as large local velocity gradients can result in unequal particle displacements causing one part of an interrogation region to correlate significantly differently to another.
- **Out-of-Plane motion.** Flow across the light sheet plane restricts measurements to regions of nearly planer flow and restricts the minimum permissible width of the sample volume, thereby restricting spatial resolution (Hart, 1998).
- **Spurious data points.** Spurious or outlier data points are defined as being a data point which is very different from the rest of the data based on some measure. High quality data typically exhibits less than 1% of spurious vectors under regular conditions and less than 5% under challenging experimental situations (Raffel, et al., 2007). Outlier data points (or vectors if you like) are a consequence of the statistical nature of PIV and are often found to occur at the edge of an image or near a solid boundary. Spurious data points are normally filtered out.

- **Filling-in of empty spaces**. During post-processing and after the filtering of outlier vectors, it is sometimes necessary to fill-in empty spaces with information from data interpolated from the surrounding areas. It is obviously risky to be over-reliant on this feature so it is advantageous to scrutinise the percentage of vectors which the software has had to add.